Study of Ice Jam Events on Missouri River During the Winter Seasons

By

Nikit Bhattarai

A thesis submitted to the Graduate Faculty of
Auburn University
in partial fulfillment of the
requirements for the Degree of
Masters of Science

Auburn, Alabama
August 6, 2022

Keywords:
Sub-zero temperature, Gage height, Landsat, Ice cover, Ice jam, Water temperature

Approved by
Dr. Xing Fang, Chair, Arthur H. Feagin Chair Professor of Civil Engineering, Auburn University
Dr. Luke Marzen, Professor of Geosciences, Auburn University
Dr. Liping Jiang, Associate Professor of Civil Engineering, Montana Technological University

ABSTRACT

Rivers are hugely affected by river ice processes for a significant portion of the year causing river ice jams in Northern rivers such as the Missouri River in Montana. Ice jamming is an accumulation of ice in a river, stream, or other flooding sources that reduces the cross-sectional area available to carry the flow and increases the water-surface elevation. Several researchers have conducted a variety of river ice studies over the years which resulted in a comprehensive dataset including meteorological, hydrometric, and river ice data. The analyses of these data provide evidence of a highly complex ice regime. This study of ice jam events in the Missouri River is conducted as a part of the project "Studying effects of sub-zero temperatures on the volume of water and discharge in the Missouri River" funded by Northwestern Energy Hydro.

The flow analysis using the USGS hydrometric data (discharge, gage height, and water temperature) is carried out from the Holter, MT to Great Falls, MT at the Missouri River which is ~100 river miles. Several ice jam events during the winter from 2014–2022 were analyzed, studying the discharge loss downstream of the ice jam location, gage height increases upstream of the ice jam location, and air temperature during the ice formation event. Flow analysis spreadsheet capable of automatically downloading hydrometric data available at the USGS gage stations from the Holter to Morony Dam is prepared which also downloads the visual crossing website weather data for historical and future periods for Great Falls. This spreadsheet is used to identify a potential ice jamming event from freezing degree hours during any event.

The model preparation of HEC-RAS is done for the Missouri River using the Lidar data and USGS data with the bathymetry data provided by Northwestern Energy Hydro. The flow and water temperature simulations are then carried out for Missouri River during the identified ice jam events using the meteorological parameters. The water temperature simulation results show the evidence of ice cover/jam formation as the water temperature stays at 0 ^{o}C during the event. Ice jam simulation is carried out in HEC-RAS after knowing the river distance that is covered by ice. The HEC-RAS ice jam simulation model do not consider the meteorological parameters for ice jam simulation and do not consider the dynamic process involved in river ice processes, which is why River1D model is selected for river ice modeling. River1D has the ability to perform thermal ice jam simulation which incorporates the dynamic processes involved in river ice jam formation.

ACKNOWLEDGEMENT

The author would like to express special gratitude to the academic advisor, Professor Dr. Xing Fang for the devotion, guidance, mentorship, and support provided throughout this research. The amount of work and professionalism he showed during this time will always be carried as motivation in any future work. The author would also like to thank Dr. Liping Jiang, for the time and supervision she provided during the whole course of the project. And the author would like to thank Prof. Dr. Luke Marzen, for the knowledge the author gained about Geographical Information System and Remote Sensing & Aerial Photogrammetry which was utilized in the course of the project. The author would also like to thank Jeremy Butcher for the valuable inputs provided during the research and the Northwestern Energy Hydro that funded the project.

The author would like to especially thank his parents Dhurba Bhattarai and Rama Poudel Bhattarai, and his brother Ankit Bhattarai who through love, hard work, and a lot of sacrifices provided the author support throughout his educational endeavor.

Finally, the author would like to thank Auburn University and the Department of Civil Engineering for providing the author an opportunity to pursue Masters in Hydrology/Hydraulics with financial support and an assistantship opportunity.

TABLE OF CONTENTS

ABSTRACT ii

ACKNOWLEDGEMENT iii

TABLE OF FIGURES vii

LIST OF TABLES xvii

CHAPTER 1. INTRODUCTION 1

1.1 BACKGROUND 1

1.2 SCOPES AND OBJECTIVES 5

1.3 THESIS ORGANIZATION 6

CHAPTER 2. LITERATURE REVIEW 7

2.1 OVERVIEW OF RIVER ICE PROCESSESS 7

2.2 CHALLENGES OF RIVER ICE PROCESSES AND BENEFITS OF RIVER ICE MODELING 17

CHAPTER 3. DATA ANALYSIS FOR FLOW DECREASE EVENTS 20

3.1 INTRODUCTION 20

3.2 SPECIAL EVENTS IN THE WINTER OF 2014–2015 21

3.3 SPECIAL EVENTS IN THE WINTER OF 2015–2016 28

3.4 SPECIAL EVENTS IN THE WINTER OF 2016–2017 33

3.5 SPECIAL EVENTS IN THE WINTER IN 2018 39

3.6 SPECIAL EVENT IN THE WINTER OF 2019 50

3.7 SPECIAL EVENTS IN THE WINTER OF 2020 58

3.8 SPECIAL EVENTS IN WINTER OF 2021 65

3.9 SPECIAL EVENTS IN WINTER OF 2022 68

3.10 CATEGORIZATION OF FLOW LOSS EVENTS BASED ON THE LOCATION OF ICE JAM FORMATION 71
3.11 FLOW ANALYSIS SPREADSHEET 73
CHAPTER 4. LAND COVER CLASSIFICATION OF STUDY AREA 81
4.1 INTRODUCTION 81
4.2 METHODOLOGY 81
4.3 RESULTS 83
4.4 DISCUSSION 91
CHAPTER 5. HEC-RAS MODEL SET UP 92
5.1 INTRODUCTION TO HEC-RAS 92
5.2 BATHYMETRY DATA ACQUISITION 97
5.3 BOUNDARY CONDITIONS 106
5.4 PROFILE ELEVATION COMPARISON 109
5.5 HEC-RAS MODEL RESULTS 110
CHAPTER 6. ICE COVER AND ICE JAM SIMULATION IN HEC-RAS 119
6.1 INTRODUCTION 119
6.2 MODELING ICE-COVERED RIVERS 120
6.3 TESTING OF RIVER ICE DATA 123
6.4 ICE JAM SENSITIVITY ANALYSIS 128
6.5 MODELING ICE-COVER IN MISSOURI RIVER 131
6.6 ICE JAM SENSITIVITY ANALYSIS FOR MISSOURI RIVER 133
CHAPTER 7. WATER TEMPERATURE SIMULATION 140
7.1 INTRODUCTION 140
7.2 INPUT DATA 141
7.3 RESULTS 147

7.4 DISCUSSION 149
CHAPTER 8. RIVER1D 150
8.1 INTRODUCTION 150
8.2 RIVER1D MODEL DESCRIPTION 153
8.3 RIVER1D APPLICATION 155
8.4 COMPARISON TO HEC-RAS 162
CHAPTER 9. SUMMARY AND CONCLUSIONS 164
9.1 SUMMARY 164
9.2 CONCLUSIONS 165
9.3 FUTURE WORK 168
REFERENCES 170

TABLE OF FIGURES

Figure 1.1 (a) Ice jam formation in Yellowstone River at Miles City, Montana in 2018 (https://www.youtube.com/watch?v=6VTEAMYHShI), and (b) Ice jam formation before a bridge in Gallatin River near Logan, Montana in January 2022 (https://www.youtube.com/watch?v=z_TDNNVxQBc). 2
Figure 1.2 Google Earth image showing river ice jam in Missouri River in December 2004. 3
Figure 1.3 Google map showing the Missouri River from Holter Dam (upstream) to Great Falls (downstream) and I15 through Craig, Cascade, and Ulm in Montana. 5
Figure 2.1 Border ice forms along the riverbank (photo from S. Beltaos). 8
Figure 2.2 Frazil ice (photo by R. Andrishak, University of Alberta) 8
Figure 2.3 Anchor ice on the riverbed of Ram River, Alberta (photo by R. Brown) 9
Figure 2.4 Frazil pans formed after collision (photo by F. Hicks) 9
Figure 2.5 Bridging process starting at river bends and constricted areas (photo by R. Gerard, University of Alberta) 10
Figure 2.6 Ice pans and border beginning to merge; start of the bridging process (photo by R. Gerard, University of Alberta) 11
Figure 2.7 Bridging of rivers from the collision of ice pans and border ice (photo by F. Hicks) 11
Figure 2.8 Hummocky ice cover at Bow River, Calgary (2005) (photo by Julia Blackburn) 12
Figure 2.9 Longitudinal profile of hanging dams accumulated from frazil slush at LaGrande River, Quebec, 1973 (photo from Michel and Drouin, 1979) 13
Figure 2.10 Thermal break-up of ice cover because of snowmelt on the ice cover (photo by F. Hicks) 14
Figure 2.11 Thermal break-up of ice cover because of development of open water leads (photo by F. Hicks) 14
Figure 2.12 Thermal break-up of ice cover because of thermal deterioration of the ice cover (photo by F. Hicks) 15
Figure 2.13 Dynamic breakup of river ice with rising water level along thalweg (photo by F. Hicks) 16
Figure 2.14 (a) River ice run, (b) ice jam, and (c) flooding due to an ice jam. 17

Figure 2.15 River ice processes simulated in RIVEICE (adopted from Sheikholeslami et al., 2012) 19
Figure 3.1 Discharge (cfs) below Morony Dam and air temperature (Montana Department of Natural Resources & Conservation) at Great Falls from December 1, 2014, to March 31, 2015, showing events of large flow decrease. 22
Figure 3.2 Discharge below Morony with air temperature for the event on Dec-28, 2014 to Dec-31, 2014..... 23
Figure 3.3 Discharge below Holter for the event between Dec-28, 2014 to Jan-5, 2015..... 24
Figure 3.4 Discharge below Morony and Air Temperature for the event on Jan-27, 2015 to Jan-29, 2015..... 26
Figure 3.5 Gage height change at Cascade for the event on Jan-27, 2015 to Jan-29, 2015 26
Figure 3.6 Discharge below Morony and air temperature for the event on Jan-31, 2015 to Feb-02, 2015..... 27
Figure 3.7 Discharge below Morony for the event on Mar-02, 2015 to Mar-03, 2015..... 28
Figure 3.8 Discharge and air temperature below Morony from Dec-1, 2015 to Mar-31, 2016 showing events of high flow loss..... 29
Figure 3.9 Discharge below Morony and air temperature for the event on Dec-16, 2015 to Dec-17, 2015..... 30
Figure 3.10 Discharge below Morony and Air Temperature for the event on Dec-20, 2015 to Dec-27, 2015..... 31
Figure 3.11 Gage height at Cascade at the event on Dec-20, 2015 to Dec-27, 2015 32
Figure 3.12 Discharge below Morony and Air Temperature for the event for Jan-30, 2016 to Jan-31,2016..... 33
Figure 3.13 Discharge and air temperature below Morony from Dec-1, 2016 to Mar-31,2017 showing events of high flow loss..... 34
Figure 3.14 Discharge below Morony for the event on Dec-07, 2016 to Dec-08, 2016. 35
Figure 3.15 Discharge below Holter for the event on Dec-07, 2016 to Dec-08, 2016..... 35
Figure 3.16 Gage height at Cascade for the event on Dec-07, 2016 to Dec-08, 2016..... 35
Figure 3.17 Discharge below Morony for the event between Dec-16, 2016 to Dec-19, 2016..... 37
Figure 3.18 Gage Height at Cascade for the event between Dec-16, 2016 to Dec-19, 2016 37

Figure 3.19 Discharge below Morony for two events between Dec-21 to Dec-25, 2016 and Dec-25 to Dec-28, 2016 38
Figure 3.20 Gage Height at Cascade for the event between Dec-21, 2016 to Dec-25, 2016 and Dec-25, 2016 to Dec-28, 2016 39
Figure 3.21 Discharge and air temperature below Morony from Jan-1, 2018 to Mar-31,2018 showing events of high flow loss. 40
Figure 3.22 Discharge below Morony and air temperature at Great Falls for the event between Jan-10 to Jan-13, 2018. 41
Figure 3.23 Gage Height near Ulm for the event between Jan-10 to Jan-13, 2018 42
Figure 3.24 Gage Height at Cascade for the event between Jan-10 to Jan-13, 2018 42
Figure 3.25 Discharge below Morony and air temperature at Great Falls for the event between Feb-04 to Feb-05, 2018. 43
Figure 3.26 Gage height near Ulm for the event between Feb-04 to Feb-05, 2018 43
Figure 3.27 Discharge and air temperature below Morony for the event between Feb-09 to Feb-11, 2018 and Feb-18 to Feb-20, 2018. 44
Figure 3.28 Gage height near Ulm for the event between Feb-09 to Feb-11, 2018 and Feb-18 to Feb-20, 2018. 45
Figure 3.29 Gage height at Cascade for the event between Feb-09 to Feb-11, 2018 and Feb-18 to Feb-20, 2018. 46
Figure 3.30 Discharge and air temperature below Morony for the event between Mar-14 to Mar-15, 2018 and Mar-17 to Mar-21, 2018 47
Figure 3.31 Gage height near Ulm for the event between Mar-14 to Mar-15 and Mar-17 to Mar-21, 2018 48
Figure 3.32 Gage height at Cascade for the event between Mar-14 to Mar-15, 2018 and Mar-17 to Mar-21, 2018 48
Figure 3.33 Discharge below Morony and air temperature at Great Falls for the event between Mar-26 to Mar-27, 2018 49
Figure 3.34 Gage height near Ulm for the event between Mar-26 to Mar-27, 2018 50
Figure 3.35 Discharge below Morony and air temperature at Great Falls from Jan-1 to Mar-31, 2019 showing events of high flow loss. 51

Figure 3.36 Discharge and air temperature for the event between Dec-30, 2018 to Jan-02, 2019 and Jan-04, 2019 to Jan-09, 2019 52
Figure 3.37 Gage heights at Cascade and near Ulm for two events from Dec-30, 2018 to Jan-02, 2019 and Jan-04 to Jan-09, 2019 with flow below Morony 53
Figure 3.38 Discharge below Morony and air temperatrue at Great Falls for three events from Jan-21 to Jan-31, 2019..... 54
Figure 3.39 Gage heights at Cascade and near Ulm for three events from Jan-21 to Jan-25, Jan-27 to Jan-28, and Jan-31, 2019 with flow below Morony 55
Figure 3.40 Discharge and air temperature for the event from Feb-03, 2019 to Feb-05, 2019. ... 56
Figure 3.41 Gage height at Cascade and near Ulm for the event from Feb-03 to Feb-05, 2019 with flow below Morony..... 57
Figure 3.42 Discharge below Morony and air temperaure at Great Falls for the event from Mar-28 to Mar-30, 2019 57
Figure 3.43 Gage height at Cascade and near Ulm for the event from Mar-28 to Mar-30, 2019 with flow below Morony..... 58
Figure 3.44 Discharge below Morony and air temperature at Great Falls from Jan-1 to Mar-31, 2020 showing events of high flow loss. 59
Figure 3.45 Discharge below Morony and air temperaure at Great Falls for the event from Jan-1 to Jan-14, 2020..... 60
Figure 3.46 Gage height at Cascade and near Ulm for the event from Jan-1 to Jan-14, 2020 with flow data below Mornoy and below Holter. 61
Figure 3.47 Discharge below Morony and air temperaure for the event from Feb-2 to Feb-5, 2020 62
Figure 3.48 Gage height at Cascade and near Ulm for the envent from Feb-2 to Feb-5, 2020 with flow below Morony..... 62
Figure 3.49 Discharge below Morony and air temperaure at Great Falls for the event from Mar-14 to Mar-16, 2020 and on Mar-19, 2020..... 63
Figure 3.50 Gage height at Cascade, near Ulm and at Great Falls for the event from from Mar-14 to Mar-19 and on Mar-19, 2020 with flow below Morony..... 64
Figure 3.51 Discharge below Morony and air temperaure at Great Falls for eight events with large flow loss from December 1, 2020 to March 13, 2021. 66

Figure 3.52 Gage height at Cascade, near Ulm and at Great Falls for the event from December 16, 2020, to March 10, 2021 with flow below Morony and below Holter. 67
Figure 3.53 Discharge below Morony and air temperaure at Great Falls for eight events with large flow loss from December 12, 2021 to March 15, 2022. 70
Figure 3.54 Gage height at Cascade, near Ulm and at Great Falls for the event from December 24, 2021, to March 13, 2022, with flow below Morony and below Holter. 71
Figure 3.55 User interface of flow analysis spreadsheet with USGS gage station map from Holter to Great Falls. 73
Figure 3.56 Flow analysis spreadsheet for USGS gaging station at Holter showing the discharge, gage height, and water temperature from March 11 to March 24, 2020. 75
Figure 3.57 Plotted discharge and gage height in the flow analysis spreadsheet for USGS gaging station below Morony Dam from March 11 to March 24, 2020. 75
Figure 3.58 Plotted stage hydrographs in the flow analysis spreadsheet for USGS gaging station at Ulm and Cascade from March 11 to March 24, 2020. 77
Figure 3.59 Plotted discharge hydrographs in the flow analysis spreadsheet for USGS gaging station at Ulm and Cascade from March 11 to 24, 2020. 77
Figure 3.60 Discharge and gage height rating curves at USGS gaging stations Ulm and Cascade using 2020 summer data (April 1 to October 31). 78
Figure 3.61 Visualcrossing weather data user interface to download data from www.visualcrossing.com from Feb-29 2020 to March-19 2020. 79
Figure 3.62 Freezing event analysis developed from flow analysis spreadsheet. 80
Figure 4.1 Workflow of land cover classification using ERDAS Imagine and ArcMAP after the ice jam event is identified in CHAPTER 3. 82
Figure 4.2 Land cover map of study on Missouri River proximities showing Land, Water/Shadow, and Snow Cover for 15/12/2015, classified using the LANDSAT-8 satellite image. 84
Figure 4.3 Land cover map of study on Missouri River proximities showing Land, Water/Shadow, and Snow Cover for 02/24/2007, classified using the LANDSAT-5 satellite image. 85
Figure 4.4 Land cover map of study on Missouri River proximities showing Land, Water/Shadow, and Vegetation for 09/05/2019, classified using the LANDSAT-8 satellite image. 86
Figure 4.5 Missouri River from Holter to Great Falls classified for ice, water, and snow cover for 01 March, 2018 using LANDSAT 8 image. 87

Figure 4.6 Hourly air temperature data at Great Falls from February 20 to March 5, 2018 generated using the flow analysis spreadsheet. 88
Figure 4.7 Discharge below Morony from February 20 to March 05, 2018. 89
Figure 4.8 Gage height at Cascade and Ulm from February 20 to March 05, 2018..... 90
Figure 4.9 Simulated water temperature (^{o}C) at Cascade using HEC-RAS from February 20 to March 05, 2020. 90
Figure 5.1 Lidar data of Missouri River covering region from upstream of Dearborn River, MT to Great Falls, MT, imported to the RAS Mapper of HEC-RAS. 95
Figure 5.2 Digitization of river center line (blue line), bank lines (two red lines), flow paths (two light green-blue lines), and cross-sections (yellow lines) of Missouri river on Lidar data using RAS Mapper 96
Figure 5.3 Sample of cross-section data obtained after digitization on RAS Mapper. 96
Figure 5.4 Lidar DEM digitized on RAS Mapper in HEC-RAS for Missouri River where bathymetry data is collected using contour map method. 99
Figure 5.5 C-Map genesis social map obtained from https://www.genesismaps.com/SocialMap/ for Missouri river. (Accessed on 06/29/2022) 99
Figure 5.6 Contour lines on the C-Map Genessis map with map scale on the bottom right corner. 100
Figure 5.7 Screenshot of the cross-sections taken from HEC-RAS Mapper 100
Figure 5.8 Screenshot taken from the C-Map genesis website for the same segment in Figure 5.7. 101
Figure 5.9 Cross section with bathymetry data from contour method imported to HEC-RAS (green dashed line is the simulated energy grade line). 102
Figure 5.10 Projection of surveyed point data and Lidar data on the study area on ArcGIS Pro104
Figure 5.11 Detail image of surveyed point data overlying on the boundary of raster surface.. 105
Figure 5.12 Sample of cross-section with bathymetry data obtained from GIS method for Missouri river. 105
Figure 5.13 HEC-RAS window for entering steady flow boundary conditions. 107
Figure 5.14 Bottom elevation comparison along the main channel distance of the minor channel elevation obtained from GIS method and Manual method (Contour map method) 109

Figure 5.15 Steady flow simulation for open water season with flow change location at the junction of Dearborn river and Missouri River when Lidar DEM (GIS method) geometry data is used. 110
Figure 5.16 Boundary condition set up for Missouri River at downstream using normal depth when Lidar DEM (GIS method) geometry data is used. 110
Figure 5.17 Profile plot with the water surface elevation and bottom channel elevation of Missouri River after steady flow simulation for open water case using Lidar DEM and GIS method.. ... 112
Figure 5.18 Steady flow simulation for open water season with flow change location at the junction of Dearborn river and Missouri River when USGS DEM (GIS method) geometry data is used. 113
Figure 5.19 Profile plot with water surface elevation and bottom channel elevation of Missouri River after steady flow simulation for open water case using USGS DEM and GIS method.... 113
Figure 5.20 Boundary conditions of unsteady flow simulation in HEC-RAS from Holter to Cascade. 114
Figure 5.21 Flow hydrograph at Holter for June 1st – July 15th, 2020 used as boundary conditions for unsteady flow simulation. 115
Figure 5.22 Water surface elevation of 15 July2020 23:45 for open water unsteady flow simulation on 1 June – 15 July, 2020 using geometry data obtained from GIS method (Lidar DEM). 115
Figure 5.23 Water surface elevation of 15 July2020 23:45 for open water unsteady flow simulation on 1 June – 15 July, 2020 using geometry data obtained from GIS method (USGS Dem). 116
Figure 5.24 Outflow hydrograph and stage hydrograph at Cascade obtained in HEC-RAS from the unsteady simulation for open water from 1 June – 15 July, 2020 using geometry data obtained from GIS method (Lidar DEM). 116
Figure 5.25 Outflow hydrograph and stage hydrograph at Cascade obtained in HEC-RAS from the unsteady simulation for open water from 1 June – 15 July, 2020 using geometry data obtained from GIS method (USGS Dem)..... 117
Figure 5.26 Simulated hydrograph vs Observed hydrograph at Cascade from June 1st – July 15th using geometry data obtained from GIS method (Lidar DEM). 117
Figure 5.27 Simulated hydrograph vs observed hydrograph at Cascade from June 1st – July 15th using geometry data obtained from GIS method (USGS DEM). 118
Figure 6.1 Ice cover editor window in HEC-RAS 119
Figure 6.2 Ice cover editor table window in HEC-RAS 120

Figure 6.3 Profile plot of Thames River for open water case. 124
Figure 6.4 Profile plot of Thames River for ice cover case. 125
Figure 6.5 Ice cover data editor table for ice jam analysis. 126
Figure 6.6 Profile plot of Thames River for ice jam case 127
Figure 6.7 Comparison of the profile plot of Thames River for open water case, ice cover case, and ice jam case. 127
Figure 6.8 Comparison of profile plot of Thames River for ice jamming case when the steady flow is changed..... 128
Figure 6.9 Comparison of ice cover thickness at varying steady flow with initial ice cover thickness of 1.0 m. 129
Figure 6.10 Comparison of ice cover thickness at varying steady flow with initial ice cover thickness of 1.5 m. 130
Figure 6.11 Comparison of ice thickness simulated on Thames River using HEC-RAS when the initial thickness is varied (a) when the flow rate is 131.5 cms (b) when the flow rate is 261 cms (c) when the flow rate is 522 cms and (d) when the flow rate is 783 cms. 131
Figure 6.12 Ice jam analysis on Missouri River using steady flow simulation. 132
Figure 6.13 Missouri River ice jam analysis on selected river reach on HEC-RAS using bathymetry data obtained from GIS Method (Lidar DEM). 133
Figure 6.14 Google Earth image of the Missouri River in December 2006, (a) showing ice cover from downstream of Dearborn River and upstream of Cascade, (b) zoomed view near upstream, and (c) zoomed view near downstream ice cover. 134
Figure 6.15 Google Earth image of Missouri River showing the ice bridging locations. (a) Portion of Missouri River with narrow width, and bifurcation of river with small higher elevation land mass in the river. (b) Enlarged portion of (a) showing the bifurcation portion of the river and immediately a constriction downstream. (c) Portion of the Missouri River with trifurcation of the river with small land masses in the river serving as constriction to the flow. 135
Figure 6.16 Ice thickness at Missouri River simulated from HEC-RAS ice jam simulation with varying discharges of 4000 cfs, 5000 cfs, and 6500 cfs. 137
Figure 6.17 Total ice volume on the main channel at the Missouri River during ice jam simulation with varying discharges of 40000 cfs, 5000 cfs, and 6500 cfs. 137
Figure 6.18 Discharge below Morony from December 1, 2006, to December 31, 2006. 138

Figure 6.19 Ice cover thickness simulated from HEC-RAS for a discharge of 5000 cfs with varying ice cover distance. 139
Figure 7.1 Atmospheric pressure time series input data for water temperature modeling from February 5,2022 – March 1, 2022..... 142
Figure 7.2 Air temperature (ºC) time series input data for water temperature modeling from February 5,2022 – March 1, 2022..... 143
Figure 7.3 Relative Humidity (%) time series input data for water temperature modeling from February 5,2022 – March 1, 2022..... 143
Figure 7.4 Solar wave radiation (W/m^2) time series input data for water temperature modeling from February 5,2022 – March 1, 2022. 144
Figure 7.5 Cloudiness (fraction of 0-1) time series input data for water temperature modeling from February 5,2022 – March 1, 2022..... 145
Figure 7.6 Wind speed (m/s) time series input data for water temperature modeling from February 5,2022 – March 1, 2022. 145
Figure 7.7 Comparison of historical and forecast data obtained from www.visualcrossing.com with NOAA data from 9/13/2021 to 9/23/2021 146
Figure 7.8 User interface of an Excel spreadsheet to import weather parameters from www.visualcrossing.com website to excel worksheet. 147
Figure 7.9 Water temperature (^oC) versus channel distance (m) from downstream, Cascade to Holter. 148
Figure 7.10 Discharge time series at Below Morony Dam from Feb-15, 2022 to Mar-02, 2022. 148
Figure 7.11 Simulated water temperature time series at Cascade showing periods (events) when the water temperature reaches 0^oC..... 148
Figure 8.1 Cross-section definition sketch of the vertical processes considered in the model for (a) moving surface ice layers, (b) anchor ice, and (c) stationary surface ice layers with moving under-cover frazil layer (Blackburn and She 2019) 152
Figure 8.2 Longitudinal profile definition sketch showing the modelled ice layers. 153
Figure 8.3 Inflow and outflow boundary conditions for open channel simulation on River1D for Missour River simulations. 156

Figure 8.4 Profile view at 455.25 hours of steady state simulation and discharge (cfs) along distance (mile) for open water of Missouri River in River1D. 156
Figure 8.5 Profile view at 455.25 hours of transient (unsteady) simulation and discharge (cfs) along distance (mile) for open water of Missouri River in River1D. 157
Figure 8.6 Hydrograph view for transient (unsteady) solution for open water case of Missouri River on River1D. 157
Figure 8.7 Profile view at 160 hours of simulation for open water case showing discharge (cfs) along the distance (mile) on River1D 158
Figure 8.8 Comparison of unsteady flow simulation from River1D and HEC-RAS 158
Figure 8.9 Profile view at 455.25 hours of steady state simulation and discharge (cfs) along distance (mile) for static ice conditions of Missouri River in River1D. 160
Figure 8.10 Profile view at 455.25 hours of transient simulation and discharge (cfs) along distance (mile) for static ice conditions of Missouri River in River1D. 160
Figure 8.11 Profile view showing elevation and water temperature with distance for the Sustina River, Alaska. 162
Figure 8.12 Profile view showing the formation of moving frazil slush and solid ice on River1D with bridging location. 162
Figure 8.13 Comparison of ice thickness simulated by HEC-RAS and River1D. 163

LIST OF TABLES

Table 3.1 Station number, station name, and earlies date with discharge and gage height for the study area 20
Table 3.2 Summary of flow decrease events observed between December 1, 2014, to March 31, 2015..... 21
Table 3.3 Flow decrease summary on Dec-28, 2014 to Dec-31, 2014. 23
Table 3.4 Air temperature change within the event during the flow-decreasing event from Dec-28, 2014 to Dec-31, 2014..... 24
Table 3.5 Flow decrease summary on Jan-27 to Jan-29, 2015. 25
Table 3.6 Third flow loss event of 2014/15..... 27
Table 3.7 Fourth flow loss event of 2014/15 28
Table 3.8 Summary of flow decrease events observed between December 1, 2015, to March 31, 2015..... 29
Table 3.9 First flow loss event in 2015/16..... 30
Table 3.10 Second flow loss event of 2015/2016 31
Table 3.11 Third flow loss event of 2015/2016. 32
Table 3.12 Summary of flow decrease events observed between December 1, 2016, to March 31, 2017..... 33
Table 3.13 First flow loss event 2016/2017..... 34
Table 3.14 Second flow loss event of 2016/2017. 36
Table 3.15 Third and fourth flow loss events in 2016/2017. 38
Table 3.16 Summary of flow decrease events observed between January 1, 2018, to March 31, 2018..... 40
Table 3.17 First flow loss event in 2018. 41
Table 3.18 Second flow loss event in 2018 43
Table 3.19 Third and fourth flow loss events in 2018 44
Table 3.20 Fifth and sixth flow loss events in 2018 47
Table 3.21 Seventh flow loss event in 2018 49
Table 3.22 Summary of flow decrease events observed from January 1 to March 31, 2019 51
Table 3.23: First and second flow loss events in 2019. 52

Table 3.24 Third, fourth, and fifth flow loss events in 2019 54
Table 3.25 Sixth flow loss event in 2019. 56
Table 3.26 Seventh flow loss event in 2019 57
Table 3.27 Summary of flow decrease events observed between January 1 to March 31, 2020 . 59
Table 3.28 Second and third flow loss events in 2020. 60
Table 3.29: Fourth flow loss event in 2020 62
Table 3.30 Fourth and fifth flow loss events in 2020 63
Table 3.31 Summary of flow decrease events observed between Dec-1, 2020 to Mar-31, 2021. 65
Table 3.32 Summary of flow decrease events observed between Dec-1, 2021 to Mar-31, 2022. 68
Table 3.32 Classification of flow loss events based on the estimated location of ice jamming and events with no ice jamming. 72
Table 3.33 Classification of flow loss events based on the predicted location of ice jamming and special events. 72
Table 4.1 Ice jam events selected from Chapter 3 and classified upon which satellite image is used for land cover classification. 83
Table 4.2 Analysis of daily weather data from February 20 to March 05, 2018 showing the average air temperature, freezing degree days, and snow depth (inch) 88
Table 5.1 Available and extracted information of an example surveyed point data..... 104
Table 5.2 Detailed output table at Cascade from HEC-RAS by steady state simulation. 112
Table 6.1 Manning's *n* value for river ice covers under different conditions..... 121
Table 6.2 Manning's *n* values for different types of ice with varying ice thickness 122
Table 6.3 Average ice cover thickness for varying discharge simulated from HEC-RAS for the Missouri River 137
Table 9.1 Events identified after analyzing the discharge, water temperature, and gage height on CHAPTER 3. 165

CHAPTER 1. INTRODUCTION

1.1 BACKGROUND

Ice cover and ice jam formation in rivers during the winter seasons in the cold regions involves dynamic and complex processes. River ice jams occur during the transitional periods of freeze-up and breakup, marking the beginning and end of an ice cover season. It may also occur in mid-winter in temperate regions, during so-called “mid-winter thaws”. Jams often extend for many kilometers and aggregate thickness of several meters along a river reach (Beltaos 2008).

Ice jamming (Figure 1.1) in the river is simply the accumulation of ice in rivers, streams, or other sources which reduces the cross-sectional area, and increases the water-surface elevation (Federal Emergency Management Agency 2018). Ice jams are a buildup of water behind ice in a river to potentially cause floods because of snowmelt runoff adding more water to the river. Ice jams can result in higher water levels at lower discharges than open water floods, posing a greater risk to flood-prone (Lindenschmidt et al. 2016). The US Army Corps of Engineers develops the Ice Jam Database and the associated website https://icejam.sec.usace.army.mil/ to provide the information of ice jams formed in all northern USA states. Ice forms at a natural or man-made obstacle, e.g., a bridge (Figure 1.1(b)), when a somewhat abrupt change in slope, alignment, cross-section shape, or depth, occurs (Federal Emergency Management Agency 2018). Ice jams are typical where a tributary stream reaches a big river (Lindenschmidt et al. 2016), and the channel grade changes from relatively steep to mild. Ice jams frequently result in significant increases in upstream water-surface elevation and flooding usually occurs quickly after the blockage forms (Federal Emergency Management Agency 2018).

(a)

(b)

Figure 1.1 (a) Ice jam formation in Yellowstone River at Miles City, Montana in 2018 (https://www.youtube.com/watch?v=6VTEAMYHShI), and (b) Ice jam formation before a bridge in Gallatin River near Logan, Montana in January 2022 (https://www.youtube.com/watch?v=z_TDNNVxQBc).

Looking from the hydraulics perspective, ice-covered rivers have different properties than a river with a free surface. The presence of ice covers increases the wetted perimeter of the channel and decreases the cross-sectional area. This increases the flow resistance hence decreasing the flow velocity and discharge capacity of the flow. The presence of ice covers also changes the flow velocity distribution from one point to another at a given cross-section. The altered velocity distribution has important implications for the energy principle of the flow hydraulics (Khan 2006).

The Missouri River is the longest in the United States and starts from the Ricky Mountains of Southwestern Montana (MT). The river is responsible for the drainage of a sparsely inhabited, semi-arid watershed that is more than 500,000 square miles (1,300,000 km²) in size and includes portions of ten states in the United States and two provinces in Canada. Although it is technically considered to be a tributary of the Mississippi, the Missouri River is considerably longer than the Mississippi River is above its confluence and transports an amount of water that is roughly equivalent to that of the Mississippi. When coupled with the lower Mississippi River, the two rivers create the river system that is the fourth longest in the world.

Along many rivers and streams in Montana, destructive floods brought on by ice jams are an unavoidable reality of life. The majority of ice jams are reported to take place in February and March in Montana, which has the largest number of documented ice jams in the continental United

States. During this period, when the cold temperatures are replaced with mild warmer temperatures with high temperatures reaching 30 ºF to lower 40 ºF, the potential for ice jam flooding in Montana is very high. The ice jams in the Missouri river are mostly observed in areas where rivers are meandering. The ice-jammed river on such a river bend is shown in Figure 1.2 for Missouri River. Montana river ice and ice jam awareness website provides rich ice cover and ice jam information https://www.arcgis.com/apps/Cascade/index.html?appid=c42b2df23a8c42ff9a2aef37843bdccb.

More than 80 percent of ice jams and associated flooding in Montana take place between January and March, with the highest number occurring in March when the air temperature rises above freezing. The most ice jams ever recorded in a single season were 75 in 1996. In more recent years, 2004 saw 40 ice jams, 2006 produced 14, and 23 were recorded in 2011 (Montana Department of Natural Resources & Conservation 2022).

Figure 1.2 Google Earth image showing river ice jam in Missouri River in December 2004.

The study area of ice jam events is the ~100 river miles between Holter Dam and the five Great Falls dams at the Missouri River in Montana. As shown in Figure 1.3, the upstream boundary of the study area is Holter Dam, a hydroelectric gravity dam on the Missouri River about 45 miles northeast of Helena, MT. The reservoir formed by the dam, Holter Lake (also known as Holter Reservoir) is 25 miles long and has a storage capacity of 243,000 acre-feet of water when full. The

Holter Dam is a "run-of-the-river" dam because it generates electricity without needing to store additional water supplies behind the dam. The downstream boundary of the study area is at Great Falls, MT, which has five dams with hydropower turbines owned by the NorthWestern Energy (NWE) Hydro (The Black Eagle Falls Dam, Rainbow Falls Dam, Cochrane Dam, The Great Falls Ryan Dam, and Morony Dam).

The study area such as Great Falls has a cold semi-arid climate, and winters are very cold, long (~3 months), and often snowy. There is an average of more than 20 days with air temperature below 0 ^{o}F (-17.8 ^{o}C), and the record low temperature in February was -49 ^{o}F at Great Falls. It becomes above 32^{o}F on some winter days (January–March). Therefore, the Missouri River from Holter Dam to Great Falls often develops ice cover and ice jams during the winter period, which reduce the available flow to hydropower turbines at five dams below Great Falls. NWE Hydro needs to know the flow decrease due to ice cover/jam during the winter in order to purchase an adequate amount of electricity from other power companies to satisfy the power demand from its customers. More accurate prediction or forecast of the flow decreases is important in helping NWE Hydro to determine the necessary amount of electricity to purchase during ice jam events.

River ice jamming is seen mostly in adverse weather conditions, which make data collection and ground survey of ice cover/jam characteristics very difficult. Despite a very high significance of ground-surveyed data in research, it is dangerous to do field measurements directly on ice jams. Hence, remote sensing technology is of great boon in this sector of study. Much of the previous studies on river hydraulics have dealt with open channels that have a free surface. Little research work has been done on ice-covered rivers. As a result, our understanding of the hydraulics of ice-covered rivers is limited, mainly because of the difficulty in obtaining field data from ice-covered rivers.

Various numerical models have been developed and applied to analyze and predict the ice cover and ice jam processes in rivers. HEC-RAS and River1D are two of these models developed which can be used for river ice process modeling. HEC-RAS is a computer program for modeling water flowing through systems of open channels and computing water surface profiles, developed by the United States Army Corps of Engineers. River1D is a software developed by the Department of Civil and Environmental Engineering, University of Alberta which was adapted to incorporate a comprehensive thermal ice process into an open water hydrodynamic model.

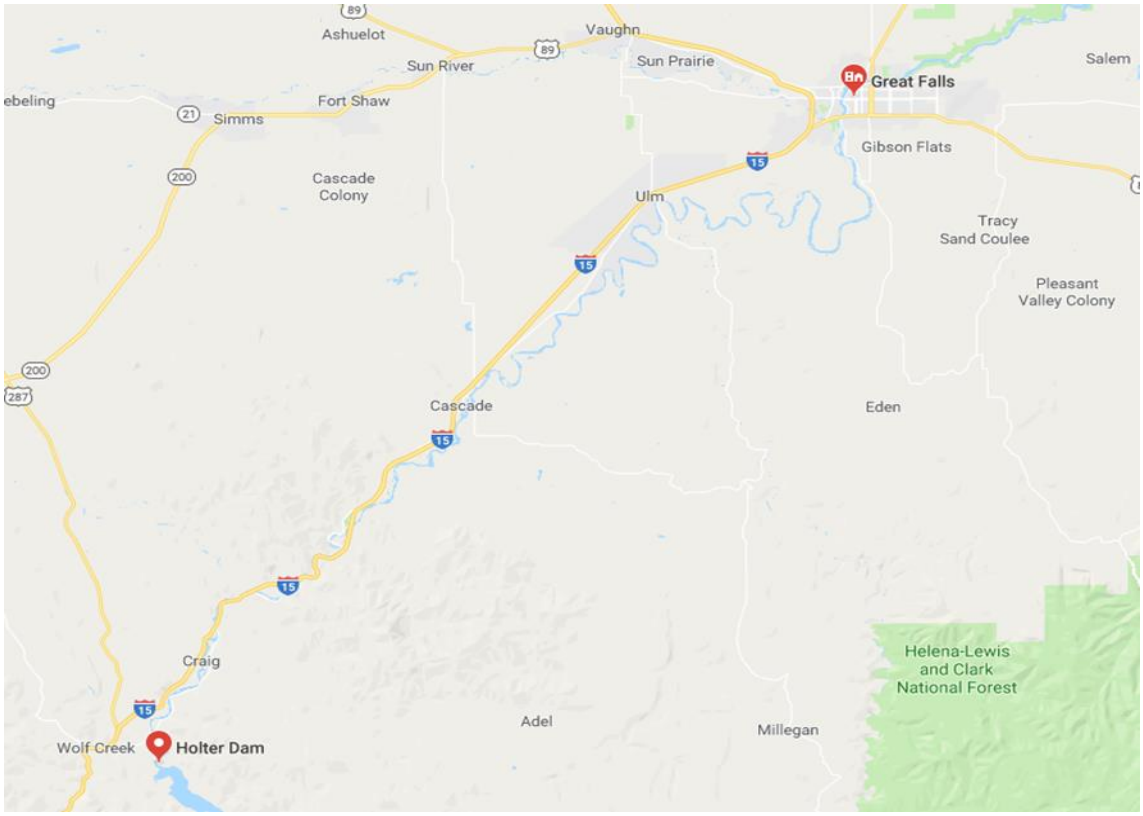

Figure 1.3 Google map showing the Missouri River from Holter Dam (upstream) to Great Falls (downstream) and I15 through Craig, Cascade, and Ulm in Montana.

1.2 SCOPES AND OBJECTIVES

The study area of the Missouri river from Holter dam to Great Falls as shown in Figure 1.3 is the river used for hydroelectricity production by Northwestern Energy Hydro. The river ice jam events affect the production of electricity in the hydropower yearly during the winter season, causing a huge amount of loss. This study is done as a part of the project which has the primary objective of developing a predictive model to forecast the amount of river discharge during an ice jamming event. This study helps in the development of the predictive model.

The primary objectives of this study are:

1) To analyze the discharge, gage height, and air temperature data of gage stations between the Holter dam to the Morony dam, from the 2014 to 2020 winter seasons to identify the ice jamming events.

2) Acquisition of bathymetry data of Missouri River in order to develop hydraulic models to predict and forecast the flow reduction in the ice cover/jam events.
3) Develop HEC-RAS models of Missouri River for open channel case, ice cover case, and ice jam case.
4) Develop the HEC-RAS model for water temperature simulation in Missouri River and validate the model with the ice jam events identified in the first objective.
5) Develop and test the River1D model for Missouri River for transient simulation and compare its result with HEC-RAS.

1.3 THESIS ORGANIZATION

This thesis is organized into nine different chapters. Chapter one covers the background, scope and objectives, and thesis organization. This section introduces the river ice jam and the study area for the project.

Chapter two provides the literature review for the river ice process, its challenges, and the benefits of river ice modeling. It discusses the recent advancement of river ice process. Chapter three explains the data analysis process to identify flow decrease events. It explains the use of discharge, water temperature, and gage height to identify and locate ice jam events. Chapter four explains the process involved in developing a land cover classification map using LANDSAT image for the study area.

Chapter five discusses the HEC-RAS model setup; input data required on HEC-RAS with steps involved in bathymetry data acquisition. Chapter six aids in understanding and testing river ice cover and ice jam simulation of Missouri River on HEC-RAS. Chapter seven discusses the further use of HEC-RAS with water temperature simulation for steady flow analysis on HEC-RAS for Missouri River.

Chapter eight focuses on River1D, its understanding and testing, and its ability to perform complex river processes. Finally, chapter nine contains the summary, conclusions, and scope for future studies.

CHAPTER 2. LITERATURE REVIEW

2.1 OVERVIEW OF RIVER ICE PROCESSESS

River ice can negatively affect fish habitat, impede hydropower development, block water intakes and outfalls, and other things in many northern regions. Any area where river ice is present may have these unfavorable effects. Some of the most important studies on river ice dynamics and hydraulics dates to the 1960s, making it a relatively new topic of study. The two most important factors in determining how ice forms are temperature and turbulence (Michel and Ramseier 1971). Temperature is related to local climate and turbulence is affected by the size of the water body (lake or river) and the materials that make up the bottom and sides of that water body. Turbulence in rivers is driven by the water velocity and by the channel materials. To describe its development, several review papers have been published over the past few decades, such as Beltaos (1987), Shen (2003), Hicks (2016), etc. Because rivers frequently have non-negligible flow velocities and turbulence, the ice formation process in the northern river rivers is significantly different from that of lakes; consequently, both flow hydraulics and meteorological conditions play a significant role in ice formation and deterioration in rivers.

On northern rivers, freeze-up normally starts in the late fall or January and is the time when a stable ice cover occurs. Heat transfer from river water (≥ 0 ^{o}C or 32 ^{o}F) to cooler air above is the main source of heat loss from the cooling of river water to ice formation. Precipitation (often snowfall) and heat loss to the riverbed and banks both have the potential to result in additional heat loss. Depending on the level of mixing and turbulence after river water has been supercooled (water becomes slightly below 0 ^{o}C) (Hicks 2016), ice may start to form in one of two ways. In slow-moving and shallow river sections, such as those near banks, in eddies, or around islands, the turbulence is frequently insufficient to entrain ice particles (Ashton 1979) or combine supercooled water at the surface with the flow below (Clark 2013). In some areas, a thin layer of skim ice will develop on the water's surface. Static border ice (Figure 2.1), similar to lake ice, is skim ice that develops laterally from a riverbank toward the center river channel (Shen 2010). In the early phases of freeze-up, border ice thickens and develops laterally as heat is transferred from the riverbank to the surrounding cold air.

Figure 2.1 Border ice forms along the riverbank (photo from S. Beltaos).

The second way that ice originates in rivers is through secondary nucleation on already-formed ice crystals, which are known as seed crystals (Kalke et al. 2019). Fracture and the generation of more frazils can result from the collision of active frazil particles (Figure 2.2). Anchor ice may form due to the adhesive nature of frazil, flocculation, and the production of frazil flocs, or if frazil adheres to the riverbed as shown in Figure 2.3 Anchor ice on the riverbed of Ram River, Alberta (photo by R. Brown)Figure 2.3. Frazil flocs often referred to as frazil slush, remain in suspension until their buoyancy is sufficient to overcome the flow's turbulence and rise to the surface. A piece of the slush is exposed above the water, leading to the creation of ice pans due to interstitial freezing of water in this exposed section. Individual pans increase in thickness and surface area as new flocs adhere laterally and to the pan's underside. Pan collisions (Figure 2.4) may result in crustal thickening, hydraulic thickening, or edge-to-edge freezing.

Figure 2.2 Frazil ice (photo by R. Andrishak, University of Alberta)

Figure 2.3 Anchor ice on the riverbed of Ram River, Alberta (photo by R. Brown)

Figure 2.4 Frazil pans formed after collision (photo by F. Hicks)

Ice pans may contribute to border ice formation through a process known as buttering (Clark 2013; Hicks 2016) or hydraulic accumulation by sticking to previously produced border ice via thermal growth (Shen 2010). The streamwise forces acting upon an ice pan, such as drag and gravity, must

be balanced by the friction force between the ice pan and the bordering ice, for border ice growth to occur in this mode (Shen 2010).

Around river bends and in constricted areas, such as between bridge piers or in regions where border ice has decreased the channel width, ice pan concentration increases. Under those conditions, it becomes probable that the ice pans will become wedged, and it is said that bridging has occurred. Figure 2.6, Figure 2.7, and Figure 2.7 show the ice pans and border ice beginning to merge and starting the bridging process of river ice.

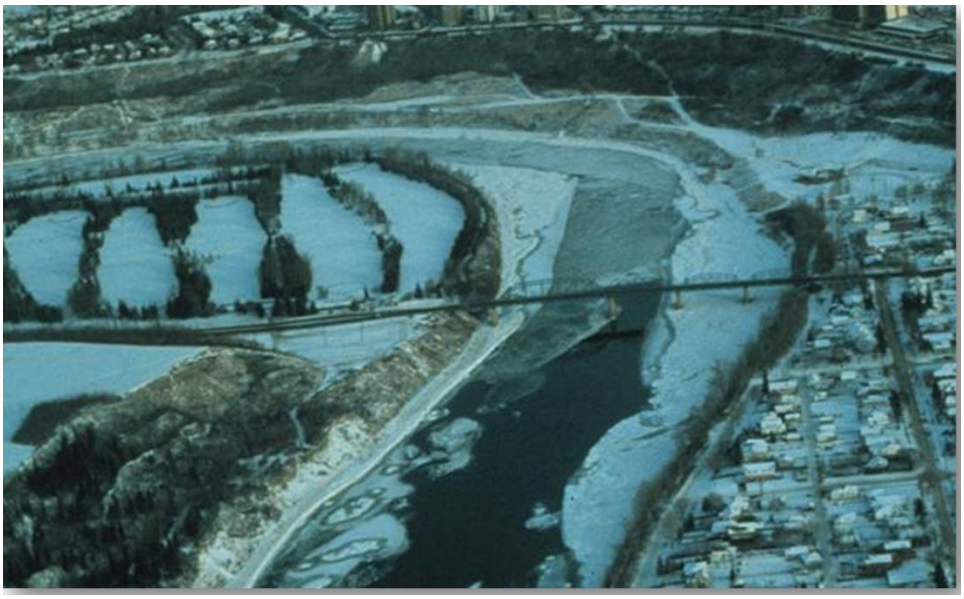

Figure 2.5 Bridging process starting at river bends and constricted areas (photo by R. Gerard, University of Alberta)

For bridging to occur (Figure 2.7), the forces operating on the pans in the streamwise direction, such as the current, hydrodynamic forces, and streamwise weight, must be balanced by the opposing forces of bank shear, ice strength, and downstream resistance given by any impediments (Shen 2010). In the absence of opposing forces to counterbalance the pushing pressures, the ice pans will either be forced through the constriction or will consolidate prior to jamming or releasing from the location of the bridge. Surface and depth-averaged water velocities, water surface width or the width of the gap in the surface obstruction, water depth, meteorological conditions, strength and thickness of ice pans, channel geometry (including bank roughness, slope, and curvature of channel bends), surface pan concentration, pan shape, Froude number, water discharge, and density and porosity of ice pans all influence the bridging process (Urroz and Ettema 1994; Wang et al. 2011). There may be multiple bridging places inside a single research reach, even when study

reaches are quite short (Jasek and Pryse-Phillips 2015; Howley et al. 2019). This may result in the propagation of a disjointed or fragmented ice front. River1D software allows users to define multiple bridge locations along a river reach, but a minimum of one briging location is needed to start thermal ice simulation using River1D.

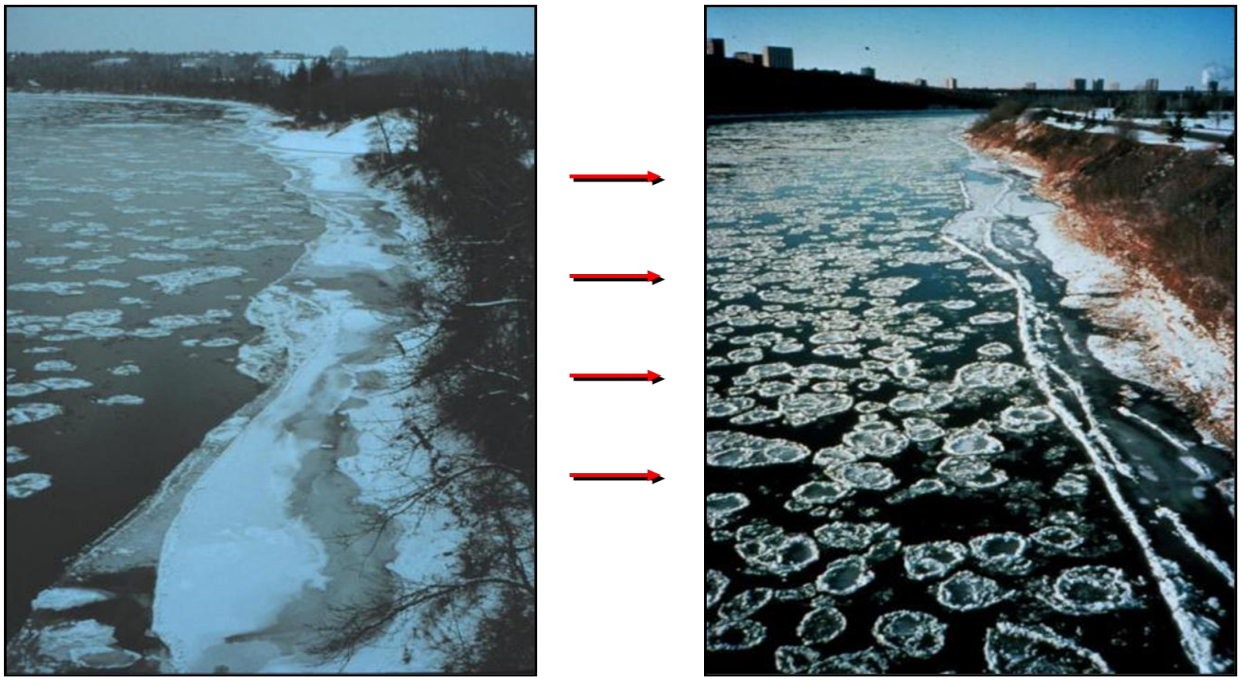

Figure 2.6 Ice pans and border beginning to merge; start of the bridging process (photo by R. Gerard, University of Alberta)

Figure 2.7 Bridging of rivers from the collision of ice pans and border ice (photo by F. Hicks)

The ice front progression rate, the rate at which an ice cover advances upstream, is a function of the channel geometry, gradient (slope), water velocity, discharge, surface ice concentration, and

the upstream propagation mode. An ice pan advancing downstream towards an ice front may come to rest edge-to-edge with the ice front, extending the ice front upstream and creating a juxtaposed ice cover. The ice front will continue to propagate upstream in a juxtaposed manner unless the streamwise forces acting on an ice cover outbalance the internal strength of the ice cover. If this happens, the ice cover may collapse or shove, and mechanical thickening will occur, resulting in a hummocky ice cover and/or freeze-up ice jams (Hicks 2016), shown in Figure 2.8. Alternatively, an incoming ice pan may submerge beneath the ice front and be deposited to the underside of the ice cover, thickening the ice cover in a process called hydraulic thickening (Hicks 2016). Whether or not an incoming pan will submerge beneath an ice cover is largely controlled by the flow velocity, with the probability of submergence increasing with water velocity. Pan geometry, porosity, and density also play a role in this process (Beltaos 2013). It should be noted that it is also possible for this type of ice cover to collapse, inducing additional mechanical thickening.

Figure 2.8 Hummocky ice cover at Bow River, Calgary (2005) (photo by Julia Blackburn)

River hydraulics are significantly impacted by immobile ice. A full or partial ice cover, including border ice, causes the channel's hydraulic efficiency to decrease and increases its wetted perimeter. Furthermore, the Manning's n roughness of an ice cover's underside can range from roughly 0.01 to 0.1 (Hicks 2016). As ice cover develops, these factors result in a decrease in the hydraulic efficiency of the channel and a sudden rise in stage, often known as stage-up.

Once it has developed, an ice cover protects the water below from the chilly air above while preventing additional supercooling and the generation of frazil. Continuous frazil production, however, is possible anywhere open leads exist, such as in places where warm water influxes occur or where the flow velocity is high enough to prevent the formation of an ice cover. The resulting frazil will flow downstream and either form ice pans or be swept behind an existing ice cover, where it may be deposited and thickened. A hanging dam will form if enough frazil is dumped in one place (Ashton 1979). Figure 2.9 shows the longitudinal profile of hanging dams at LaGrande River accumulated from the frazil slush.

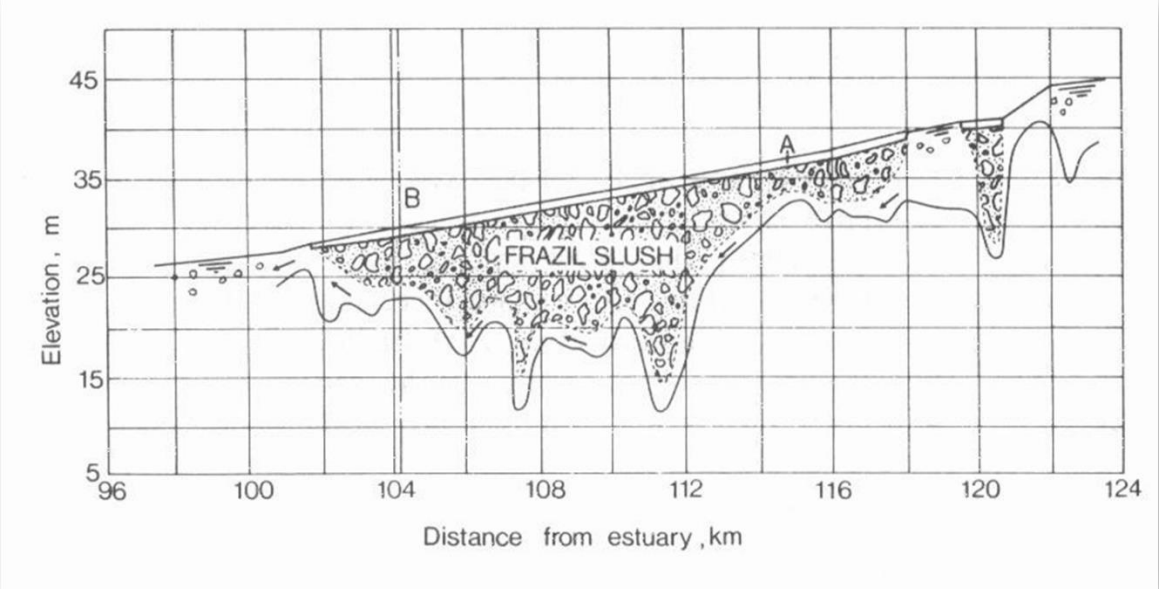

Figure 2.9 Longitudinal profile of hanging dams accumulated from frazil slush at LaGrande River, Quebec, 1973 (photo from Michel and Drouin, 1979)

An ice cover's thickness will typically increase over the winter. Heat loss through the ice cover itself to the cold air above could cause the underside of the ice cover to thicken. Thermal growth is the term for this. Snow accumulation on an ice cover may result in the ice cover depressing or submerging, which will cause river water to up well. Snow starts to saturate and turn into slush, then freezes to become snow ice.

Rising air temperatures (> 32 ^{o}F) trigger the break-up process, which can either be thermal or dynamic in nature. Ice covering melting in-situ causes thermal break-up, which is directly influenced by meteorological circumstances. It frequently happens when air temperatures are gradually rising. The timing of thermal break-up typically varies greatly in space and is fragmented. The spatial diversity of shading effects and ice thickness is responsible for this. As a

result, open leads frequently materialize during the breakup process. Such open leads cause the river water to warm, which may, in turn, help the downstream ice cover's underside melt thermally. A thermal breakup can be because of the snowmelt on the ice cover. Ice cover reduces the ice jam surface albedo and permits more of the sun’s heat energy to get into the ice (Figure 2.10). It can also be because of the development of open water leads, which allows a lot of solar heat energy to enter the flow and this warmed water melts the ice from the underside (Figure 2.11). Thermal break-up can also be because of the thermal deterioration of the ice cover, which occurs at an increasing rate as the surface albedo decreases (Figure 2.12). The ice cover melts in place in river or lake, and it typically results very little ice movement.

Figure 2.10 Thermal break-up of ice cover because of snowmelt on the ice cover (photo by F. Hicks)

Figure 2.11 Thermal break-up of ice cover because of development of open water leads (photo by F. Hicks)

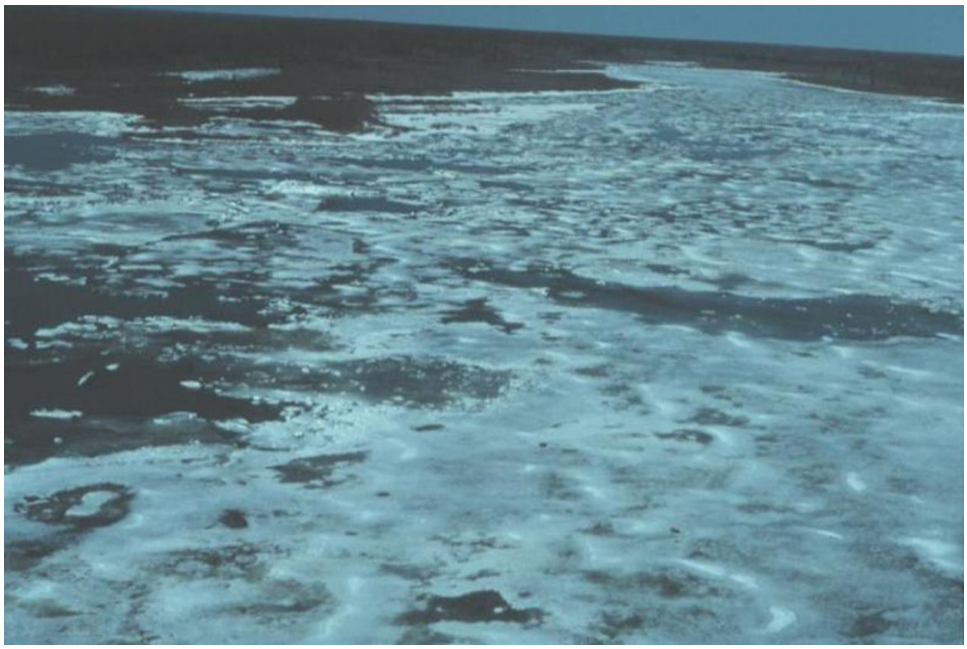

Figure 2.12 Thermal break-up of ice cover because of thermal deterioration of the ice cover (photo by F. Hicks)

The mechanical breaking of the ice cover is the consequence of dynamic break-up, which is primarily driven by hydraulic processes. A considerable increase in discharge (due to melting snow or ice or upstream release) raises the water level, raising/lifting the ice cover in the center portion of the channel and separating it from the shore-fast border ice into floating ice sheets. When water levels rise, the channel top width increases, and then large floating ice sheets can move/pass downstream to form an ice run (Figure 2.14a) when the flow width gets large enough. Hinge cracks form parallel to the banks, and then border ice becomes inundated and melts away quickly. For narrow channels, a single crack may form down the middle of the channel. Break-up ice jams can form if the ice run is arrested at a narrow-restricted cross-section called the bridging location in various ice jam models, and dynamic break-up is also fragmented (Figure 1.1a). When ice jams form (Figure 2.14b), an upstream cascade effect may result, whereby waves that are traveling upstream trigger or assist in the mechanical release of unbroken upstream ice covers. Ice debris will be able to move downstream once an ice jam has been released, but it may block up again at the next restriction or obstruction (Jasek 2019). Most of the ice stays in the channel and the ice jam accumulation is thick. After the release of an ice jam, remnant ice can pile up along the banks and cover entire islands in the middle of a river.

Therefore, an ice run moving downstream can stop to form an ice jam, and then an ice jam breakup or release occurs later when water level rise builds up large enough hydrostatic forces; the process of stop and release of ice floes continues to happen. Small ice floes can freeze and connect to form large ice blocks when the air temperature drops below freezing. Dynamic break-up often begins like a thermal ice break-up. It starts with snow melt on ice cover, with development of open leads which often form along the thalweg where the flow is highly turbulent and fast, and the ice cover is often the thinnest. This results in overflow from open leads indicating rapid water level rise (Figure 2.13) to result flooding due to an ice jam (Figure 2.14c).

Figure 2.13 Dynamic breakup of river ice with rising water level along thalweg (photo by F. Hicks)

When there is a sudden increase in air temperature or when there is a rainfall event that causes the snowpack to quickly melt and the hydrograph of a river to increase sharply, the dynamic break-up is far more likely to occur. Dynamic break-up may also be influenced or caused by additional variables, such as increasing releases from hydropower plants, dams, or reservoirs.

(a) Mackenzie River photo by Faye Hicks

(b) Hay River photo by R. Gerard, UofA

(c)Hay River photo by Faye Hicks

Figure 2.14 (a) River ice run, (b) ice jam, and (c) flooding due to an ice jam.

2.2 CHALLENGES OF RIVER ICE PROCESSES AND BENEFITS OF RIVER ICE MODELING

For engineers and geoscientists, river ice dynamics provide a variety of difficulties. Water quality and ecology are significantly impacted by river ice (Whitfield and McNaughton 1986; Brown et al. 2000; Prowse 2001; Lindenschmidt et al. 2018) as are river scour (Hains and Zabilansky 2005), flooding (Gebre et al. 2014; Kempema et al. 2019) power outages and operational issues at hydroelectric generating stations (Beltaos and Burrell 2003; Daly and Ettema 2006; Gebre et al. 2014). Even though ice jams are frequently viewed as harmful processes, they are really beneficial and required for inland deltas, supplying vital nutrients to places like the Peace-Athabasca Delta, a UNESCO World Heritage Site (Rokaya et al. 2019).

Although there has been significant progress in our understanding of river ice processes over the past few decades, the difficulty of data collection remains one of the biggest barriers to increased knowledge and understanding. Turcotte et al. (2017) provide an excellent account of some of the

difficulties and issues related to installing and relocating equipment for the gathering of river ice data. The most prevalent issues are inclement weather, a limited amount of time to collect data, anchor and frazil ice buildup on equipment, equipment loss, damage, or theft, and battery failure.

Hypothermia is a severe concern when falling through the ice, and prolonged exposure can be lethal. Victims may be swept downstream by river currents below the ice, driving them below the ice (Jasek and Lavalley 2003). There are several ways to reduce or remove these hazards, such as through formal training, experience, and work avoidance (Jasek and Lavalley 2003). A potential substitute for large and expensive field research for data collecting is the use of river ice models.

Investigating these issues and phenomena has always benefited greatly from river ice models. It can offer quantitative descriptions of the river ice conditions as well as perception into a particular ice regime or process (Blackburn and She, 2019; Shen, 2010). It is also possible to locate and/or address gaps in the river ice community's comprehension of processes by running model simulations and comparing the results to observable data from the field.

Numerical models have been employed in a number of projects to date, including determining the timing of freeze-up and break-up (Prowse et al. 2007; Bijeljanin and Clark 2011; Rokaya 2020), forecasting floods (Rokaya et al. 2019), determining flood risk (Lindenschmidt 2017) and assessing the advantages and drawbacks of installing or building flood defenses (Lindenschmidt 2017) examining the potential implications of flow regime change and evaluating the impacts of climate change (Andrishak and Hicks 2005; Liu et al. 2015; Turcotte et al. 2019).

In the discipline of river ice engineering, numerical models range from component models, which are used to explore a single distinct variable or process, to comprehensive models, which are created to replicate a river's whole winter regime. One-dimensional (1D) steady-state ice jam profile models like HEC-RAS (Beltaos, 2013; Daly, 2003), RIVJAM (Beltaos and Wong 1986), ICEJAM (Flato and R. 1986), and ICETHK are the most popular models (Tuthill et al. 1998). Under steady state conditions, these models are commonly employed to produce an ice jam profile and the associated water levels. While most of these models can provide ice jam profiles for non-equilibrium jams, others can solve the equilibrium ice jam equation. Although two-dimensional (2D) steady state-ice jam profile models need more processing, they often perform better in situations where there are strong 2D flow effects, such as in braided channels or deltas, or in situations where the dynamics of structures and outfalls are important. Stable ice process models

like ICEPRO (Malenchak 2012), ICESIM (Carson and Groeneveld 1997) and SIMGLACE (Malenchak 2012) may be employed when more processes or variables need to be considered.

There are also a number of thorough one- and two-dimensional unstable ice process models. One-dimensional models are frequently chosen over two-dimensional models in practical applications because they require less computing power and typically run simulations significantly faster. CRISSP (developed by Clarkson University under contract to CEA Technologies, Inc.), MIKE-ICE (developed by Danish Hydraulic Institute's (DHI) in conjunction with La Groupe-Conseil Lasalle Inc.), River1D (developed by University of Alberta), and RIVICE (developed by a consortium of organizations and engineering firms and completed by KGS Group, Figure 3.14) are some of the most well-liked one-dimensional complete river ice models.

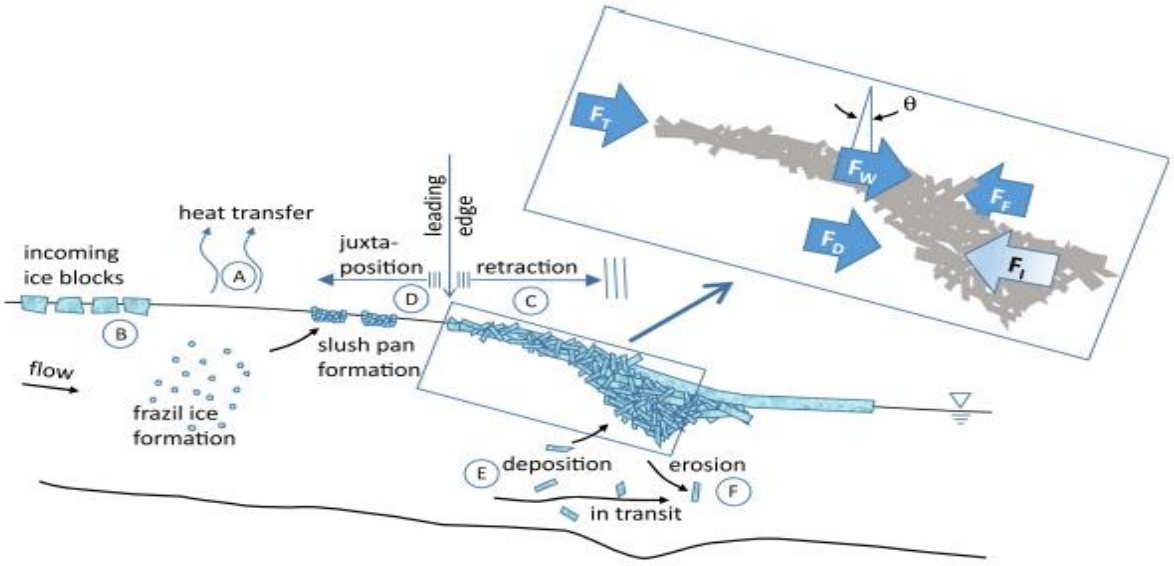

Figure 2.15 River ice processes simulated in RIVEICE (adopted from Sheikholeslami et al., 2012)

CHAPTER 3. DATA ANALYSIS FOR FLOW DECREASE EVENTS

3.1 INTRODUCTION

This data analysis was to identify the special events that occurred in the Missouri River from below Holter Dam to Great Falls, Montana, and their characteristics since 2014. The special events in the Missouri River refer to when the flow rate or discharge at the USGS gage station below Morony has reduced abruptly (e.g., roughly 500 cfs or more per day) in December, January, February, and March. Table 3.1 lists the information of USGS gaging station number, station name, and earlies date with discharge and gage height for the study area. There are no valuable data at Cascade and Ulm during the winter period before 2014. Three stations also have water temperature data from 10/1/2011 or 4/1/2012 to today. The gage station below Morony, USGS 06090300 Missouri River near Great Falls MT, is located a short distance downstream from the Morony Dam, one of five hydroelectric power generation facilities near Great Falls, and is used to analyze the flow rate decrease of more than 500 cfs in this study. The abrupt flow decreases in the Missouri River during the winter period (December–March) could be due to various reasons, e.g., ice formation, ice jam formation, etc., which are related to the cold weather conditions. The hourly weather data were obtained from the National Climatic Data Center's (NCDC) Climate Data Online (CDO) website for the weather station of Great Falls Airport, MT, US. The weather data downloaded includes air temperature, precipitation, and wind speed; but only air temperature was analyzed.

Table 3.1 Station number, station name, and earlies date with discharge and gage height for the study area

Site Number	Station Name	Early Date with Data	
		Discharge	Gage Height
06066500*	Missouri River bl Holter Dam nr Wolf Cr MT	10/1/1994	10/1/2007
06074000	Missouri River at Cascade MT	5/21/2014	6/16/2011
06078200	Missouri River near Ulm MT	10/1/1994	7/1/2017
06090000	Missouri River at Great Falls MT		5/21/2014
06090300	Missouri River near Great Falls MT (bl Morony Dam)	10/1/1994	10/1/2007
06071300	Little Prickly Pear Cr at Wolf Cr MT	10/1/2007	10/1/2007
06073500*	Dearborn River near Craig MT	10/1/1995	10/1/2007
06077500*	Smith River near Eden MT	3/1/2006	10/1/2007
06089000	Sun River near Vaughn MT	10/1/1994	10/1/2007

Note: * indicates the station has water temperature data from 10/1/2011 or 4/1/2012.

3.2 SPECIAL EVENTS IN THE WINTER OF 2014–2015

First, time series of discharge below Morony and air temperature at Great Falls were plotted for each winter period to identify those special events of the abrupt flow decreases. Figure 3.1 shows the air temperature time series from 12/1/2014 to 3/31/2015 with a reference line of 32˚F or 0˚C to indicate the dates when the air temperature was notably below the freezing point. Figure 3.1 shows whenever air temperature went below the freezing point, the discharge below Morony was highly affected and typically decreased. Those special events were marked and indicated in Figure 3.1 when the flow decrease was larger than 500 cfs or more. From Figure 3.1, four special events are noted with high flow loss along with the corresponding temperature drop. The characteristics of four special events are summarized in Table 3.2 including the start and end time, total flow decrease (cfs), the lowest air temperature (Montana Department of Natural Resources & Conservation) during the flow decrease, and the rate of flow decrease over the flow-decreasing period (cfs/hr). The lowest air temperatures during the flow decrease events ranged from 24 ^{o}F to -20 ^{o}F. When the flow below Morony decreased 500 cfs in one day (24 hours), the rate of flow decrease was 20.8 cfs/hr (500 cfs/24 hours). The rate of flow decreases in these identified events ranged from 32.9 cfs/hr to 107.6 cfs/hr, which means these events had flow decreases much larger than 500 cfs per day.

There was no gage height data before 6/16/2011 at Cascade and before 7/1/2017 at Ulm in the Missouri River; therefore, water level changes at Ulm are unknown for these four events. Each special event is discussed and analyzed in detail below.

Table 3.2 Summary of flow decrease events observed between December 1, 2014, to March 31, 2015.

S.N.	Period of the decrease	Total flow decrease (cfs)	Lowest temperature during the decrease	Rate of the flow decrease (cfs/hour)
1	Dec 28 to Dec 31, 2014	2770 cfs	-20 ^{o}F	32.9
2	Jan 27 to Jan 29, 2015	3570 cfs	24 ˚F	107.6
3	Jan 31 to Feb 02, 2015	1960 cfs	-8 ^{o}F	56.0
4	Mar 02 to Mar 03, 2015	1650 cfs	-6 ^{o}F	90.5

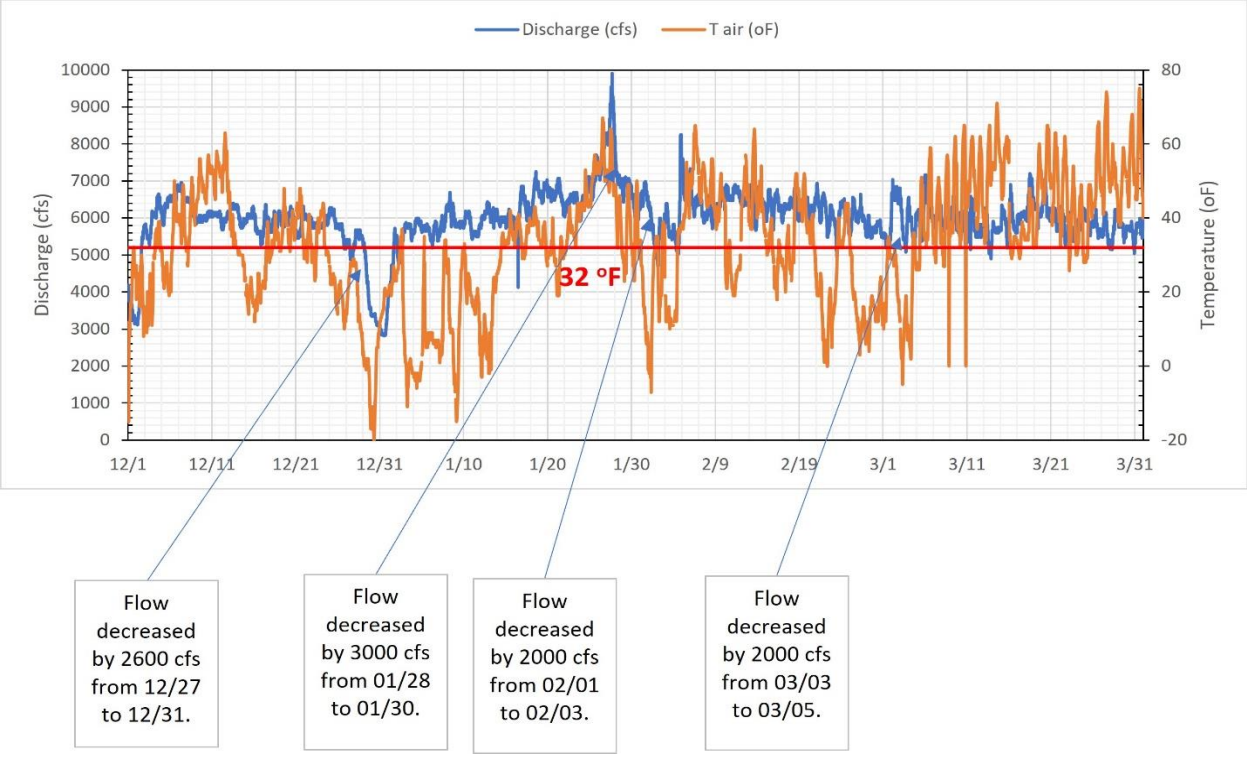

Figure 3.1 Discharge (cfs) below Morony Dam and air temperature (Montana Department of Natural Resources & Conservation) at Great Falls from December 1, 2014, to March 31, 2015, showing events of large flow decrease.

3.2.1 SPECIAL EVENT FROM DEC-28 TO DEC-31, 2014

The flow decrease was 2770 cfs between 4:45 December 28 and 17:00 December 31 when air temperature dropped from 26 °F to -20 °F (the lowest temperature) and started to increase after that (Figure 3.1). The discharge below Morony had a sharp decrease on December 29 from 5240 cfs to 3370 cfs (77.9 cfs/hr) when the air temperature was mostly below 32 °F (red horizontal line in Figure 3.2). The flow had a small decrease on December 28 and a decrease of 530 cfs from December 30 to December 31 7:00 (17.1 cfs/hr). The flow also decreased ~1000 cfs from 12:00 on December 25 to 12:00 on December 27 (20.8 cfs/hr) when the air temperature was ~25–10 °F. The flow started to increase from ~18:00 on December 31, 2014, to January 3, 2015, when there was a short period with air temperature > 32 °F. The air temperature decreased from 35 °F to -10 °F from ~17:00 on January 2 but the flow was almost no change.

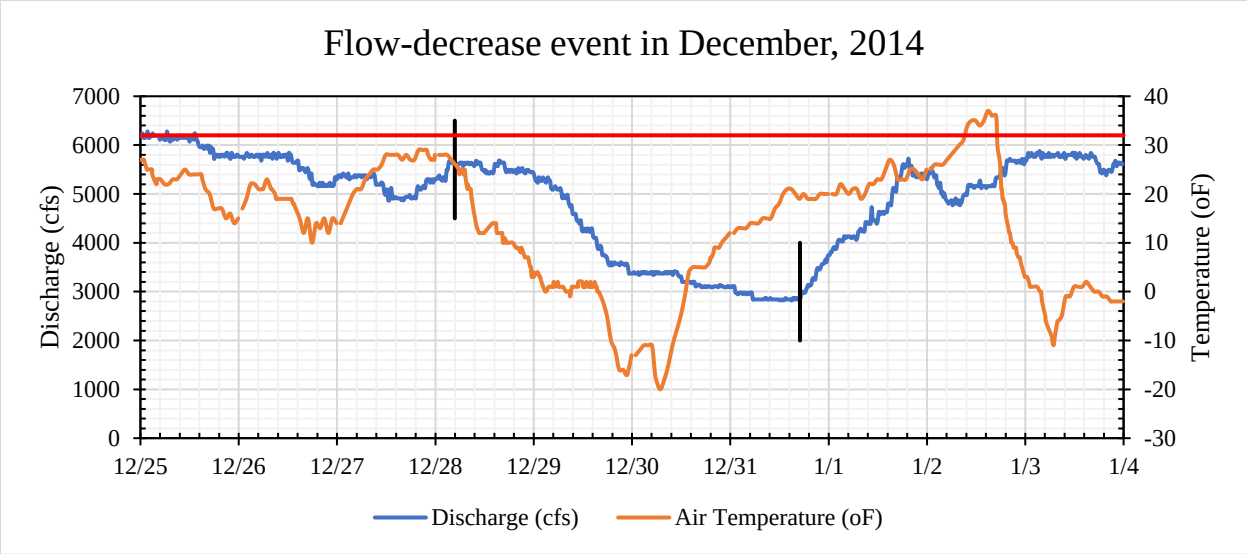

Figure 3.2 Discharge below Morony with air temperature for the event on Dec-28, 2014 to Dec-31, 2014

Table 3.3 Flow decrease summary on Dec-28, 2014 to Dec-31, 2014.

Event 1	Values	Discharge (cfs)
Beginning time	12/28/14 4:45	5610
End time	12/31/14 17:00	2840
Total Minutes	5055	
Total Hours	84.3	
Flow decrease	2770	cfs
Flow decrease rate	32.9	cfs/hour

Measured flow at Missouri River below Holter Dam near Wolf Creek (USGS Gage station number: 0606650) was available from October 1994 and water temperature from October 2011. Figure 3.3 shows the time series of discharge below Holter from 12/20/2014 to 12/31/2014. There was a small increase of ~200 cfs on 12/27 to 12/29 and then a large increase of ~800 cfs from 12/29/2014 until 12/31/2014, Figure 3.3. Considering the time delay, a part of the flow increases below Morony (Figure 3.2) from 12/31/2014 could be due to the inflow increase at the below Holter. Because there was no gage height data at Cascade and Ulm, it is difficult to know whether or where ice jams were formed in Missouri River for the flow decrease from 12/28/2014 to 12/31/2014 (Figure 3.2). Water temperature below Holter was above 34 ^{o}F and had a small decrease of ~2 ^{o}F (Figure 3.3).

Table 3.3 shows the change in air temperature within the event. The initial temperature at the beginning of the event, the lowest temperature reached during the event, the drop in temperature,

and rate of decrease of temperature are noted. After the lowest temperature, the rise of temperature from the lowest point to the temperature at the final point of the event is recorded and the rate of increase of temperature is calculated.

Table 3.4 Air temperature change within the event during the flow-decreasing event from Dec-28, 2014 to Dec-31, 2014

Parameter	Temperature (Montana Department of Natural Resources & Conservation)	Time
Initial	26	12/28/2014 4:53
Lowest	-20	12/30/2014 6:53
Drop	46	
Hours	50	hours
Decrease rate	0.92	^{o}F/hour

Lowest	-20	12/30/2014 6:53
Final	19	12/31/2014 16:53
Increase	39	
Hours	33	hours
Increase rate	1.18	^{o}F/hour

The temperature first dropped to the lowest point of -20 ^{o}F and then rises to 39 ^{o}F when the flow below Morony dam was also dropping (Figure 3.1).

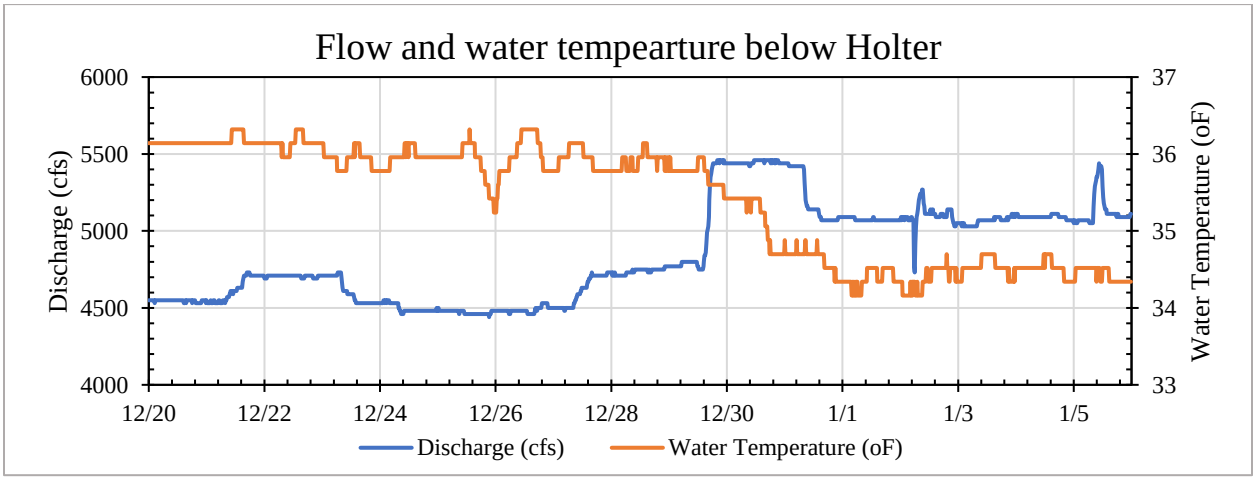

Figure 3.3 Discharge below Holter for the event between Dec-28, 2014 to Jan-5, 2015

The increase in the discharge below Morony Dam after Dec-31 (Figure 3.2, from 2840 cfs to 5720 cfs), could not only be due to the increase in discharge below Holter after Dec-29 (Figure 3.3

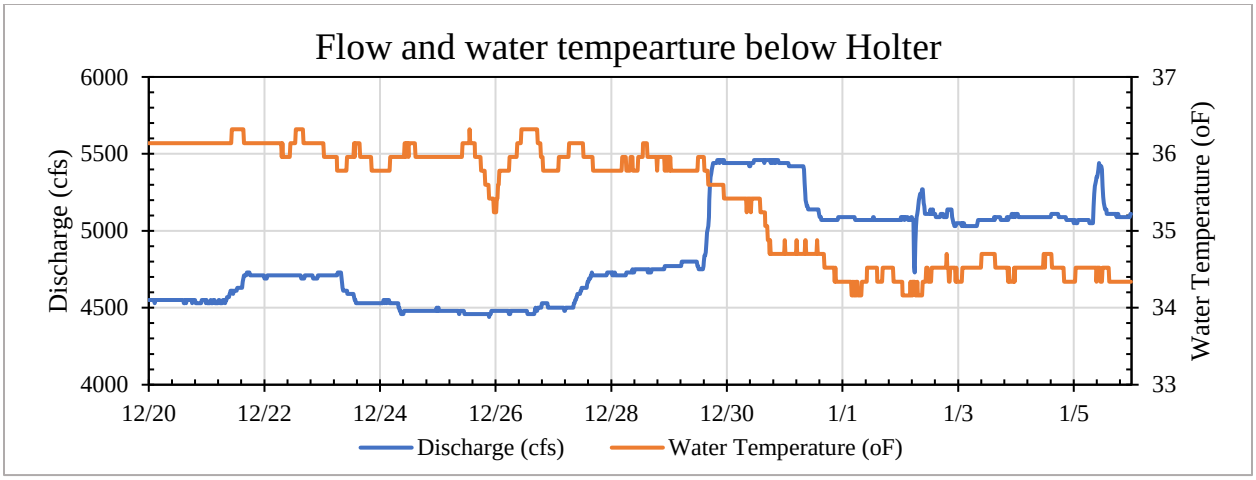

, ~800 cfs). The increase in discharge below Holter is typically a management strategy implemented by NWE Hydro and is mostly not related to any temperature changes at Great Falls. Therefore, the increase could be due to the breakup of ice cover or ice jams formed before December 31, which released the large amount of water stored behind the ice jams (flooding overbank areas). Gage height at Cascade had an increase of 5 ft from December 31 to January 2, which indicated certain flooding issue (flow increase from Holter shown in Figure 3.3).

Figure 3.2 shows a flow loss of 2770 cfs from December 28 to 31. The significant drop down in air temperature indicated a major chance of ice jam development between Holter and Morony. The specific place of ice jamming cannot be specified.

3.2.2 SPECIAL EVENT FROM JAN-27 TO JAN-29, 2015

This event has a decrease in discharge of 3570 cfs below Morony Dam (Table 3.5). This corresponds with the simultaneous temperature decrease from 60 ˚F to 22 ˚F as seen in Figure 3.4. Discharge below Holter did not change much (~300 cfs). The gage height at Cascade was increased by only 0.2 ft from Jan-25 to Jan-26 (Figure 3.5). This increase in gage height is not significant enough to cause that amount of water loss (Figure 3.4).

The possible reasoning could be ice jam formation downstream of Cascade to Ulm or Great Falls. Considering the lag time (~2 days) from Holter to Morony and quite high air temperature (> 50 ^{o}F), any ice formation is questionable; therefore, the reason for this flow-decreasing event at Morony is unclear.

Table 3.5 Flow decrease summary on Jan-27 to Jan-29, 2015.

Event 2	Time	Discharge (cfs)

Beginning Time	1/27/2015 17:00	9900
End Time	1/29/2015 01:15	6430
Total Minutes	1935	
Total Hours	32.25	
Flow Loss	3570	cfs
Flow decrease rate	107.60	cfs/hour

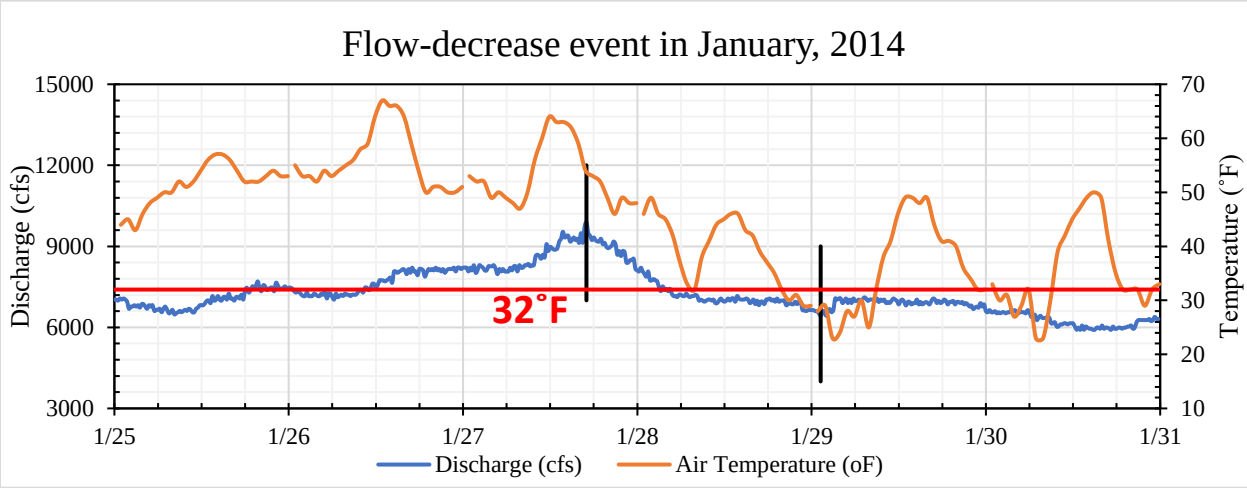

Figure 3.4 Discharge below Morony and Air Temperature for the event on Jan-27, 2015 to Jan-29, 2015

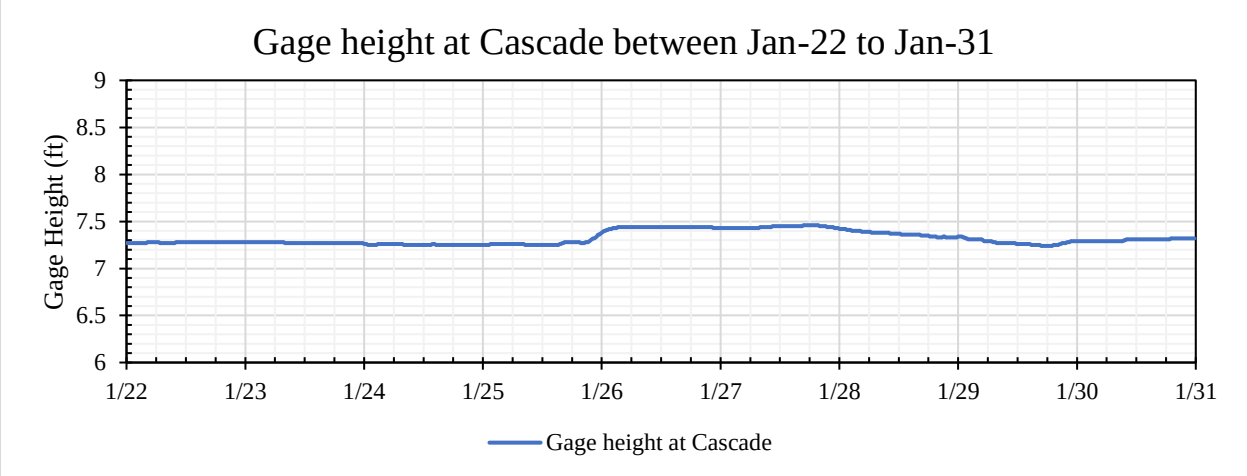

Figure 3.5 Gage height change at Cascade for the event on Jan-27, 2015 to Jan-29, 2015

3.2.3 SPECIAL EVENT FROM JAN-31 TO FEB-02, 2015

This event had a flow loss of 1960 cfs within a period of 35 hours (Table 3.6). Similar to the last event (Section 3.2.2), the flow loss at Morony corresponds a large air temperature drop (Figure 3.6, circled).

The flow loss of 1960 cfs or a rate of 56 cfs/hour could result from ice jam formation under freezing temperature. From the data analysis, there was no specific change in discharge below Holter, and neither there was much change in gage height at Cascade. Thus, the ice jam formation could be downstream of Cascade to Ulm or Great Falls.

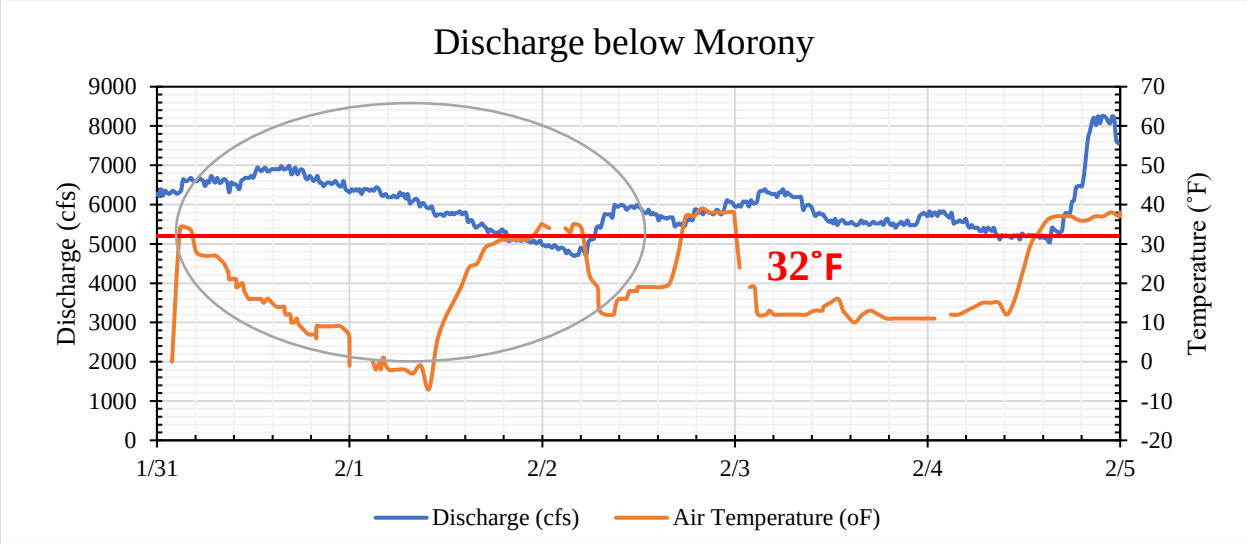

Figure 3.6 Discharge below Morony and air temperature for the event on Jan-31, 2015 to Feb-02, 2015

Table 3.6 Third flow loss event of 2014/15

Event 3	Date	Discharge
Beginning Time	1/31/2015 18:30	6680
End Time	2/2/2015 5:30	4720
Total Minutes	2099	
Total Hours	35	
Flow loss	1960	cfs
Flow Decrease Rate	56	cfs/hour

3.2.4 SPECIAL EVENT FROM MAR-02 TO MAR-03, 2015

This is the last event of major flow decrease that was noticed in between Holter to Great Falls during the winter of 2014/2015. A flow decrease of 1650 cfs at a rate of 90.5 cfs/hour on March 3

is found (Table 3.7) and corresponds to temperature dropping and maintaining below 32˚F throughout the event, causing the decrease in flow. The data analysis shows there is no discharge changes at below Holter and almost no change of gage height at Cascade.

After a flow increase during the night on March 3, there is a subsequent flow loss of around 1200 cfs on March 4 (Figure 3.7) when air temperature was still below freezing. These flow losses were quite dynamic and could be due to ice jam formation, break up, and formation again in another downstream location. There is no evidence seen in the Cascade and Holter showing ice jamming. The air temperature was lowed to -6˚F and remained below 32˚F for 3 days. Thus, like previous events, there could be ice jam formation downstream Cascade to Ulm or Great Falls.

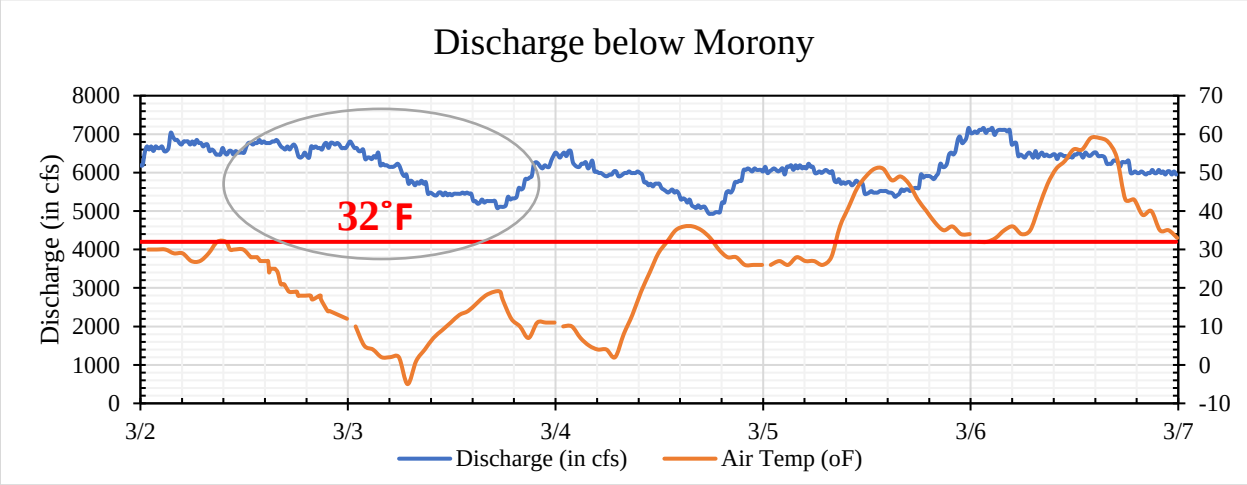

Figure 3.7 Discharge below Morony for the event on Mar-02, 2015 to Mar-03, 2015

Table 3.7 Fourth flow loss event of 2014/15

Event 4	Time	Discharge (cfs)
Beginning time	3/2/2015 23:00	6730
End time	3/3/2015 17:15	5080
Total Minutes	1094	
Total Hours	18.2	
Flow Loss	1650	cfs
Flow decrease rate	90.5	cfs/hour

3.3 SPECIAL EVENTS IN THE WINTER OF 2015–2016

The time series of discharge and air temperature from Dec-01, 2015 to Mar-30, 2016 is plotted indicating three events with flow decrease in Figure 3.8. Three events marked with high flow loss are shown in Table 3.8. The lowest air temperature during the flow-decrease events ranged from

22 ^{o}F to -4 ^{o}F. The rate of flow decreases in three identified events ranged from 81.5 cfs/hour to 15.1 cfs/hour. Three individual events in Table 3.8 are discussed below.

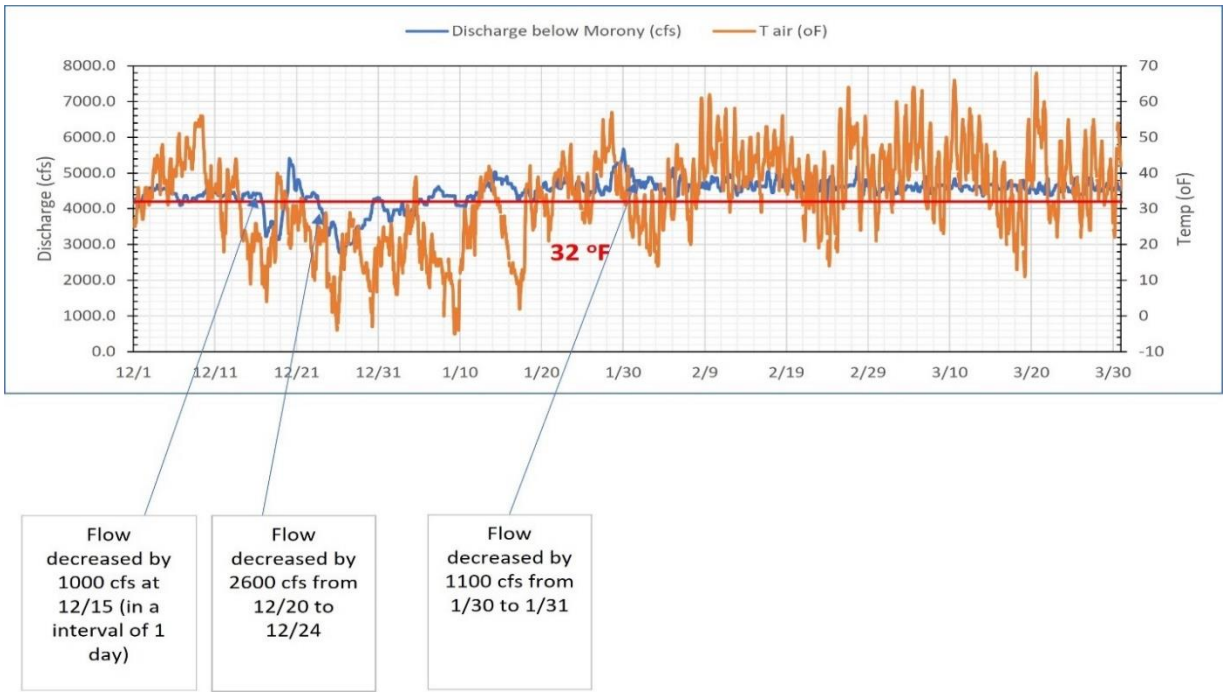

Figure 3.8 Discharge and air temperature below Morony from Dec-1, 2015 to Mar-31, 2016 showing events of high flow loss.

Table 3.8 Summary of flow decrease events observed between December 1, 2015, to March 31, 2015.

S.N.	Date	Flow decreased	Lowest Temperature	Flow decreases rate (cfs/hour)
1	Dec 16 to Dec 17, 2015	1057 cfs	4 ^{o}F	81.5
2	Dec 20 to Dec 27, 2015	2480 cfs	-4 ^{o}F	15.1
3	Jan 30 to Jan 31, 2016	1040 cfs	22 ^{o}F	29.1

3.3.1 SPECIAL EVENT FROM DEC-16 TO DEC-17, 2015

For the first flow loss event from Dec-16 to Dec-17, 2015, a flow loss of 1057 cfs is observed with a flow decrease rate of 81.5 cfs/hour (Table 3.9). The flow decrease was observed between 17:00 December 16 and 06:00 December 17, 2015, with the air temperature dropping to 4˚F (Figure 3.9). The data analysis of discharge below Holter from Dec-12 to Dec-21 gives a discharge of 3434.8 cfs and no flow loss at below Holter. And the gage height at Cascade shows an average height of 6.7 ft throughout the event, thus indicating no ice jam formation in this time period between Cascade and Ulm that might have resulted in flow loss. The corresponding temperature reading at

and before this event shows potential case of ice formation, with temperatures well below the freezing point for 3 to 4 days (Figure 3.9).

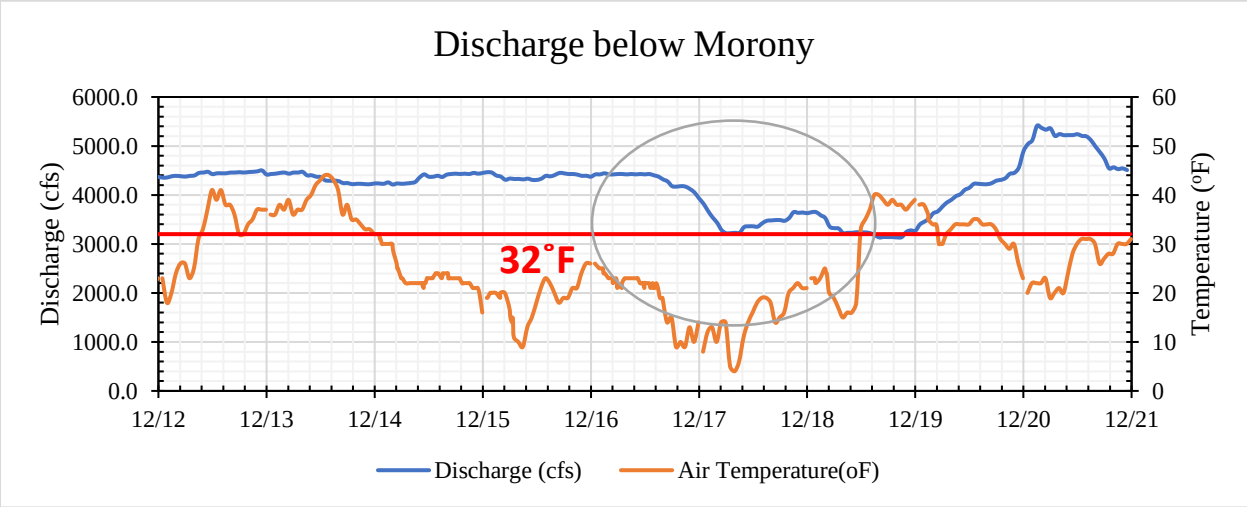

Figure 3.9 Discharge below Morony and air temperature for the event on Dec-16, 2015 to Dec-17, 2015

Table 3.9 First flow loss event in 2015/16

Event 1	Date	Discharge
Beginning Time	12/16/15 17:00	4277.5 cfs
End Time	12/17/15 6:00	3220.0 cfs
Total Minutes	779	
Total Hours	13.0	
Flow Loss	1057.5	cfs
Flow decrease rate	81.5	cfs/hour

In this event, from Figure 3.9, ice jamming is a possibility, but as no specific traces of it are noticed at discharge reading for below Holter and gage height reading at Cascade, the possibility of ice jam formation in between Ulm and Morony dam is seen viable. Also, as the temperature goes up after Dec-18, flow increases at Morony, without any changes to the discharge at Holter or gage height at Cascade. This must be a result of the ice melting between Ulm and Morony.

3.3.2 SPECIAL EVENTS FROM DEC-20 TO DEC-27, 2015

The second flow loss event is a longer event, of around 7 days, from Dec-20 to Dec-27, 2015. where a gradual loss in discharge of 2480 cfs at the rate of 15.1 cfs/hour is observed from 4:45 December 20 to 00:30 December 27, 2015 (Table 3.10). The air temperature has dropped from 32˚F to -4˚F over throughout this event (Figure 3.10). This indicates a possibility of ice cover/jam

formation. The analysis of the discharge below Holter at the event does not show a significant change and has an average discharge of 3419.7cfs.

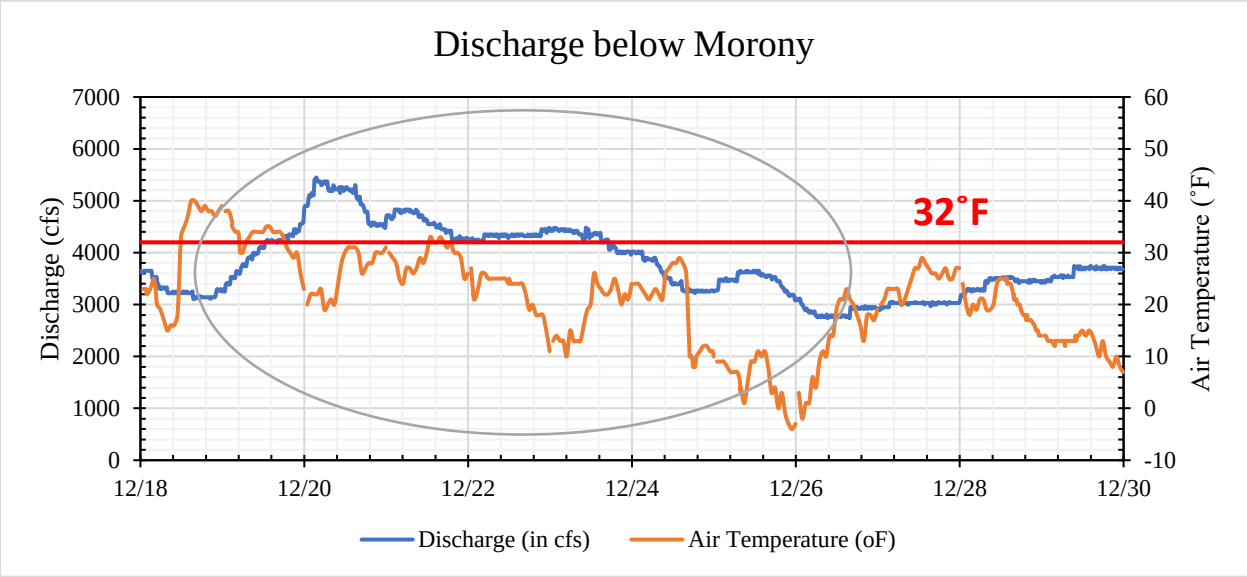

Figure 3.10 Discharge below Morony and Air Temperature for the event on Dec-20, 2015 to Dec-27, 2015.

Table 3.10 Second flow loss event of 2015/2016

Event 2	Time	Discharge
Beginning time	12/20/2015 4:45	5370
End time	12/27/15 0:30	2890
Total Minutes	9825	
Total Hours	163.8	
Flow Loss	2480	cfs
Flow decrease rate	15.1	cfs/hour

The gage height at Cascade is constant at the beginning of the event, but we can see beginning of ice jam formation start after Dec-26 in Figure 3.11. The gage height has raised by 1.7 ft during this event. Initially, the flow loss from Dec-20 to Dec-25 below Morony (Figure 3.10) could be due to ice cover/jam formation between Ulm and Morony because the gage height at Cascade was not affected during this flow loss. Again, for the most abrupt flow loss seen from Dec-25 to Dec-27 of the event, gage height at Cascade (Figure 3.11) shows the evidence of ice cover/jam formation in between Cascade and Ulm. Thus, this is the case of ice cover/jam formation in both the places i.e., between Cascade and Ulm, and/or between Ulm and Morony.

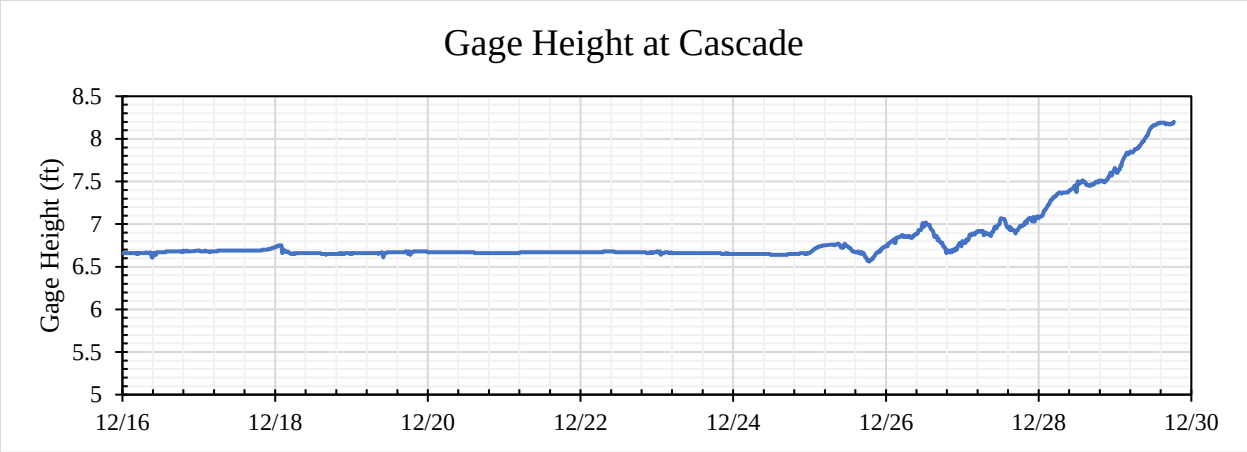

Figure 3.11 Gage height at Cascade at the event on Dec-20, 2015 to Dec-27, 2015

3.3.3 SPECIAL EVENT FROM JAN-30 TO JAN-31, 2016

The third flow loss event of 1040 cfs was from Jan-30 to Jan-31, 2016 at the rate of 29.1 cfs/hour (Figure 3.12). Figure 3.12 shows the discharge below Morony along with the air temperature change during from Jan-28 to Feb-05. The air temperature in the flow loss event was dropped from around 32˚F to 20˚F. The air temperature stayed below the freezing point after Jan 30 (Figure 3.12).

The data analysis of the discharge and gage height below the Holter and Cascade, respectively, shows that the discharge below Holter shows no major loss or increase and had an average flow of 3881.9 cfs, while the gage height at Cascade was consistent throughout this event with an average gage height of 6.8 ft. There was no data at Ulm gaging station. Air temperature was below 32˚F for a period of 12 hours (Figure 3.12), this event most likely was not due to ice jam formation upstream Cascade but could be from Cascade to Ulm or Great Falls.

Table 3.11 Third flow loss event of 2015/2016.

Event 3	Time	Discharge
Beginning time	1/30/2016 5:15	5520
End time	1/31/2016 17:00	4480
Total Minutes	2145	
Total Hours	35.8	
Flow Loss	1040	Cfs
Flow decrease rate	29.1	cfs/hour

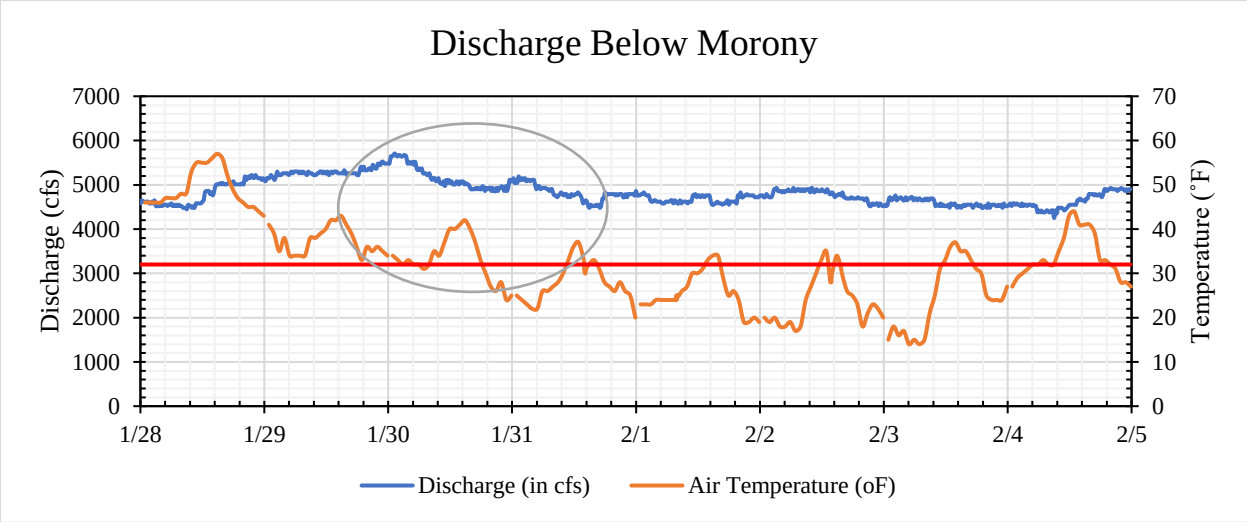

Figure 3.12 Discharge below Morony and Air Temperature for the event for Jan-30, 2016 to Jan-31,2016

3.4 SPECIAL EVENTS IN THE WINTER OF 2016–2017

The time series of discharge and air temperature from Dec-01, 2016 to Mar-31, 2017 is plotted indicating the events with flow decrease on Figure 3.13. From the graph of discharge and air temperature with date, five events with high flow loss and the corresponding air temperature are identified. The special scenarios that are marked with high flow loss are shown in Table 3.12. The lowest air temperature during the flow decrease events ranged from 32 ^{o}F to -6 ^{o}F. The rate of flow decreases in these identified events ranged from 56.7 cfs/hour to 16.25 cfs/hour. The largest flow decrease was 2000 cfs which was observed from Feb-19, 2017 to Feb-26, 2017, with the flow decrease rate of 20.83 cfs/hour.

Table 3.12 Summary of flow decrease events observed between December 1, 2016, to March 31, 2017

S.N.	Date	Flow Decreased (cfs)	Temperature after drop	Flow decrease rate (cfs/hour)
1	Dec-07 to Dec-08	1290	-6 ^{o}F	56.7
2	Dec-16 to Dec-19	1890	32 ^{o}F	30.12
3	Dec-21 to Dec-25	1280	10 ^{o}F	16.25
4	Dec-25 to Dec-28	1100	32 ^{o}F	17.00
5	Feb-19 to Feb-26, 2017	2000	24 ^{o}F	20.83

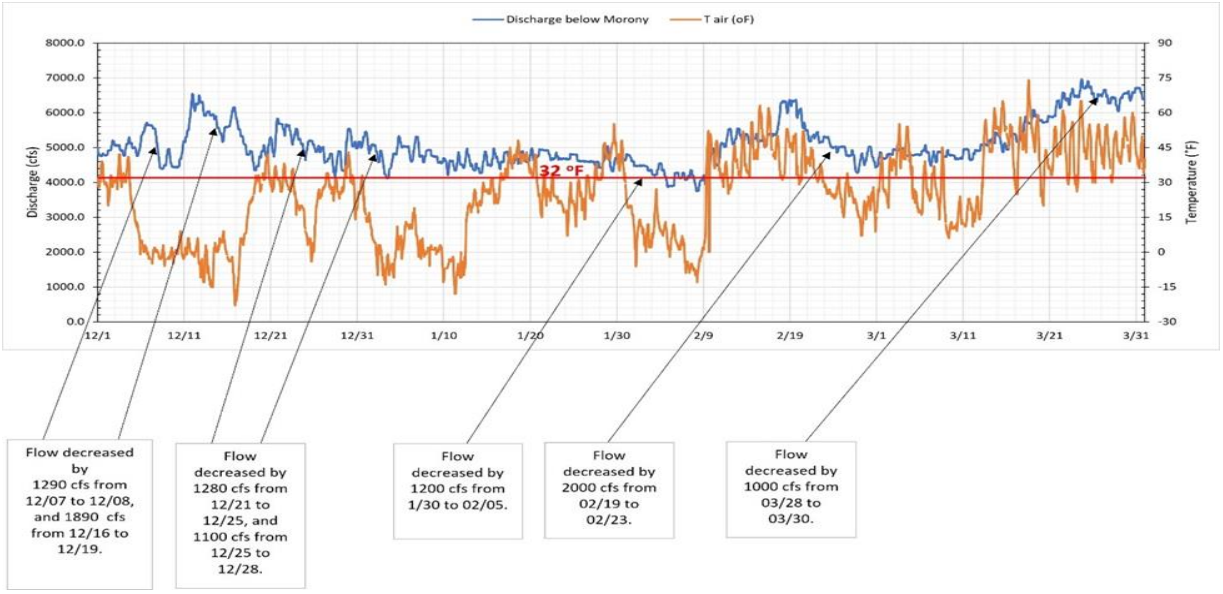

Figure 3.13 Discharge and air temperature below Morony from Dec-1, 2016 to Mar-31,2017 showing events of high flow loss.

3.4.1 SPECIAL EVENT FROM DEC-07 TO DEC-08, 2016

The first flow loss event of the winter of 2016 was observed from 06:30 December 7 to 5:15 December 8, 2016 (Figure 3.14). A total flow loss of 1290 cfs is seen during this event at the flow decrease rate of 56.7 cfs. The air temperature started to drop below freezing on December 4 and reached around 0˚F from December 6 to 10 (Figure 3.14). There was temperature drop to below the freezing point from late hours on Dec-04, with the rise in discharge between Dec-06 to Dec-07 albeit the temperature was decreasing, which is because of the increase (1000 cfs) in discharge at 8:00 below Holter on Dec-04 (Figure 3.15), 16:00 on Dec-04 at Cascade, 8:00 on Dec-05 at Ulm, and an increase in gage height (0.5 ft) at Cascade at Dec-05 (Figure 3.16), most likely managed release by NWE Hydro. The loss in discharge from Dec-07 to Dec-08 was most possibly due to ice cover/jam formation from Cascade to Ulm or Morony since air temperature was so low, but water temperature at Holter was high and continuously dropped from 43.4 ºF to 39.9 ºF.

Table 3.13 First flow loss event 2016/2017

Event 1	Time	Discharge
Beginning time	12/7/2016 6:30	5710
End time	12/8/2016 5:15	4420
Total Minutes	1364	
Total Hours	22.7	
Flow loss	1290	cfs
Flow decrease rate	56.7	cfs/hour

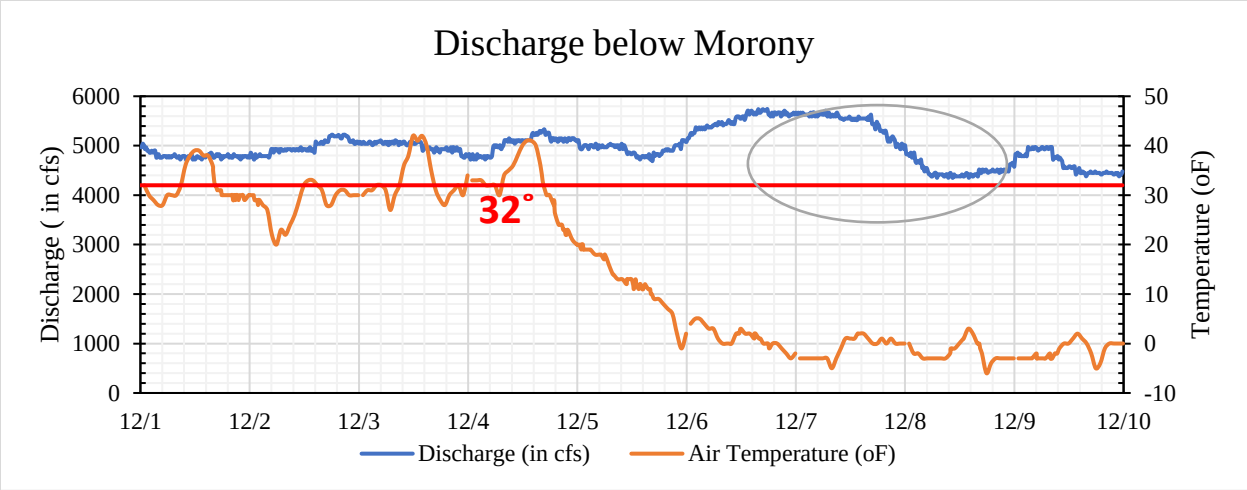

Figure 3.14 Discharge below Morony for the event on Dec-07, 2016 to Dec-08, 2016.

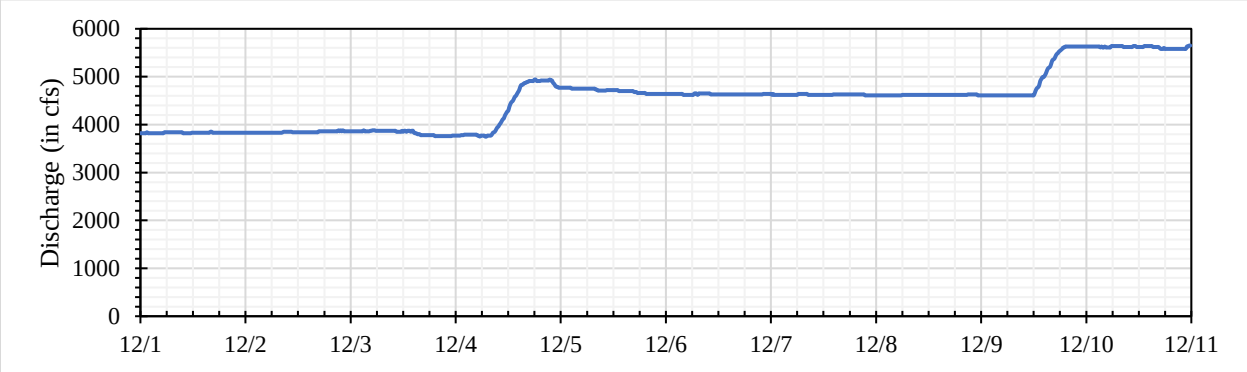

Figure 3.15 Discharge below Holter for the event on Dec-07, 2016 to Dec-08, 2016

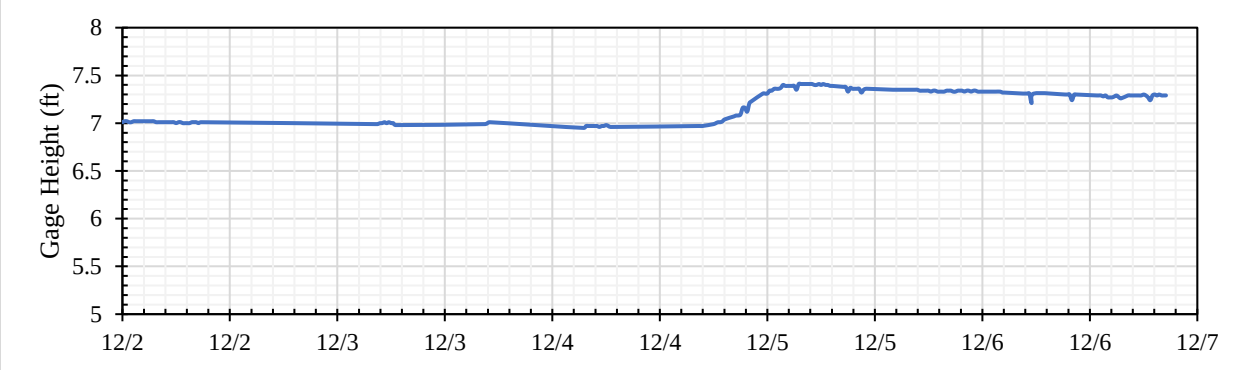

Figure 3.16 Gage height at Cascade for the event on Dec-07, 2016 to Dec-08, 2016

3.4.2 SPECIAL EVENT FROM DEC-16 TO DEC-19, 2016

The second flow loss event from 16:45 December 16 to 7:30 December 19, 2016, was observed with flow loss of 1890 cfs in a span of 2 days (Figure 3.17) at the rate of 30.12 cfs/hour (Figure 3.17).The minimum air temperature during at this event was around -21˚F and the air temperature

remains under the freezing point from before and throughout the event. Discharge from Holter Dam was 5620 cfs on December 13 and dropped to 4500 cfs on December 16: decrease of 1120 cfs, smaller than the drop in Morony. The reason for flow loss can be predicted at the very low temperatures, which possibly caused the ice cover formation.

The gage height data at Cascade is studied to check the ice jam formation between Cascade and Ulm. The observed gage height data at Cascade from December-15 to December-23 shows a rise of 5 ft on December 17 (Figure 3.18) and remain at high level up to the end of December 20. Water temperature at Holter dropped from 36.3 ^{o}F on December 15 to 34.9 ^{o}F on December 17–21.

Figure 3.18 shows a potential ice jam formation near Cascade on Dec-17. As there was an increase in gage height at Cascade (Figure 3.18) and flow loss at Morony (Figure 3.17), we can conclude there was an ice jam between Cascade and Morony. The flow loss from Dec-16 to Dec-18 is the result of low air temperature for ice jam formation and the flow loss at Holter before the event, even Missouri River below Holter had a constant discharge from December 17–19.

Table 3.14 Second flow loss event of 2016/2017.

Event 2	Time	Discharge
Beginning Time	12/16/2016 16:45	6210
End Time	12/19/2016 7:30	4320
Total Minutes	3765	
Total Hours	62.75	
Flow Loss	1890	cfs
Flow decrease rate	30.12	cfs/hour

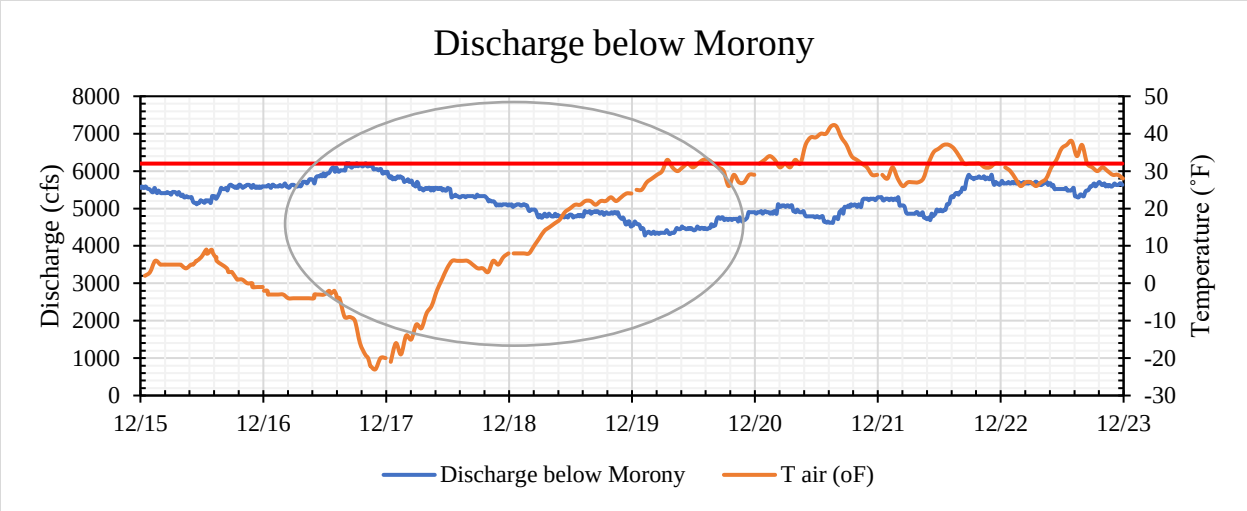

Figure 3.17 Discharge below Morony for the event between Dec-16, 2016 to Dec-19, 2016

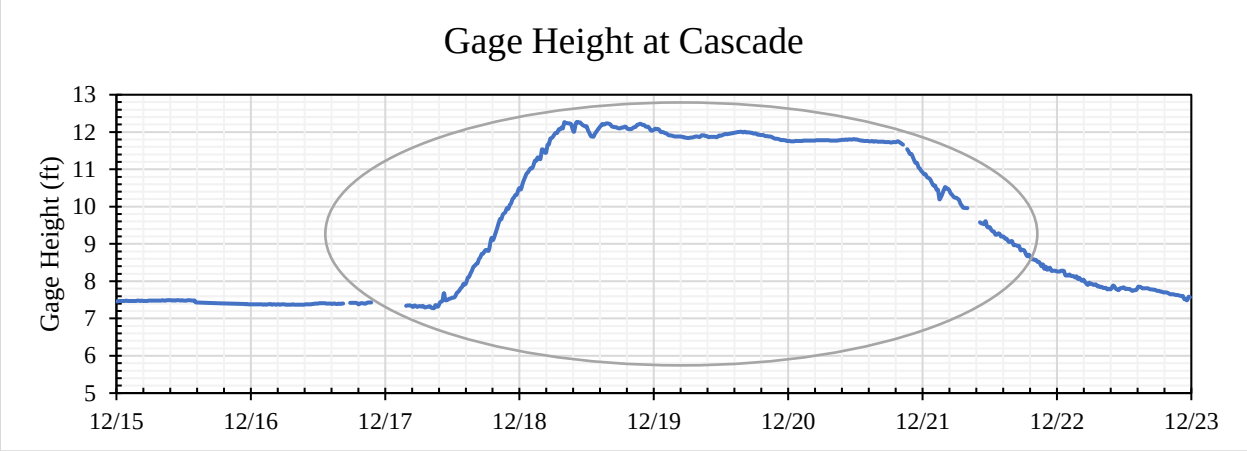

Figure 3.18 Gage Height at Cascade for the event between Dec-16, 2016 to Dec-19, 2016

3.4.3 SPECIAL EVENTS FROM DEC-21 TO DEC-25 AND DEC-25 TO DEC-28, 2016

The third flow loss event was observed from 17:45 December 21 to 00:30 December 25, 2016 with flow loss of 1280 cfs in a span of around 4 days (Figure 3.19) at the flow loss rate of 16.25 cfs/hour (Table 3.15). The minimum air temperature at this event is 16˚F (Figure 3.19). Figure 3.18 shows ice cover/jam formation on December 17, continuous buildup/development up to the end of December 20, and then ice jam breakup on December 21–23. This leads the flow increase (~100 cfs) at Morony on December 22. The flow loss from December 22 to 25 could be due to low and fluctuating air temperature (below the freezing point of 32˚F over some hours) and another ice cover/jam formation.

For another event from 18:00 December 25 to 10:45 December 28, 2016, flow loss of 1100 cfs is observed at the rate of 17 cfs/hour (Table 3.15). Initially the air temperature is at -5˚F, and the temperature remains below the freezing point for the most part of the flow loss evet, which has caused the reduction in flow below Morony.

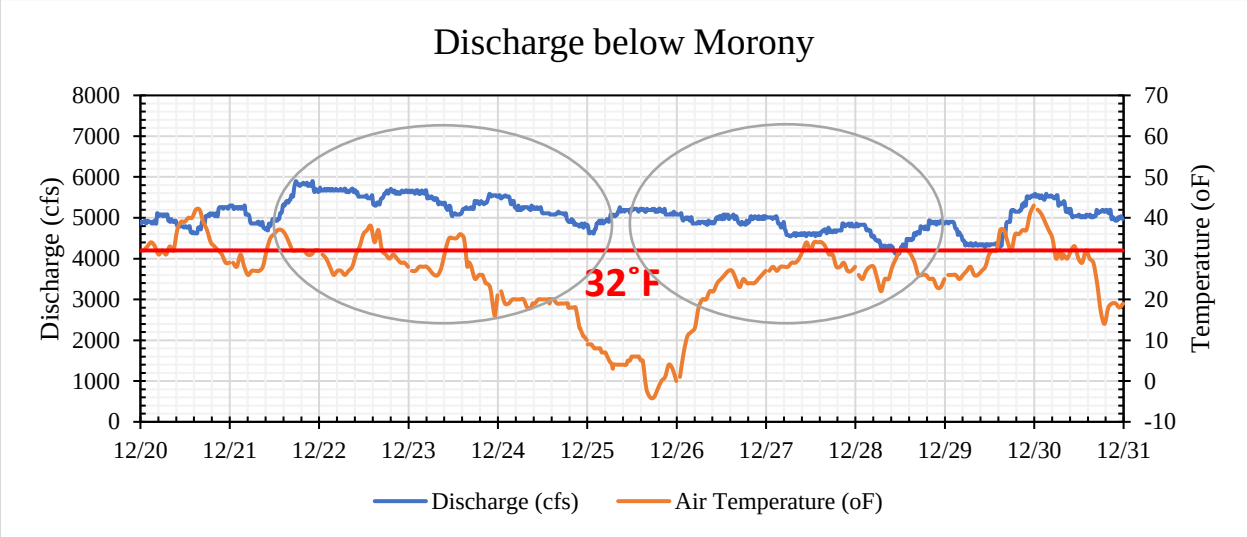

Figure 3.19 Discharge below Morony for two events between Dec-21 to Dec-25, 2016 and Dec-25 to Dec-28, 2016

Table 3.15 Third and fourth flow loss events in 2016/2017.

Event 3	Time	Discharge
Beginning Time	12/21/16 17:45	5900
End Time	12/25/16 0:30	4620
Total Minutes	4725	
Total Hours	78.75	
Flow Loss	1280	cfs
Flow Decrease Rate	16.25	cfs/hour

Event 4	Time	Discharge
Beginning Time	12/25/16 18:00	5220
End Time	12/28/16 10:45	4120
Total Minutes	3884	
Total Hours	64.73	
Flow Loss	1100	cfs
Flow Decrease Rate	17	cfs/hour

The fourth flow loss event from December 25 to December 28 also shows ice jam formation, as an increment in gage height is observed at Cascade after Dec-26 (Figure 3.20). There is an

increment of around 4 ft in gage height at Cascade, thus indicating ice jamming in between Cascade and Ulm.

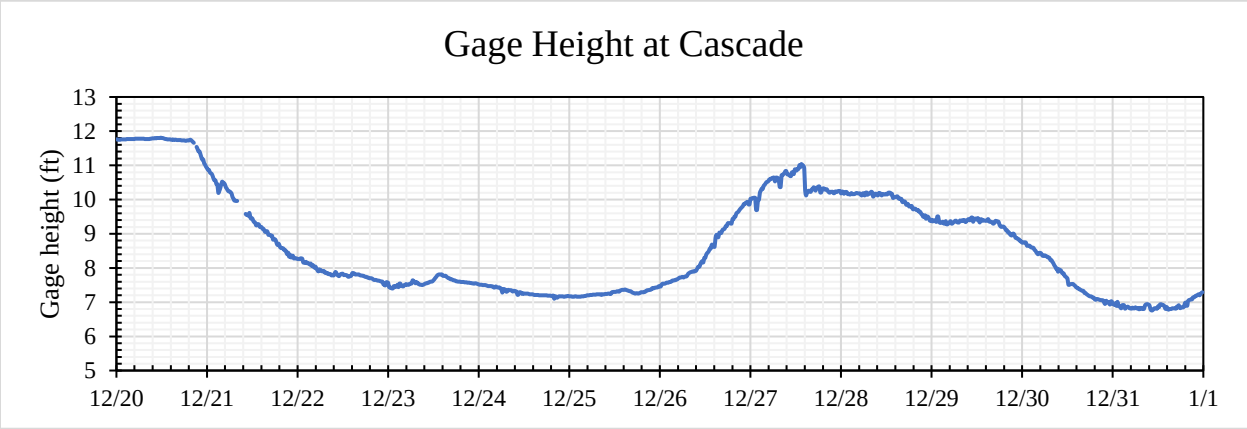

Figure 3.20 Gage Height at Cascade for the event between Dec-21, 2016 to Dec-25, 2016 and Dec-25, 2016 to Dec-28, 2016

The data analysis of discharge at Holter indicates no significant flow loss and gain at Holter during both of these events, which substantiates the hypothesis of ice jam formation somewhere between Cascade and Ulm for the event of Dec-25 to Dec-28, 2016.

3.5 SPECIAL EVENTS IN THE WINTER IN 2018

The time series of discharge and air temperature from Jan-01, 2018 to Mar-31, 2018 is plotted indicating the events with flow decrease on Figure 3.21. From the graph of discharge and air temperature with date (Figure 3.21) six events when there was high flow loss and the corresponding air temperature at those dates were identified. The special events that are marked with high flow loss are summarized in Table 3.16. The lowest air temperature during the flow decrease events ranged from 32 ^{o}F to -20 ^{o}F. The rate of flow decreases in these identified events ranged from 235.8 cfs/hour to 22.5 cfs/hour. The largest flow decrease observed was 3640 cfs from Mar-17 to Mar-21, 2018, with the flow decrease rate of 38.6 cfs/hour.

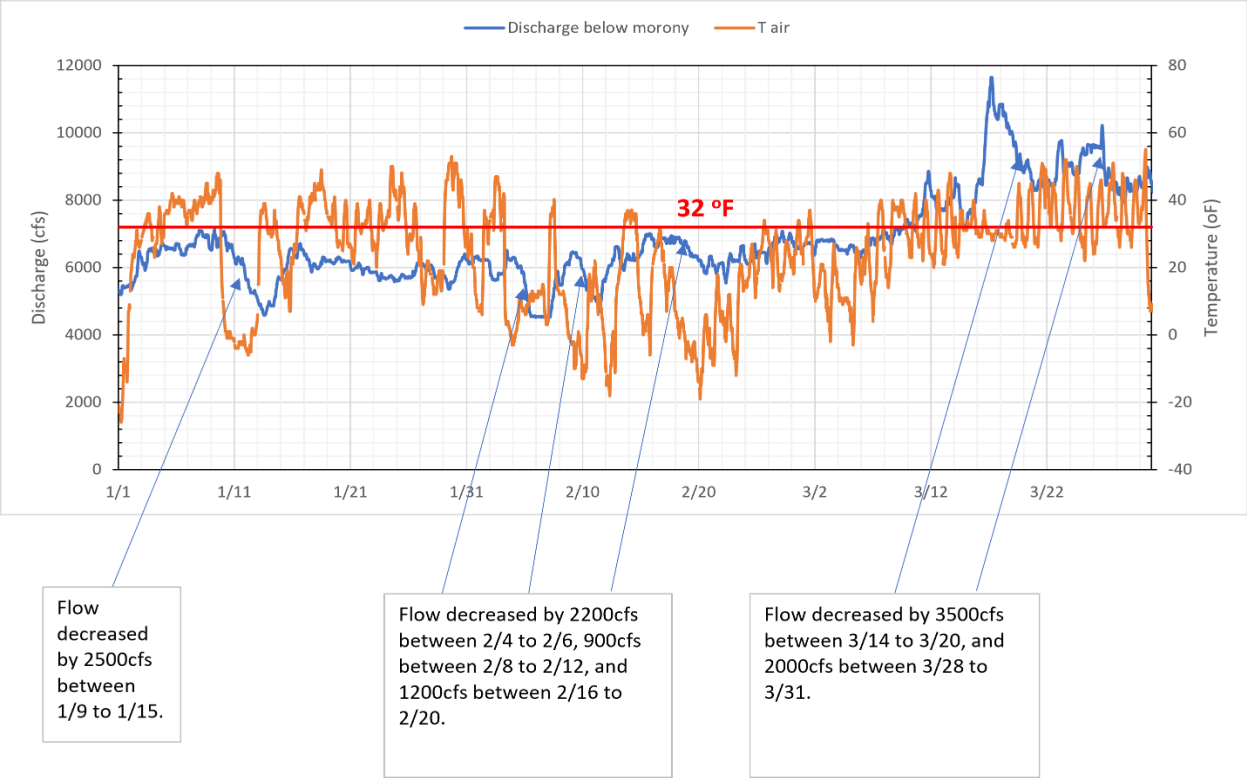

Figure 3.21 Discharge and air temperature below Morony from Jan-1, 2018 to Mar-31,2018 showing events of high flow loss.

Table 3.16 Summary of flow decrease events observed between January 1, 2018, to March 31, 2018

S.N.	Date	Flow Decreased (cfs)	Temperature after drop	Flow decrease rate (cfs/hour)
1	Jan-10 to Jan-13	2480 cfs	-6 °F	30.1
2	Feb-4 to Feb-5	860 cfs	26 °F	118.9
3	Feb-9 to Feb-11	1980 cfs	-14 °F	31.1
4	Feb-18 to Feb-20	1190 cfs	-20 °F	22.5
5	Mar-14 to Mar-15	2330 cfs	24 °F	101.3
6	Mar-17 to Mar-21	3640 cfs	28 °F	38.6
7	Mar-26 to Mar-27	2000 cfs	32 °F	235.8

3.5.1 SPECIAL EVENT FROM JAN-10 TO JAN-13, 2018

The first flow decrease event of 2018 is observed from 05:15 January 10 to 05:45 January 13, with a decrease in discharge of 2480 cfs below Morony at the rate of 30.1 cfs/hour (Table 3.17). There was a significant decrease in air temperature on December 10, going from high of 45˚F to 0˚F (Figure 3.22), and stayed very low (lowest at -6 °F) for more than two days. This resonates with the time of flow loss event.

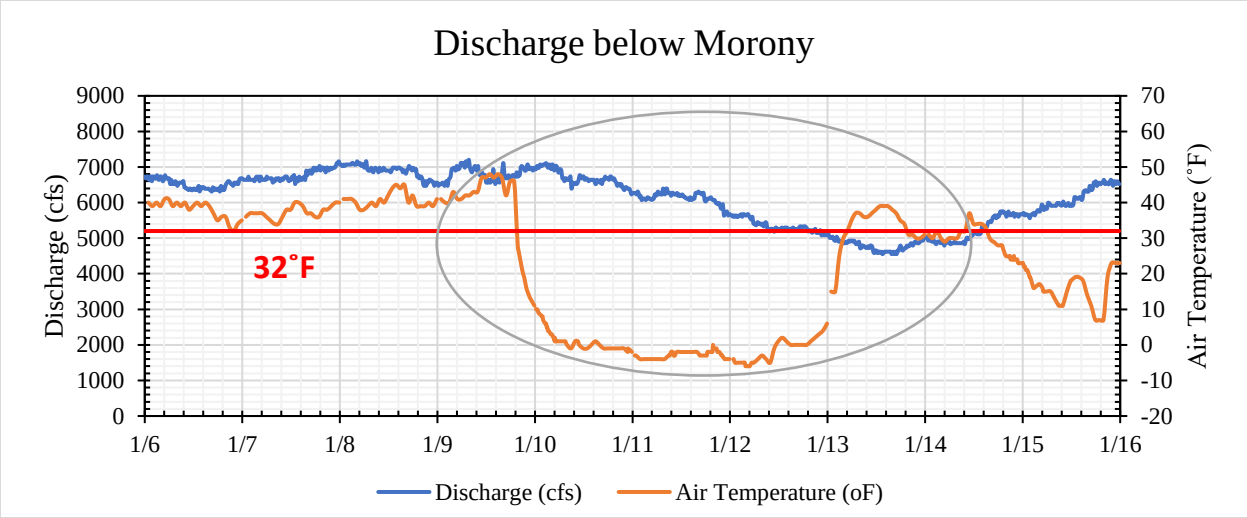

Figure 3.22 Discharge below Morony and air temperature at Great Falls for the event between Jan-10 to Jan-13, 2018.

Table 3.17 First flow loss event in 2018.

Event 1	Time	Discharge
Beginning Time	1/10/2018 5:15	7030
End Time	1/13/2018 15:45	4550
Total Minutes	4950	
Total Hours	82.5	
Flow Loss	2480	cfs
Flow decrease rate	30.1	cfs/hour

There was a gradual decrease in gage height near Ulm observed from Jan-07 to Jan-13 (Figure 3.23). The gage height at Cascade was constant on January 10–11, started to increase at 10:00 on December 11, an increase of 4.5 ft up to 5:30 on January 12 (Figure 3.24). This indicates there is ice jam formation in between Cascade and Ulm, which is the cause of this decrease in flow at Morony after December 11. The flow decrease from January 10–11 was most likely due to ice cover formation first due to sharp drop of air temperature.

The data analysis of discharge below Holter gives the evidence that the discharge below Holter is not changing but having an increase in gage height at only Cascade, supports our conclusion of ice jamming between Cascade and Ulm.

Additionally, there is flow increment at Morony after Jan-7 to Jan-9 and gage height decreases at the same time at Cascade, with temperature reading being above the freezing point of 32˚F (Figure

3.22). This indicates the increment in discharge at Morony was due to melting down of jammed ice that was formed before Jan-7 (on December 29, 2017).

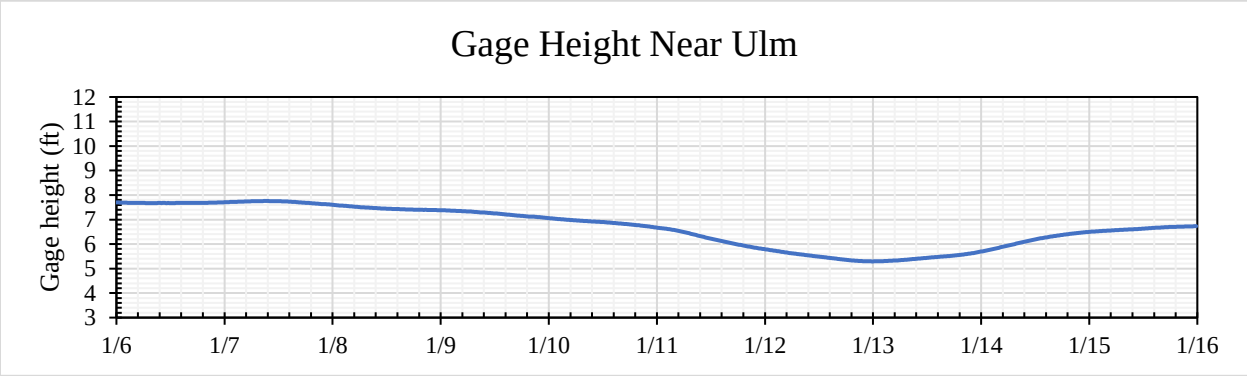

Figure 3.23 Gage Height near Ulm for the event between Jan-10 to Jan-13, 2018

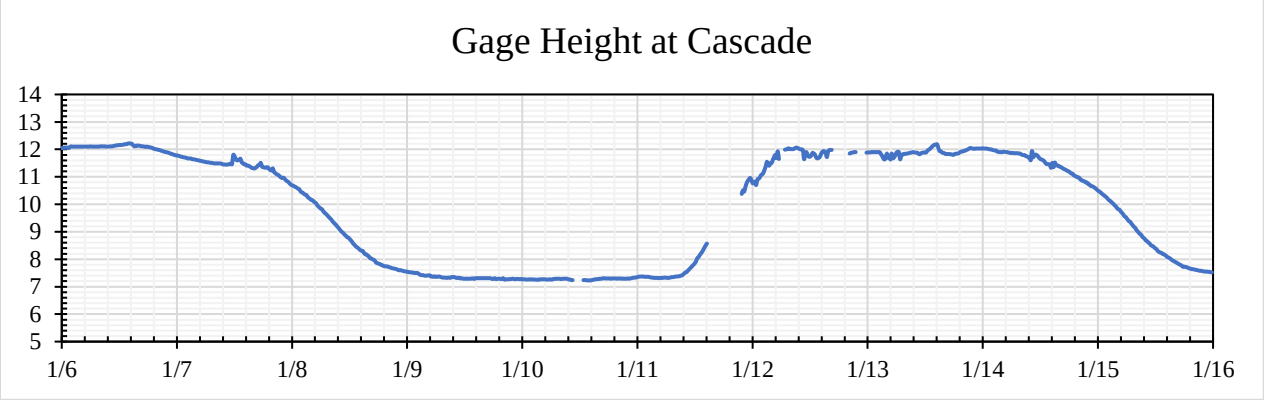

Figure 3.24 Gage Height at Cascade for the event between Jan-10 to Jan-13, 2018

3.5.2 SPECIAL EVENT FROM FEB-04 TO FEB-05, 2018

The second flow loss event from 22:15 February 04 to 05:30 February 05, 2018, has a flow loss of 860 cfs in a span of 7 hours (Table 3.18) with a flow decrease rate of 118.9 cfs/hour. Here low temperature is one of the potential reasons for flow loss. Figure 3.25 shows the discharge below Morony along with air temperature. There was an abrupt loss in flow on Feb-5 and then the reduced flow remained constant for 2 days span (Figure 3.25). This all happened when there was low temperature, and once there was an increase in temperature to above freezing, i.e., from Feb-5 to Feb-8, the discharge below Morony was increased, resulting from the ice meltdown.

Gage height increase of around 3 ft is noticed at near Ulm in between Feb-4 to Feb-5, 2018 (Figure 3.26). Thus, it can be assumed that the reason for decrease in discharge below Morony is due to ice jamming which has caused the increase in gage height near or downstream Ulm. Also, the gage

height data analysis at Cascade shows there is not any significant increase in gage height during the flow loss event (Figure 3.26). This concludes that there is ice jamming and that is somewhere in between Ulm and Morony Dam.

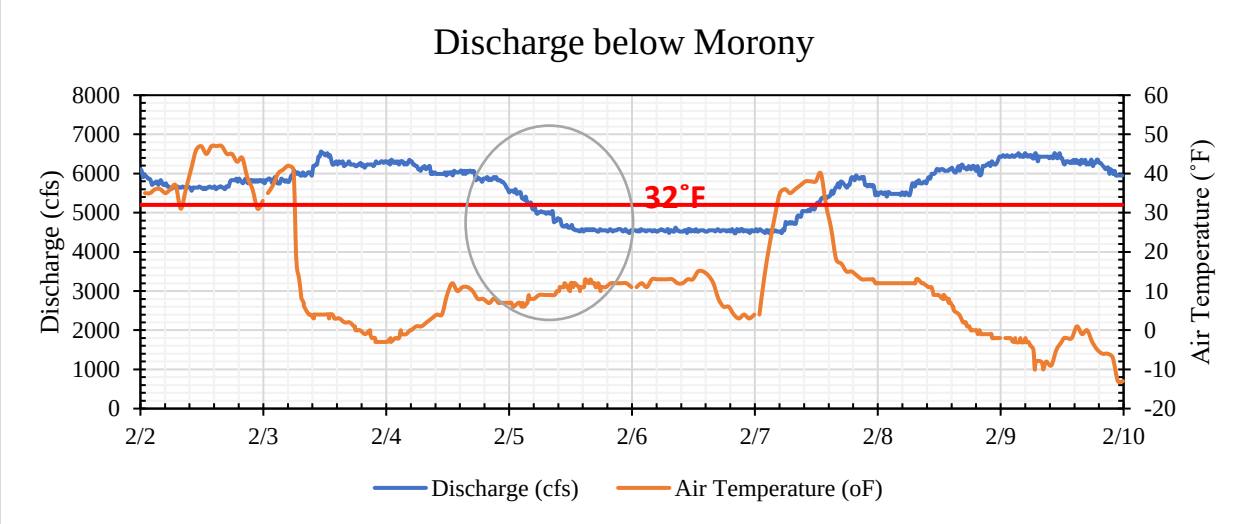

Figure 3.25 Discharge below Morony and air temperature at Great Falls for the event between Feb-04 to Feb-05, 2018.

Table 3.18 Second flow loss event in 2018

Event 2	Time	Discharge
Beginning Time	2/4/18 22:15	5830
End Time	2/5/18 5:30	4970
Total Minutes	434	
Total Hours	7.2	
Flow Loss	860	cfs
Flow decrease rate	118.9	cfs/hour

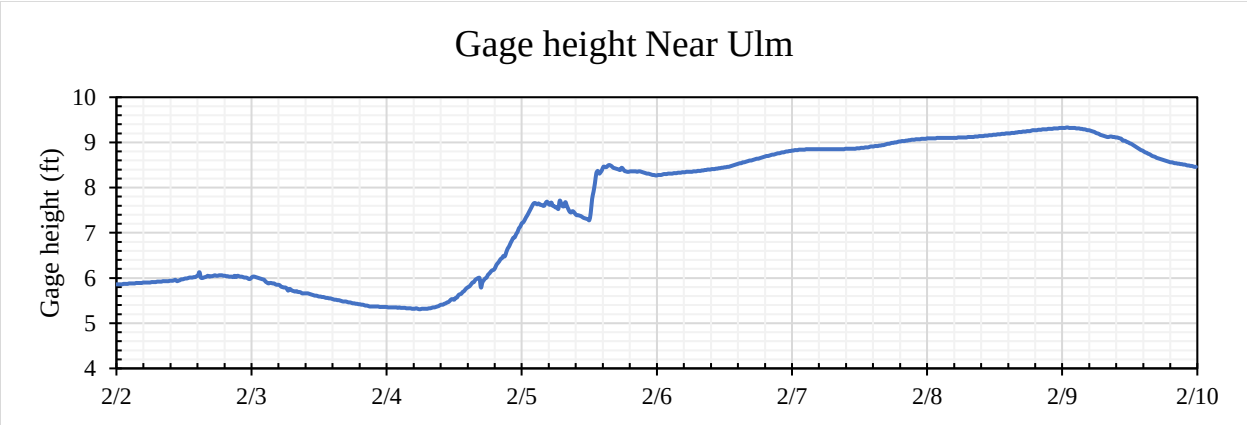

Figure 3.26 Gage height near Ulm for the event between Feb-04 to Feb-05, 2018

3.5.3 SPECIAL EVENT FROM FEB-09 TO FEB-11 AND FEB-18 TO FEB-20, 2018

The third flow loss event and the fourth flow loss event for 2018 are observed and plotted along with the air temperature on Figure 3.27. For the third flow loss event from 3:15 February 09 to 12:30 February 11, the flow loss is of 1980 cfs at the rate of 31.1 cfs/hour (Table 3.19). The temperature during the event is well below the freezing point of 32 ^{o}F and remains below 32˚F for 6 days (Figure 3.27). This indicates a possibility of ice cover/jam formation.

On the fourth event from 7:00 February 18 to 12:00 February 20, the flow loss is of 1190 cfs (Table 3.19) with a flow loss rate of 22.5 cfs/hour. The temperature during this time was well below the freezing point as well, indicating a possibility of ice cover/jam formation.

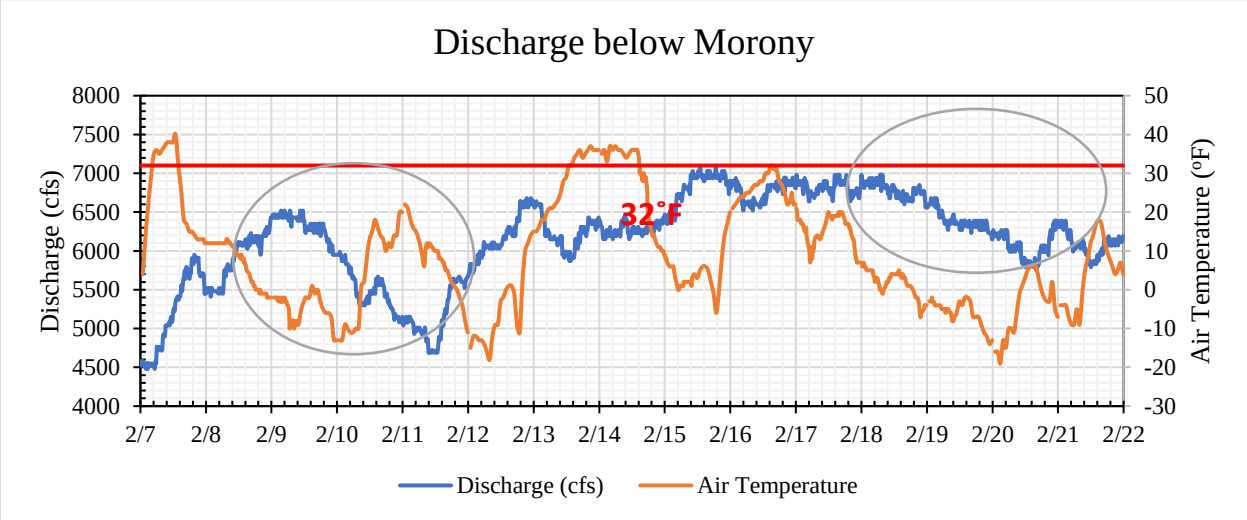

Figure 3.27 Discharge and air temperature below Morony for the event between Feb-09 to Feb-11, 2018 and Feb-18 to Feb-20, 2018.

Table 3.19 Third and fourth flow loss events in 2018

Event 3	Time	Discharge
Beginning Time	2/9/18 3:15	6470
End Time	2/11/18 12:30	4690
Total Minutes	3435	
Total Hours	57.3	
Flow Loss	1980	cfs
Flow decrease rate	31.1	cfs/hour

Event 4	Time	Discharge
Beginning Time	2/18/18 7:00	6980
End Time	2/20/18 12:00	5790

Total Minutes	3180	
Total Hours	53.0	
Flow Loss	1190	cfs
Flow decrease rate	22.5	cfs/hour

For the event between Feb-09 to Feb-11, there was about 0.3–0.4 ft increase of gage height at Cascade on February 8 and 10. The gage height near Ulm started to increase from 5.4 ft at 8:00 on February 4 to 8.4 ft at 16:00 on February 5 then gradually increased to 9.4 ft at 4:30 on February 9, which indicates the possibility of ice jam formation between Ulm and Morony (Figure 3.28). For the event between Feb-18 to Feb-20, there is no gage height increment near Ulm around Feb-18 observed to indicate the ice jam formation.

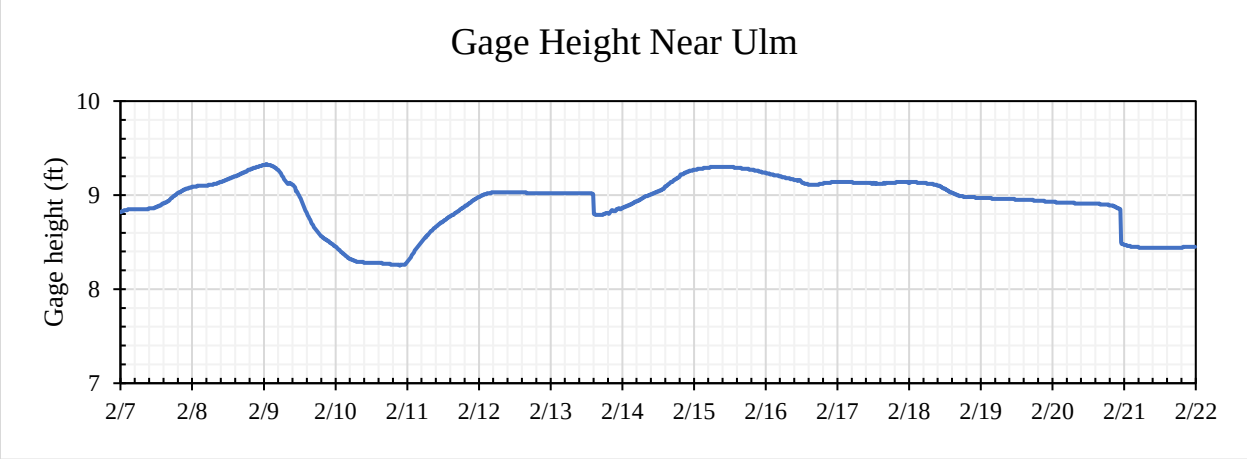

Figure 3.28 Gage height near Ulm for the event between Feb-09 to Feb-11, 2018 and Feb-18 to Feb-20, 2018.

From Figure 3.29, the gage height at Cascade for both of these events has small or no change in gage height on and before Feb-08 and Feb-19. Thus, ice jamming is between Ulm and Morony and not between Cascade and Ulm for the event between Feb-09 to Feb-11.

On the other hand, there is not any change in increment in gage height before Feb-19 noticed either on Cascade or Ulm. Also, gage height has increased after Feb-21 at Cascade, but this increase in gage height cannot be the reason for the decrease in discharge below Morony on Feb-18, as the impact of gage height increase in Cascade can only be seen after a day in Morony.

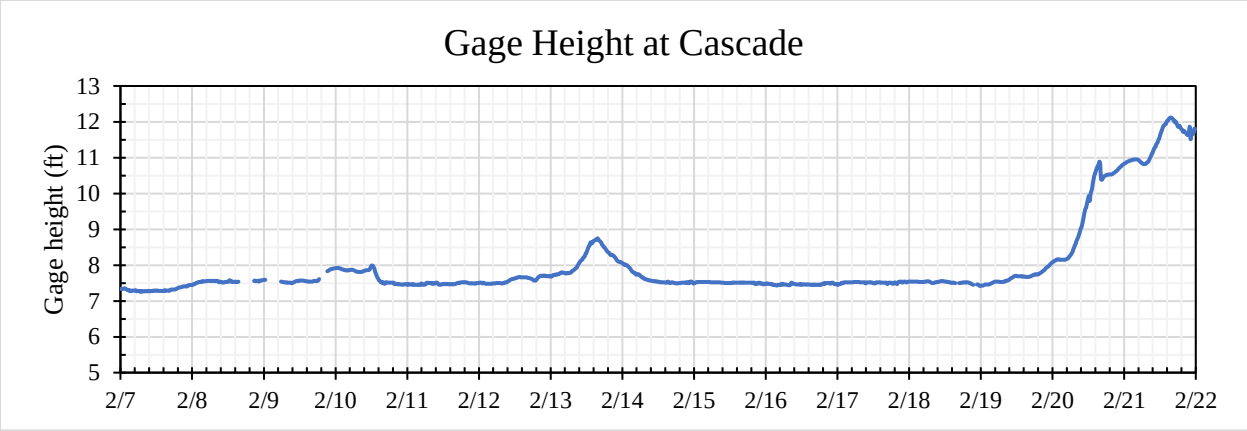

Figure 3.29 Gage height at Cascade for the event between Feb-09 to Feb-11, 2018 and Feb-18 to Feb-20, 2018.

The data analysis of discharge below Holter shows an increment (<600 cfs) of discharge on Feb-07 and is fairly constant throughout the event. Thus, after analyzing all the information, the third flow loss event on Feb-9 to Feb-11 was due to ice jam formation between Ulm and Morony. While, the fourth flow loss event is a special event, where the reason of flow loss cannot be specified, as the ice cover formation was possible because of very low air temperature but the location could not be predicted accurately.

3.5.4 SPECIAL EVENTS FROM MAR-14 TO MAR-15 AND MAR-17 TO MAR-21, 2018

The fifth flow loss event of 2018 is from 02:15 March 14 to 01:15 March 15,2018, where a flow loss of 2330 cfs with a flow decrease rate of 101.3 cfs/hour (Table 3.20) is observed. Air temperature before and at this event was fluctuating around the freezing point of 32 ^{o}F (Table 3.30), so the ice cover formation during night was possible. Since the amount of flow loss was huge, an ice jam formation would be most likely to occur.

The sixth flow loss event of 2018 is from 04:45 March 17 to 03:00 March 21, where a flow loss of 3640 cfs in a span of 4 days at a rate of 38.6 cfs/hour is observed (Table 3.20). The temperature at the time of this event is below the freezing point of 32˚F and has the possibility of ice cover/jam formation. As there is an increase in gage height near Ulm during Mar-16 by around 1.5 ft, the possibility of ice jam formation between Ulm and Morony is predicted for this event (Figure 3.31).

The data analysis of discharge below Holter shows there is no significant decrease in discharge below Holter on the event between Mar-14 to Mar-15.

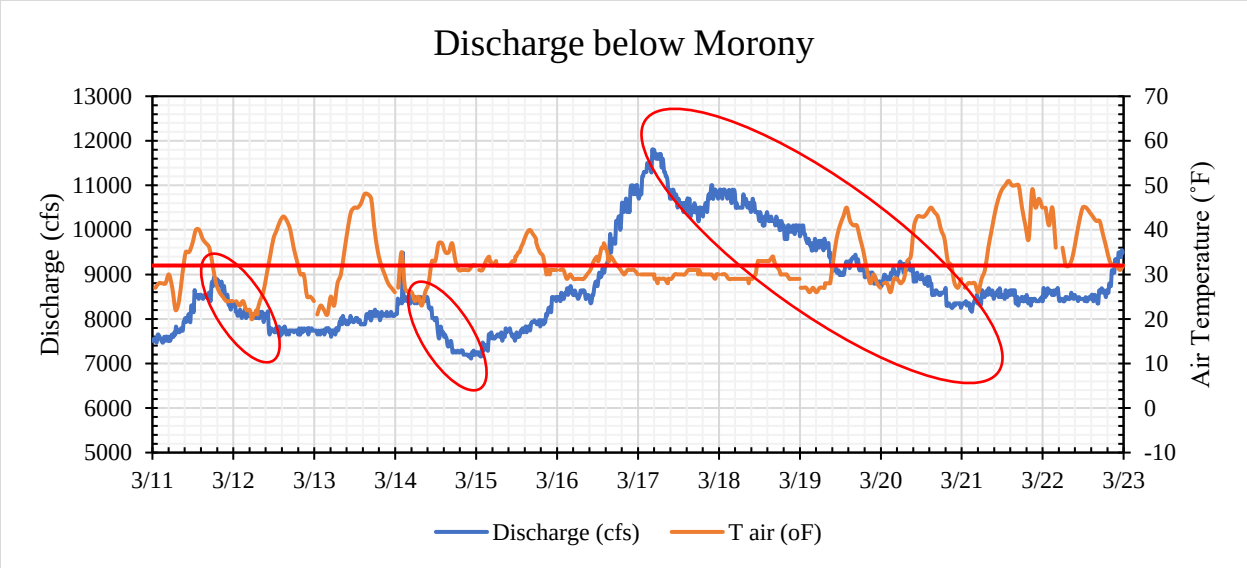

Figure 3.30 Discharge and air temperature below Morony for the event between Mar-14 to Mar-15, 2018 and Mar-17 to Mar-21, 2018

Table 3.20 Fifth and sixth flow loss events in 2018

Event 5	Time	Discharge
Beginning Time	3/14/18 2:15	9490 cfs
End Time	3/15/18 1:15	7160 cfs
Total Minutes	1380	
Total Hours	23.0	
Flow Loss	2330	cfs
Flow decrease rate	101.3	cfs/hour

Event 6	Time	Discharge
Beginning Time	3/17/18 4:45	11800 cfs
End Time	3/21/18 3:00	8160 cfs
Total Minutes	5655	
Total Hours	94.3	
Flow Loss	3640	cfs
Flow decrease rate	38.6	cfs/hour

The gage height at Ulm was seen decreasing by around 4 ft from Marc-11 to Mar-14 (Figure 3.31) and could a breakup of ice jam formed before, which should have resulted in increase in discharge from Mar-15 to Mar-17 below Morony dam (Figure 3.30). The flow decrease on March 14 could be a temporary ice jam formation at a bridging (narrow or restriction) location from Ulm to Great Falls.

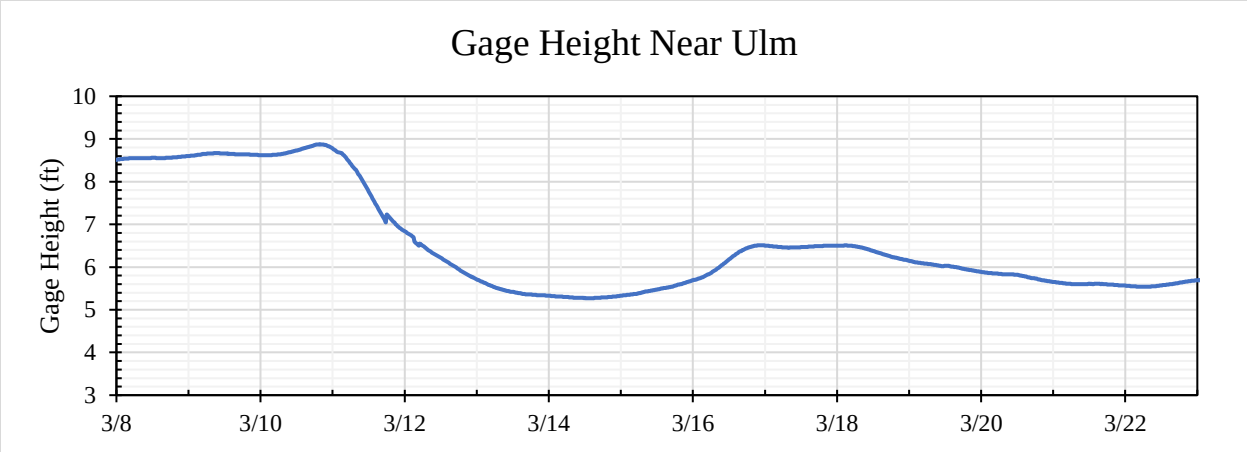

Figure 3.31 Gage height near Ulm for the event between Mar-14 to Mar-15 and Mar-17 to Mar-21, 2018

The gage height at Cascade before Mar-14 (Figure 3.32) had no change. Thus, the chance of ice jam formation in between Cascade and Ulm for this event is not predicted. For the other event between Mar-17 to Mar-21, there was an increase in gage height at Cascade by ~0.7 ft and at Ulm by 1.2 ft around March 16. This indicates ice jam formation in between Cascade and Ulm or Great Falls for this event.

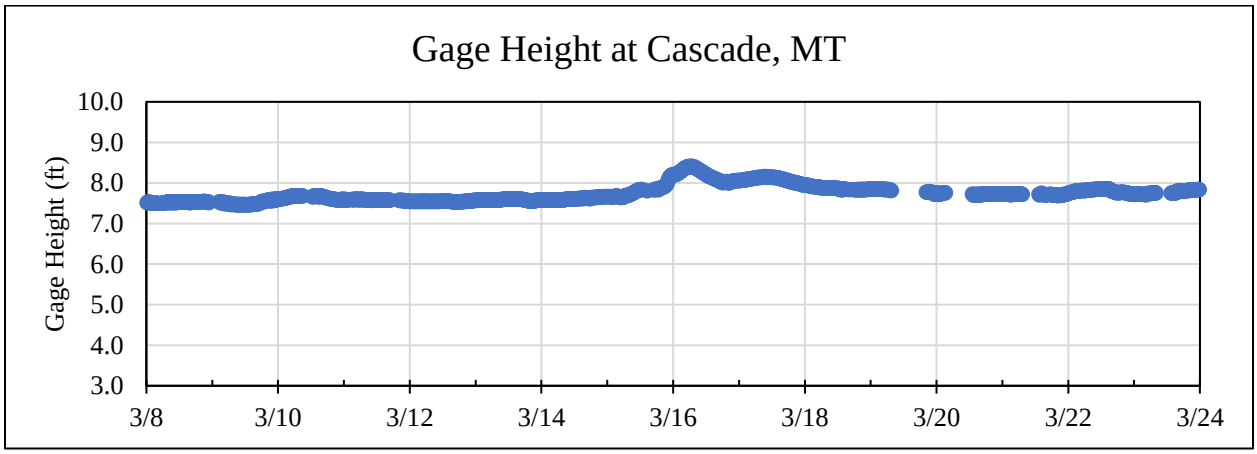

Figure 3.32 Gage height at Cascade for the event between Mar-14 to Mar-15, 2018 and Mar-17 to Mar-21, 2018

After analyzing the information above, the event between Mar-14 to Mar-15 is categorized as one of the special events, where there is flow decrease, when the gage height is decreased, thus the reason of flow decrease or the location of ice jam formation if formed cannot be predicted. And, for the other event Mar-17 to Mar-21, the possibility of ice jamming is in both the places, i.e., between Cascade and Ulm, and between Ulm and Morony, which have resulted in flow loss.

3.5.5 SPECIAL EVENT FROM MAR-26 TO MAR-27, 2018

The sixth flow loss event of 2018 is observed from 17:45 March 26 to 02:15 March 27. In this event there was a flow loss of 2000 cfs, in a span of 8.5 hours with a flow decrease rate of 235.8 cfs/hour (Table 3.21). After a small increase (~600 cfs) of discharge, discharge below Morony started to gradually decrease up to noon of March 28. Using a longer duration of flow loss, the flow decrease rate would be smaller than 235.8 cfs/hour. Figure 3.33 shows the discharge below Morony and air temperature between March-24 to April-1. The corresponding temperature at the flow loss event is fluctuating above the freezing point (Figure 3.33). The data analysis of the discharge below Holter shows a small decrease after Mar-25, but this decrease is not significant enough to cause the 2000 cfs decrease at Morony.

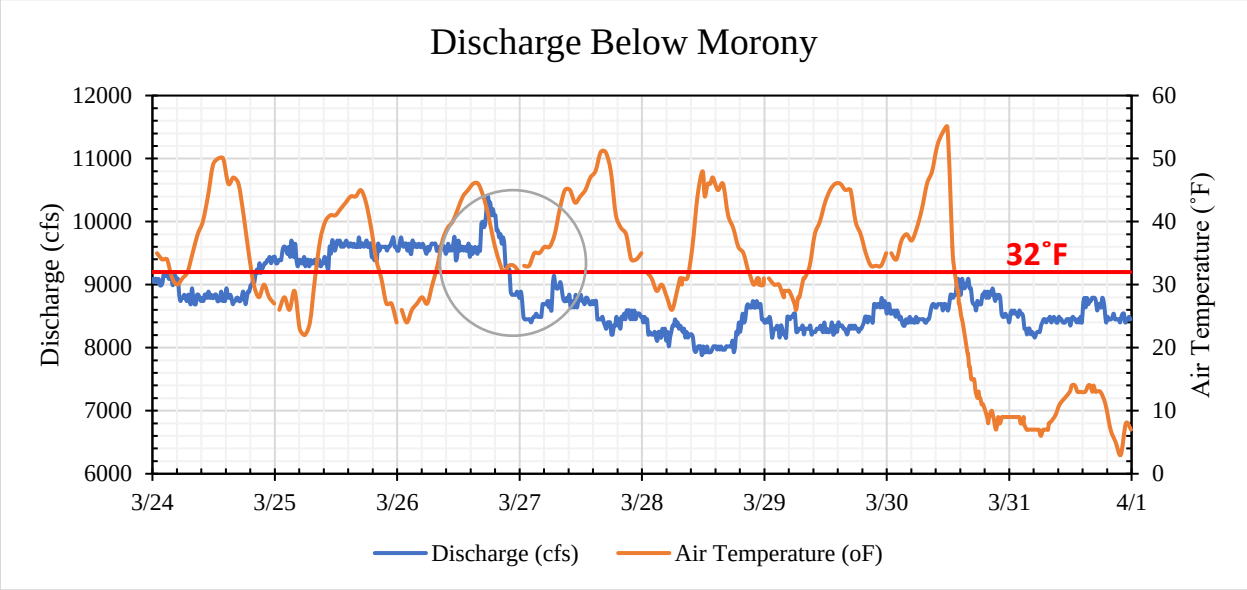

Figure 3.33 Discharge below Morony and air temperature at Great Falls for the event between Mar-26 to Mar-27, 2018

Table 3.21 Seventh flow loss event in 2018

Event 7	Time	Discharge
Beginning Time	3/26/18 17:45	10400
End Time	3/27/18 2:15	8400
Total Minutes	509	
Total Hours	8.5	
Flow Loss	2000	cfs
Flow decrease rate	235.8	cfs/hour

Looking at the gage height near Ulm in Figure 3.51 for the event of Mar-26 to Mar-27, there is a decrease in gage height of 0.3 ft, which indicates the possibility of ice jam breakup moving from

Ulm and Morony. The data analysis of gage height at Cascade shows no change on Mar-26. Hence, after analyzing the above graphs and conditions, the conclusion could be made that there was ice jam formation between Ulm and Morony.

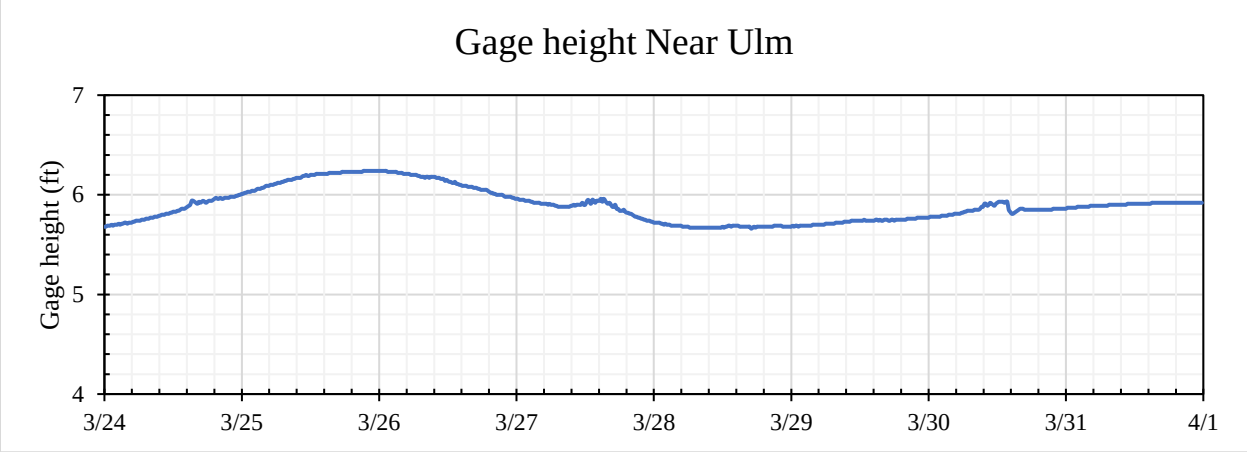

Figure 3.34 Gage height near Ulm for the event between Mar-26 to Mar-27, 2018

3.6 SPECIAL EVENT IN THE WINTER OF 2019

The time series of discharge and air temperature from Jan-01, 2019 to Mar-31, 2019 is plotted indicating the events with flow decrease on Figure 3.35. From the graph of discharge and air temperature with date (Figure 3.35), five events with high flow loss were identified. Characteristics of these special events are summarized in Table 3.16. The lowest air temperature during the flow decrease events ranged from 32 ^{o}F to -13 ^{o}F. The rate of flow decreases in these identified events ranged from 180.3 cfs/hour to 20.7 cfs/hour. The largest flow decrease observed was 7230 cfs from Mar-29 2018 to Mar-31, 2019, with the flow decrease rate of 180.3 cfs/hour.

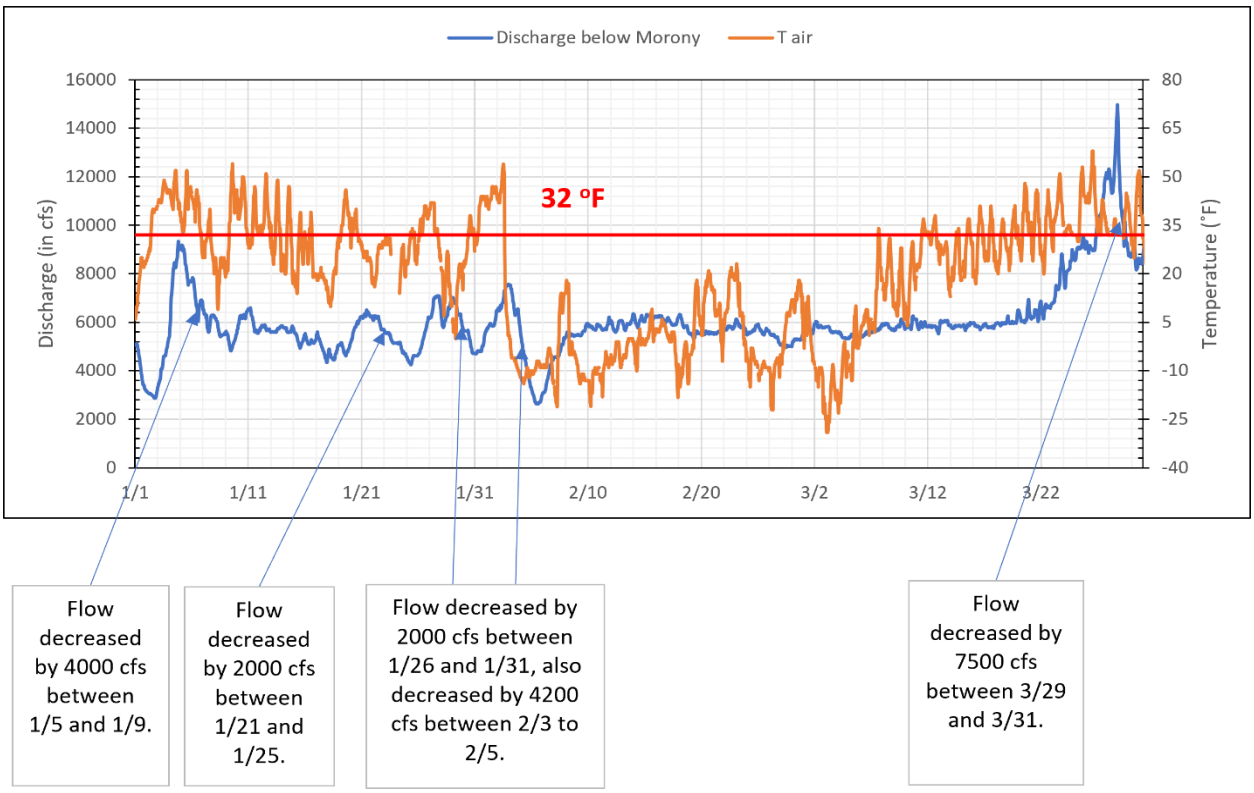

Figure 3.35 Discharge below Morony and air temperature at Great Falls from Jan-1 to Mar-31, 2019 showing events of high flow loss.

Table 3.22 Summary of flow decrease events observed from January 1 to March 31, 2019

S.N.	Date	Flow Decreased (cfs)	Temperature after drop	Flow decrease rate (cfs/hour)
1	Dec-30, 2018 to Jan-02, 2019	3680	6 °F	49.9
2	Jan-4 to Jan-9, 2019	4000	7 °F	41.7
3	Jan-21 to Jan-25, 2019	2120	20 °F	20.7
4	Jan-27 to Jan-28, 2019	1360	9 °F	115.7
5	Jan-29 to Jan-31, 2019	2330	0 °F	46.8
6	Feb-03 to Feb-05, 2019	5060	32 °F	91.2
7	Mar-28 to Mar-30, 2019	7230	32 °F	180.3

3.6.1 TWO EVENTS FROM DEC-30, 2018 TO JAN-09, 2019

The first event of flow loss in 2019 is observed from 16:30 December 30, 2018 to 18:15 January 02, 2019 where a flow loss of 3680 cfs is observed, in a span of around 3 days at a flow loss rate of 49.9 cfs/hour (Table 3.23). The air temperature reading was dropped down well below the freezing point to 6˚F, which gives a possibility of ice jam formation (Figure 3.36).

The second event of flow loss of 2019 is observed from 20: 45 January 04 to 13:00 January 09, 2019, with a flow loss of 4650 cfs, in a span of around 5 days at a flow loss rate of 41.4 cfs/hour. The air temperature reading was dropped down from around 50˚F to 10˚F (Figure 3.36). The data analysis of the discharge below Holter shows no change in discharge for both events.

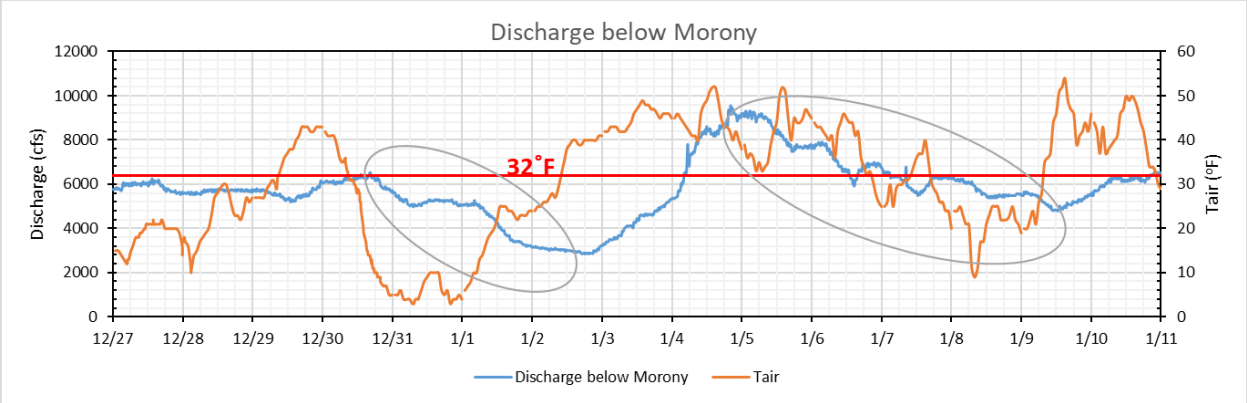

Figure 3.36 Discharge and air temperature for the event between Dec-30, 2018 to Jan-02, 2019 and Jan-04, 2019 to Jan-09, 2019

Table 3.23: First and second flow loss events in 2019.

Event 1	Time	Discharge
Beginning time	12/30/2018 16:30	6520
End time	1/2/2019 18:15	2840
Total Minutes	4424	
Total Hours	73.7	
Flow Loss	3680	cfs
Flow decrease rate	49.9	cfs/hour

Event 2	Time	Discharge
Beginning time	1/4/2019 20:45	9440
End time	1/9/2019 13:00	4790
Total Minutes	6734	
Total Hours	112.2	
Flow Loss	4650	cfs
Flow decrease rate	41.4	cfs/hour

The gage heights at Cascade and near Ulm from December 27, 2018 to January 11, 2019 is analyzed in Figure 3.37. Initially, during the first event from Dec-30 to Jan-02, there is a small spike (0.5 ft) seen in the gage height at Ulm on Dec-29, which may be due to ice jamming in a small amount in between Ulm and Morony, which resulted in the decrease in discharge in Dec-31 (Figure 3.36). And there is also a spike of gage height on Jan-02 of around 3 ft, which is an

indication of possible ice jam formation, which resulted in the second flow loss event from Jan-04 to Jan-09.

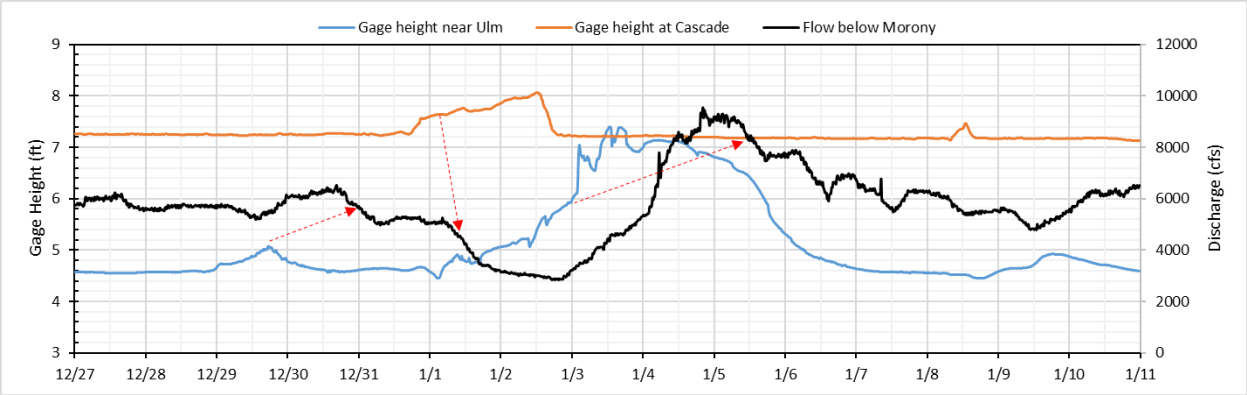

Figure 3.37 Gage heights at Cascade and near Ulm for two events from Dec-30, 2018 to Jan-02, 2019 and Jan-04 to Jan-09, 2019 with flow below Morony

The increase in gage height at Cascade can be due to ice jam formation between Cascade and Ulm. This water level increase was formed after the small of amount of ice jam was formed on Dec-29 between Ulm and Morony, which aided in the loss of discharge below Morony from Jan-01 to Jan-02 (flow was about constant on December 31). The temperature goes above 32˚F, after Jan-02, which made the ice melt, causing the discharge to increase below Morony from Jan-02 to Jan-05 (Figure 3.36). Once the temperature went down to 32˚F, after Jan-6, the melting stopped, and the discharge below Morony was again reduced (ice formation). The increment of gage height at Ulm on Jan-02 was large, and this supports ice jam formation in between Ulm and Morony, which resulted in the flow loss from Jan-04 to Jan-09 (Table 3.23).

3.6.2 THREE EVENTS FROM JAN-21 TO JAN-31, 2019

There are three flow-decrease events shown in Figure 3.38 with the discharge below Morony and air temperature from January 16 to February 03. The third event of flow loss of 2019 is observed from 02:00 January 21 to 08:30 January 25, which shows a flow loss of 2120 cfs in a span of 102.5 hours (Table 3.24), with a flow loss rate of 20.7 cfs/hour. The minimum air temperature during this event is at 20˚F.

The fourth event of flow loss of 2019 is observed from 18:15 January 27 to 06:00 January 28, which shows a flow loss of 1360 cfs, in a span of 11.8 hours at the flow loss rate of 115.7 cfs/hour (Table 3.24) and the air temperature decreases up to 9˚F.

The fifth event of flow loss is observed from 0:15 January 29 to 02:00 January 31which shows a flow loss of 2330 cfs, in a span of 49.8 hours at the flow loss rate of 46.8 cfs/hour (Table 3.24) and the air temperature goes to a minimum of 0˚F. All these readings show a possibility of ice jam formation for third, fourth, and fifth flow loss events. The data analysis of the discharge below Holter shows that the discharge below Holter does not show any significant change throughout three events.

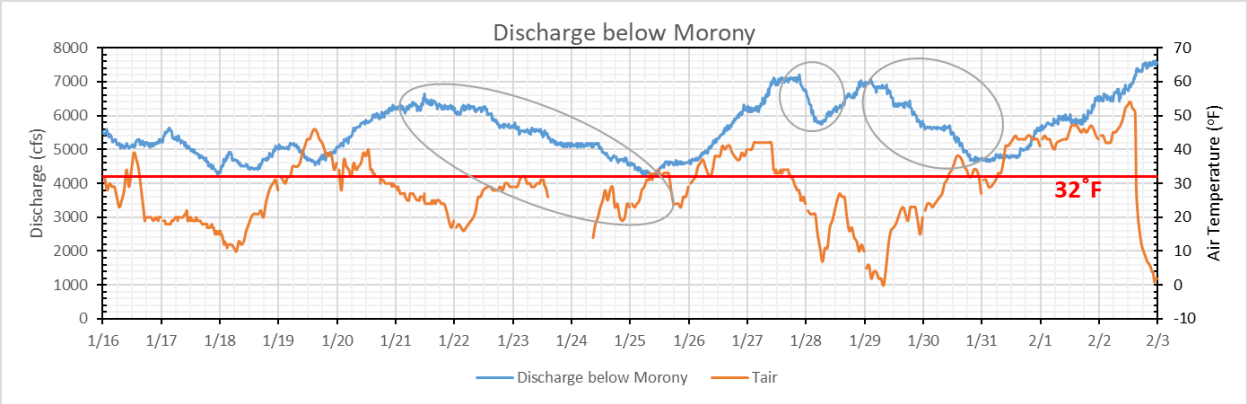

Figure 3.38 Discharge below Morony and air temperatrue at Great Falls for three events from Jan-21 to Jan-31, 2019

Table 3.24 Third, fourth, and fifth flow loss events in 2019

Event 3	Time	Discharge
Beginning Time	1/21/19 2:00	6310
nd Time	1/25/19 8:30	4190
Total Minutes	6149	
Total Hours	102.5	
Flow Loss	2120	cfs
Flow decrease rate	20.7	cfs/hour

Event 4	Time	Discharge
Beginning Time	1/27/2019 18:15	7110
End Time	1/28/19 6:00	5750
Total Minutes	705	
Total Hours	11.8	
Flow Loss	1360	cfs
Flow decrease rate	115.7	cfs/hour

Event 5	Time	Discharge
Beginning Time	1/29/2019 0:15	6980
End Time	1/31/19 2:00	4650

Total Minutes	2985	
Total Hours	49.8	
Flow Loss	2330	cfs
Flow decrease rate	46.8	cfs/hour

Figure 3.39 shows increases in gage height at the first two events near Ulm, which shows there were possibilities of ice jam formation in between Ulm and Morony. The gage height is increased by 1 ft before the flow loss event from Jan-21 to Jan-25, 3 ft before the flow loss event from Jan-27 to Jan-28 and decreased by 2ft before the event from Jan-29 to Jan-31, 2019. The decrease in gage height on Jan-29 could be ice jam breakup due to the rise in air temperature on Jan-29 which resulted in an increase in discharge after Jan-31 (Figure 3.38). Although there is a decrease in the gage height for the event from Jan-29 to Jan-31, as the gage height is increasing from Jan-23 to Jan-28, this caused the decrease in discharge below Morony.

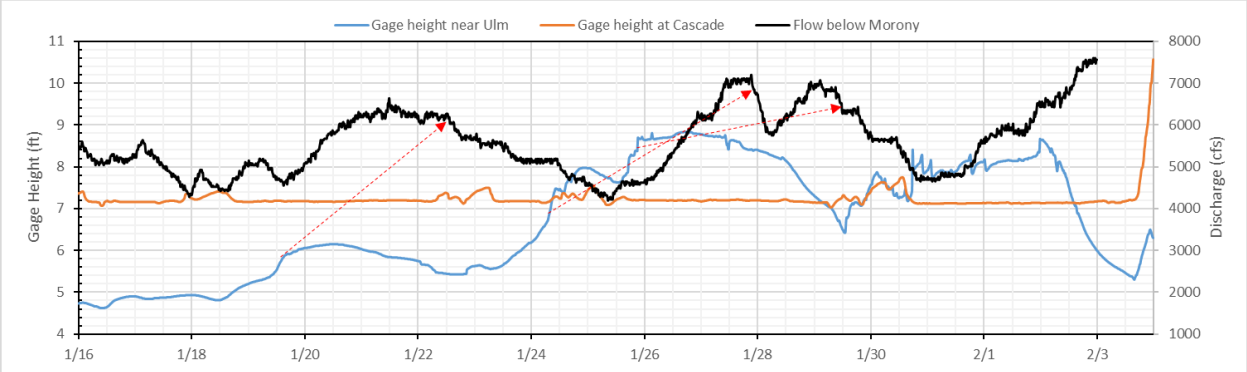

Figure 3.39 Gage heights at Cascade and near Ulm for three events from Jan-21 to Jan-25, Jan-27 to Jan-28, and Jan-31, 2019 with flow below Morony

The gage height at Cascade does not show any significant change to indicate there may be ice jam formation in between Ulm and Cascade, but the small spike in the events supports the claim that there may be ice jam formation in between Ulm and Morony. Thus, there were ice jam formations between Ulm and Morony during all these events.

3.6.3 SPECIAL EVENT FROM FEB-03 TO FEB-05, 2019

The sixth event of flow loss of 2019 is observed from 04:30 February 3 to 12:00 February 5, with a flow loss of 5060 cfs at the flow decrease rate of 91.2 cfs/hour (Table 3.25). Air temperature had a sharp drop on February 2 to -10 ^{o}F, reached -13 ˚F, and remained well below the freezing point of 32˚F for about 5 days (Figure 3.40), showing a possibility of ice cover/jam formation.

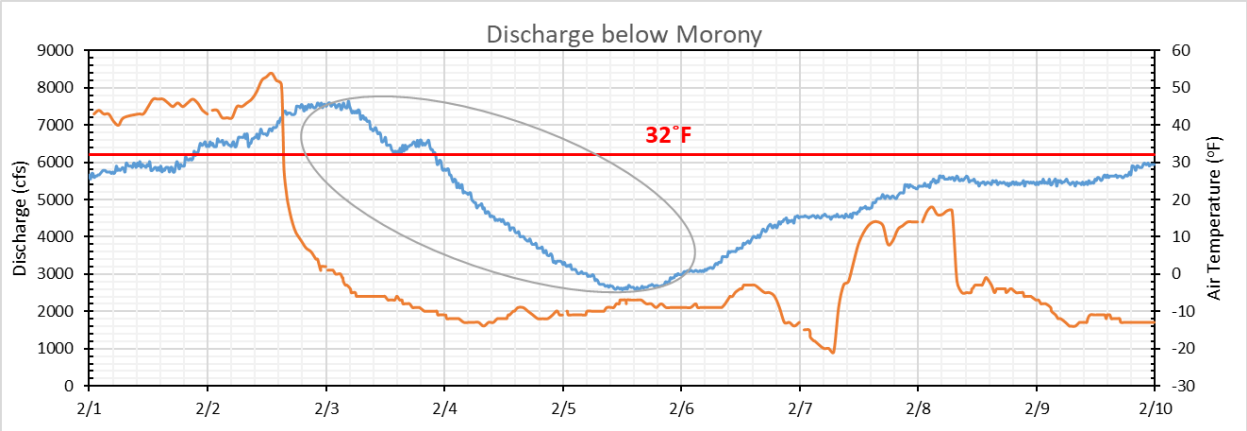

Figure 3.40 Discharge and air temperature for the event from Feb-03, 2019 to Feb-05, 2019.

Table 3.25 Sixth flow loss event in 2019.

Event 6	Time	Discharge
Beginning Time	2/3/19 4:30	7650
End Time	2/5/19 12:00	2590
Total Minutes	3330	
Total Hours	55.5	
Flow Loss	5060	cfs
Flow decrease rate	91.2	cfs/hour

The gage height data at Cascade and near Ulm are analyzed using Figure 3.41 to show that initially there is a decrease in gage height of around 3 ft near Ulm on February 2–3. The gradual increase of discharge below Morony on February 1–2 (Figure 3.40) when the air temperature was above the freezing point was the case of ice melting (jam breakup or release). The sharp drop of air temperature from afternoon of February 2 led ice cover/jam formation downstream Ulm to Great Falls. About 1 ft increase in gage height in late hours on Feb-03 (Figure 3.41) further indicated the ice jamming in between Ulm and Morony.

Also, the gage height at Cascade Figure 3.41 had about 4 ft of increase, but this does not explain the flow loss at the initial part of the event from Feb 3 to Feb 4 but explains the massive decrease in discharge below Morony from Feb 4 to Feb 5, which was due to ice jam formation between Cascade and Ulm.

Hence, this event can be categorized as the event where the ice jam for the initial flow loss from Feb 3 to Feb 4 was downstream Ulm, but the flow loss from Feb 4 to Feb 5 could be due to the ice jam location between Cascade and Ulm and between Ulm and Morony.

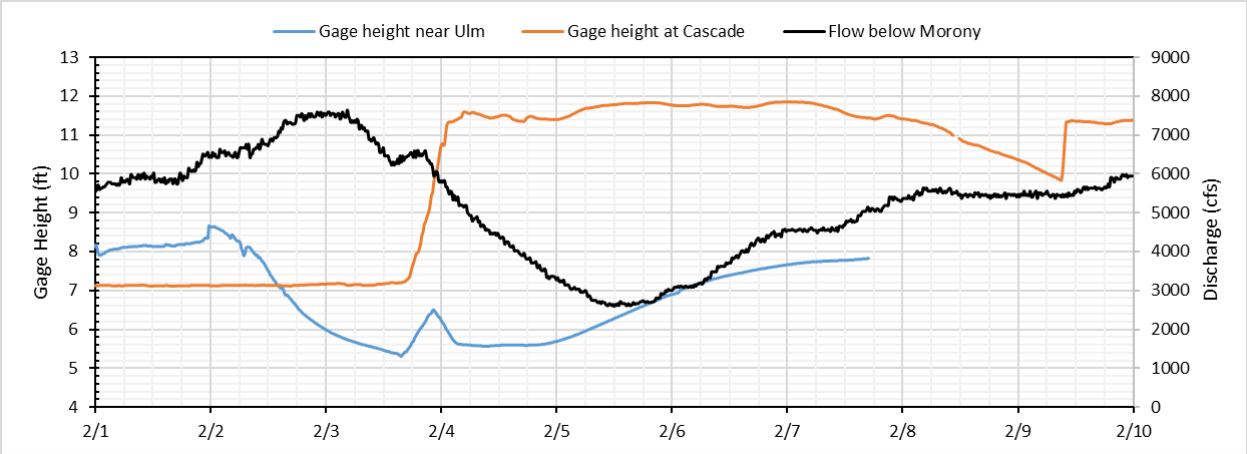

Figure 3.41 Gage height at Cascade and near Ulm for the event from Feb-03 to Feb-05, 2019 with flow below Morony.

3.6.4 SPECIAL EVENT FROM MAR-28 TO MAR-30, 2019

The seventh event of flow loss of 2019 is observed from 18:30 March 28 to 10:30 March 30 which shows a major loss in discharge, i.e., 7230 cfs, at a flow loss rate of 180.8cfs/hour (Table 3.26). The temperature reading corresponding to this event is at about the freezing point line of 32 ºF. (Figure 3.42).

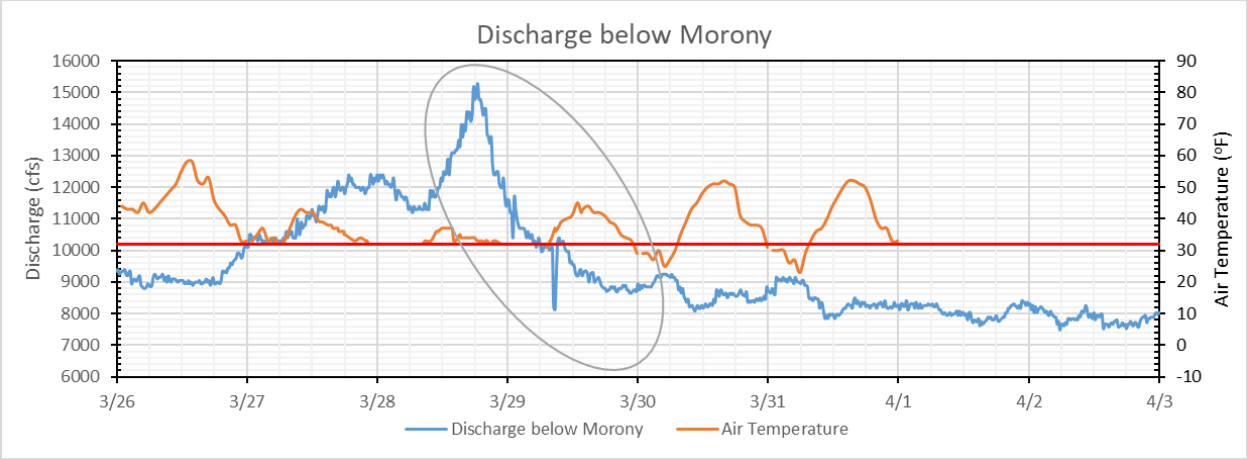

Figure 3.42 Discharge below Morony and air temperaure at Great Falls for the event from Mar-28 to Mar-30, 2019

Table 3.26 Seventh flow loss event in 2019

Event 7	Time	Discharge
Beginning Time	3/28/2019 18:30	15300
End Time	3/30/19 10:30	8070
Total Minutes	2399	
Total Hours	40.0	

Flow Loss	7230	cfs
Flow decrease rate	180.8	cfs/hour

The gage height at Cascade and near Ulm is analyzed from March 26 to April 3 (Figure 3.43). There is a rise in gage height by 2.6 ft at Ulm prior to the event from Mar 26 to Mar 27, Figure 3.43 showing the possibility of ice jam formation in between Ulm and Morony. The rise of gage height by 0.8 ft on Mar-26 and 0.4 ft on Mar-27 is noticed at Cascade, Figure 3.43 showing the possibility of ice jam formation in between Cascade and Ulm too. There is a rise (700 cfs) in discharge at Holter on Mar-28, which would not impact the discharge below Morony since the ice jam between Cascade and Ulm would block the flow increase to reach up to Morony.

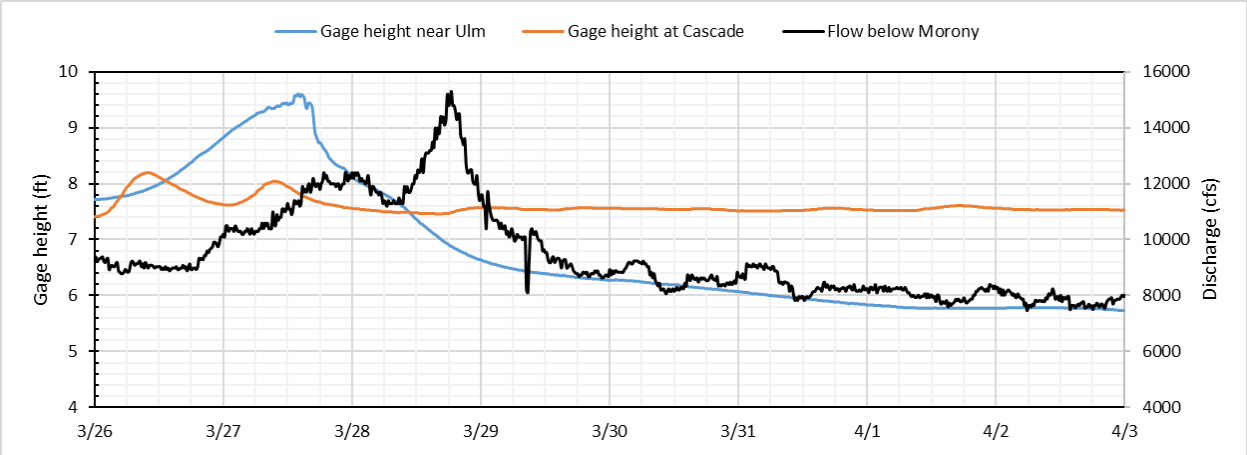

Figure 3.43 Gage height at Cascade and near Ulm for the event from Mar-28 to Mar-30, 2019 with flow below Morony.

Hence, there is ice jam formation seen in both the places with larger ice jamming seen between Ulm and Morony and relatively smaller ice jamming between Cascade and Ulm. Ice jamming at both these places could be the reason of such a huge flow loss.

3.7 SPECIAL EVENTS IN THE WINTER OF 2020

The time series of discharge and air temperature from Jan-01 to Mar-31, 2020 is plotted indicating the four events with flow decrease on Figure 3.44. The special event that are marked with high flow loss are shown in Table 3.27. The lowest air temperature during the flow decrease events ranged from 20 ^{o}F to -15 ^{o}F. The rate of flow decreases in these identified events ranged from 131.1 cfs/hour to 25.7 cfs/hour. The largest flow decrease observed was 2320 cfs which was observed from Mar-14 to Mar-18, 2020, with the flow decrease rate of 48.3 cfs/hour.

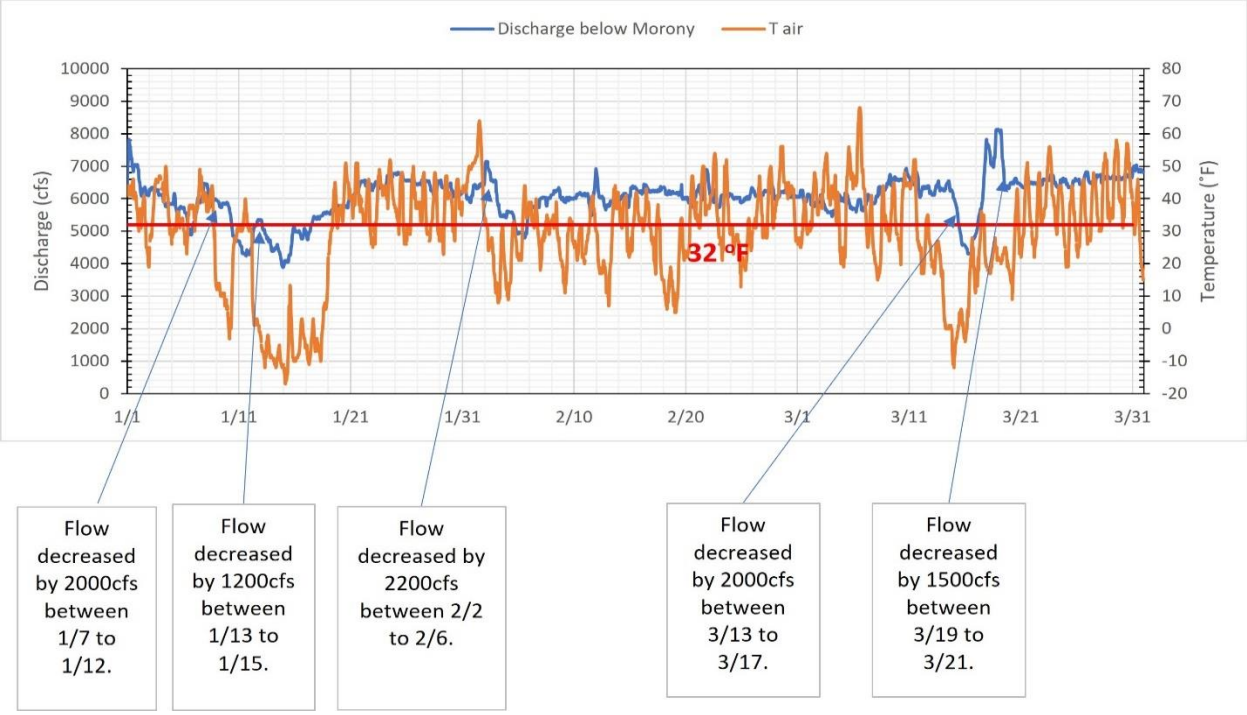

Figure 3.44 Discharge below Morony and air temperature at Great Falls from Jan-1 to Mar-31, 2020 showing events of high flow loss.

Table 3.27 Summary of flow decrease events observed between January 1 to March 31, 2020

S.N.	Date	Flow Decreased (cfs)	Temperature after drop	Flow decrease rate (cfs/hour)
1	Jan-8 and Jan-12	2020cfs	-2 ^{o}F	26.5
2	Jan-13 to Jan-14	1570cfs	-15 ^{o}F	33.8
3	Feb-2 to Feb-5	1810cfs	9 ^{o}F	25.7
4	Mar-14 to Mar-18	2320cfs	-11 ^{o}F	48.3
5	Mar-19	2030cfs	20 ^{o}F	131.1

3.7.1 SPECIAL EVENTS FROM JAN-1 TO JAN 14

The first event of the flow loss in 2020 was observed from 4:30 January 1 to 15:30 January 6, where the flow loss of 2970 cfs is observed at the rate of 26.5 cfs/hour. The second event of the flow loss in 2020 was observed from 3:00 January 8 to 16:45 January 12, where the flow loss of 2270 cfs is observed at the rate of 26.5 cfs/hour (Table 3.28), with the air temperature being reduced up to -2 ˚F during this event (Figure 3.45). In this event, initially the flow loss is gradual but gets steep after Jan-10, showing the possibility of ice jamming after Jan-10.

The third event of the flow loss in 2020 was observed from 01:15 January 13 to 23:45 January 14, where the flow loss of 1570 cfs was observed at the rate of 33.8 cfs/hour (Table 3.28), with air temperature going down to -15˚F (Figure 3.45). There is a possibility of ice cover formation seen in the second and third cases.

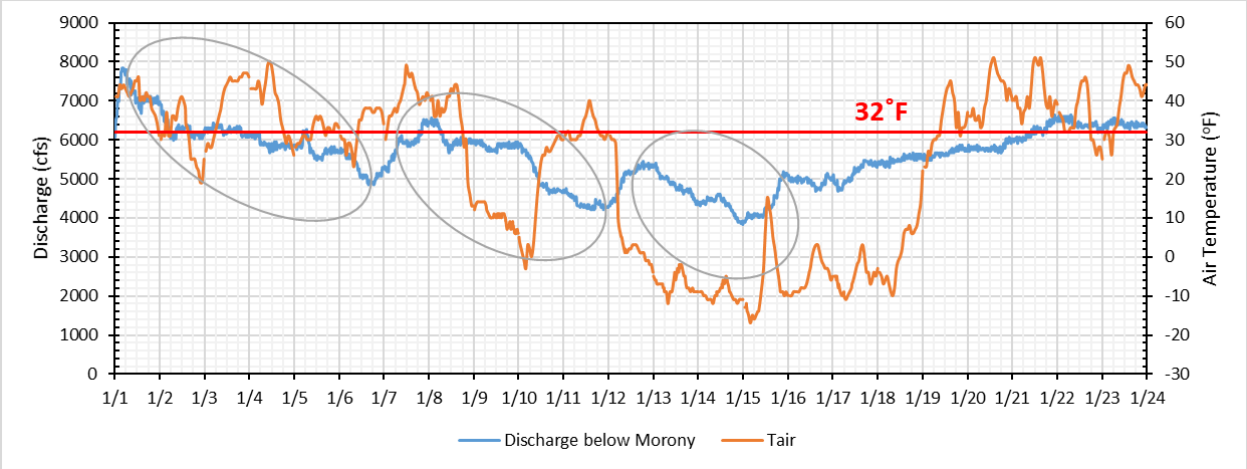

Figure 3.45 Discharge below Morony and air temperaure at Great Falls for the event from Jan-1 to Jan-14, 2020

Table 3.28 Second and third flow loss events in 2020.

Event 1	Time	Discharge
Beginning time	1/8/2020 3:00	6520
End time	1/11/2020 16:45	4250
Total Minutes	5144	
Total Hours	85.7	
Flow Loss	2270	cfs
Flow decrease rate	26.5	cfs/hour

Event 2	Time	Discharge
Beginning time	1/13/2020 1:15	5410
End time	1/14/2020 23:45	3840
Total Minutes	2790	
Total Hours	46.5	
Flow Loss	1570	Cfs
Flow decrease rate	33.8	cfs/hour

The gage height at Cascade and near Ulm (Figure 3.46) shows almost no change to account for the flow losses of the first and second events. Flow below Holter was increased by ~1200 cfs from January 9 to 11 that could explain the flow increase (~1200 cfs) below Morony on January 12. The

gage height increased after Jan-10, with an increase of around 4 ft near Ulm and 1 ft at Cascade, the third event is thus justified to be termed as due to ice jam formation between Ulm and Morony.

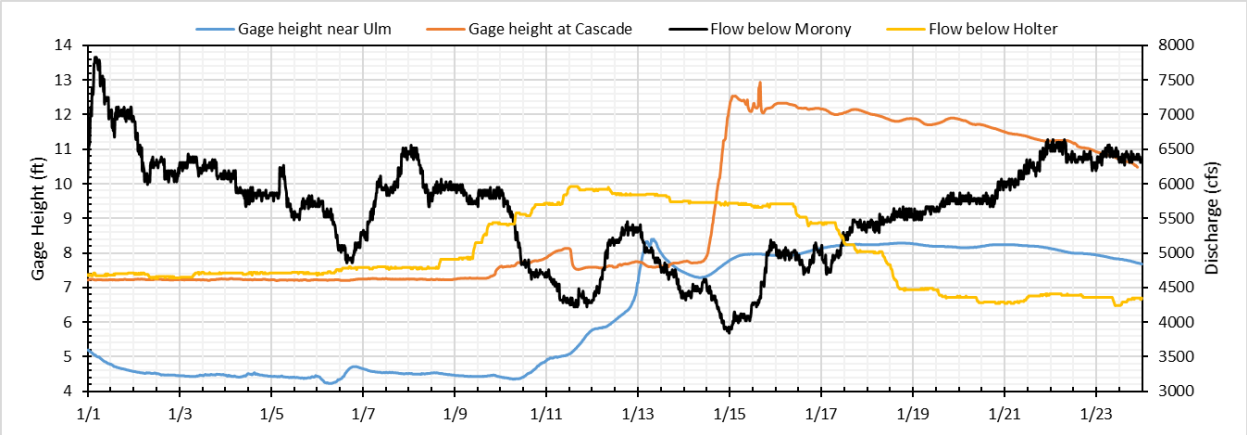

Figure 3.46 Gage height at Cascade and near Ulm for the event from Jan-1 to Jan-14, 2020 with flow data below Mornoy and below Holter.

There was a large increase in gage height (~5ft) at Cascade on January 14, Figure 3.46 clearly indicating the ice jam formation between Cascade and Ulm; but it would explain the flow loss from January 13 to 14 (third event). Strangely, the flow below Morony did not decrease but started to increase from January 15 to 22, which might be due to the high flow at Holter over six days plus air temperature above freezing after January 19 (Figure 3.45).

Hence, there was ice jam formation downstream Ulm on January 11–12 and between Cascade and Ulm on January 14 even though their connection with flow loss events is weak.

3.7.2 SPECIAL EVENT FROM FEB-2 TO FEB-5, 2020

The fourth event of flow loss in 2020 was observed from 17:30 February 02 to 16:00 February 05, where a flow loss of 1810 cfs within a span of around 3 days with a flow loss rate of 25.7 cfs/hour is observed (Table 3.29). The air temperature reading corresponding to this event is well below 32˚F, with a minimum air temperature showing 9 ºF, showing the possibility of ice cover/jam formation (Figure 3.47).

The gage height at Cascade shows almost no changes to account for the flow loss, thus indicating no ice jam formation between Cascade and Ulm. The discharge below Holter was almost no change before and during this event to account for the loss in discharge below Morony. Figure 3.48 shows there was a decrease (~1.8 ft) in gage height at Ulm prior to this event from Feb 01 to Feb 02 to indicate an ice jam breakup (since above freezing temperature since January 30). The ice jam could

move downstream and stop at certain location before Great Falls (minor impact to Ulm) to have a decrease in discharge noticed at Morony.

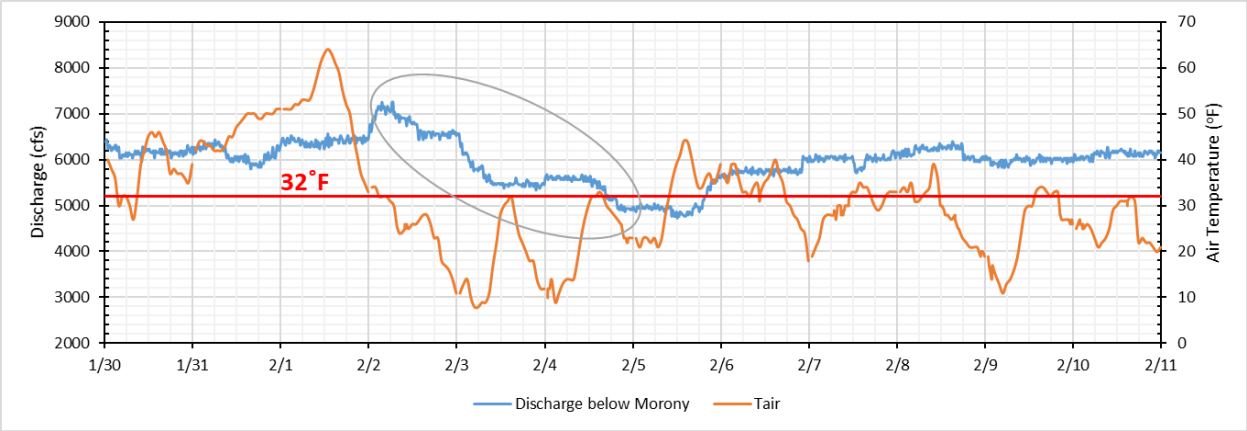

Figure 3.47 Discharge below Morony and air temperaure for the event from Feb-2 to Feb-5, 2020

Table 3.29: Fourth flow loss event in 2020

Event 3	Time	Discharge
Beginning time	2/2/20 17:30	6600
End time	2/5/20 16:00	4790
Total Minutes	4230	
Total Hours	70.5	
Flow Loss	1810	cfs
Flow decrease rate	25.7	cfs/hour

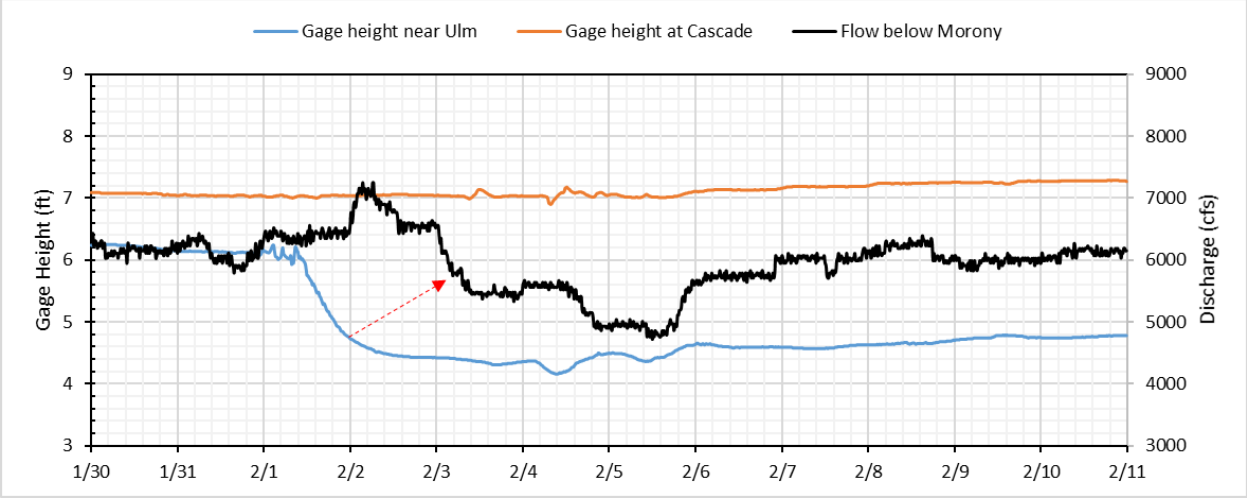

Figure 3.48 Gage height at Cascade and near Ulm for the envent from Feb-2 to Feb-5, 2020 with flow below Morony.

Hence, this event is categorized as a special event, as there is an anomaly seen in this event than the rest of the events, where although the gage height at Cascade is decreasing, indicating the meltdown of ice covers, the discharge at Morony is not increasing, but decreasing. Here the temperature readings and the amount of flow loss give the evidence of ice jam formation but the gage height at Ulm and Cascade shows otherwise.

3.7.3 SPECIAL EVENT FROM MAR-14 TO MAR-16 AND ON MAR-19, 2020

There are two events of flow loss shown in Figure 3.49. The first event is between Mar-14 to Mar-16, with flow loss of 2320 cfs within a span of 2 days, with a flow loss rate of 48.3 cfs/hour (Table 3.30). The temperature readings at this event shows a possibility of ice cover/jam formation.

The second event is on Mar-19 within the span of 15.5 hours, with a flow loss rate of 130.96 cfs/hour (Table 3.30). The temperature reading corresponding to this event also shows the possibility of ice cover/jam formation as it is well below the freezing point.

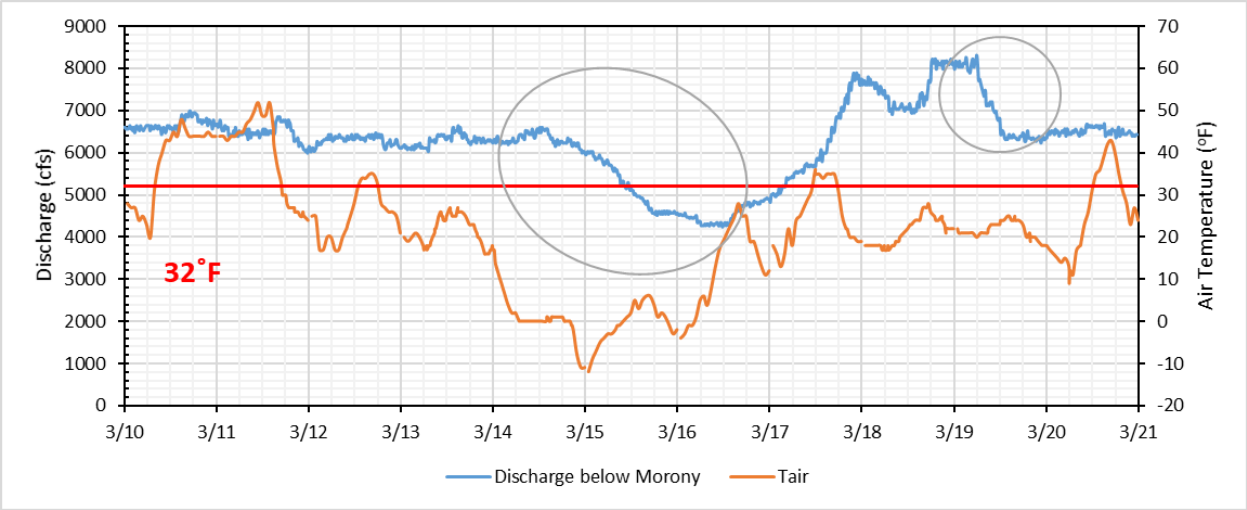

Figure 3.49 Discharge below Morony and air temperaure at Great Falls for the event from Mar-14 to Mar-16, 2020 and on Mar-19, 2020

Table 3.30 Fourth and fifth flow loss events in 2020

Event 4	Time	Discharge
Beginning time	3/14/20 12:45	6600
End time	3/16/20 12:45	4280
Total Minutes	2880	
Total Hours	48	
Flow Loss	2320	cfs
Flow decrease rate	48.3	cfs/hour

Event 5	Time	Discharge
Beginning time	3/19/20 6:00	8300
End time	3/19/20 21:30	6270
Total Minutes	930	
Total Hours	15.5	
Flow Loss	2030	cfs
Flow decrease rate	130.96	cfs/hour

Figure 3.50 shows there is increment in gage height at Ulm starting from Mar-15, thus indicating ice jam formation started from Mar-15 between Ulm and Morony. While the flow decrease started at Mar-14, the initial loss in flow at the first event is not due to ice jam formation. Also in the second event, there is no indication of ice jam formation seen at Ulm as there is no change in gage height prior to Mar-19. The gage height at Cascade has no evidence of ice jam formation in between Cascade and Ulm for the second event on Mar-19. The discharges below Holter had very less change at both these events that could cause the loss in discharge below Morony. However, the gage height at Great Falls had 2 ft increase on March 15 to indicate ice jam at Black Eagle Falls Dam for the flow loss at Morony.

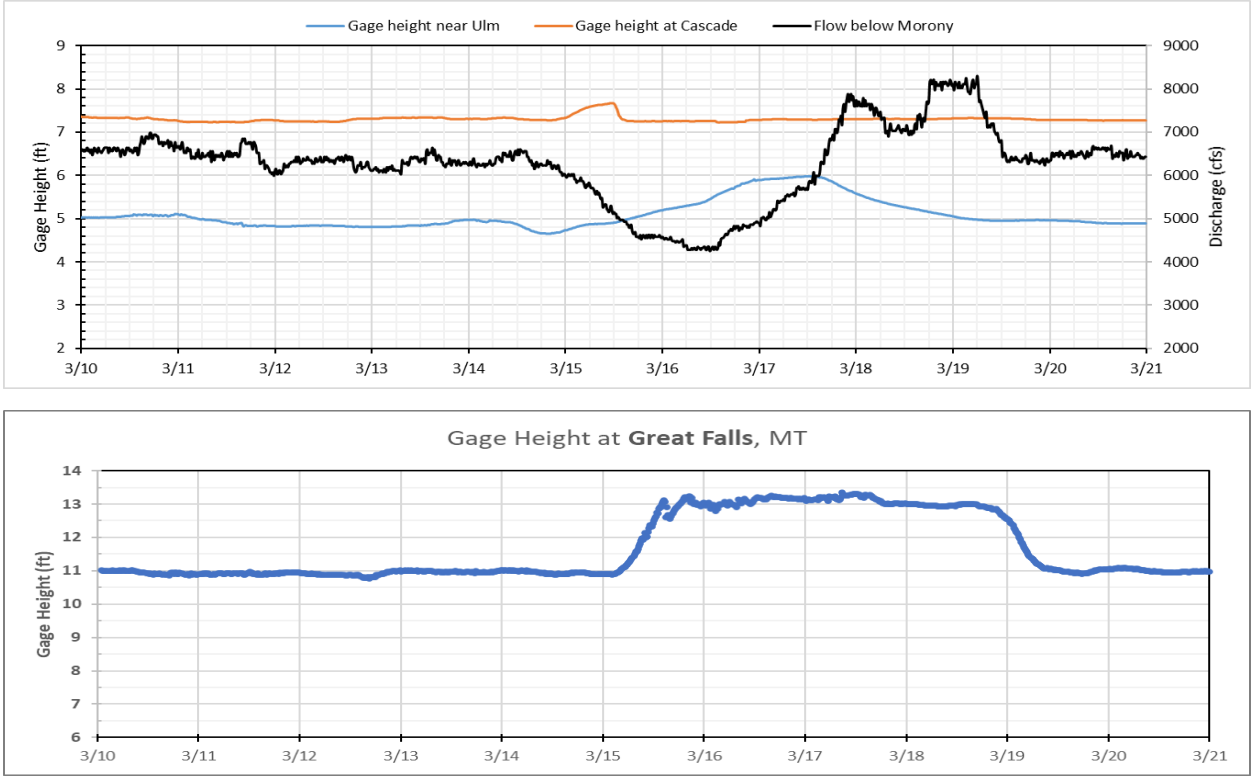

Figure 3.50 Gage height at Cascade, near Ulm and at Great Falls for the event from from Mar-14 to Mar-19 and on Mar-19, 2020 with flow below Morony.

Hence, the first event of flow loss from Mar-14 to Mar-16, 2020, was due to ice jam formation at Great Falls, but it is not clear why the flow below Morony increased from noon on March 16 to middle night on March 17. The second event of flow loss on Mar-19 could still be due to the ice jam at Black Eagle Falls Dam since the water level remained high for over 3 days at Great Falls.

3.8 SPECIAL EVENTS IN WINTER OF 2021

The time series of discharge and air temperature from Dec-01, 2020 to Mar-31, 2021 is plotted for four periods to show the eight events with flow decrease on Figure 3.51. The special events marked with high flow loss are summarized in Table 3.31. The lowest air temperature during the flow decreases events ranged from 12 ^{0}F to -16 ^{o}F. The rate of flow decreases in these identified events ranged from 54.2 cfs/hour to 7.6 cfs/hour. The largest flow decrease observed was 3050 cfs which was observed from Feb-5 to Feb-7, 2021, with the flow decrease rate of 54.2 cfs/hour.

Table 3.31 Summary of flow decrease events observed between Dec-1, 2020 to Mar-31, 2021

S.N.	Date	Flow Decreased (cfs)	Lowest temperature during drop	Flow decrease rate (cfs/hour)
1	Dec-11 to Dec-14	960	2 ^{o}F	11.1
2	Dec-17 to Dec-24	2270	12 ^{o}F	12.4
3	Dec-27 to Dec-30	1140	11 ^{o}F	14
4	Jan-17 to Jan-28	2010	7 ^{o}F	7.6
5	Feb-5 to Feb-7	3050	-16 ^{o}F	54.2
6	Feb-15 to Feb-18	970	-12 ^{o}F	11.1
7	Feb-25 to Mar-1	1090	11 ^{o}F	10.9
8	March -7	1590	25 ^{o}F	18.5

Time series of gage height at Cascade, near Ulm, and at Great Falls for four of the eight events are plotted in Figure 3.52 including flow time series below Holter and below Morony. The first event from December 11 to 14, 2020 most likely had ice formation to loss water under below freezing temperatures and had 1.8 ft of water level increase at Great Falls on December 14 and 15. The flow increase and decrease from December 14 to 24 is not explainable by gage height data, air temperature variation, and no flow change below Holter. The flow below Morony decreased by 2290 cfs from 15:00 January 13 to 16:30 January 28, 2021, with a few short periods of small flow increase. The flow decreases below Morony from January 13 to 22 can not be explained by changes of gage heights and flow below Holter; but the water level increase of 1.5 ft on January 22 at Great Falls supports the continuous decrease from January 22 to 28.

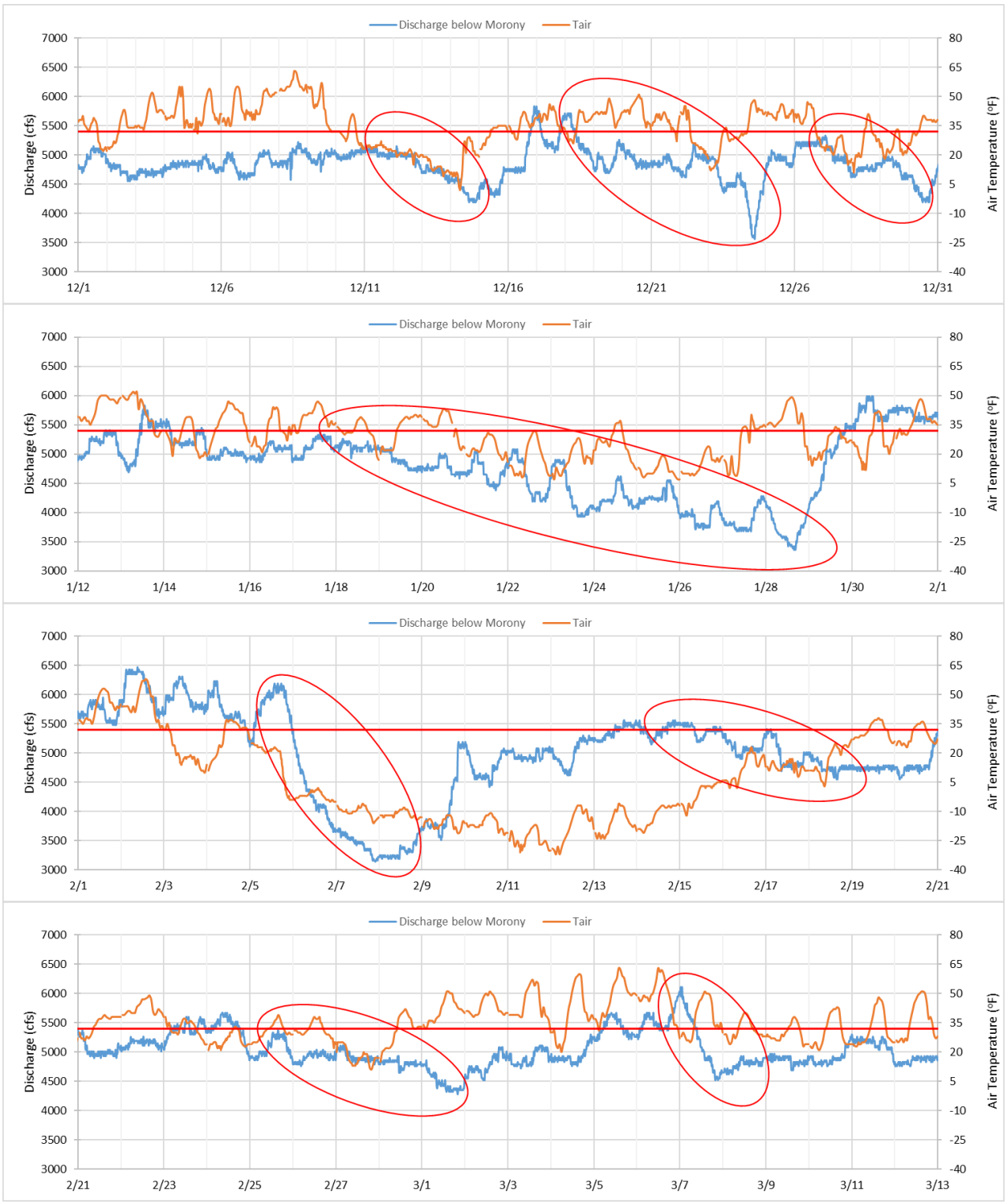

Figure 3.51 Discharge below Morony and air temperaure at Great Falls for eight events with large flow loss from December 1, 2020 to March 13, 2021.

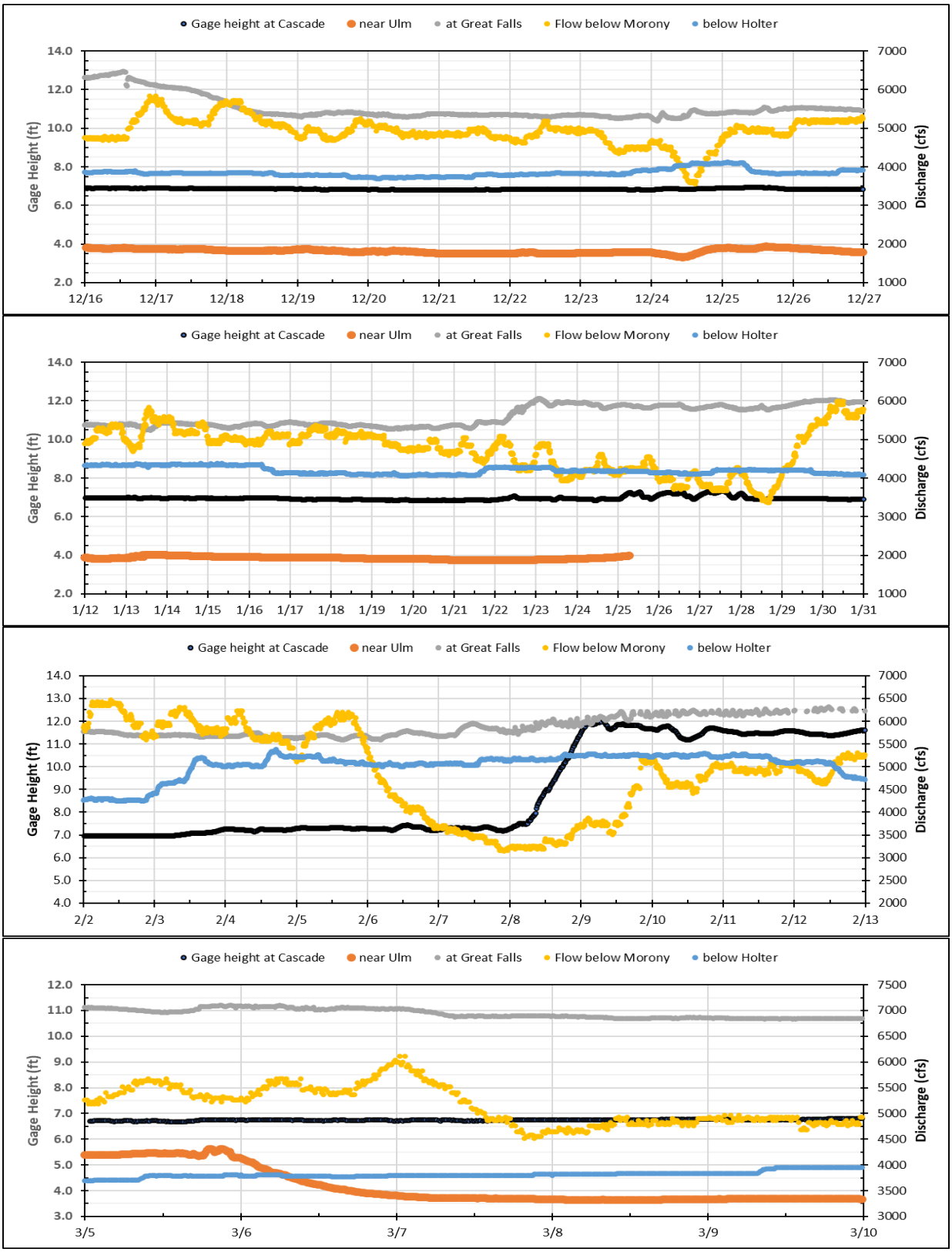

Figure 3.52 Gage height at Cascade, near Ulm and at Great Falls for the event from December 16, 2020, to March 10, 2021 with flow below Morony and below Holter.

A large flow decrease (3050 cfs) occurred from February 5 to 7, 2021, although flow below Holter increased ~800 cfs on February 3 and stayed at 505 cfs up to February 11, when air temperature dropped continuously from February 5 and reached -30 ^{o}F at 9:15 on February 11. This flow loss could be due to ice formation since there were no above freezing temperatures to melt any snow and ice to form ice run moving downstream. The flow decrease below Morony on March 7 could be due to an ice jam between Ulm and Great Falls when the decrease of 1.5 ft in water level at Ulm from March 6 to 7 with above freezing temperature indicated an ice jam broke/released, moved downstream but did not reach Great Falls (no water level change).

3.9 SPECIAL EVENTS IN WINTER OF 2022

The time series of discharge and air temperature from Dec-01, 2021 to Mar-31, 2022 is plotted for four periods to show the eight events with flow decrease on Figure 3.53. The special events marked with high flow loss are summarized in Table 3.32. The lowest air temperature during the flow decrease events ranged from 15 ^{o}F to -23 ^{o}F. The rate of flow decreases in these identified events ranged from 89.7 cfs/hour to 13.6 cfs/hour. The largest flow decrease observed was 2580 cfs which was observed from Dec-25 to Dec-27, 2021, with the flow decrease rate of 37.1 cfs/hour.

Table 3.32 Summary of flow decrease events observed between Dec-1, 2021 to Mar-31, 2022

S.N.	Date	Flow Decreased (cfs)	Lowest temperature during drop	Flow decrease rate (cfs/hour)
1	Dec-16 to Dec-17	1620	-11 ^{o}F	46.3
2	Dec-25 to Dec-27	2580	-23 ^{o}F	37.1
3	January 6	1300	-15 ^{o}F	89.7
4	Jan-18 to Jan-20	920	1 ^{o}F	13.6
5	Feb-2 to Feb 3	1970	-20 ^{o}F	44.5
6	Feb-21 to Feb-22	2400	-21 ^{o}F	55.8
7	Mar-3 to Mar-5	2490	15 ^{o}F	64.7
8	Mar-9 to Mar-10	1530	-4 ^{o}F	35

The first event from December 16 to 17, 2021 most likely had ice formation to loss water under below freezing temperatures and had a small continuous increase of water level at Great Falls from December 16 and 21 (Figure 3.54). About 2 ft increase of water level at Ulm on December 18 could not explain the flow increase after December 18 to 22. The flow decrease and increase from December 25 to 29 is not explainable by gage height data, air temperature variation, and small flow increase below Holter. The increase of 3.9 ft in water level on December 27 is not linked to

the increase of flow on December 28 and might link to 760 cfs decrease over a few hours on December 29, 2021. The flow below Morony decreased by ~2000 cfs from February 2 to 4, 2022 can be linked to ice jams between Ulm and Great Falls (> 2 ft water level decrease at Ulm) and between Cascade and Ulm (~2.8 ft water level increase at Cascade on February 2). The flow decrease of 2150 cfs below Morony (Figure 3.54c) from February 21 to 22 could be due to ice jams near Grate Falls (0.5 ft increase in water level at early hours on February 21) and between Ulm (1.5 ft increase in water level) and Great Falls. However, about 3.5 ft increase of water level at Cascade from February 22 to 23, 2022, could not explain the flow increase below Morony from February 23 to 26 with below freezing air temperatures. The flow decrease below Morony from March 3 to 4 (Figure 3.54d) can be due to an ice jam between Ulm and Great Falls when the decrease of 2.0 ft in water level at Ulm on March 3 with above freezing temperature after February 28 indicated an ice jam broke/released, moved downstream but did not reach Great Falls (no water level change). The decrease of 1380 cfs below Morony from March 9 to 10 could be due to ice formation below freezing temperatures (Figure 3.53d) but not be explained by gage height increase of ~2.8 ft at Ulm on March 10, 2022 (Figure 3.54d).

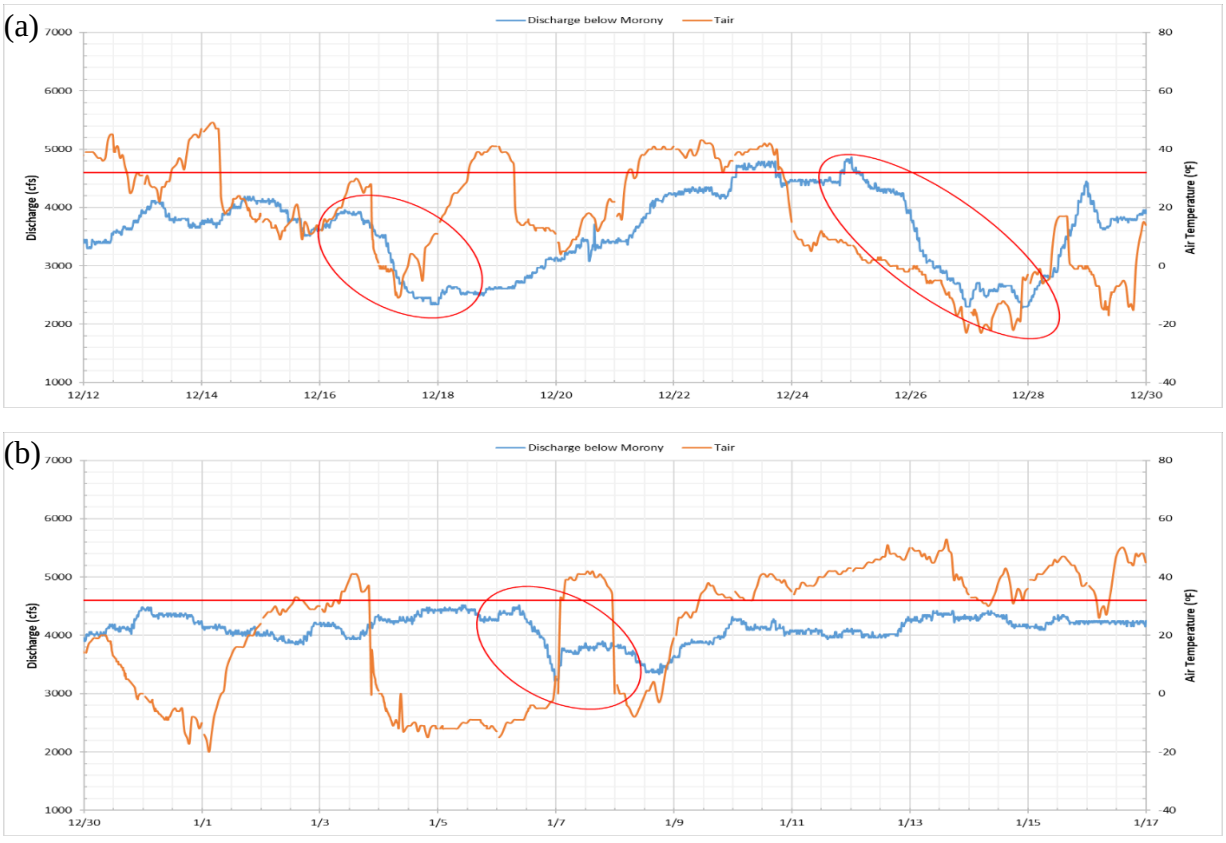

Figure 3.53 Discharge below Morony and air temperaure at Great Falls for eight events with large flow loss from December 12, 2021 to March 15, 2022.

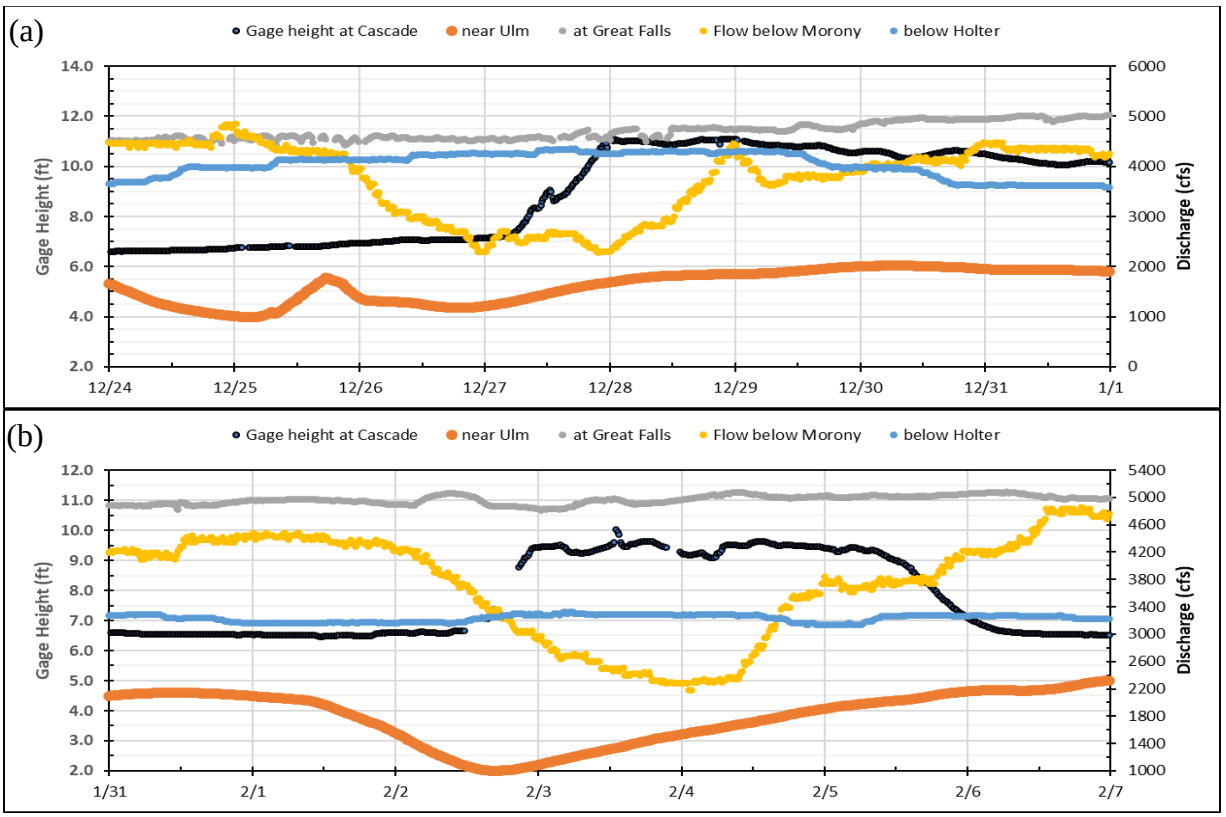

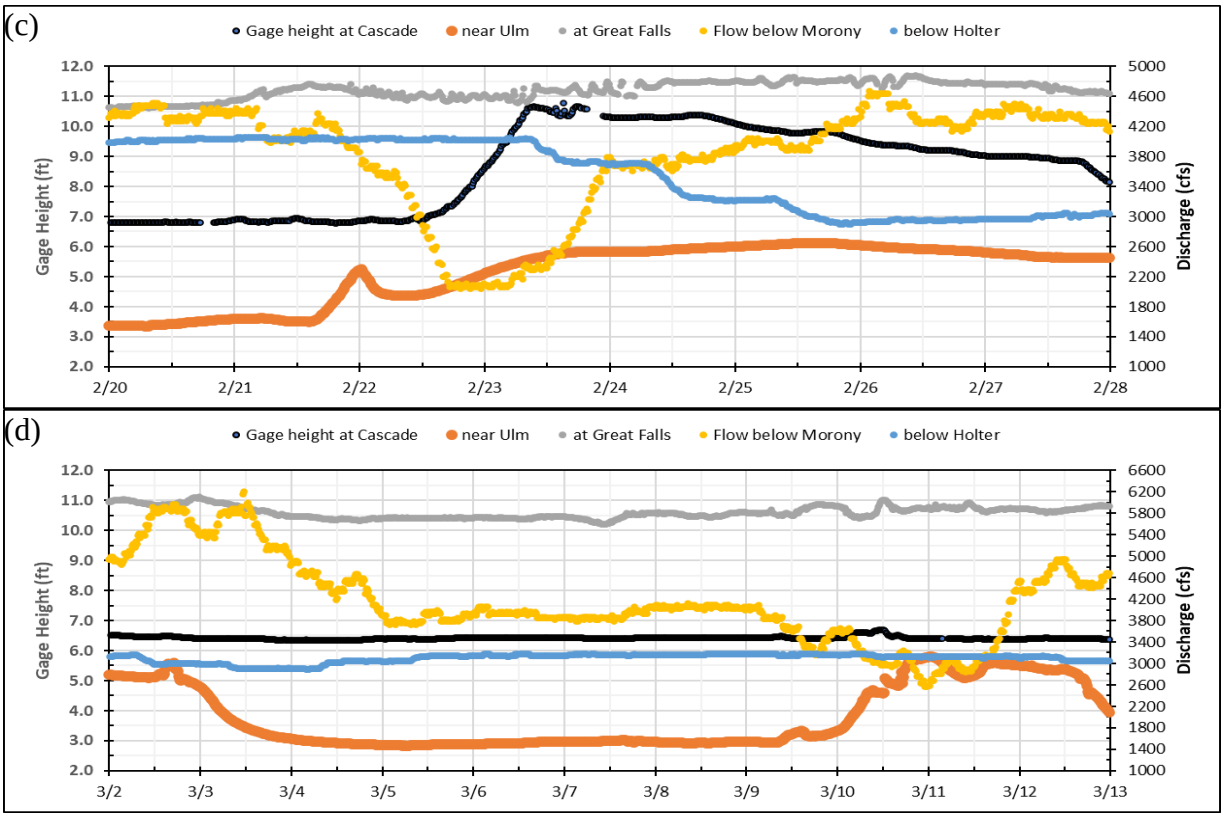

Figure 3.54 Gage height at Cascade, near Ulm and at Great Falls for the event from December 24, 2021, to March 13, 2022, with flow below Morony and below Holter.

3.10 CATEGORIZATION OF FLOW LOSS EVENTS BASED ON THE LOCATION OF ICE JAM FORMATION

Table 3.33 shows the locations where ice jamming events up to 2020 were estimated to occur after analyzing the discharge, air temperature, and gage height data. The events where flow loss is seen without evidence of ice jamming are kept under no ice jamming. These are the events where flow loss is noticed initially, but after analyzing the available data, classified as events without ice jamming. The events where the ice jamming was estimated to occur between Cascade and Ulm are classified under “Ice jam between Cascade and Ulm”. They are classified so after analyzing the discharge loss in Ulm, the change in gage height noticed at Cascade after the ice jamming between Cascade and Ulm, or the major loss in air temperature, or all. Similarly, the “Ice jam between Ulm and Morony” classifies those events where the ice jam is predicted to occur between Ulm and Morony. They are classified as such after analyzing the discharge loss in Morony, or the increase in gage height at Ulm and Cascade, the major loss in air temperature, or all.

Table 3.33 Classification of flow loss events based on the estimated location of ice jamming and events with no ice jamming.

No ice jamming	Ice jam between Cascade and Ulm	Ice jam between Ulm and Morony
1. Dec-21 to Dec-25, 2016	1. Dec-20 to Dec-27, 2015 2. Dec-25 to Dec-28, 2016. 3. Jan-10 to Jan-13, 2018 4. Mar-17 to Mar-21, 2018 5. Feb-3 to Feb-5, 2019 6. Mar-28 to Mar-30, 2019 7. Jan-8 to Jan-11, 2020 8. Jan-13 to Jan-14, 2020	1. Dec-15 to Dec-17, 2015 2. Feb-4 to Feb-5, 2018 3. Feb-9 to Feb-11, 2018 4. Mar-26 to Mar-27, 2018 5. Dec-30 to Jan-2, 2019 6. Jan-4 to Jan-9, 2019 7. Jan-21 to Jan-25, 2019 8. Jan-27 to Jan-28, 2019 9. Jan-29 to Jan-31, 2019 10. Mar-14 to Mar-16, 2020 11. Dec-20 to Dec-27, 2015 12. Feb-3 to Feb-5, 2019 13. Mar-28 to Mar-30, 2019 14. Jan-13 to Jan-14, 2020

Table 3.33 precisely predicts the place of ice jamming based on the location where data are analyzed, i.e., Cascade, Ulm and Morony. Table 3.34 categorizes the ice jamming events based on the location of ice jamming, but here the precise location could not be predicted. The events where the location of the ice jamming could not be determined precisely and concluded that the event must have occurred somewhere between the upstream (Holter) and downstream (Morony) of the study area, are classified under “Ice jam between Holter and Morony”. The events where the location of ice jamming was identified to occur between Cascade and Morony but could not be precisely told if it was upstream or downstream of Ulm are classified under "Ice jam between Cascade and Morony”. All the other events of flow where the reason of flow loss was not determined and could be speculated as an event due to ice jamming were categorized as “Special events”. As the change in river discharge is a dynamic process and many factors come into play, it is difficult to identify the cause of loss in discharge with available data, thus this category was created to classify those events.

Table 3.34 Classification of flow loss events based on the predicted location of ice jamming and special events.

Ice jam between Holter and Morony	Ice jam between Cascade and Morony	Special events
1. Dec-28 to Dec-31, 2014	1. Jan-27 to Jan-29, 2015 2. Jan-31, to Feb-2, 2015 3. Mar-2 to Mar-3, 2015	1. Feb-18 to Feb-20, 2018 2. Mar-14 to Mar-15, 2018 2. Feb-2 to Feb-5, 2020

	4. Jan-30 to Jan-31, 2016 5. Dec-7 to Dec-8, 2016 6. Dec-16 to Dec-19, 2016.	3. Mar-19, 2020

3.11 FLOW ANALYSIS SPREADSHEET

For the analysis of the ice jam events, with discharge, air temperature and gage height with ease, Dr. Xing Fang and Xueqian Li (Student, Auburn University) developed a spreadsheet with VBA (Visual Basic for Application) code. The spreadsheet allows users to get USGS gage station data (streamflow, stage height, and water temperature) for nine USGS gage stations (Table 3.1) from Holter to Great Falls.

The user can specify the time period, and USGS gage station of which the data is desired. Also, the user can download data for multiple locations or a single location at a the same time. Since, the USGS water data is getting updated on the website from January 1, 2023, two versions of the spreadsheet are prepared. The user interface of the spreadsheet is shown in Figure 3.55.

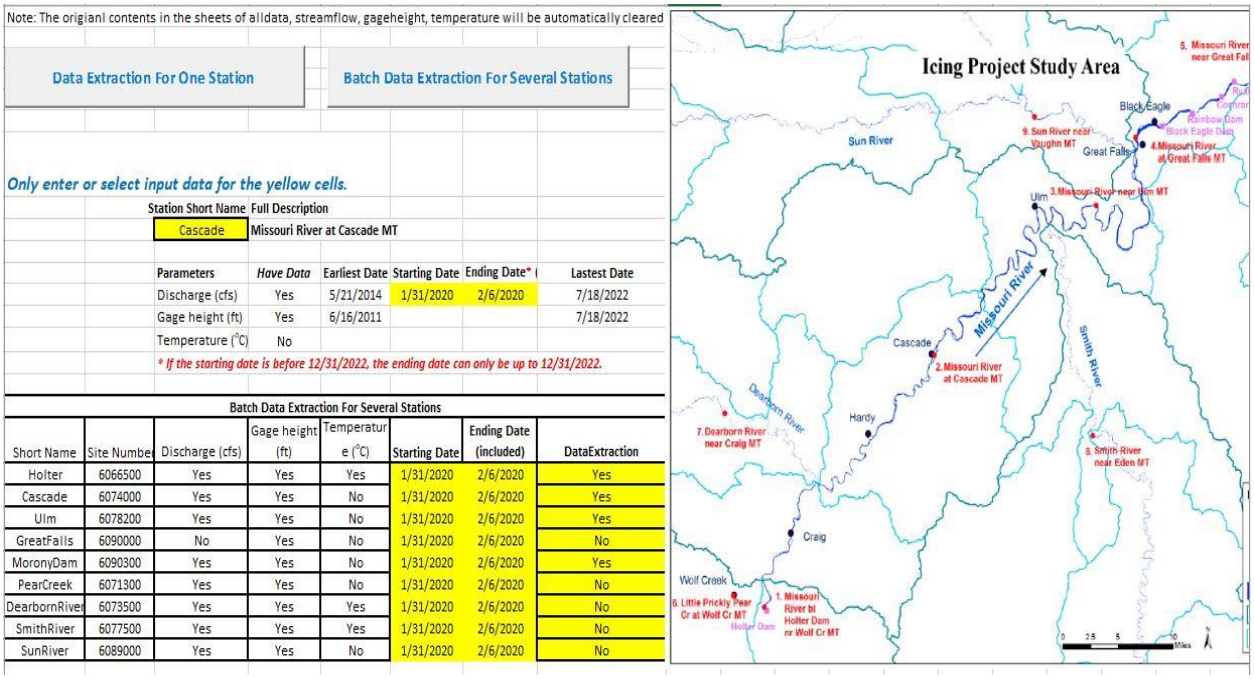

Note: The original contents in the sheets of alldata, streamflow, gageheight, temperature will be automatically cleared

Data Extraction For One Station | Batch Data Extraction For Several Stations

Only enter or select input data for the yellow cells.

Station Short Name	Full Description
Cascade	Missouri River at Cascade MT

Parameters	*Have Data*	Earliest Date	Starting Date	Ending Date*	Lastest Date
Discharge (cfs)	Yes	5/21/2014	1/31/2020	2/6/2020	7/18/2022
Gage height (ft)	Yes	6/16/2011			7/18/2022
Temperature (°C)	No				

** If the starting date is before 12/31/2022, the ending date can only be up to 12/31/2022.*

Batch Data Extraction For Several Stations

Short Name	Site Number	Discharge (cfs)	Gage height (ft)	Temperature (°C)	Starting Date	Ending Date (included)	DataExtraction
Holter	6066500	Yes	Yes	Yes	1/31/2020	2/6/2020	Yes
Cascade	6074000	Yes	Yes	No	1/31/2020	2/6/2020	Yes
Ulm	6078200	Yes	Yes	No	1/31/2020	2/6/2020	Yes
GreatFalls	6090000	No	Yes	No	1/31/2020	2/6/2020	No
MoronyDam	6090300	Yes	Yes	No	1/31/2020	2/6/2020	Yes
PearCreek	6071300	Yes	Yes	No	1/31/2020	2/6/2020	No
DearbornRiver	6073500	Yes	Yes	Yes	1/31/2020	2/6/2020	No
SmithRiver	6077500	Yes	Yes	Yes	1/31/2020	2/6/2020	No
SunRiver	6089000	Yes	Yes	No	1/31/2020	2/6/2020	No

Figure 3.55 User interface of flow analysis spreadsheet with USGS gage station map from Holter to Great Falls.

The spreadsheet displays the discharge, water temperature, and gage height data and graphs along the date in the separate worksheets for each station. The spreadsheet is coupled with the weather data analysis spreadsheet which imports data from the visual crossing website. The visual crossing

website allows users to download historical and forecast weather data of the desired location. Figure 7.2 in Chapter 7 shows the user interface of the visual crossing excel spreadsheet, which imports data from the website to spreadsheet.

The final data analysis spreadsheet thus helps for analyzing any particular events, without the hassle of going through searching every event, and graphing data for all gage stations to predict ice jamming for a single event, as it recognizes such events and plots those on a separate workbook. Figure 3.62 shows the workbook showing freezing event analysis of historical data, which is recognized by the flow analysis spreadsheet, where the temperature between this period is below 32^{o}F and chance of ice jamming is high. In addition, this spreadsheet also prepares the weather data to be ready for input into water temperature modeling in HEC-RAS.

3.11.1 SPECIAL EVENTS ANALYSIS USING FLOW ANALYSIS SPREADSHEET

The flow analysis spreadsheet prepared by Dr. Xing Fang (as discussed in 3.11) is used for analyzing the flow loss event from March 14 to March 16, 2020. For the analysis of the event, hydrometric data available from March 11 to March 24, 2020 was analyzed for the USGS gaging stations at Holter, Cascade, Ulm, below Morony at Missouri River, and Sun River.

The discharge, gage height, and water temperature data available on the USGS gage station at Holter is displayed in the flow analysis spreadsheet as Figure 3.56. The discharge and gage height at Holter only have small variations: < 350 cfs change on flow rate and < 0.2 ft change on water level. Also the water temperature at Holter was ~36–37 ^{o}F and above the freezing temperature of 32 ^{o}F. The flow loss identified in this event is seen on Figure 3.57, which shows the discharge and gage height data at below Morony dam. A flow loss of 2320 cfs (Table 3.30) is noticed from March 14 at 12:45 to March 16 at 12:45, 48 hours of flow decrease and water level drop (0.5 ft). There was also a flow drop of 2030 cfs on March 19 over 15.5 hours (Figure 3.56 and Table 3.30).

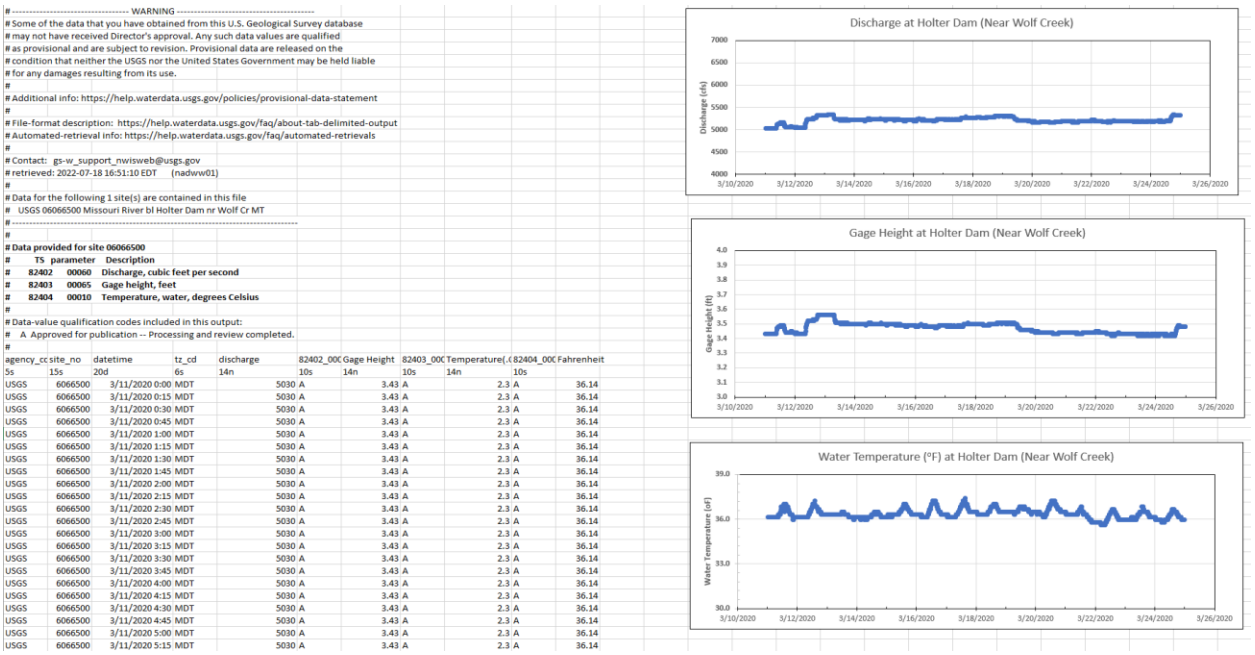

---------- WARNING ----------
Some of the data that you have obtained from this U.S. Geological Survey database
may not have received Director's approval. Any such data values are qualified
as provisional and are subject to revision. Provisional data are released on the
condition that neither the USGS nor the United States Government may be held liable
for any damages resulting from its use.
#
Additional info: https://help.waterdata.usgs.gov/policies/provisional-data-statement
#
File-format description: https://help.waterdata.usgs.gov/faq/about-tab-delimited-output
Automated-retrieval info: https://help.waterdata.usgs.gov/faq/automated-retrievals
#
Contact: gs-w_support_nwisweb@usgs.gov
retrieved: 2022-07-18 16:51:10 EDT (nadww01)
#
Data for the following 1 site(s) are contained in this file
USGS 06066500 Missouri River bl Holter Dam nr Wolf Cr MT

#
Data provided for site 06066500
TS parameter Description
82402 00060 Discharge, cubic feet per second
82403 00065 Gage height, feet
82404 00010 Temperature, water, degrees Celsius
#
Data-value qualification codes included in this output:
A Approved for publication -- Processing and review completed.
#

agency_cc	site_no	datetime	tz_cd	discharge	82402_00(	Gage Height	82403_00(	Temperature(.(	82404_00(	Fahrenheit
5s	15s	20d	6s	14n	10s	14n	10s	14n	10s	
USGS	6066500	3/11/2020 0:00	MDT	5030	A	3.43	A	2.3	A	36.14
USGS	6066500	3/11/2020 0:15	MDT	5030	A	3.43	A	2.3	A	36.14
USGS	6066500	3/11/2020 0:30	MDT	5030	A	3.43	A	2.3	A	36.14
USGS	6066500	3/11/2020 0:45	MDT	5030	A	3.43	A	2.3	A	36.14
USGS	6066500	3/11/2020 1:00	MDT	5030	A	3.43	A	2.3	A	36.14
USGS	6066500	3/11/2020 1:15	MDT	5030	A	3.43	A	2.3	A	36.14
USGS	6066500	3/11/2020 1:30	MDT	5030	A	3.43	A	2.3	A	36.14
USGS	6066500	3/11/2020 1:45	MDT	5030	A	3.43	A	2.3	A	36.14
USGS	6066500	3/11/2020 2:00	MDT	5030	A	3.43	A	2.3	A	36.14
USGS	6066500	3/11/2020 2:15	MDT	5030	A	3.43	A	2.3	A	36.14
USGS	6066500	3/11/2020 2:30	MDT	5030	A	3.43	A	2.3	A	36.14
USGS	6066500	3/11/2020 2:45	MDT	5030	A	3.43	A	2.3	A	36.14
USGS	6066500	3/11/2020 3:00	MDT	5030	A	3.43	A	2.3	A	36.14
USGS	6066500	3/11/2020 3:15	MDT	5030	A	3.43	A	2.3	A	36.14
USGS	6066500	3/11/2020 3:30	MDT	5030	A	3.43	A	2.3	A	36.14
USGS	6066500	3/11/2020 3:45	MDT	5030	A	3.43	A	2.3	A	36.14
USGS	6066500	3/11/2020 4:00	MDT	5030	A	3.43	A	2.3	A	36.14
USGS	6066500	3/11/2020 4:15	MDT	5030	A	3.43	A	2.3	A	36.14
USGS	6066500	3/11/2020 4:30	MDT	5030	A	3.43	A	2.3	A	36.14
USGS	6066500	3/11/2020 4:45	MDT	5030	A	3.43	A	2.3	A	36.14
USGS	6066500	3/11/2020 5:00	MDT	5030	A	3.43	A	2.3	A	36.14
USGS	6066500	3/11/2020 5:15	MDT	5030	A	3.43	A	2.3	A	36.14

Figure 3.56 Flow analysis spreadsheet for USGS gaging station at Holter showing the discharge, gage height, and water temperature from March 11 to March 24, 2020.

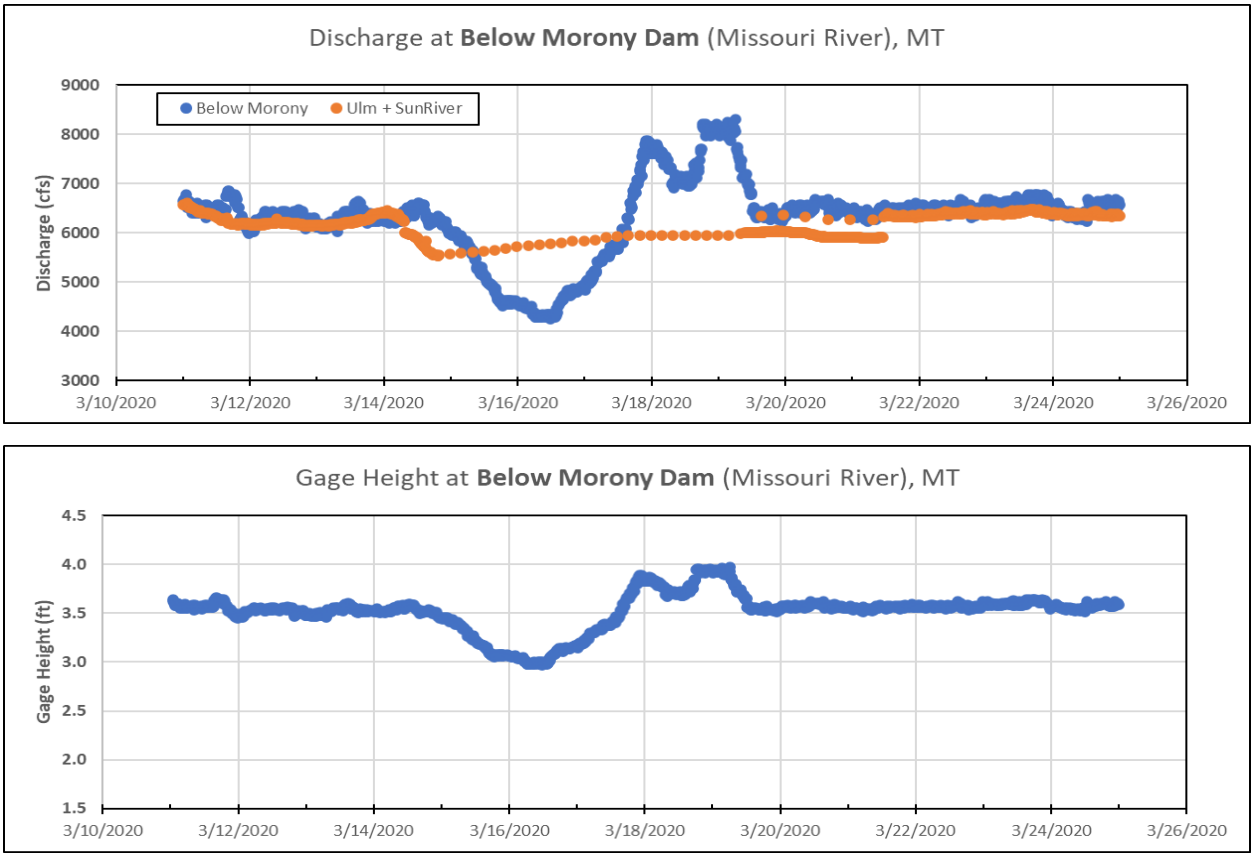

Figure 3.57 Plotted discharge and gage height in the flow analysis spreadsheet for USGS gaging station below Morony Dam from March 11 to March 24, 2020.

The continuous measured gage height data (Figure 3.58) available at Ulm and Cascade for the event are displayed in the flow analysis spreadsheet. The gage height at Ulm increased more than 1 ft (4.65–6.0 ft) from March 14 at 12:45 to March 16, 2020, and <0.4 ft at Cascade over 17.5 hours on March 15. These stage height changes indicate the ice jamming or ice cover formation below Ulm to Great Falls, as analyzed in Section 3.7.3 and Table 3.33. The gage heights at Ulm and Cascade prior to the event were fairly consistent (with small variations).

The plotted discharge hydrographs at USGS gaging stations Ulm and Cascade are displayed in the flow analysis spreadsheet as 2. The discharges at Ulm and Cascade just prior to and after the water level spike were plotted based on 15-minute verified streamflow data, which were determined from a rating curve. Without knowing the rating curves used by USGS, discharge and gage height rating curves at USGS gaging stations Ulm and Cascade were developed using 2020 summer data (April 1 to October 31) as shown in Figure 3.60. The fitted rating equations have very high accuracy (R^2 > 0.99) with respect to the summer data. Figure 3.60 shows calculated discharges (orange dots) from two regression rating equations that match very well with USGS streamflow data before and after the stage spikes but greatly overestimate discharges during the spike periods for both Ulm and Cascade gaging stations. USGS website only provides the verified and estimated discharges every 4 hours during the stage spike periods. At Cascade, there are five estimated discharges (five blue dots, Figure 3.60) over 17.5 hours that seem to be linearly interpolated from discharges before and after the spike (5440 cfs to 5380 cfs). At Ulm, there are 28 estimated discharges (blue dots) from 19:45 on March 14 to 9:30 on March 19 that are linearly interpolated from discharges before and after the spike plus some constant discharges.

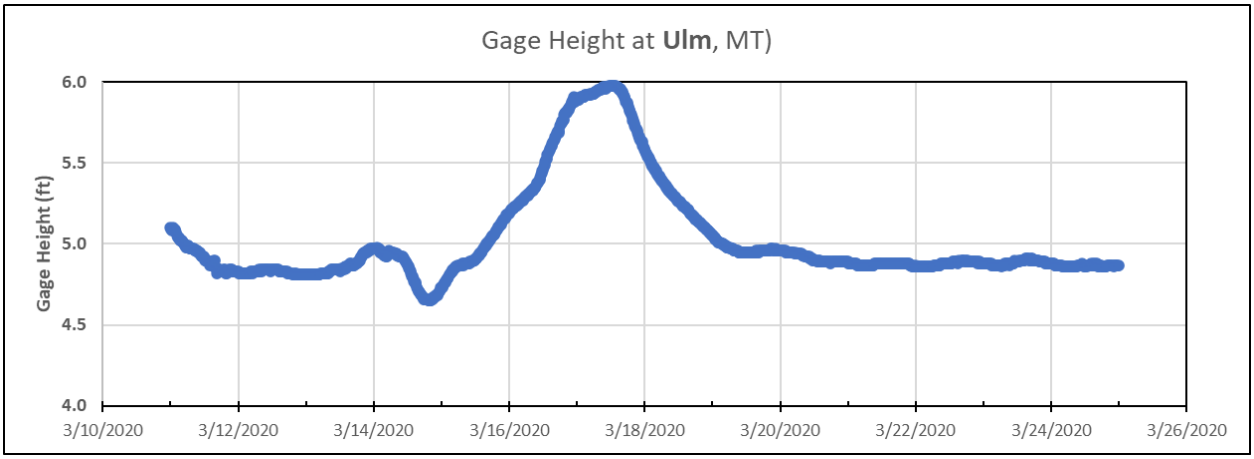

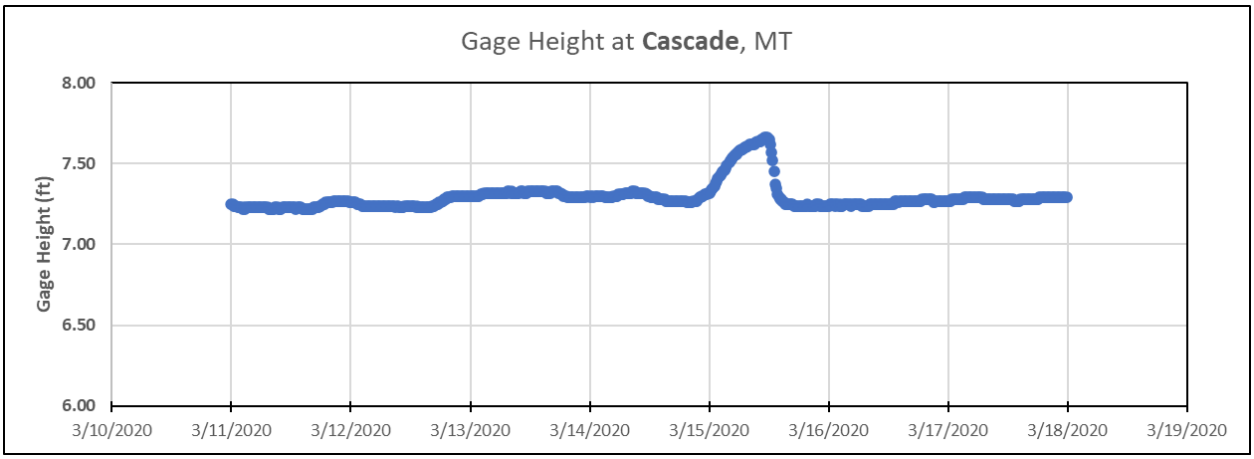

Figure 3.58 Plotted stage hydrographs in the flow analysis spreadsheet for USGS gaging station at Ulm and Cascade from March 11 to March 24, 2020.

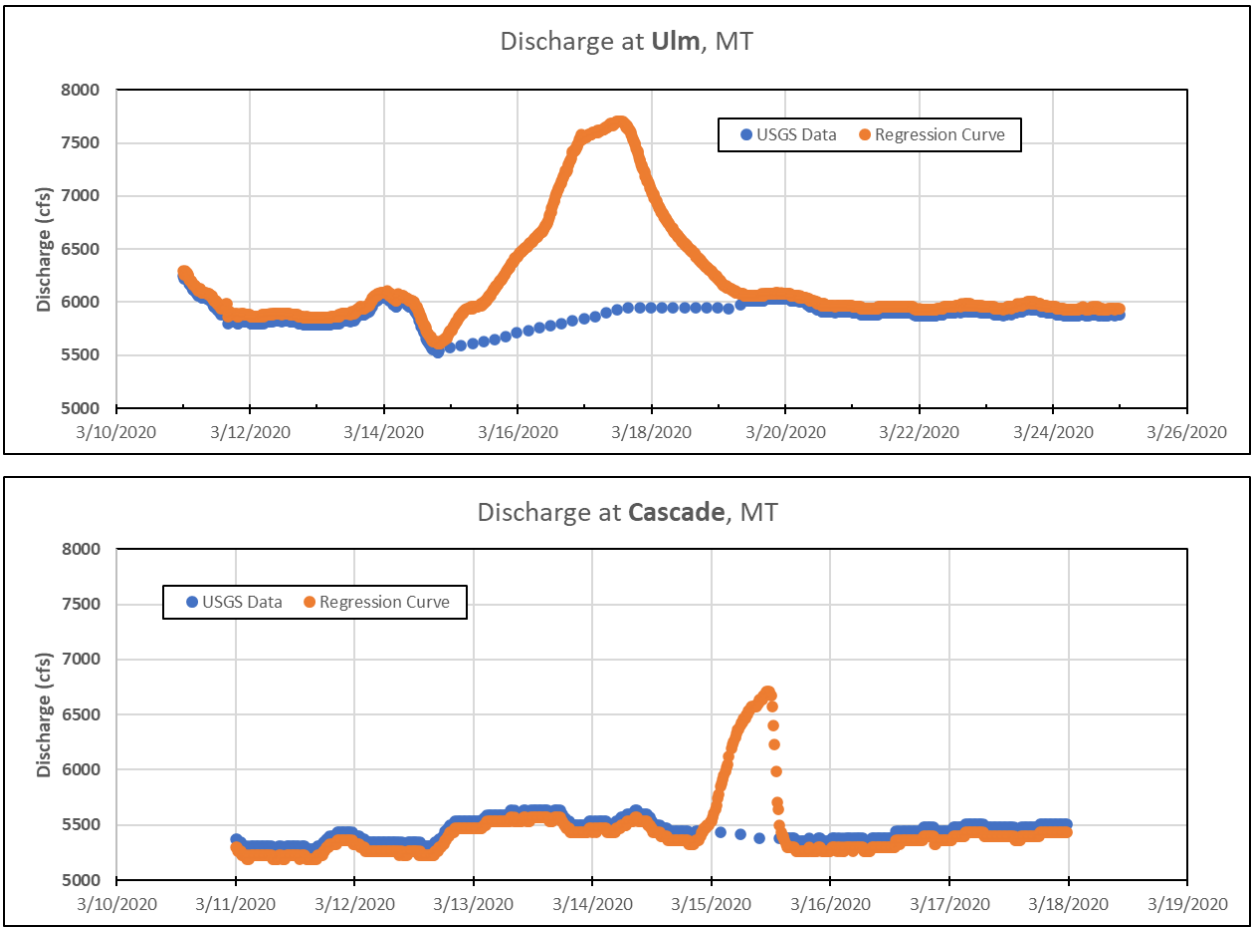

Figure 3.59 Plotted discharge hydrographs in the flow analysis spreadsheet for USGS gaging station at Ulm and Cascade from March 11 to 24, 2020.

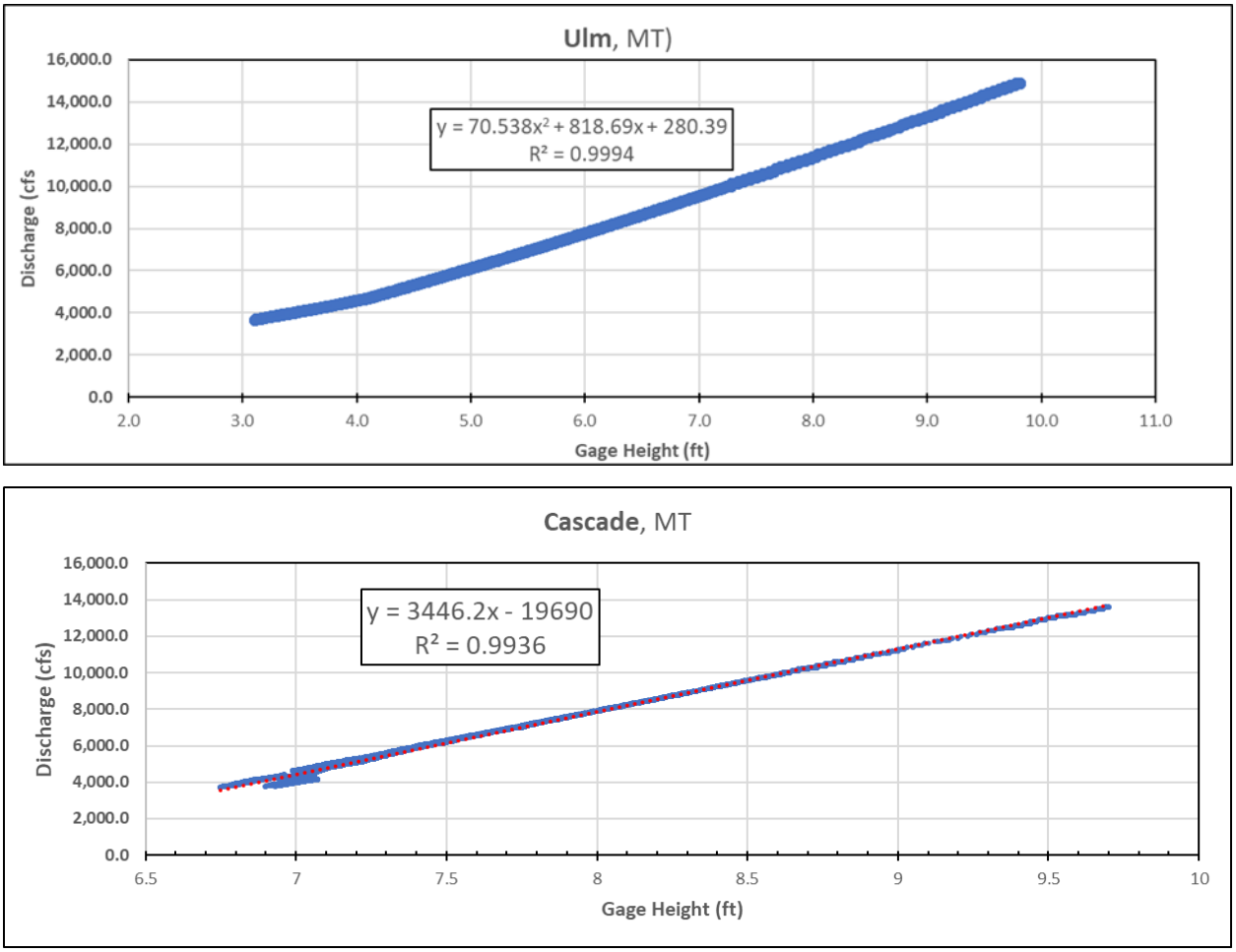

Figure 3.60 Discharge and gage height rating curves at USGS gaging stations Ulm and Cascade using 2020 summer data (April 1 to October 31).

Figure 3.57 also shows the sum of discharges from Missouri River at Ulm and Sun River but the summation does not support the flow drops at the USGS gaging station below Morony Dam at all. This could indicate that USGS estimated discharges at Cascade, Ulm, and Sun River during the ice cover or jamming event are not correct or quite different from the reality.

Figure 3.61 shows the user interface of the visual crossing weather data spreadsheet which is coupled with the flow analysis spreadsheet. This spreadsheet is set to provide us the weather data starting from February 29, 2020 to March 19, 2020. It has the ability to access forecast data for up to 15 days period, while it can also provide the historical weather data over the selected period.

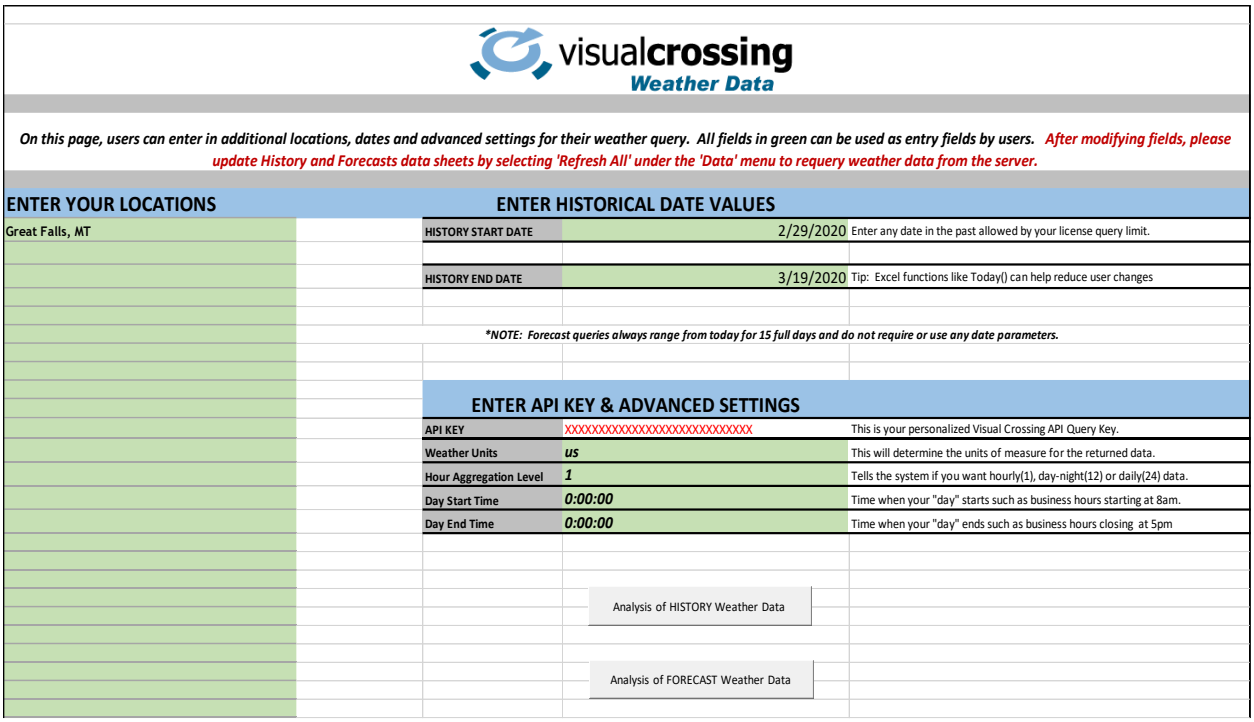

Figure 3.61 Visualcrossing weather data user interface to download data from www.visualcrossing.com from Feb-29 2020 to March-19 2020.

The visual crossing weather data is also analyzed with developed VBA code in the spreadsheet where all the freezing events are identified. Every instance when the air temperature goes below the freezing point of 32 ^{o}F, it is noted down on the spreadsheet, as in Figure 3.62. For the weather data analyzed period from February 29 to March 19, it was identified that 12 freezing events was taken place. The initial temperature reading noted after the temperature reaches below the freezing point, final temperature before the temperature goes above the freezing point, lowest temperature reached during every freezing event are identified. The duration of every freezing period and the average temperature maintained during the event are also identified in the analysis. The freezing degree hours for every event are also calculated in the spreadsheet. The spreadsheet also provides the daily average air temperature within the event and calculates the freezing degree days for every day.

Freezing Event Analysis of History Data

FreezingEvents	Starting DateHour	Temperature (°F)	Ending DateHour	Temperature (°F)	Duration (hours)	Average Temperature	LowestTemp	FreezingDegreeHours
1	02/29/20 09:00:00 PM	29.2	03/01/20 12:00:00 PM	30.4	16	27.54	25.1	71.4
2	03/01/20 08:00:00 PM	31.9	03/02/20 04:00:00 AM	30.8	9	30.60	29.6	12.6
3	03/02/20 06:00:00 AM	31.2	03/02/20 07:00:00 AM	31.3	2	31.25	31.2	1.5
4	03/04/20 07:00:00 PM	31.5	03/05/20 08:00:00 AM	28.2	14	23.33	19.9	121.4
5	03/07/20 06:00:00 AM	30.2	03/07/20 12:00:00 PM	31.9	7	28.54	25.4	24.2
6	03/07/20 06:00:00 PM	29.3	03/08/20 02:00:00 PM	28.7	20	20.66	15.4	226.8
7	03/09/20 12:00:00 AM	29.9	03/09/20 12:00:00 AM	29.9	1	29.90	29.9	2.1
8	03/09/20 02:00:00 AM	30	03/09/20 10:00:00 AM	31.5	9	29.43	27	23.1
9	03/09/20 10:00:00 PM	29.7	03/10/20 09:00:00 AM	31.5	12	27.46	22.9	54.5
10	03/11/20 07:00:00 PM	30	03/12/20 01:00:00 PM	28.4	19	23.92	18.2	153.5
11	03/12/20 08:00:00 PM	27.8	03/17/20 12:00:00 PM	31	113	10.48	-11.8	2431.8
12	03/17/20 07:00:00 PM	31	03/19/20 12:00:00 AM	22	30	21.69	17.1	650.7

Date	DailyAverage	FreezingDegreeDays
02/29/2020	40.10	-8.10
03/01/2020	30.58	1.42
03/02/2020	37.58	-5.58
03/03/2020	44.61	-12.61
03/04/2020	37.63	-5.63
03/05/2020	38.69	-6.69
03/06/2020	52.85	-20.85
03/07/2020	31.80	0.20
03/08/2020	25.42	6.58
03/09/2020	34.13	-2.13
03/10/2020	36.81	-4.81
03/11/2020	41.46	-9.46
03/12/2020	26.25	5.75
03/13/2020	21.94	10.06
03/14/2020	3.08	28.92
03/15/2020	-1.34	33.34
03/16/2020	11.05	20.95
03/17/2020	23.83	8.17
03/18/2020	21.23	10.78
03/19/2020	22.00	10.00

ours of weather forecast
456
Total hours of weather forecast with Air Temperature below FREEZING
252
Total hours of weather forecast Air Temperature ABOVE FREEZING"
204

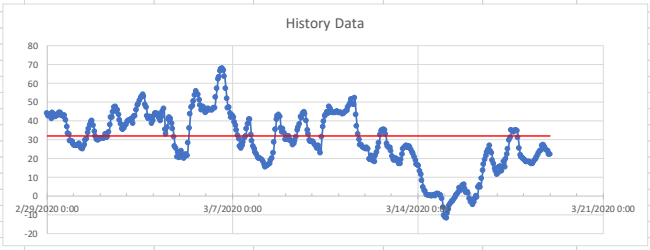

Figure 3.62 Freezing event analysis developed from flow analysis spreadsheet.

For the event of flow loss from March 14 to March 16, 2020 February, air temperature started to drop below the freezing point at 8:00 on March 12 and reached the lowest temperature of -11.8 ^{o}F on March 14 when flow at Morony started to decrease (Figure 3.57). Air temperature remained below the freezing up to 12:00 on March 17 but the flow at Morony started to increase from 12:45 on March 16, 2020. The freezing degree hours from 8:00 on March 12 to 12:00 on March 17 were 2431.8 ^{o}F-hour. The freezing degree hours on March 14, 15, and 16 were greater than 20 ^{o}F-hour and mean air temperatures were 3.08, -1.34, and 11.05 ^{o}F, respectively.

The flow analysis spreadsheet with history weather data analysis provides rich information for us to understand the ice jamming event as demonstrated using one example here. All ice jamming events in Table 3.31 will be further analyzed and summarized for Northwestern Energy.

CHAPTER 4. LAND COVER CLASSIFICATION OF STUDY AREA

4.1 INTRODUCTION

Since 1980s, global ground-based observational recordings have decreased dramatically, and satellite remote sensing has assumed a greater role in monitoring river and lake ice (Duguay et al. 2015). Satellite remote sensing augments the temporal and spatial coverage of terrestrial observations (Duguay et al. 2015). In a recent study conducted in the Susquehanna River, one of the longest and widest rivers in the northeastern United States, an automated approach that incorporated a threshold-based decision-tree image classification algorithm was used to determine the ice extent from MODIS (visible and near-infrared bands at 250m) on the Terra satellite. A good agreement was observed with aerial photographs, in situ observations-based ice charts, and LANDSAT imagery (Chaouch et al. 2012). Recent research on the 4400-kilometer-long Lena River uses remote sensing data from which river ice velocities are extracted to monitor ice along several hundreds of kilometers (Altena and Kaab 2021).

In Chapter 4, the land cover classification of the study area for different time and seasons is done to portray the amount of ice/snow seen in a winter period, and the condition of the river during summer season.

4.2 METHODOLOGY

Remote sensing data is accessed for the land cover classification mapping of the study area. For this study LANDSAT-5 and LANDSAT-8 imagery are used. LANDSAT-5 is used for the events before 2010 and LANDSAT-8 is used for the events after 2010. From the study conducted in Chapter 3, some of the events of ice jamming are identified with their probable location and date of ice jam formation.

USGS earth explorer (https://earthexplorer.usgs.gov/) is used to multiple images of LANDSAT-5 and LANDSAT-8 for the study location at the date when the ice jam occurred. These images are then used for land-ice cover classification, using the ERDAS Imagine and ArcGIS software. The study area with cloud cover of less than 50% is identified in the USGS earth explorer and used.

The workflow of the methodology is given in Figure 4.1:

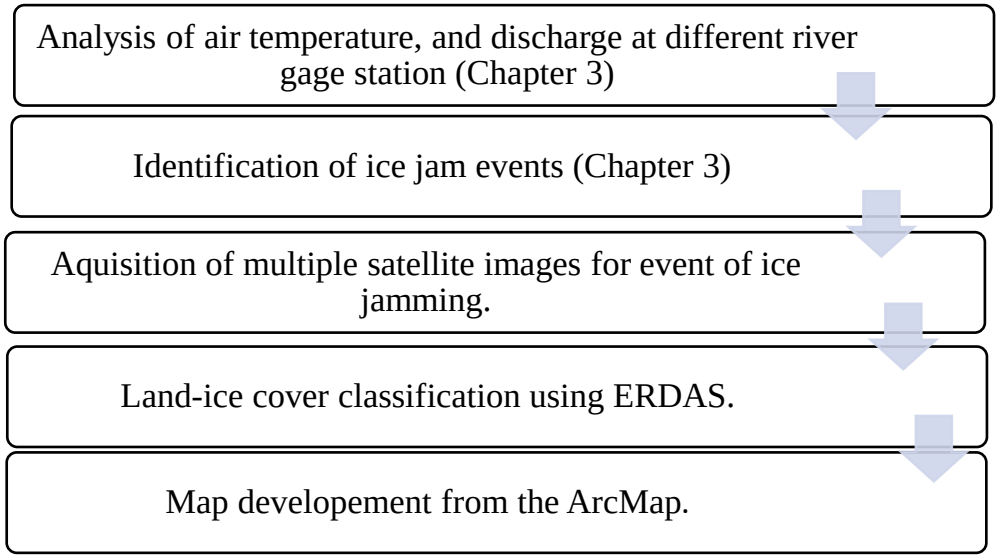

Figure 4.1 Workflow of land cover classification using ERDAS Imagine and ArcMAP after the ice jam event is identified in CHAPTER 3.

4.2.1 BAND COMPOSITION

The sensors on each of the LANDSAT satellites acquire data in different ranges of frequencies along the electromagnetic spectrum. The LANDSAT 1-5 Multispectral Scanner (MSS) images consist of four spectral bands with 60 meters spatial resolution, whereas the LANDSAT 4-5 Thematic Mapper (Montana Department of Natural Resources & Conservation) images consist of seven spectral bands with spatial resolution of 30 meters for bands 1 to 5 and 7. LANDSAT-8 Operational Land Imager (OLI) and Thermal Infrared Sensor (TIRS) images consist of nine spectral bands with a spatial resolution of 30 meters for bands 1 to 7 and 9. Band composition of downloaded LANDSAT-5 and LANDSAT-8 images is carried out using the ArcMAP software.

4.2.2 SHAPEFILE ACQUISITION

A shapefile format is a digital vector format for storing geographical location and associated attribute information (ESRI 1998). The study area of our site ranges from the Holter dam (upstream) to the Great Falls (downstream). As the study area is large and we are only concerned for the river proximities (Missouri River), a shapefile is created using the Google Earth Pro software.

Polygon feature in the Google Earth Pro is used to identify the study area, which is then saved as a shapefile, and added to the ArcGIS. Here, the shape file is overlaid on the composite imagery of

the LANDSAT images, and “Extraction of mask” tool is used to extract the desired study area. This file is now used in ERDAS Imagine software and is ready for classification.

4.2.3 CLASSIFICATION

Classification of the LANDSAT map acquired after the extraction of mask is then done using ERDAS Imagine software. In this project, unsupervised classification is adopted because of the lack of extensive prior knowledge of the area and unsupervised classification creates class purely based on spectral information (Olaode et al. 2014).

Unsupervised classification is also called clustering because it is based on the natural grouping of pixels in image data (Canada 2013). Unsupervised classification is performed using the Isodata algorithm. The image is then classified into 30 classes using 10 iterations. The classified image is then further classified upon mainly three categories, i.e., Land, Snow Cover, and Water using the thematic recode function. The classified image is then imported in the ArcMap to produce the map.

4.3 RESULTS

Some of the events were taken from CHAPTER 3 where the ice jamming was predicted. And for the selected events, land cover classification is done. Two events after 2010 were classified and one event before 2010 was used (Table 4.1).

Table 4.1 Ice jam events selected from Chapter 3 and classified upon which satellite image is used for land cover classification.

LANDSAT-8	LANDSAT-5
12/15/2015	02/24/2007
09/05/2019	

Figure 4.2, Figure 4.3, and Figure 4.4 shows the land cover map of study area of the Missouri River proximities starting from the Holter Lake (upstream) to the Great Falls (downstream). The overbank areas of the river are also included in the map. This map has three classifications, and some of the iced portion of the river are classified as river water.

The map on Figure 4.3 has comparatively lower snow cover than the Figure 4.2 and Figure 4.4 Here, the river can be seen entirely, but still the USGS discharge at this time shows a loss of 1057.5 cfs (Table 3.8). This map also has three classifications, and some of the iced portion of the river as classified as river water.

Figure 4.2 and Figure 4.3 are the map classification of winter season where flow loss event was identified in CHAPTER 3, and Figure 4.4 is the map classification of the study area for summer season showing the Missouri River without any ice cover present.

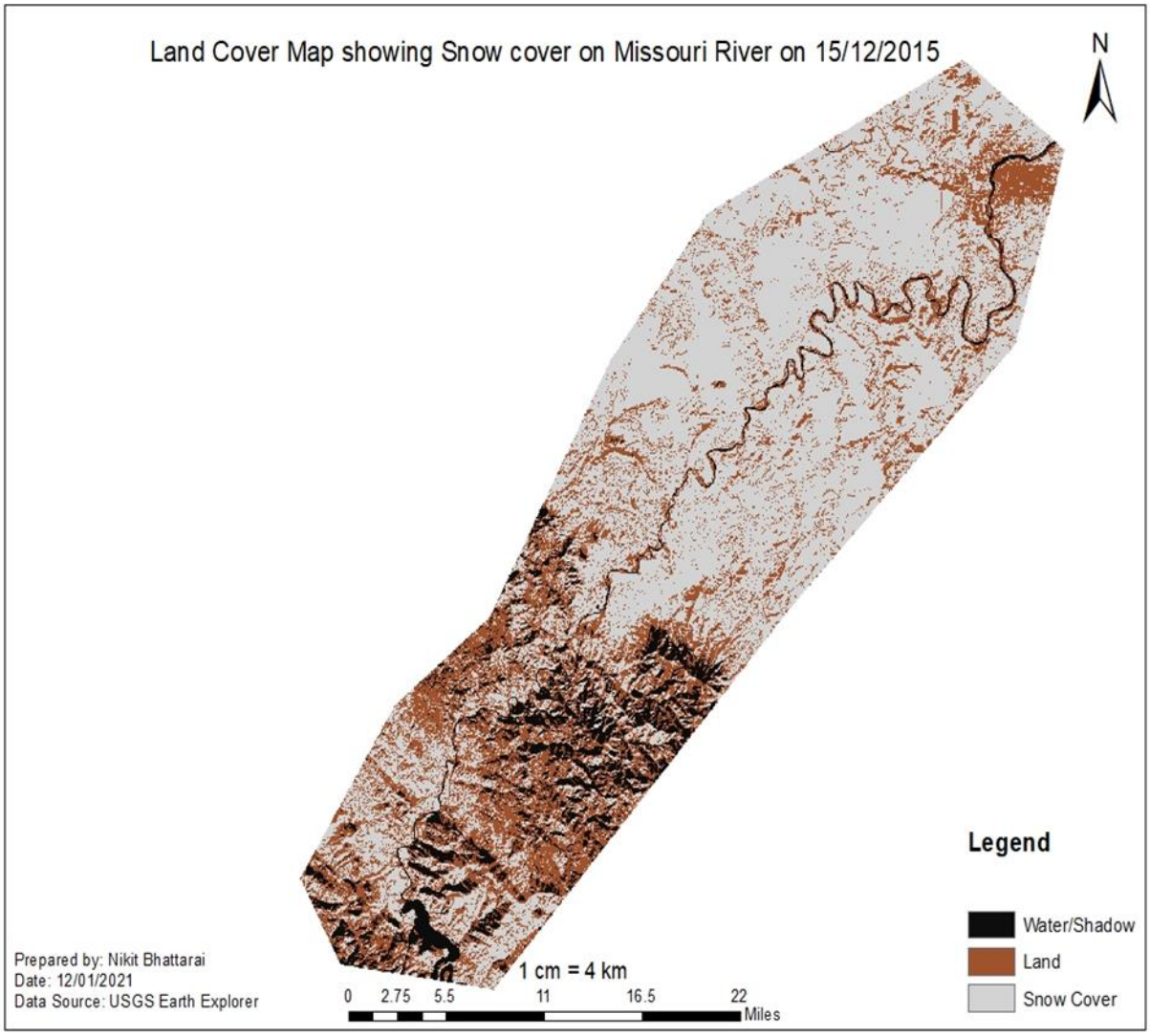

Figure 4.2 Land cover map of study on Missouri River proximities showing Land, Water/Shadow, and Snow Cover for 15/12/2015, classified using the LANDSAT-8 satellite image.

The map on Figure 4.3 shows the satellite image acquired from LANDSAT-5. It has relatively equal distribution of snow cover and open land. On the downstream of the river, snow cover is much more than the upstream section of the river, and covering some portions of the river reach.

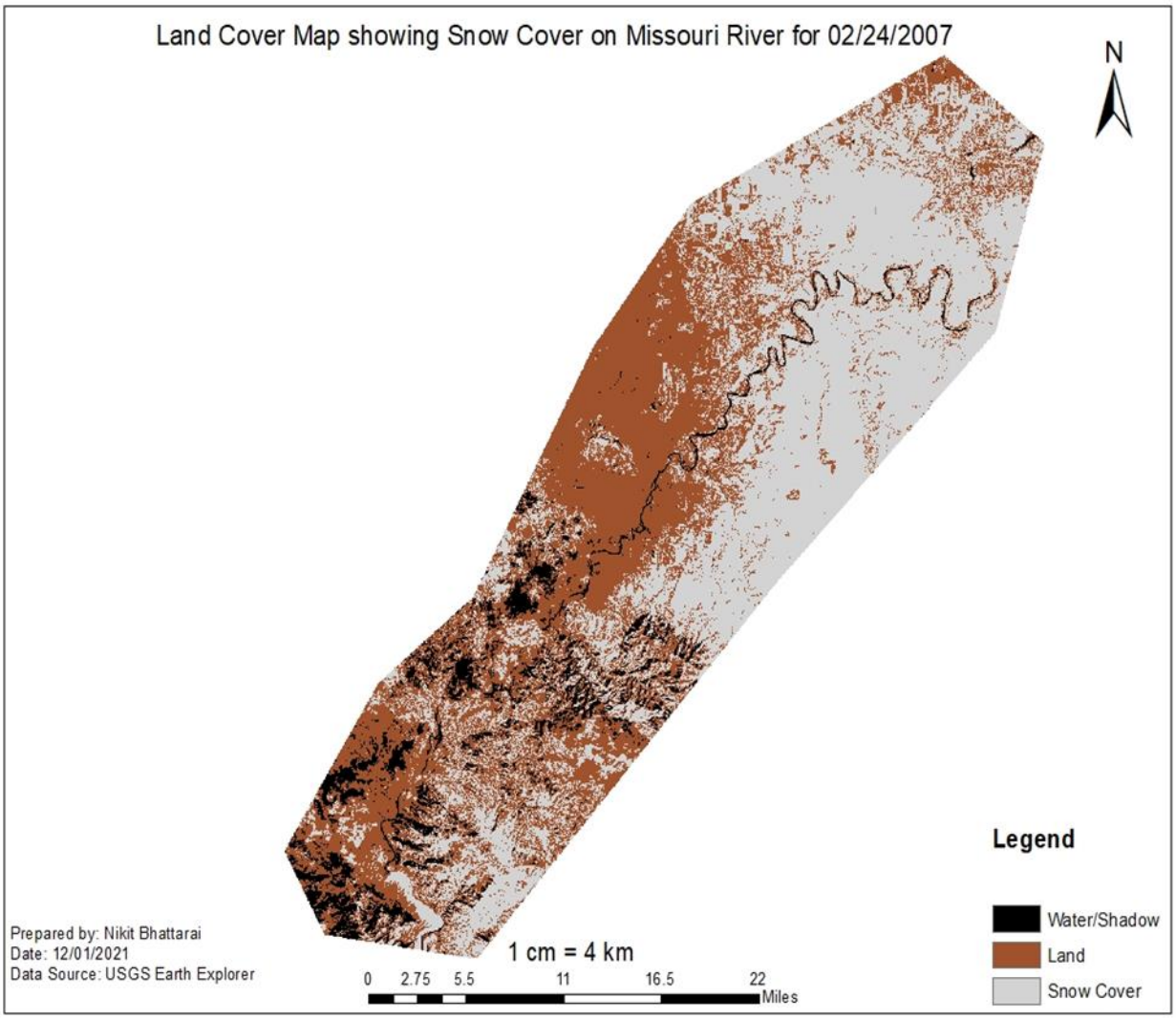

Figure 4.3 Land cover map of study on Missouri River proximities showing Land, Water/Shadow, and Snow Cover for 02/24/2007, classified using the LANDSAT-5 satellite image.

The map on Figure 4.4 shows the satellite image acquired from LANDSAT-5. It has relatively equal distribution of snow and land, but on the downstream of the river, snow cover is much more than the upstream section of the river.

The map on Figure 4.4 shows the summer season vegetation of the study area. The river width across the study area is visible here, compared to the Figure 4.2 and Figure 4.3. This land cover classification shows rivers, barren lands, and vegetation land. The vegetation land here includes the green topped part of the area, whereas the barren land includes the hills and the area with settlements.

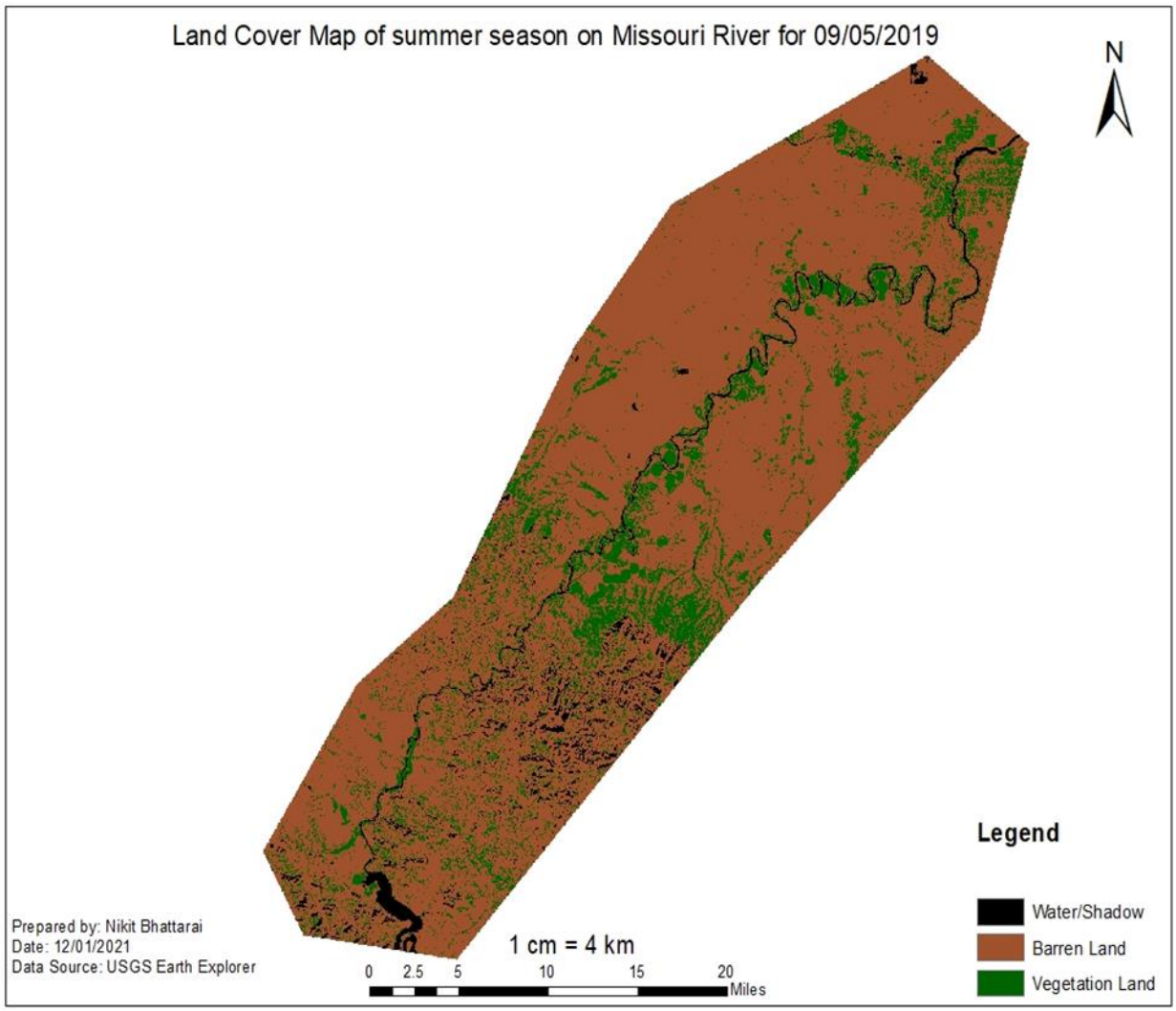

Figure 4.4 Land cover map of study on Missouri River proximities showing Land, Water/Shadow, and Vegetation for 09/05/2019, classified using the LANDSAT-8 satellite image.

4.3.1 MISSOURI RIVER CLASSIFICATION

A land cover classification of only the Missouri River from Holter to Great Falls is done using LANDSAT 8 image. Supervised image classification technique is carried out to classify the study area, and a polygon of the Missouri river is created using Google Earth Pro, which extracts only the river stretch from the study area. Figure 4.5 shows the image classification for 2018 March 01, where the water body is classified as water, ice, and snow cover. Some of the important locations for the Missouri River reach in the study area like: Holter, junction of Dearborn River and Missouri River, Cascade, Ulm and the Great Falls are also plotted in Figure 4.5.

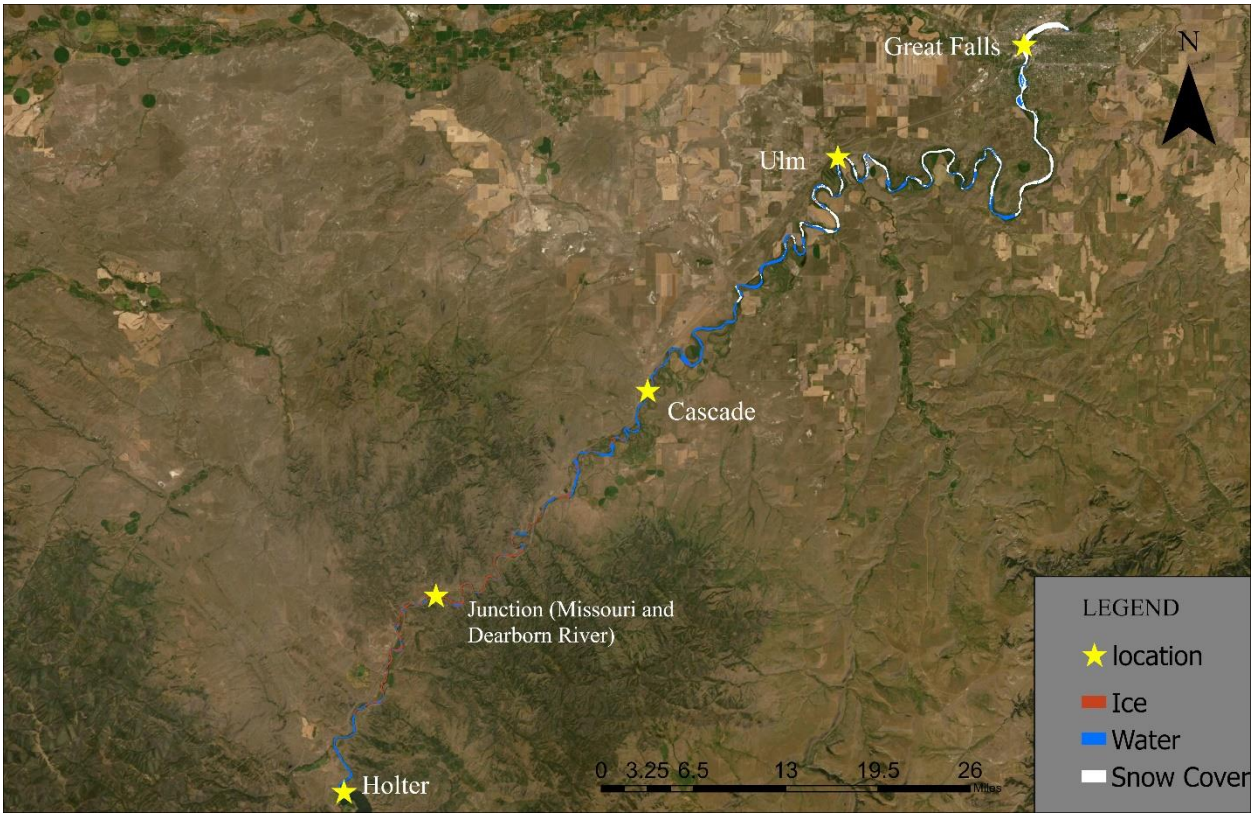

Figure 4.5 Missouri River from Holter to Great Falls classified for ice, water, and snow cover for 01 March, 2018 using LANDSAT 8 image.

The snow-covered area is seen mostly on the downstream part of the Missouri River. And, some areas with ice formation is seen on the upstream section of the Missouri River. For this event, after the image classification, it is concluded that for the river surface, 14.3 % of the river is occupied by ice, 47.1 % is occupied by snow, and 38.6 % is occupied by water.

The event of ice jam formation is not classified as special event of flow loss in Morony earlier in CHAPTER 3. To verify the ice jam formation on 01 March, 2018, the flow analysis spreadsheet discussed on Section 3.11 is used. The air temperature analysis of the study area from February 20 to March 5 shows the air temperature prior to the event on March 01 is below the freezing point of 32 ^{o}F. Table 4.2 shows the daily average air temperature, freezing degree days, and the snow depth from 20 February to 05 March 2018. Figure 4.6 shows the plot of hourly temperature from 20 February to 05 March showing above freezing temperature only to last a few hours in three days. Four freezing events is seen occurring in this period, with the total freezing degree hours of 5364 hours. This shows the evidence of ice cover/jam formation/accumulation on Missouri River

from the middle of February to early March, 2018, that is why ice cover is seen on March 1 (Figure 4.5) in 2018.

Table 4.2 Analysis of daily weather data from February 20 to March 05, 2018 showing the average air temperature, freezing degree days, and snow depth (inch)

Date	Daily average air temperature	Freezing Degree Days	Snow Depth (in)
02/20/2018	-4.38	36.38	10.26
02/21/2018	3.38	28.62	9.87
02/22/2018	3.51	28.49	9.02
02/23/2018	7.99	24.01	8.15
02/24/2018	19.91	12.09	7.14
02/25/2018	26.61	5.39	6.60
02/26/2018	23.08	8.92	6.44
02/27/2018	21.37	10.63	6.12
02/28/2018	26.03	5.98	5.31
03/01/2018	26.71	5.29	4.69
03/02/2018	16.12	15.88	4.63
03/03/2018	13.18	18.82	5.86
03/04/2018	10.78	21.22	10.10
03/05/2018	7.20	24.80	0.43

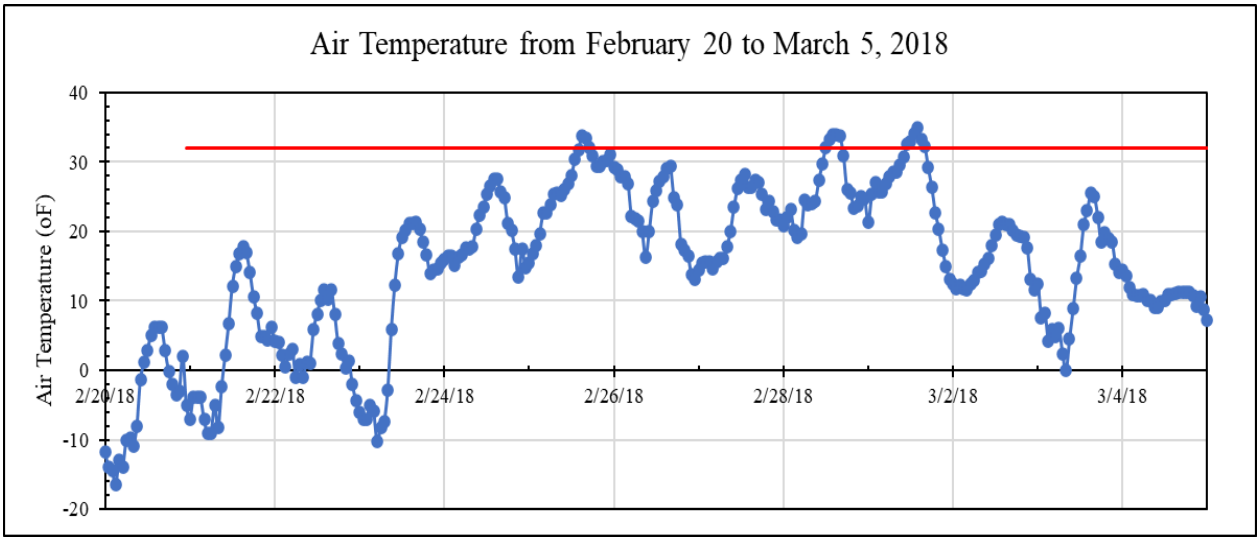

Figure 4.6 Hourly air temperature data at Great Falls from February 20 to March 5, 2018 generated using the flow analysis spreadsheet.

The discharge below Morony from February 20 to March 05 2018 shows an evidence of gradual flow increase with a few loss events prior to March 01, 2018. Although, the flow loss is not seen on March 1, but existing ice cover/jam above Cascade in Missouri River can be cross verified

using Figure 4.6 and Figure 4.8. The gage height in Cascade rises by 4 ft from February 20 to February 22, while the gage height at Ulm does not show much change during this period. As the air temperature from Figure 4.6 shows that the temperature during February 20 to February 22 is below the freezing event with lowest being -17 ^{o}F, there is high chance of ice cover formation and ice jamming during this period.

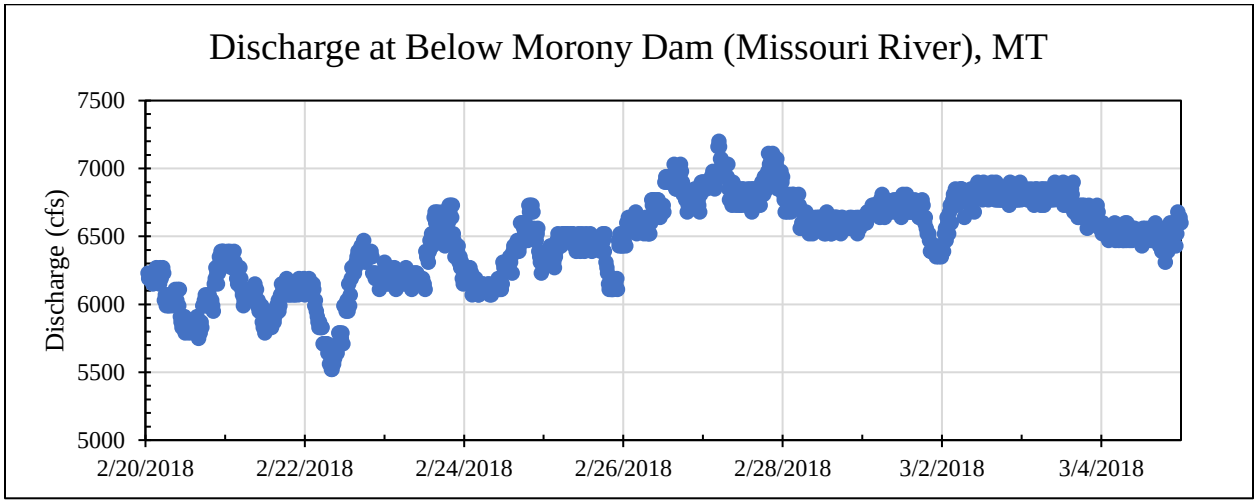

Figure 4.7 Discharge below Morony from February 20 to March 05, 2018.

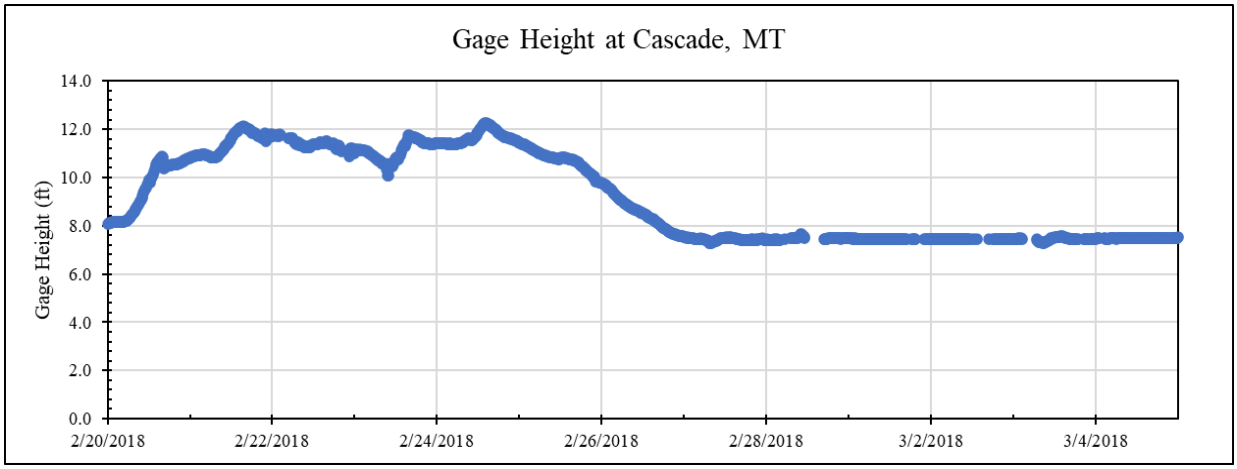

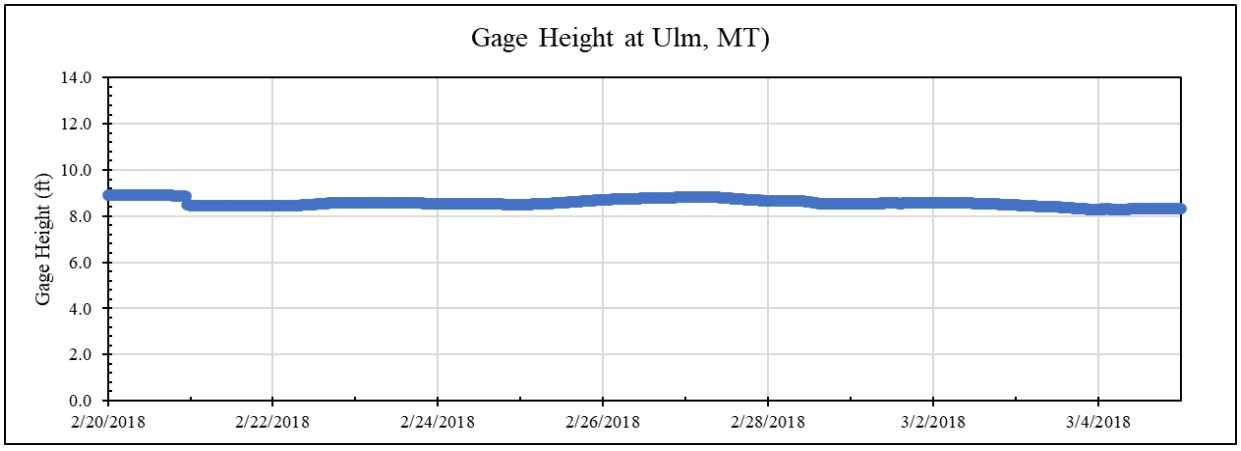

Figure 4.8 Gage height at Cascade and Ulm from February 20 to March 05, 2018

Water temperature simulation discussed on CHAPTER 4 is also applied for the duration of February 20 to March 05, 2020. The steady flow at Holter is taken as 5400 cfs, which is an average discharge measured at Holter during this time. The initial temperature is taken as 1.1 ^{o}C. Other meteorological parameters like atmospheric pressure, air temperature, wind, cloudiness, solar radiation and relative humidity for this duration is generated using the flow analysis spreadsheet. The simulated water temperature time series at Cascade using HEC-RAS water quality model is shown in Figure 4.9. The water temperature simulation on Figure 4.9 shows 13 events when the water temperature reaches 0 ^{o}C. This event supports the evidence that ice jam is formed during the period of February 20 to March 05.

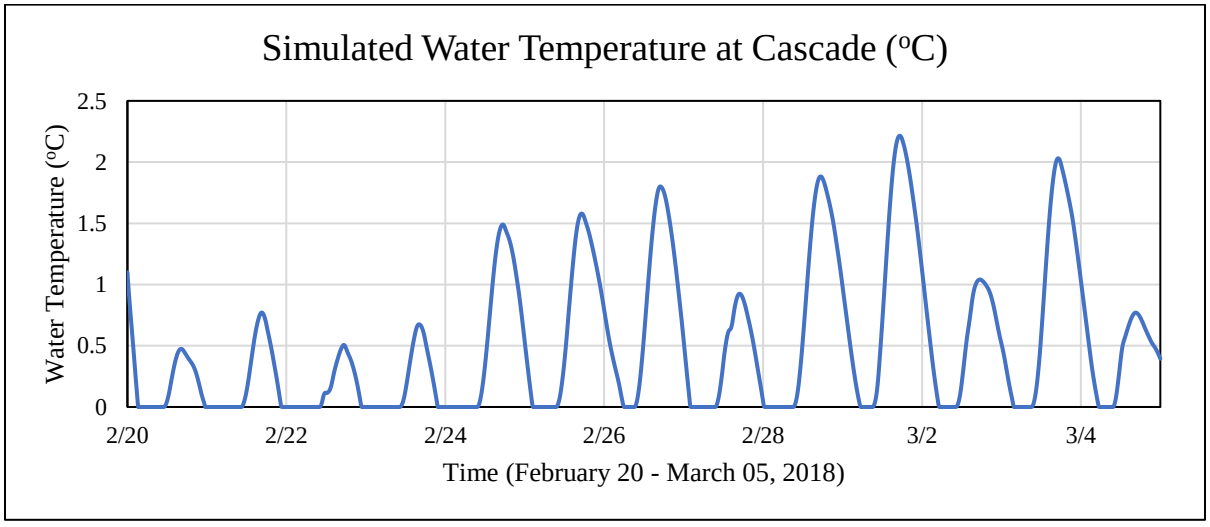

Figure 4.9 Simulated water temperature (^{o}C) at Cascade using HEC-RAS from February 20 to March 05, 2020.

4.4 DISCUSSION

The study area from Holter Dam, Montana to Great Falls, Montana along Missouri River as lies on the northern region of the country, faces huge snowfall and the air temperature goes below O^{o}C mostly during the winter season. This is seen evidently from the land cover maps of the winter seasons. This snow covering river, with low air temperatures and water temperatures causing ice jamming decreases the overall discharge of the river, which in turn effects the hydropower electricity generation on the downstream hydro powerplant. Additionally, such snow covers has a significant impact on the ecosystem residing there.

The difference in ecosystem during the summer season and the winter season is very evident from the land cover map. Also, the discharge in the Missouri river with and without the snow cover is evident as the amount of flow loss during the event shown on Figure 4.2 is 1890 cfs and Figure 4.3 is 1057.5 cfs. For the land cover classification map, classification of river water using LANDSAT images for winter season is also difficult because of the shadow regions found on the images. For every classification, water and shadow and classified together because for winter season, the shadow casted by the hills are larger and the spectral behavior is similar to that of the river, which is a limitation of this classification. The shadow regions are evidently higher on summer season compared to the winter season. Also, as ice cover and snow cover show similar spectral behavior, they are classified together. As ice covered map has a snow topping thus the classification of snow cover and ice cover distinctly is not done in the land cover classification. Additionally, although many years of discharge and air temperatures were analyzed and many such events were identified, only two events of the ice jamming are classified here. This is because there are very few events when, ice jamming date and availability of LANDSAT data with less than 50% cloud cover coincided.

The ice jam analysis using the flow analysis spreadsheet and water temperature simulation in HEC-RAS shows an example of how prediction of ice jamming can be made using the spreadsheet. The event discussed from February 20 to March 05, 2018 verifies the ice cover formation identified in Figure 4.5. This is one of the major applications of the study conducted in the thesis.

CHAPTER 5. HEC-RAS MODEL SET UP

5.1 INTRODUCTION TO HEC-RAS

HEC-RAS is a software of river analysis system (RAS) designed for interactive use in a multi-tasking environment and developed by the Hydrologic Engineering Center (HEC) of the US Army Corps of Engineers (USACE). It has a graphical user interface (GUI), separate analysis components, data storage and management capabilities, graphics and reporting capabilities, and other features. HEC-RAS is intended to perform one-dimensional and two-dimensional hydraulic calculations for a complete network of natural and man-made channels, overbank/floodplain areas, levee protected areas, and so on (USACE 2016). HEC-RAS has been developed over several decades, e.g., HEC-RAS 2.0 was released in April 1997; for this study HEC-RAS 6.1 was used.

River analysis components in the HEC-RAS 6.1 system include: (1) steady flow water surface profile computations; (2) one-dimensional and/or two-dimensional unsteady flow simulation; (3) quasi unsteady or fully unsteady flow movable boundary sediment transport computations; and (4) water quality analysis. The fact that all four components use the same geometric data representation and geometric and hydraulic computation routines is critical. Aside from the four river analysis components, the system includes several hydraulic design features that can be used once the water surface profiles have been computed (USACE 2016).

The steady flow water surface profile computations component of HEC-RAS is intended for calculating water surface profiles for steady gradually varied flow. The system may handle a channel network, dendritic system, or river reach. The steady flow component models subcritical, supercritical, and mixed flow regimes. The computation starts with the one-dimensional energy equation. Friction (Manning's equation) and contraction/expansion measure energy loss (coefficient multiplied by the change in velocity head). When the water surface profile changes quickly, to utilize the momentum equation is recommended. Mixed flow regime computations with hydraulic jumps, bridge hydraulics, and analyzing river confluence profiles (stream junctions) are also available in HEC-RAS (USACE 2016).

The one- and two- dimensional unsteady flow simulation component simulates one-dimensional, two-dimensional, and combined one/two-dimensional unsteady flow over open channels, floodplains, and alluvial fans. The unstable flow component can be utilized to calculate subcritical, supercritical, and mixed flow regimes (hydraulic jumps and drawdowns). Unsteady flow

component of HEC-RAS has some special features, which include: extensive hydraulic structure capabilities dam break analysis; leeve-breaching and overtopping; pumping stations; navigation dam operations; pressurized pipe systems; automated calibrations features; user defined rules; and combined one and two-dimensional unsteady flow modeling (USACE 2016).

The steady transport/movable boundary computations component simulates one-dimensional sediment transport/movable boundary computations across intermediate time periods (typically years, although applications to single flood events are possible). By computing sediment transport potential by grain size fraction, hydraulic sorting and armoring may be simulated. Modeling a whole network of streams, channel dredging, levee and encroachment alternatives, and sediment transport equations are major elements. The model simulates long-term patterns of scour and deposition in a stream channel caused by adjusting water discharge, stage, or channel shape. This technique can be used to analyze reservoir deposition, plan channel contractions to maintain navigation depths, anticipate the influence of dredging on deposition, estimate maximum flood scour, and evaluate sedimentation in fixed channels (USACE 2016).

The water quality analysis component analyzes riverine water quality. HEC–RAS has an advection-dispersion module to model water temperature and other water quality constituents. This new module solves the one-dimensional advection-dispersion equation using a control volume technique and a heat energy budget. HEC-RAS now includes transport and fate of some water quality elements, for example, dissolved nitrogen (NO3-N, NO2-N, NH4-N, and Org-N), dissolved phosphorus (PO4-P and Org-P), algae; dissolved oxygen (Brown et al.); and carbonaceous biological oxygen demand (CBOD) (USACE 2016).

A good river hydraulics model begins with an accurate topography model and the production of geometric data elements that depict the flow of water through the river system. These geometric data elements are river network centerlines, overbank flow pathways, main channel bank lines, cross sections, bridges, and other layers for a 1D river hydraulics model. Data elements for a 2D hydraulics model include the 2D flow region with cell sides oriented to high land, such as banks, and hydraulic structures that convey water over and through high ground, such as highways and levees. To assist the production of geometric data, RAS Mapper as GIS Tools in HEC-RAS becomes available from HEC-RAS 4.0 from 2010 and provides vector Editing Tools that allow the user to define HEC-RAS-specific geometric data items. These data are referred to as RAS

Layers. Creating RAS Layers in RAS Mapper needs the creation of a RAS Terrain Layer and its association with the geometry layer, as well as the definition of a coordinate system.

The geometry data are imported from a RAS Mapper, which requires a terrain data. The terrain can be a DEM (Digital Elevation Model) data.

5.1.1 DEM DATA

A digital elevation model (DEM) is a representation of the topographic surface of the Earth's naked ground (bare earth), devoid of any trees, structures, or other surface items. Sensors that detect the reflections of a pulsed laser beam are used to collect terrain data from aircraft utilizing the light detection and ranging (Lidar) technique. Millions of individual points, collectively referred to as a "point cloud," are collected from the reflections to depict the 3D positions of things on the surface, including as structures, plants, and the earth. Digital elevation models can be produced using Lidar data as well as data from other sources.

For higher accuracy purpose, Lidar data from Montana Lidar Inventory (https://montana.maps.arcgis.com/apps/MapSeries/index.html?appid=55cc886ec7d2416d85beca68d05686f4) has 1 m by 1 m spatial resolution and is taken, which covers about 2/3rd of the study area. The Lidar data is collected from 04/25/2020–06/23/2020. The DEM data is then uploaded to the HEC-RAS, for the extraction of geometry data for further analysis Figure 5.1.

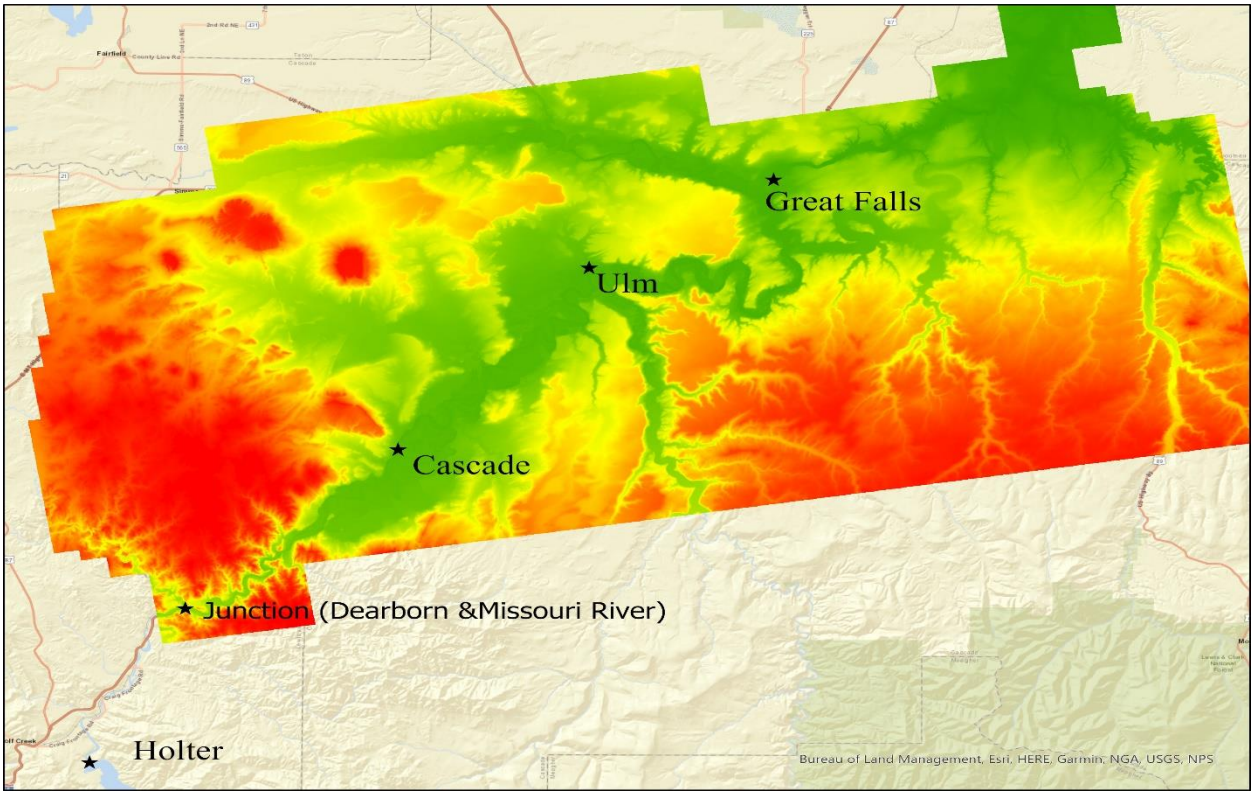

Figure 5.1 Lidar data of Missouri River covering region from upstream of Dearborn River, MT to Great Falls, MT, imported to the RAS Mapper of HEC-RAS.

The digitization of the terrain model is done to obtain the geometry data. The digitization includes creating of river centerline, main-channel bank lines, flow path, and cross sections through the river; and Figure 5.2 shows a small part of Missouri River. River centerline is used to establish the river reach network for HEC-RAS. Bank lines are used to distinguish the main channel from the overbank floodplain areas. Flow paths are used to determine the downstream reach lengths along the left overbank, the main channel, and the right over bank. The flow paths are digitized at the boundary of the floodplains (Dey and Merwade 2020). The cross section is not necessary a straight line but each part of the cross section should be more or less perpendicular to the flow direction in that part so that to estimate or predict the flow movement direction by RAS model developer is crucial for establishing a more precise and accurate hydraulic modeling using HEC-RAS. Many cross-sections along with river reach length are then obtained (Figure 5.2). The straight line on Figure 5.3 denotes the water surface level (elevation) between two bank stations denoted by red dots when Lidar data were collected. The water level in a stream varies with discharge from upstream.

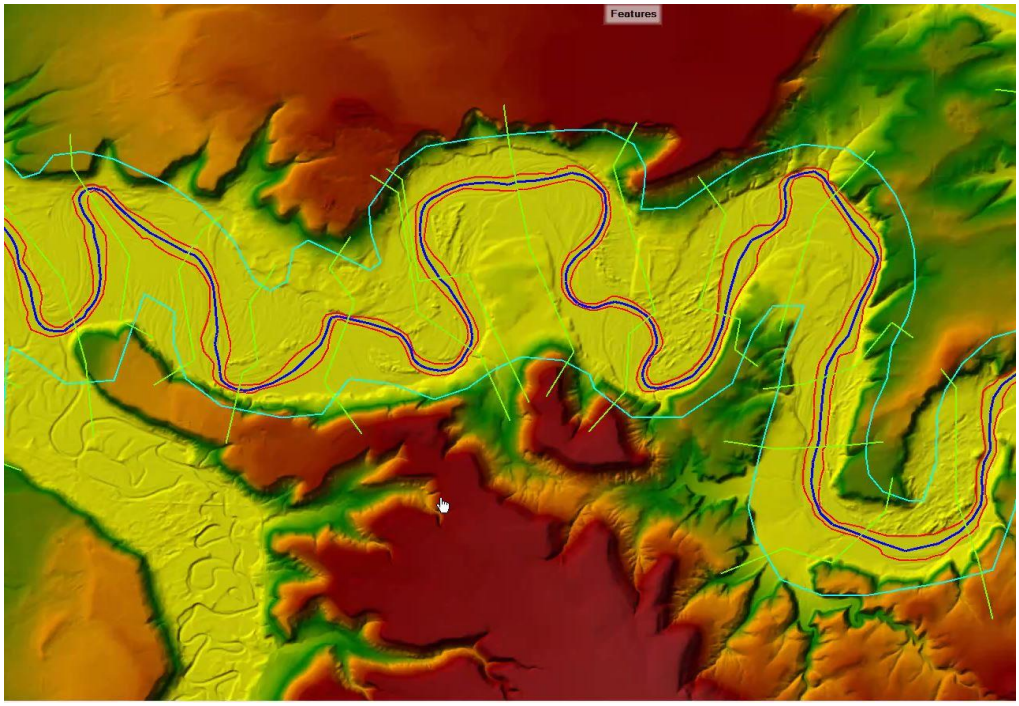

Figure 5.2 Digitization of river center line (blue line), bank lines (two red lines), flow paths (two light green-blue lines), and cross-sections (yellow lines) of Missouri river on Lidar data using RAS Mapper

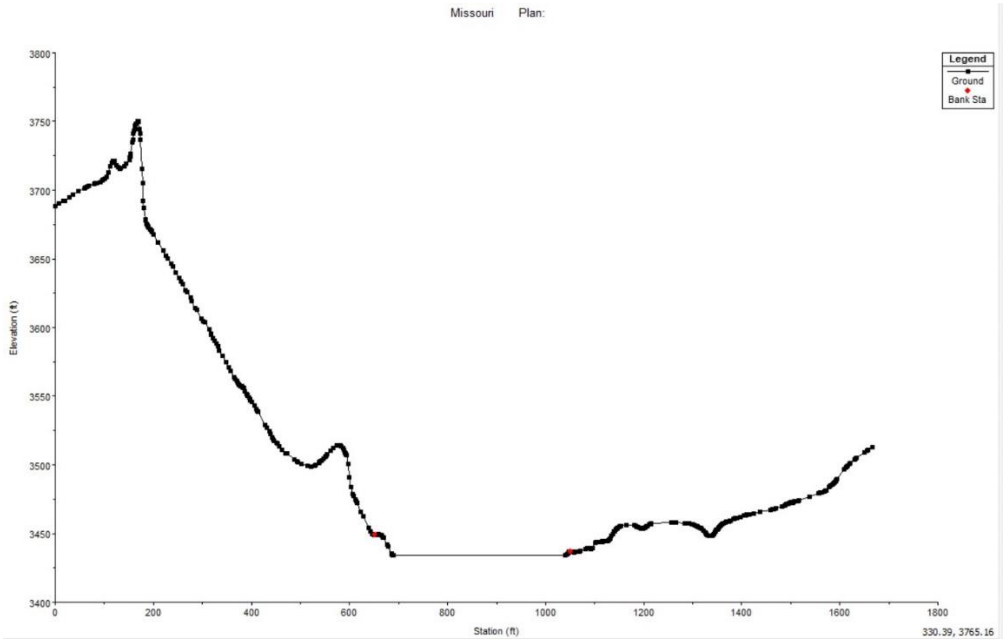

Figure 5.3 Sample of cross-section data obtained after digitization on RAS Mapper.

5.1.2 LIMITATIONS OF DEM DATA

The primary limitation of the acquired cross section (Figure 5.3) from the DEM data includes lack of bathymetry data for river channel, elevation change under the water surface. For HEC-RAS to run the river analysis, bathymetry data is required. The DEM data only provides with the elevation of the surface level at specific discharge, and for modeling using HEC-RAS, the elevations of channel bottom (including left and right over bank areas) throughout the river network are necessary. These elevation data can only be obtained using field survey, which is also one of the limitations of remotely acquired data.

5.2 BATHYMETRY DATA ACQUISITION

Bathymetry refers to the study of the "beds" or "floors" of water bodies. Bathymetric data includes information about the depths and shapes of underwater terrain. Water depth is the elevation difference between the water surface and the channel bottom.

From Figure 5.3 it is evident that the cross-section data do not have the water depth, thus acquisition of bathymetry data is a very vital step to carry out river analysis using HEC-RAS for this study. For the acquisition of bathymetric data, two approaches were carried out in this research. One is the manual method of digitizing contour map of the river, and the other is the use of GIS to process the surveyed water depth data.

5.2.1 CONTOUR MAP METHOD

In the past, lake or river contour maps were developed by professional hydrographic survey using a boat with multibeam echo sounders. Nowadays, owners of small fishing boats can equip a sonar finder with memory card to record water depth data that can be used to create high-resolution (e.g., 1-ft) contours of a lake or stream. The contour map method used to obtain the bathymetric data for the Missouri River is a manual workaround method adapted which provides depth of the river at the locations where contour lines are found. In this method, the bathymetry data for the Missouri River has been acquired using the C-Map Genesis (https://www.genesismaps.com/) map, GetData Graph Digitizer, and HEC-RAS.

C-Map Genesis is a free, global, online collection of inland and coastal platform provided by the communities of fishing, cruising, and sailing enthusiasts. C-Map Genesis contour maps are not available in all lakes or streams and only available when someone collects and uploads the data into C-Map Genesis website. These data are mostly used in boats, but we are using it to get the

contour data of Missouri river. C-Map Genesis map are primarily created for fisherman for fishing purpose. It provides contour lines on some rivers and coastal areas. Sonar technique is applied to get the river depth data here. Sonar technique is a sound propagation technique to navigate, measure distances, communicate with or detect objects on or under the surface of the water. This technique is used to obtain the bathymetry of the surveyed river, and a contour map is generated and publicly available on their website.

Figure 5.5 shows the social map with contour data (white) on the Missouri river from downstream of Holter Lake to a short distance downstream of Cascade. These contour data were collected on May 23–24, 2020 (mean daily discharge about 7092 cfs), by AMARUQ Environmental Services LLC for the Upper Missouri Watershed Alliance, which was a part of submersed aquatic vegetation survey study. Dr. Andrew Z. Skibo, President & Founder of the company, provided us the data in csv format, and we did not download it from C-Map Gensis since downloaded data can only be used with boat GPS Fishfinder units. Figure 5.6 shows a zoomed view of an example contour map (resolution of 1 ft, from 1 to 5 ft) in a small segment of Missouri River, upper portion of the study area. Currently, we do not have the contour data for Missouri River from Cascade to Great Falls (~60 river miles).

For the contour map method, the Missouri River was digitized from the upstream of Dearborn River to the downstream of Cascade (~23 river miles). The total of 87 cross-sections are developed on the RAS Mapper. The cross-sections are spaced at an average of 440 m from one another (Figure 5.4).

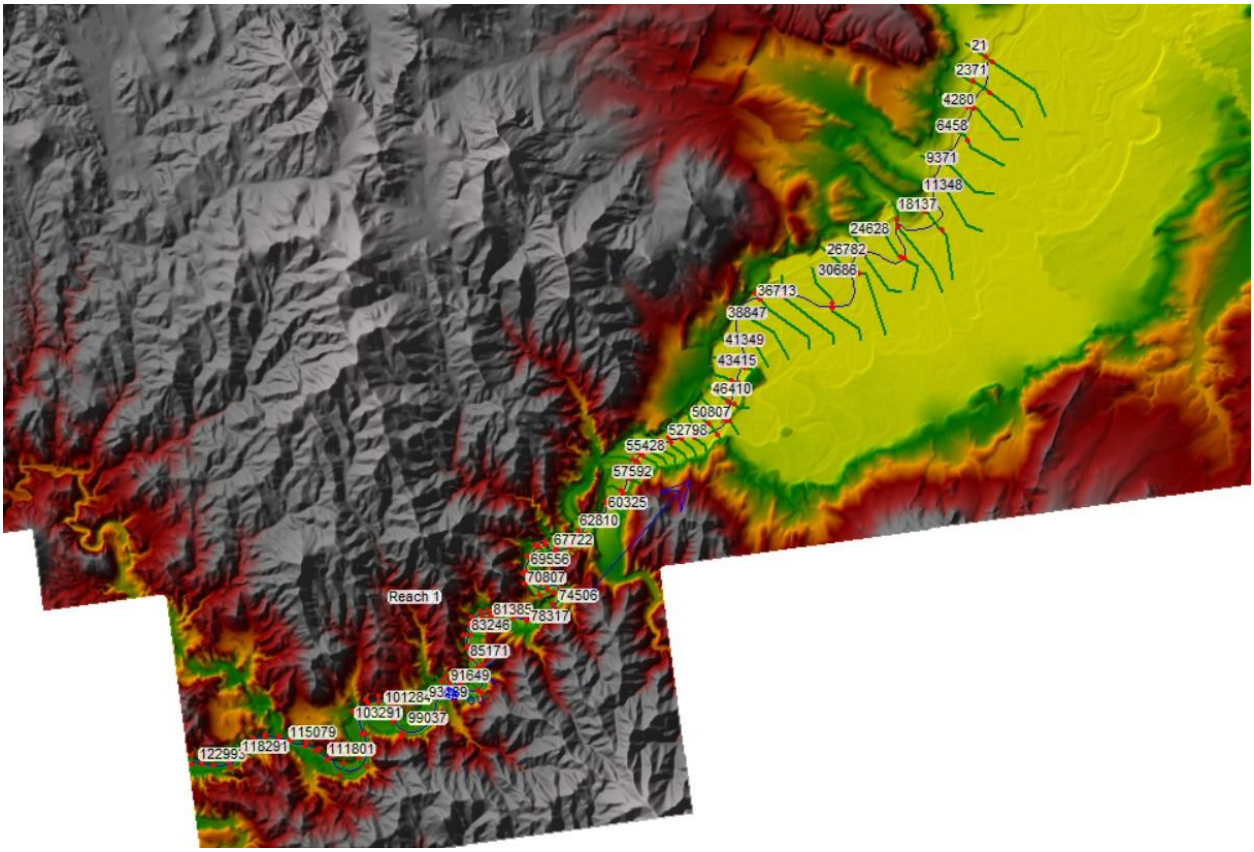

Figure 5.4 Lidar DEM digitized on RAS Mapper in HEC-RAS for Missouri River where bathymetry data is collected using contour map method.

Figure 5.5 C-Map genesis social map obtained from https://www.genesismaps.com/SocialMap/ for Missouri river. (Accessed on 06/29/2022)

Figure 5.6 Contour lines on the C-Map Genessis map with map scale on the bottom right corner.

5.2.1.1 Process to obtain bathymetry

For the bathymetric data collection from the website, the river segment where the cross-sections are digitized in HEC-RAS (Figure 5.7), is identified in the C-Map social map (Figure 5.8). Then identical cross-sections are manually outlined replicating the HEC-RAS cross-sections.

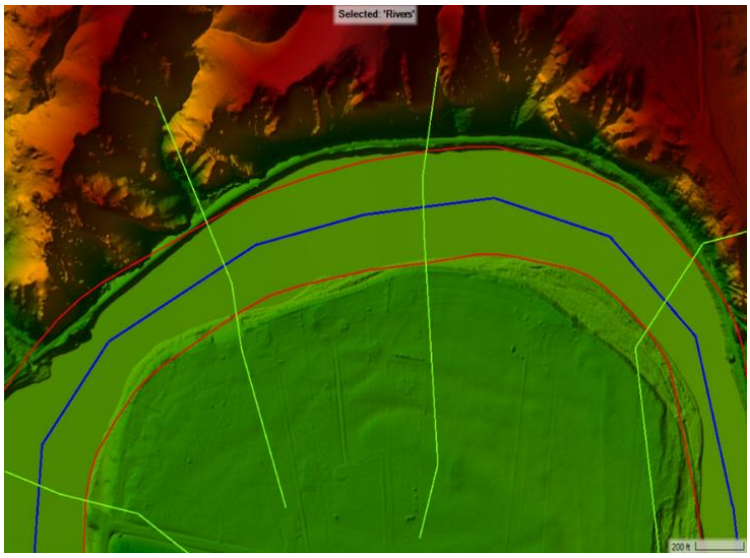

Figure 5.7 Screenshot of the cross-sections taken from HEC-RAS Mapper

Figure 5.8 Screenshot taken from the C-Map genesis website for the same segment in Figure 5.7.

Figure 5.7 and Figure 5.8 show an example of the cross-sections that were made on the identical river segment. The cross-sections on Figure 5.7 were digitized cross-sections from HEC-RAS Mapper, whereas the cross-sections on Figure 5.8 were manually made to replicate the HEC-RAS cross-sections.

The contour lines are cut by each cross section and the corresponding image is opened in GetData graph digitizer software. Here the image from C-Map Genesis is analyzed. The scale of the image is set according to the scale of the map (right lower corner of Figure 5.6 as an example). Then the points on the cross-section line crossing with the contour lines are then captured. These points provide the co-ordinates of the intersections of cross-section line and contour lines, which are used to calculate the distance in between two contour lines along the cross-section. The depth is found using the contour lines. The station of cross-section data in HEC-RAS is the distance from the most left reference point to any right point on the section when one looks downstream.

Figure 5.3 implies that the station versus elevation data above the water surface are known and we just lack the data beneath the water surface. Now, the distance between contour lines calculated using the data from GetData Graph Digitizer is cumulatively added to the station data of the most left point on the water surface, and the depth data got using C-Map genesis contours is subtracted from the elevation of water surface. This calculation provides bathymetry data on all contour lines. Figure 5.9 shows an example of the cross section after the bathymetry data is calculated.

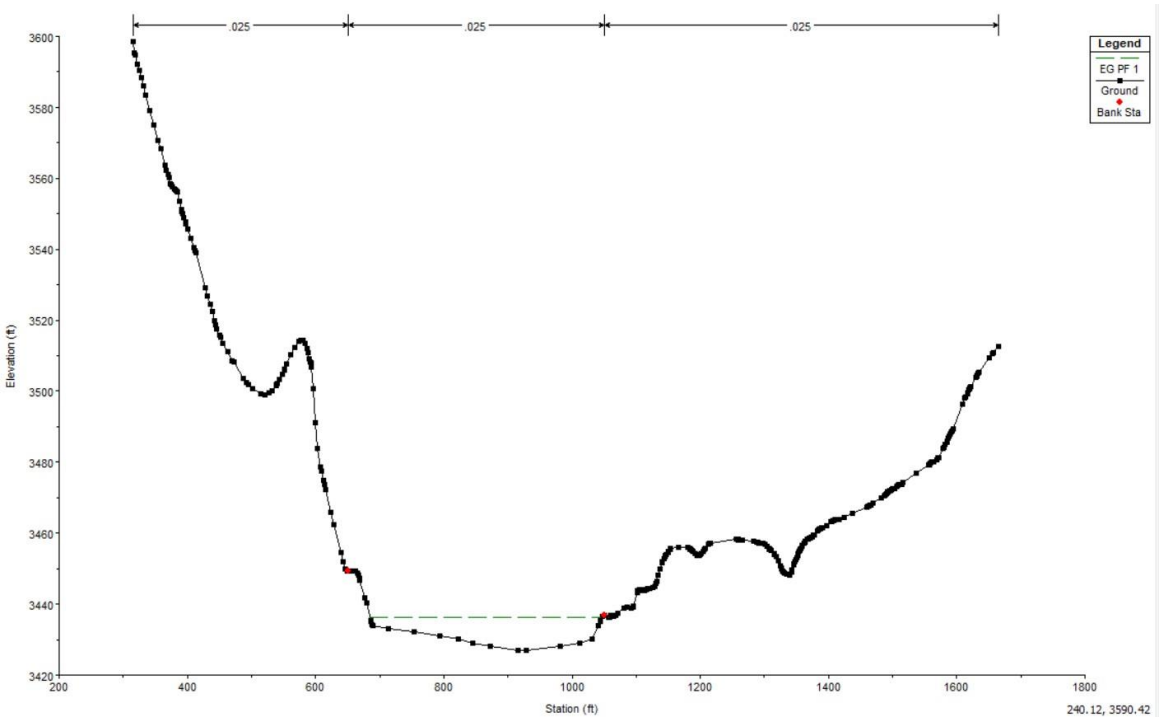

Figure 5.9 Cross section with bathymetry data from contour method imported to HEC-RAS (green dashed line is the simulated energy grade line).

5.2.2 GIS METHOD ON LIDAR DATA

A geographic information system (GIS) is a particular kind of database that combines software tools for managing, analyzing, and displaying data with spatial information. GIS can be used for various functions. The use of GIS to extract the bathymetry data is carried out. First of all, NWE (Northwestern Energy Hydro) through AMARUQ Environmental Services LLC provided the surveyed data (csv format) consisting of depths of water in feet at many points (longitude and latitude) along the upper Missouri River. The surveyed point data for every point is associated with Longitude, Latitude and Depth in feet (Table 5.1).

ArcGIS Pro is used to obtain the bottom elevation data, using techniques of GIS. The Lidar data available from Montana Lidar Inventory, (Figure 5.1) for 2/3rd of the study area is used to obtain the elevation data in the overbank areas (floodplains) with/without high-elevation areas from the bank of the rivers on both sides. The surveyed point data consisting of depth information, are merged with Lidar data to generate the cross-section geometry at the study area including the river bathymetry using GIS.

Steps involved in merging depth data with Lidar elevation data:

1. The point data consisting of latitude, longitude, and depth (in feet) is plotted in the ArcGIS Pro.
2. The Lidar data with surface elevation in "m" is also plotted in ArcGIS Pro.
3. "Extract Multi Values to Point" command is used to get surface elevation at all the points.
4. The surface elevation obtained in "m" is converted to "ft", and then depth of water available already is subtracted from the elevation, providing the bottom elevation data for all points.
5. The new point data consisting of longitude, latitude, and bottom elevation (ft) is projected in ArcGIS Pro.
6. A polygon of the river is created on ArcGIS Pro for the study area where point data is available.
7. The point data available from 5 is then interpolated using IDW command on ArcGIS Pro, which creates a raster surface using the point data and contains the bottom elevation data. The cell size of the raster surface is made same as the Lidar data.
8. The newly created raster surface on 7, is clipped with the polygon of the river on 6, which provides the raster surface with bottom elevation of river.
9. The two raster surface, created from interpolation (8) and Lidar data (2) is then merged using "Mosaic to New Raster" tool, keeping the raster with bottom elevation of river on top and Lidar data elevation on bottom on overlapping areas.
10. The resulting raster consists of elevation provided by Lidar data on the overbank regions, and the elevation provided by point data on the river channel.
11. The raster is then saved on TIFF format, which can be used on HEC-RAS. The projection of the raster is set as NAD83 / Montana (ft).

The surveyed point data and the Lidar data are projected on the ArcGIS Pro and overlaid as in Figure 5.10. The point data is available up to the Cascade from the Holter Lake. And the raster data (Lidar data) covers the region from a little upstream than Dearborn River junction point in Missouri river to the Great Falls. The bottom elevation for the overlapping region can only be extracted.

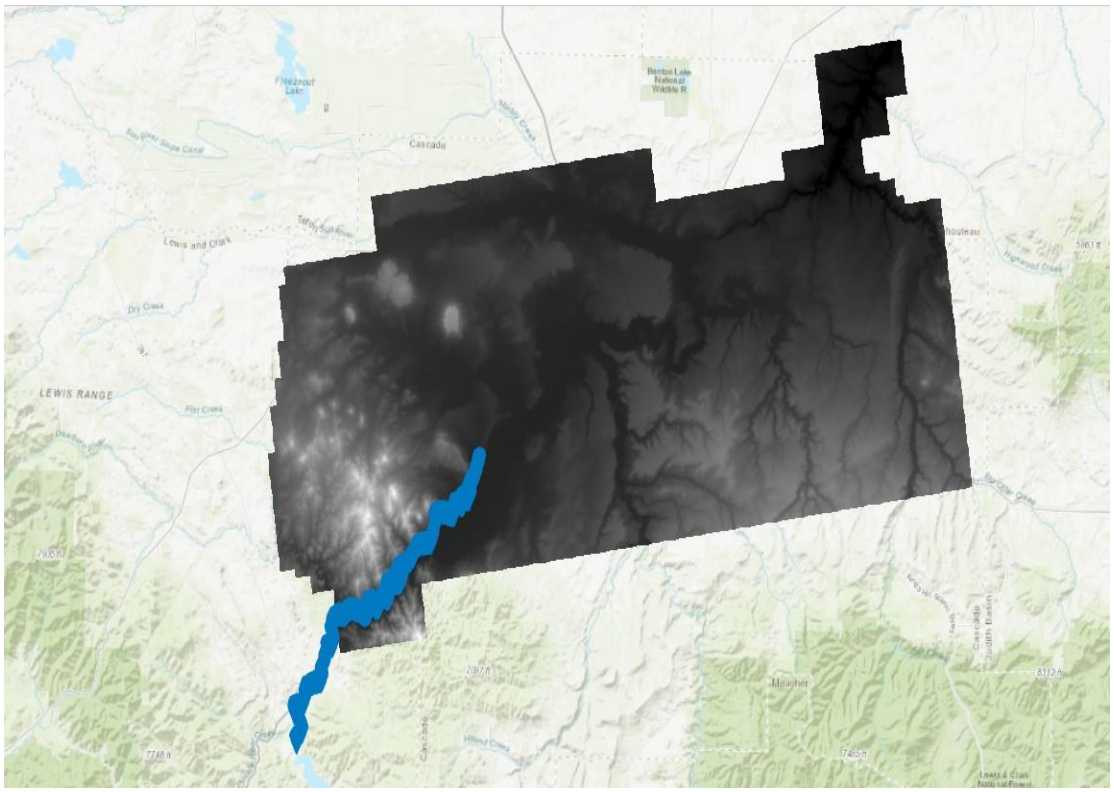

Figure 5.10 Projection of surveyed point data and Lidar data on the study area on ArcGIS Pro

Table 5.1 Available and extracted information of an example surveyed point data

Longitude	Latitude	Depth (in ft)	DEM (m)	DEM (ft)	Bottom elevation (ft)	Bottom elevation (m)
-111.94	47.12	-1.77	1046.85	3434.56	3432.79	1046.31

In addition to Longitude, Latitude, and Depth (in ft) provided on the survey point, extracted or calculated data from the Lidar data are also listed in Table 5.1. DEM (ft) is the elevation at the point that is extracted from the Lidar data using "extraction of multi values" tool. The Lidar data extracted is in "meters" initially, i.e., DEM (m) column, which is then converted to "feet". Bottom elevation (ft) is the bottom elevation after the depth of the water is subtracted from the DEM, i.e., DEM (ft) + Depth (ft). Bottom elevation (m) is the bottom elevation after converting the bottom elevation from "feet" to "meters".

Now all surveyed points that are on the overlapping region on Figure 5.10 will have bottom elevation which is then interpolated for the whole river. Figure 5.11 shows the zoomed image of point data on the boundary of available raster data. The points lying on the raster data will have its bathymetry data available, whereas the one out of the raster will not. Finally, the two surface: (1)

the interpolated surface with depth data and (2) initial Lidar data with surface elevation for floodplains, are merged which results in the DEM data with bathymetry data. The resulting cross-section after obtaining the bathymetry data is shown in Figure 5.12.

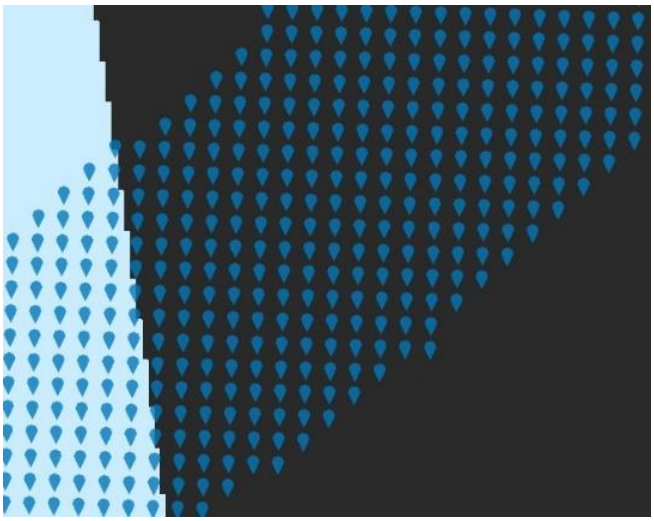

Figure 5.11 Detail image of surveyed point data overlying on the boundary of raster surface.

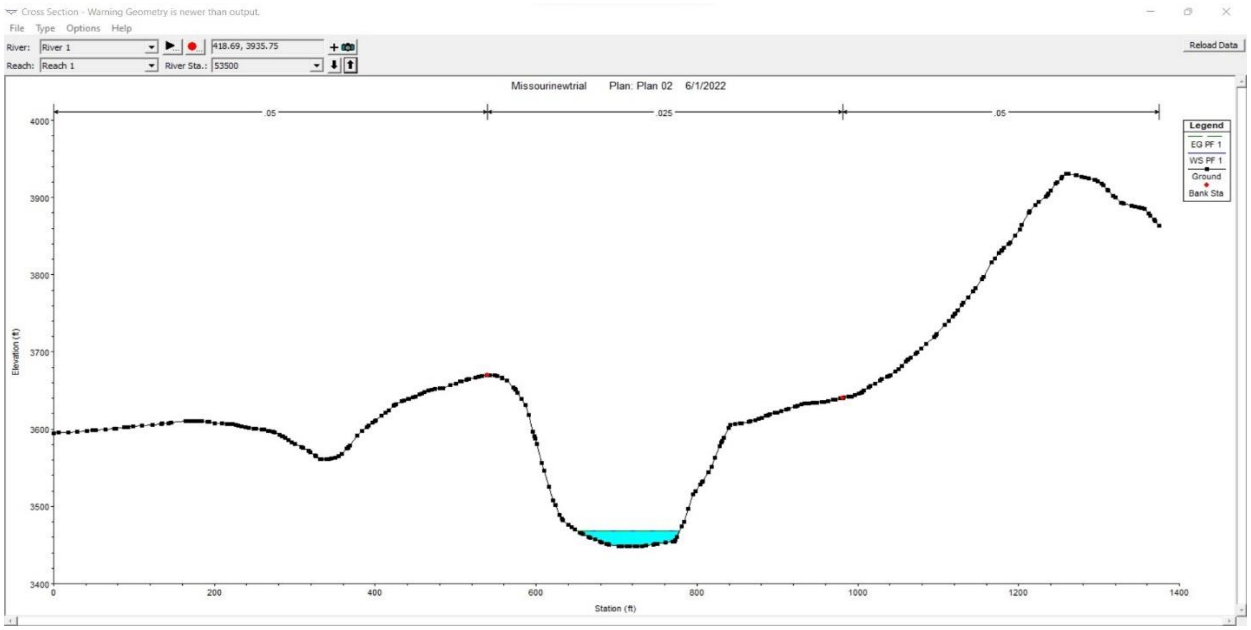

Figure 5.12 Sample of cross-section with bathymetry data obtained from GIS method for Missouri river.

5.2.3 GIS METHOD ON USGS DEM DATA

Lidar data are is not available for the entire reach of the study area. For the Missouri River, Lidar data is not available from the upstream of the Dearborn River to the Holter Lake. Due to this lack

of Lidar data availability, USGS 1/3 arc-second DEM (10 meters) resolution is used, which covers the entire study area.

For USGS 1/3 arc-second DEM is downloaded from the apps.nationalmap.gov/downloader/ for the study area, which is then merged using “Mosaic” feature in ArcGIS Pro. The resulting raster is the base raster that is used for bathymetry data acquisition process by GIS method.

The same steps as 5.2.2 GIS METHOD ON LIDAR DATA are applied on USGS DEM as well. This indicates the diminishing precision of bathymetry data as compared to the one we get from Lidar data.

5.3 BOUNDARY CONDITIONS

Boundary conditions are required to establish the starting water surface at the river system's ends (upstream and downstream). A starting water surface is required for the program to begin calculations. In a subcritical flow regime, boundary conditions are only required at the river system's downstream ends. If a supercritical flow regime is to be calculated, boundary conditions are only required at the river system's upstream ends. If a mixed flow regime calculation is to be performed, boundary conditions at all ends of the river system must be entered (USACE 2016).

The boundary conditions for steady and unsteady flow for HEC-RAS simulation are discussed on steady flow simulation and unsteady flow simulation section. Every reach is listed in a table in the boundary conditions editor. Each reach has two boundary conditions: upstream and downstream. Internal boundary conditions are connections to junctions. Internal boundary conditions are listed in the table automatically based on how the river system was defined in the geometric data editor. Only the necessary external boundary conditions must be entered by the user.

5.3.1 STEADY FLOW SIMULATION

For the steady flow simulation in HEC-RAS, four types of boundary conditions consist of:

(1) Known water surface elevations – a known water surface elevation for each of the profiles to be computed is required to input.
(2) Critical depth –HEC-RAS program calculates the critical depth of each profile using flow and cross section data at the boundary and use that as the boundary condition. No further information is required to input.

(3) Normal depth – energy slope is required to input and used in calculating normal depth by Manning's equation at the boundary. If the energy slope is unknown, the user could approximate it by providing either the slope of the water surface or the slope of the channel bottom.

(4) Rating curve – an elevation versus flow rating curve table is inputted. Then for each profile, the water surface elevation at the boundary is interpolated from the rating curve based on discharge.

For this study, "Normal Depth" is used as boundary condition, with estimated energy slope as 0.00076 at Cascade (Figure 5.13) for all profiles.

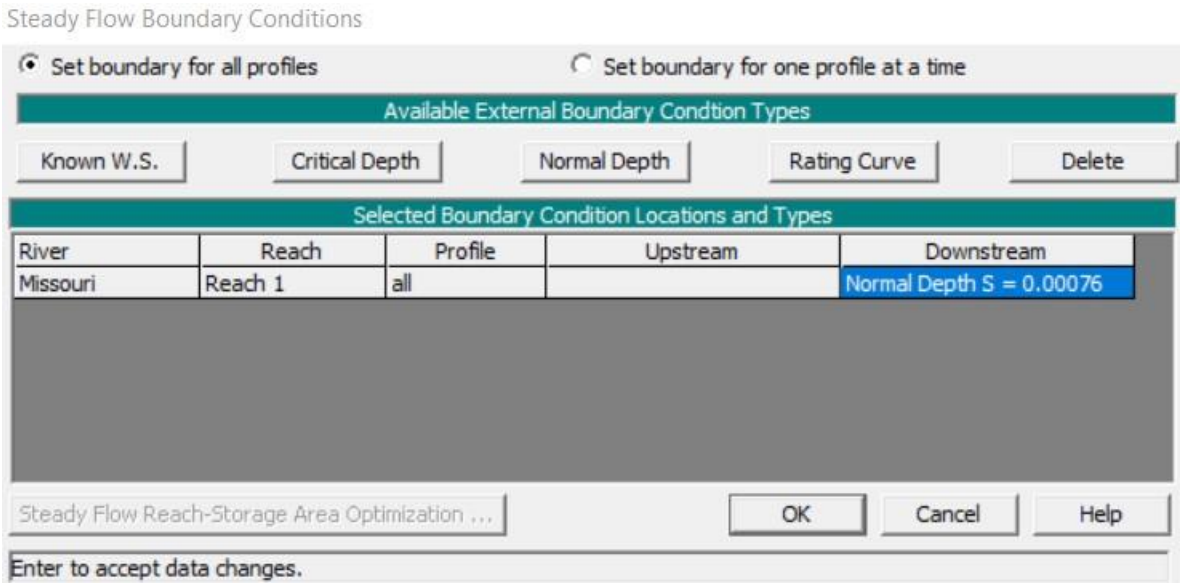

Figure 5.13 HEC-RAS window for entering steady flow boundary conditions.

5.3.2 UNSTEADY FLOW SIMULATION

For unsteady flow simulation, there are several types of boundary conditions available to the user. Some of them are discussed here:

(1) Flow hydrograph – A hydrograph is a graph of the flow in a stream cross section over a period of time. A flow hydrograph can be used as either an upstream or downstream boundary condition, while it is most frequently employed as an upstream boundary condition.

(2) Stage hydrograph – A stage hydrograph is the graph of stage of water in a stream cross section over a period of time. It can also be either used as either an upstream or downstream boundary condition.

(3) Stage and flow hydrograph – The stage and flow hydrograph option can be used as a boundary condition either upstream or downstream. The upstream stage and flow hydrograph is a mixed boundary condition. The stage hydrograph is used as the upstream boundary until it runs out of data, at which point the program automatically switches to using the flow hydrograph as the boundary condition. This kind of boundary condition is mostly used in forecast models, where the stage is based on what has been seen up to the time of the forecast, and the flow is based on a forecasted hydrograph.

(4) Rating curve – It is possible to apply the rating curve option as a downstream boundary condition. The downstream rating curve is a single valued relationship and does not represent a rating loop that might take place during an event. This presumption could lead to inaccuracies close to the rating curve. When the slope of the water surface is not steep enough to dampen the errors over a reasonably short distance, the errors become a concern for streams with mild gradients. When utilizing a rating curve, make sure it is downstream of the research area by a sufficient amount to ensure that any inaccuracies it introduces do not impair the study reach.

(5) Normal depth – Only an open-ended reach's downstream boundary condition can be utilized with the normal depth option. For each computed flow, a stage is estimated using Manning's equation. For the reach nearby, the friction slope (slope of the energy grade line) is necessary. The friction slope is frequently estimated from the slope of the water's surface, but it might be challenging to determine this in advance. The friction slope is frequently estimated using the typical bed slope in the vicinity of the boundary condition. When using this form of boundary condition, it should be put far enough downstream so that any inaccuracies it causes will not have an impact on the outcomes at the study reach, as is advised with the rating curve option.

For the unsteady flow condition in Missouri River, flow hydrograph as upstream boundary conditions and normal depth as downstream boundary conditions were taken.

5.4 PROFILE ELEVATION COMPARISON

The water surface profile is a measure of how flow depths change longitudinally throughout the river. The water surface profiles are generated after steady and unsteady flow simulation.

The profile elevation plot in HEC-RAS also gives the understanding of the riverbed elevation. The profile elevations obtained from the manual method of bathymetry data collection and the GIS method of bathymetry data collection show a difference in elevation. Figure 5.14 compares the elevation of river bottom or the minimum channel elevation, that is obtained from the GIS method (both Lidar and USGS DEM) and the Manual method (Contour map method). The main channel distance varies for the data because for the Manual method and Lidar method, the 1-m Lidar data available from upstream of Dearborn River to Cascade is used, while for the USGS DEM, the 10-m DEM data from Holter to Cascade is used. Water depths in Missouri River are all from the surveyed data (Figure 5.10 and Figure 5.11) for all the methods. The bottom elevation (ft) profiles are comparatively similar for the manual method and the GIS method using Lidar DEM, but the GIS method using USGS DEM shows some discrepancies. This is because of the difference in resolution of the DEM.

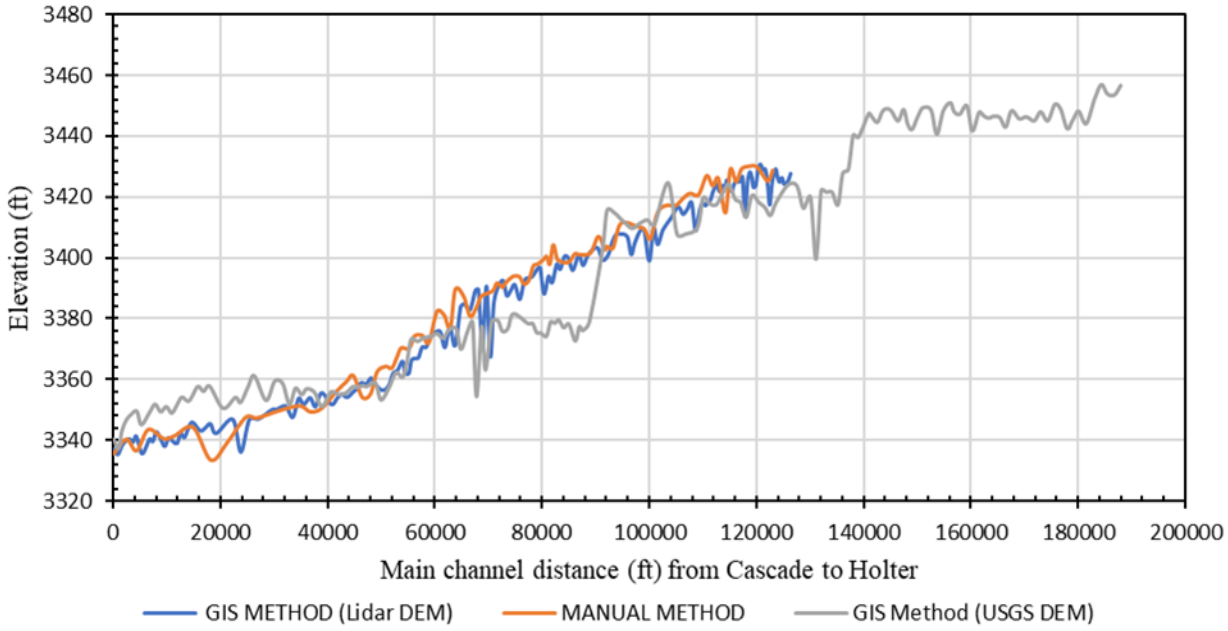

Figure 5.14 Bottom elevation comparison along the main channel distance of the minor channel elevation obtained from GIS method and Manual method (Contour map method)

5.5 HEC-RAS MODEL RESULTS

5.5.1 OPEN WATER STEADY FLOW SIMULATION

The HEC-RAS steady flow simulation is done for open water season with no ice cover and ice jamming. The steady flow is set up as 7947.63 cfs (average flow of 1 June, 2020 – 15 July, 2020), with flow change location at 1.5 miles downstream of the most upstream point of the study area above Dearborn river. It is the junction of Dearborn River and the Missouri River. This flow change location adds a discharge of 454.9 cfs (average flow of 1 June, 2020 – 15 July, 2020) (Figure 5.15). For the boundary condition on steady flow simulation, the normal depth is taken to be 0.000717, which is the slope of river bed elevation, Figure 5.16.

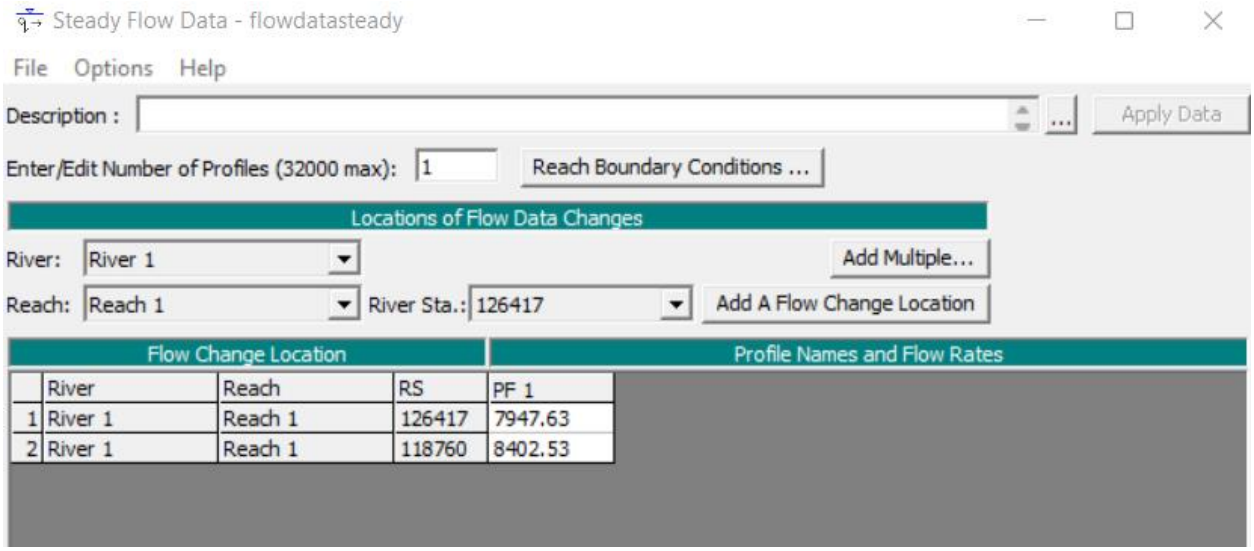

Figure 5.15 Steady flow simulation for open water season with flow change location at the junction of Dearborn river and Missouri River when Lidar DEM (GIS method) geometry data is used.

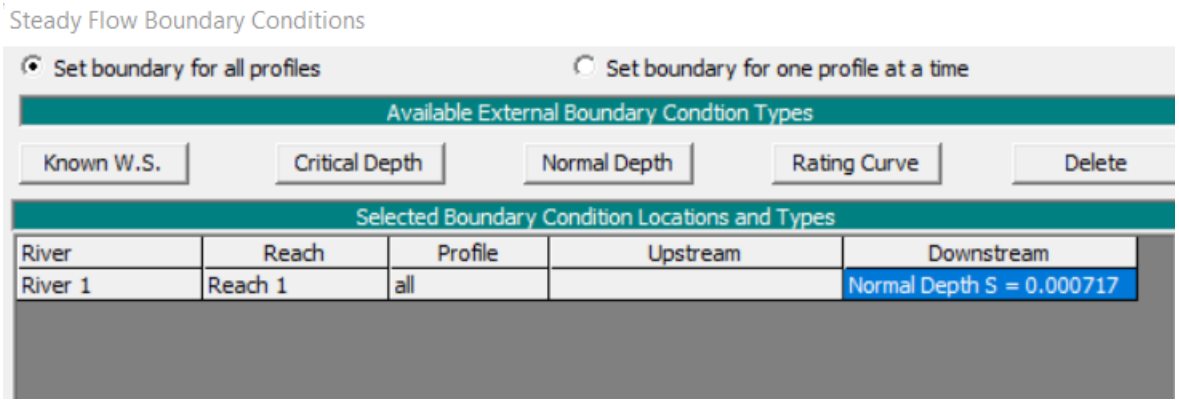

Figure 5.16 Boundary condition set up for Missouri River at downstream using normal depth when Lidar DEM (GIS method) geometry data is used.

The geometric data used for the model set up is with the one with GIS method using Lidar data. The water surface profile generated from the steady flow simulation is shown in

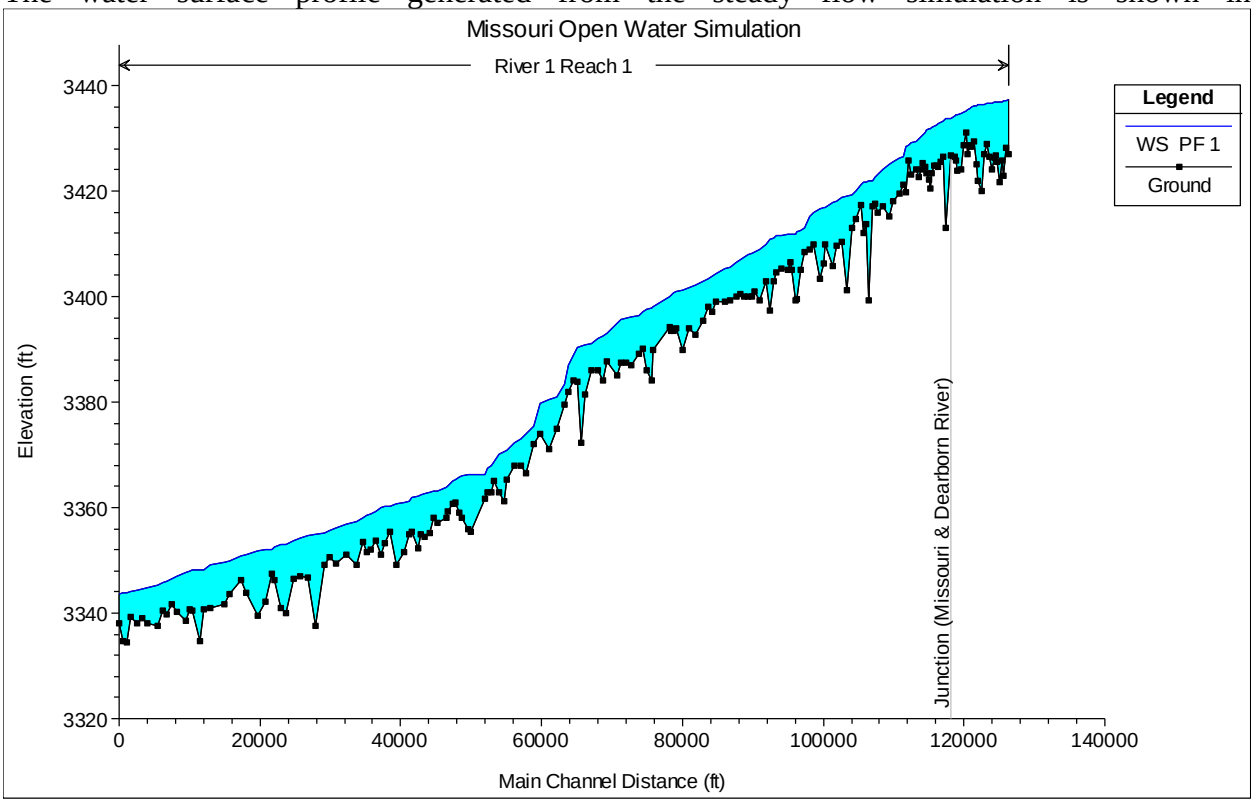

Figure 5.17. In real scenario, there is no steady flow on natural river.

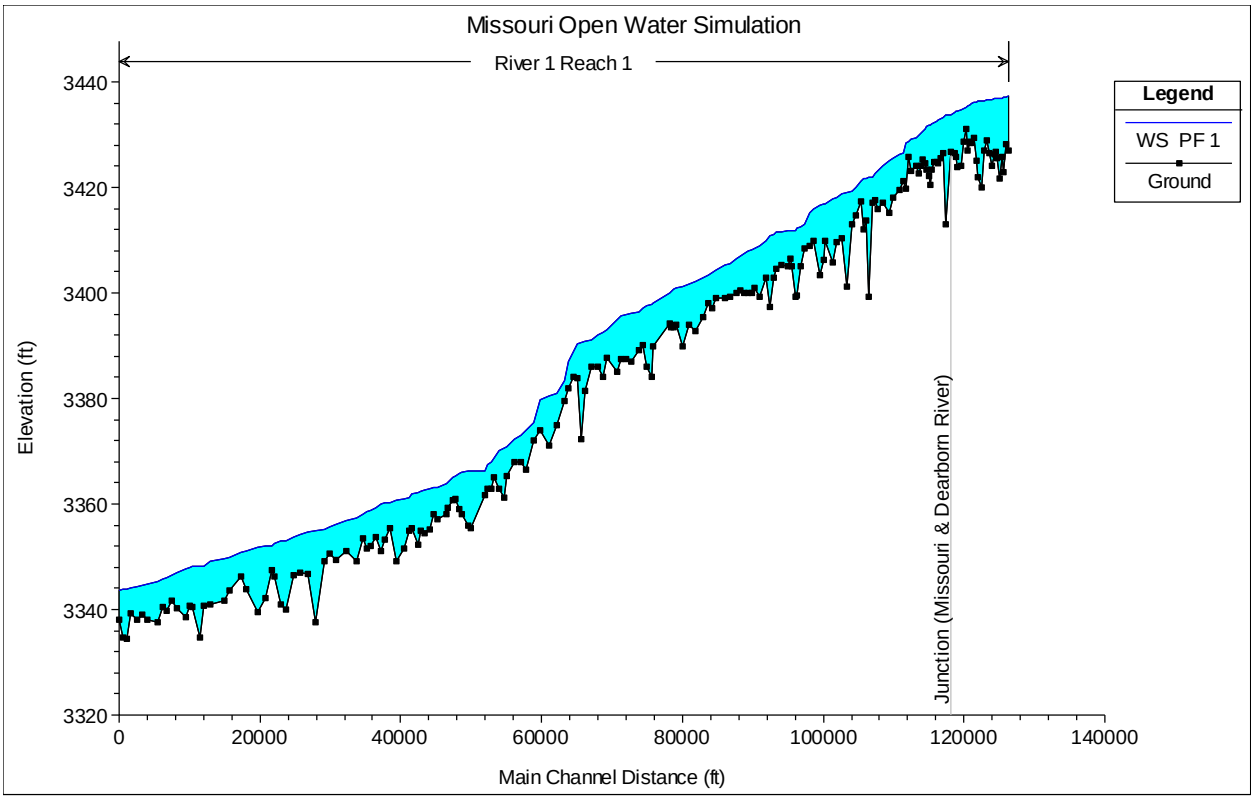

Figure 5.17 Profile plot with the water surface elevation and bottom channel elevation of Missouri River after steady flow simulation for open water case using Lidar DEM and GIS method..

The detailed output generated from the steady flow simulation at Cascade is summarized in Table 5.2.

Table 5.2 Detailed output table at Cascade from HEC-RAS by steady state simulation.

Energy grade line (E.G.) for given water surface elevation (ft)	3342.55
Velocity head (ft)	0.14
Water surface elevation (WSEl) (ft)	3342.41
Critical WSEl (ft)	3339.88
E.G. Slope (ft/ft)	0.000718
Total discharge (cfs)	5693.54
Top Width (ft)	553.07
Total velocity (ft/s)	2.95
Maximum Channel depth (ft)	5.44
Min Ch El (ft)	3336.97

The steady flow simulation for the same flow data as Figure 5.15 and boundary condition as Figure 5.16 but with the geometric data from Holter to Cascade (achieved from USGS DEM) is used is carried out next in HEC-RAS. The number of cross-sections here are 159 and the average distance between them is 360 m. The resulting profile plot showing the water surface elevation and bottom

elevation is shown in Figure 5.19. The flow change location is set at the junction of Dearborn River and Missouri River, Figure 5.18. The slope of bed or normal depth (S) in this case is 0.000619.

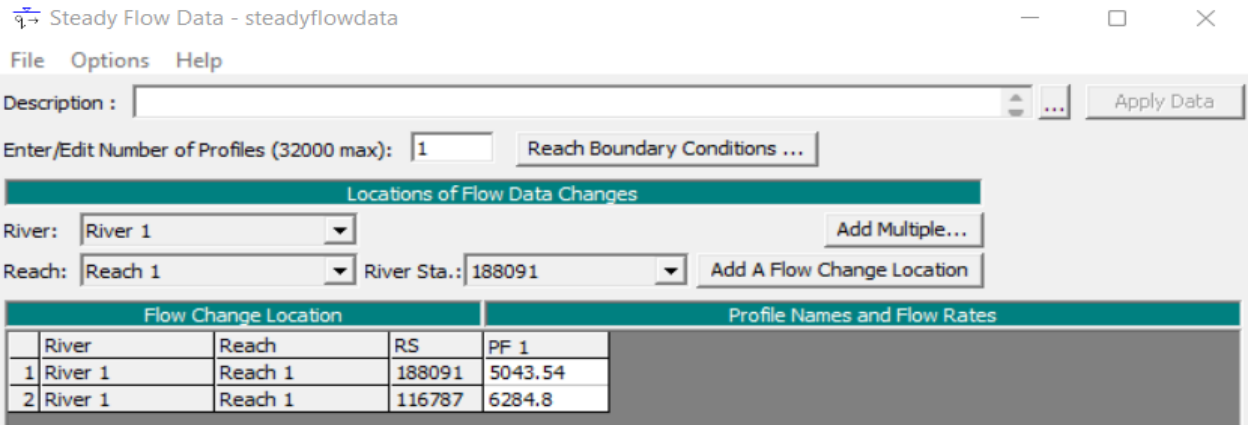

Figure 5.18 Steady flow simulation for open water season with flow change location at the junction of Dearborn river and Missouri River when USGS DEM (GIS method) geometry data is used.

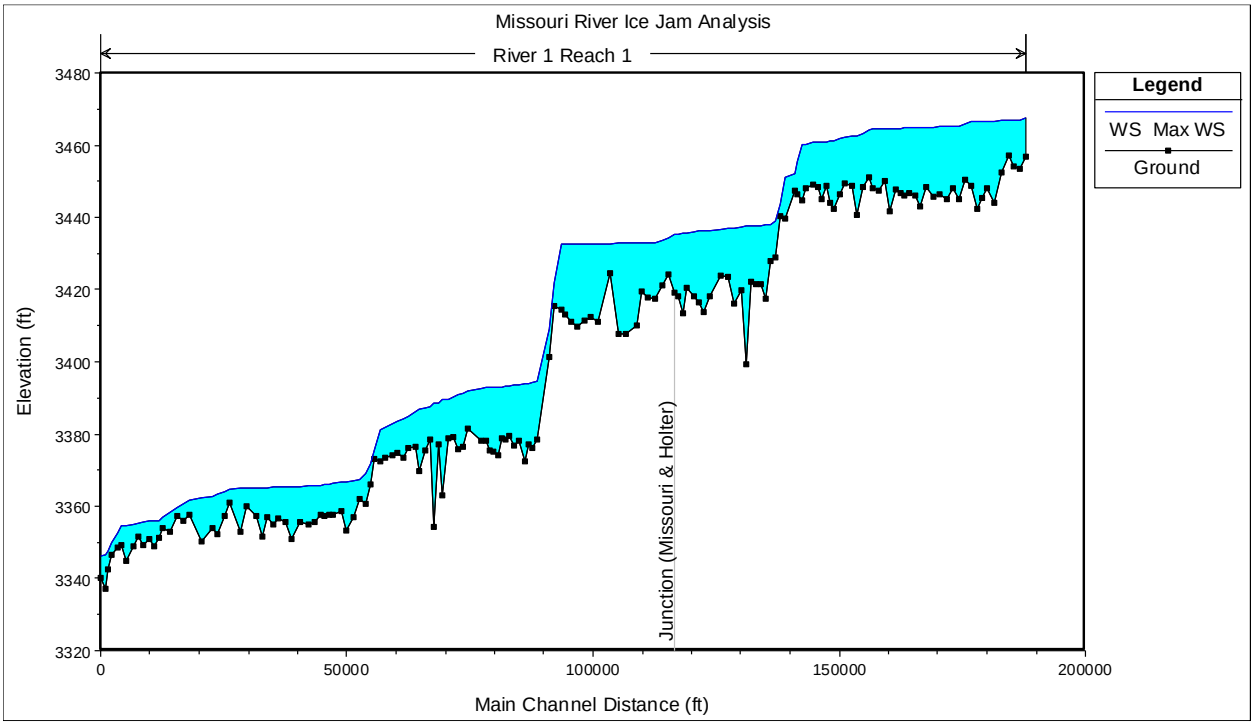

Figure 5.19 Profile plot with water surface elevation and bottom channel elevation of Missouri River after steady flow simulation for open water case using USGS DEM and GIS method.

5.5.2 OPEN WATER UNSTEADY FLOW SIMULATION

Unsteady flow simulation is also carried out for open water case with no ice cover and ice jamming. The data available on June 1, 2020 – July 15, 2020 is used for the unsteady flow simulation on the Missouri River. The unsteady flow simulation is carried for the geometry data collected from GIS

method with Lidar DEM, i.e., from 2.3 km upstream of Dearborn River and Missouri River junction to the Cascade. The boundary conditions required for unsteady flow simulation is shown in Figure 5.20. For the upstream, boundary condition is the flow hydrograph, Figure 5.21, from June 1 – July 15, 2020, flow from Holter is used for this. And for the downstream boundary condition, normal depth is used, where the slope is taken as 0.000619. A lateral inflow hydrograph is added at the junction of Dearborn River and Missouri River.

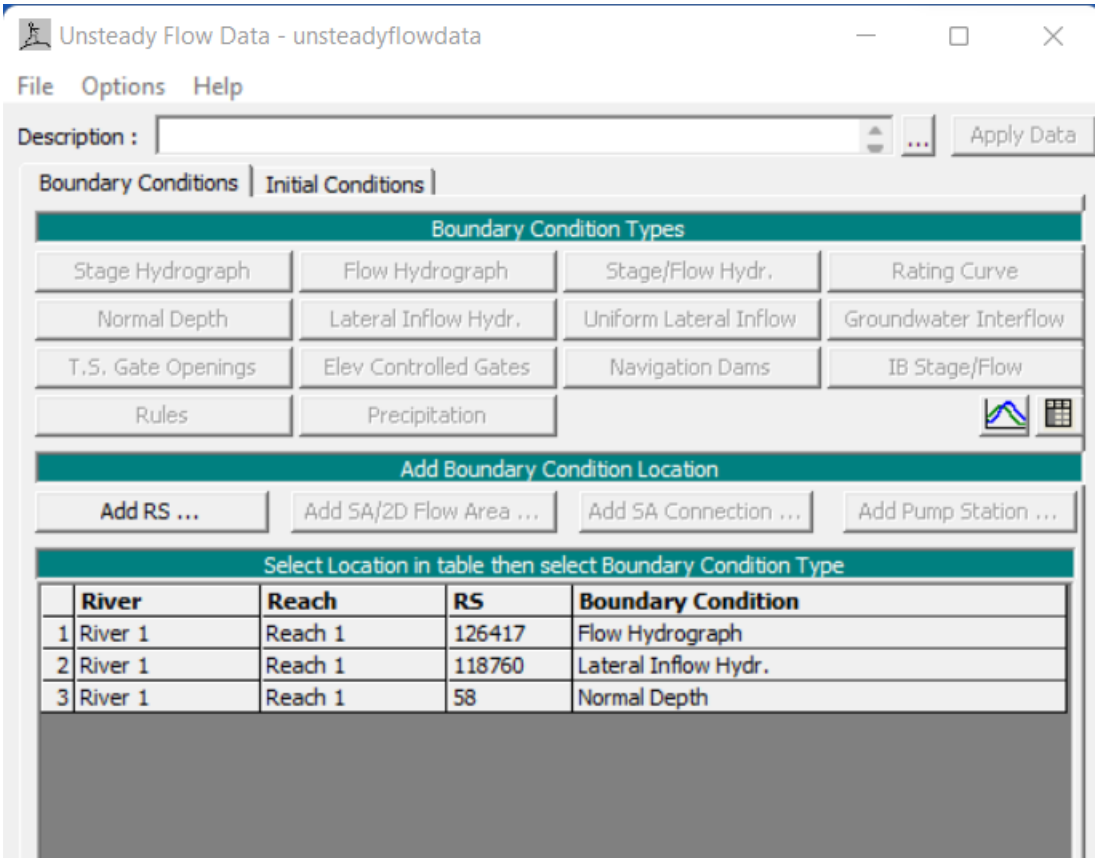

Figure 5.20 Boundary conditions of unsteady flow simulation in HEC-RAS from Holter to Cascade.

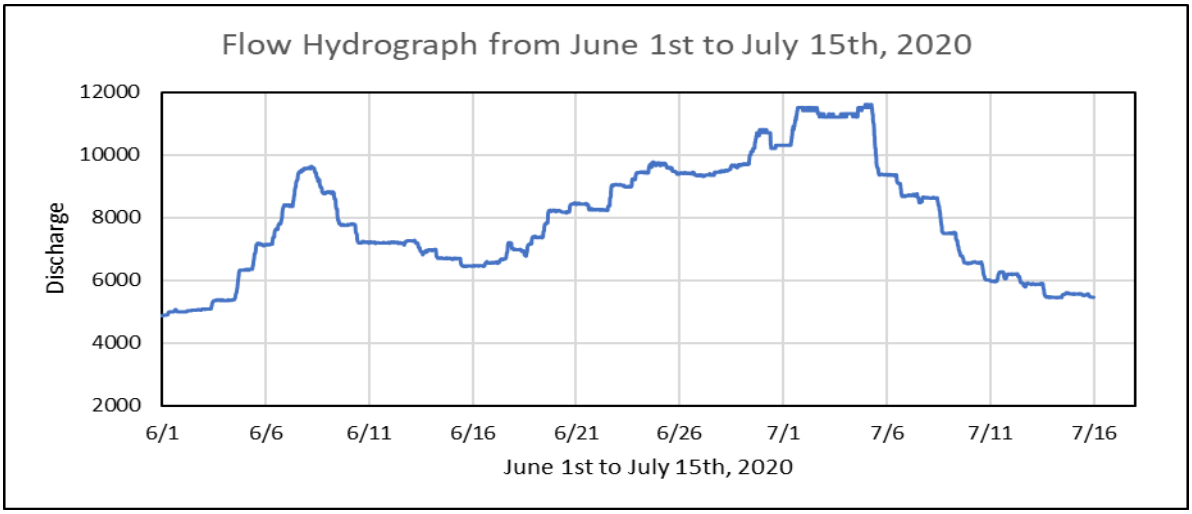

Figure 5.21 Flow hydrograph at Holter for June 1st – July 15th, 2020 used as boundary conditions for unsteady flow simulation.

The resulting profile plot showing the water surface elevation and bottom elevation on 15th July 23:45 is shown in Figure 5.23. Figure 5.25 shows the outflow hydrograph and the stream stage hydrograph at the most downstream cross-section i.e., at Cascade. These are the results obtained from the unsteady flow simulation for open water season.

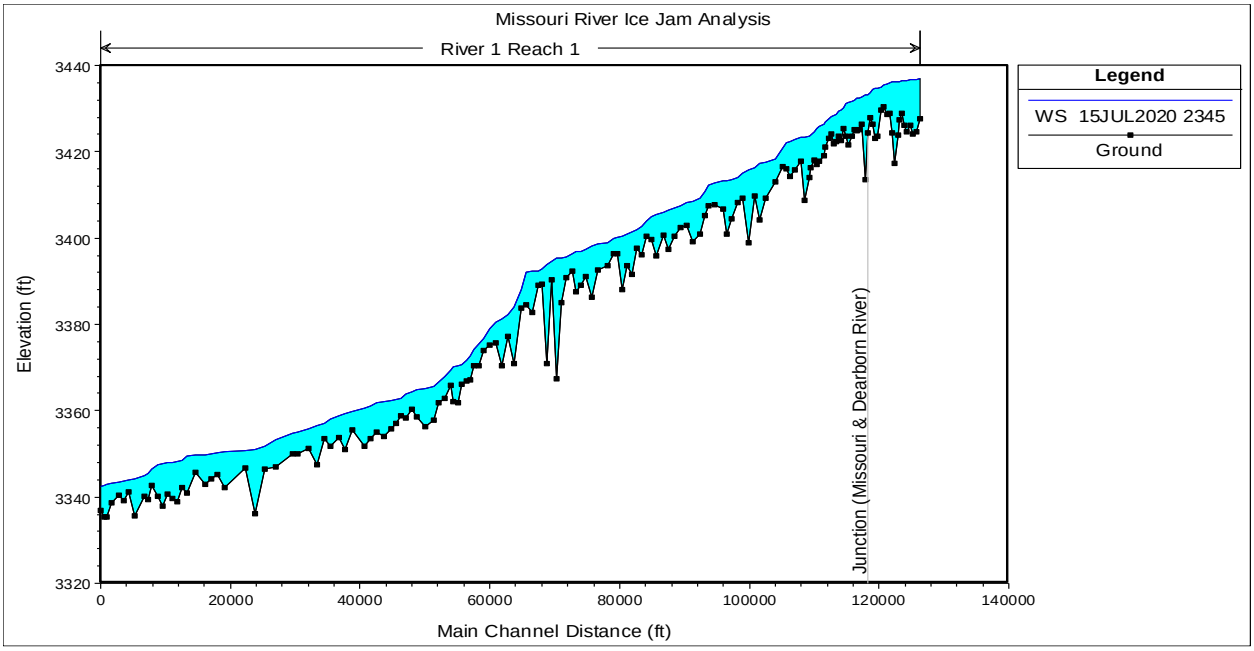

Figure 5.22 Water surface elevation of 15 July2020 23:45 for open water unsteady flow simulation on 1 June – 15 July, 2020 using geometry data obtained from GIS method (Lidar DEM).

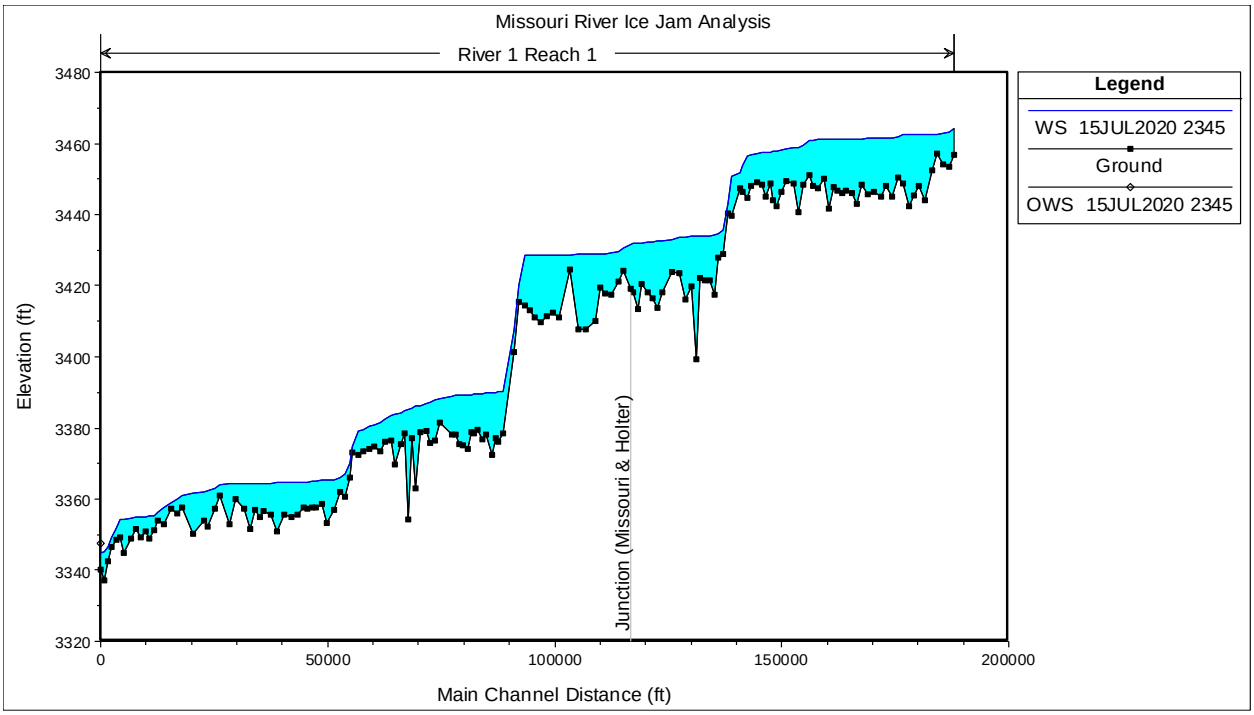

Figure 5.23 Water surface elevation of 15 July2020 23:45 for open water unsteady flow simulation on 1 June – 15 July, 2020 using geometry data obtained from GIS method (USGS Dem).

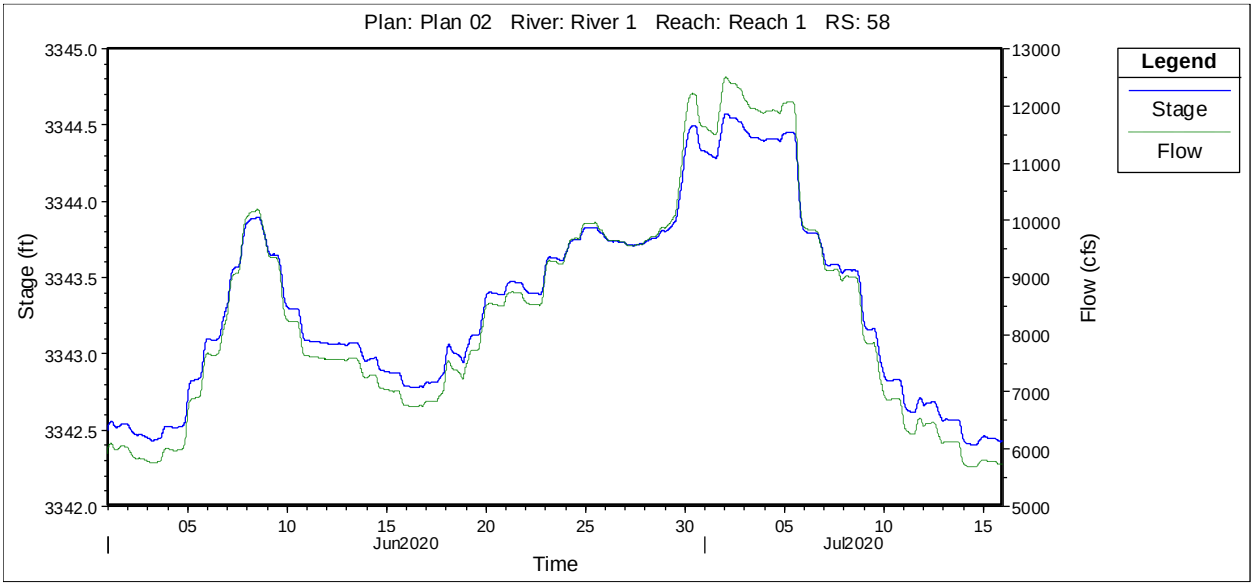

Figure 5.24 Outflow hydrograph and stage hydrograph at Cascade obtained in HEC-RAS from the unsteady simulation for open water from 1 June – 15 July, 2020 using geometry data obtained from GIS method (Lidar DEM).

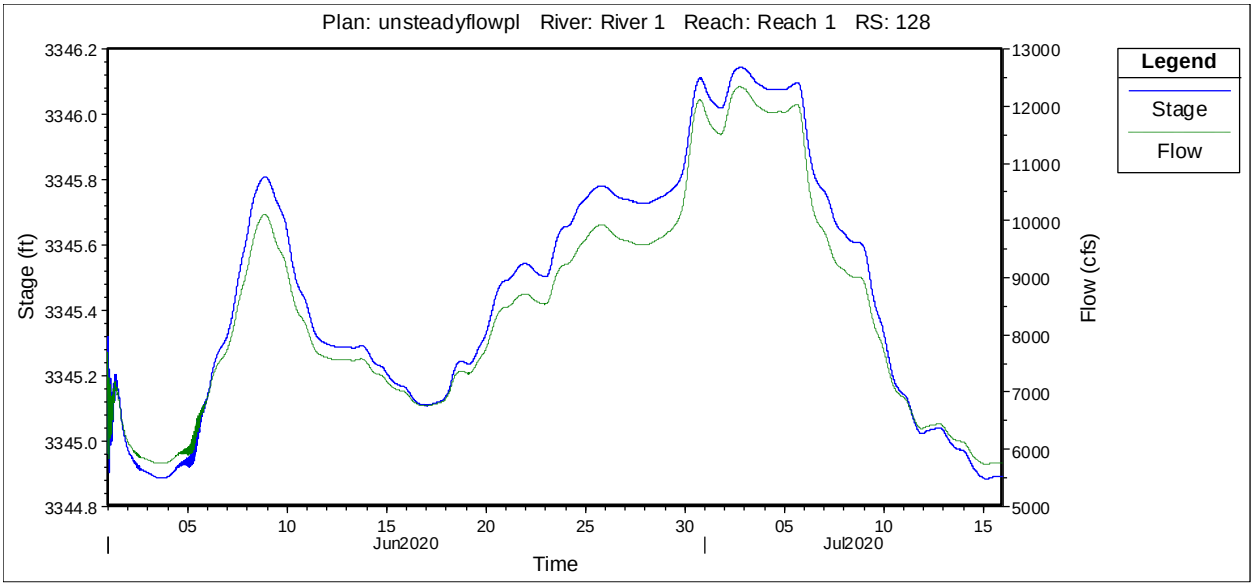

Figure 5.25 Outflow hydrograph and stage hydrograph at Cascade obtained in HEC-RAS from the unsteady simulation for open water from 1 June – 15 July, 2020 using geometry data obtained from GIS method (USGS Dem).

The outflow hydrograph observed and simulated from the HEC-RAS (Figure 5.27) shows close relationship. The simulated outflow initially shows some variations from the observed data.

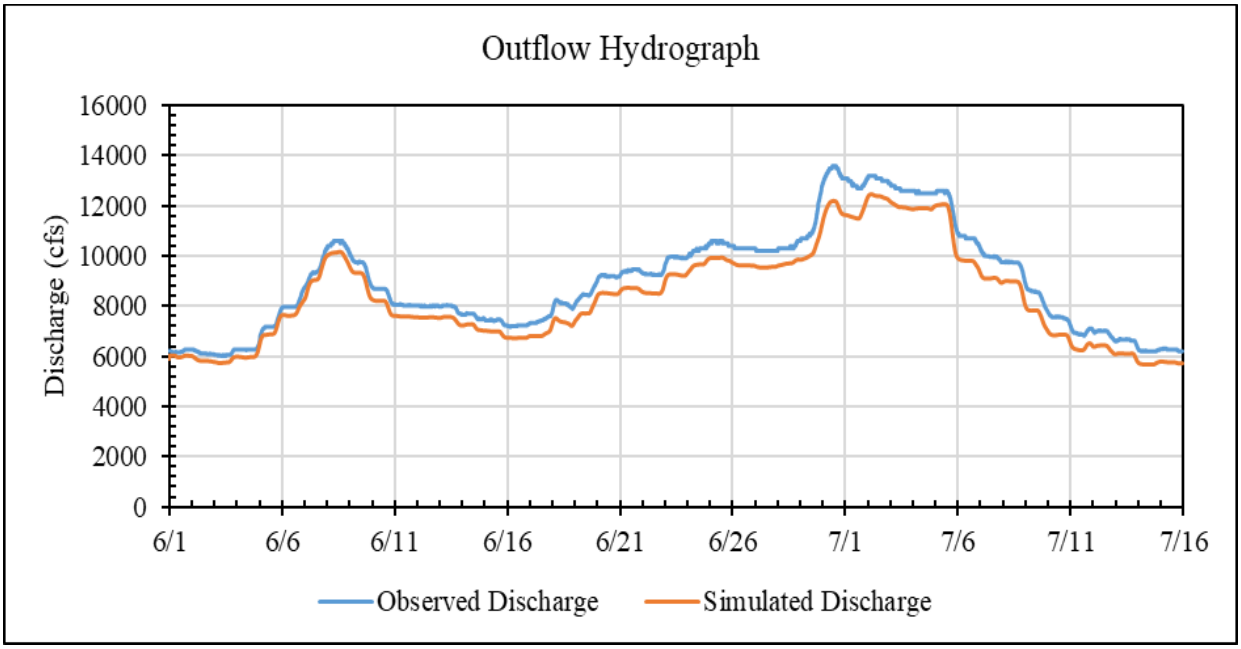

Figure 5.26 Simulated hydrograph vs Observed hydrograph at Cascade from June 1st – July 15th using geometry data obtained from GIS method (Lidar DEM).

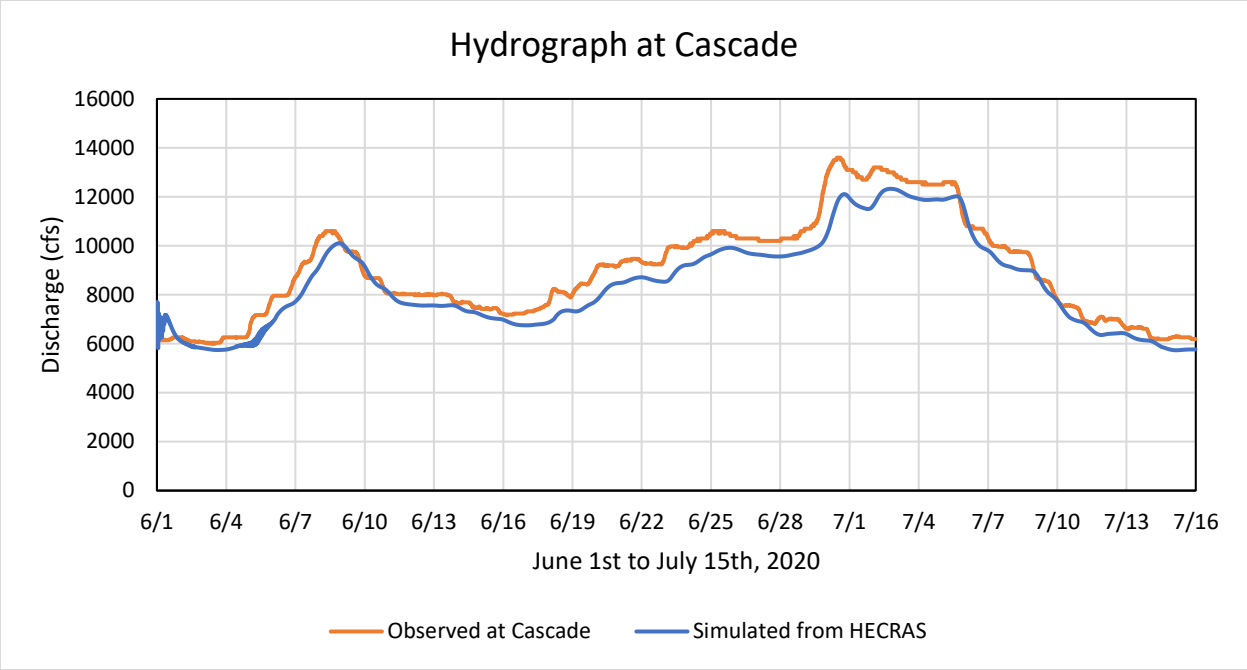

Figure 5.27 Simulated hydrograph vs observed hydrograph at Cascade from June 1st – July 15th using geometry data obtained from GIS method (USGS DEM).

CHAPTER 6. ICE COVER AND ICE JAM SIMULATION IN HEC-RAS

6.1 INTRODUCTION

HEC-RAS can be used for modeling and analysis of river ice. This chapter discusses the modeling of ice-covered rivers and testing of river ice data in HEC-RAS. River ice data can be edited in HEC-RAS using ice cover editor, Figure 6.1. When the ice cover geometry is known, i.e., if the ice cover thickness and roughness are known throughout the reaches of interest, the user can supply these data and describe the ice cover directly. If the ice cover is resulted from a wide-river type jam, HEC-RAS will estimate the jam thickness in reaches where the ice jam occurs (USACE 2016). In this case, the user can supply the material properties of the jam or use the default values.

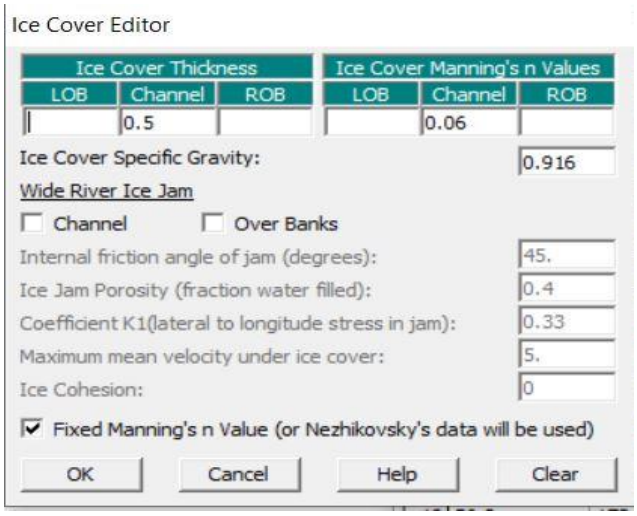

Figure 6.1 Ice cover editor window in HEC-RAS

The ice cover thickness specified in Figure 6.1 will be used as the initial estimate of the ice jam thickness and will also serve as the minimum thickness allowed for the ice jam at that section. If the jam is allowed in the overbank areas, the channel and overbanks hydraulic properties will be combined to calculate a single jam thickness for the channel and overbanks. Ice jamming is allowed by checking the box on Channel or Over Banks, on Figure 6.1.

In addition to the ice cover editor (Figure 6.1), the ice cover data can also be entered and edited using the ice cover data editor table, Figure 6.2. This is often very convenient to enter and view data for more than one cross section at a time. For example, select a column, type a value, add parameters such as ice specific gravity, friction angle porosity, stress K1 ration, maximum velocity, activate ice jam by selecting “y for yes” and “n for no”, etc. for desired cross-section at once.

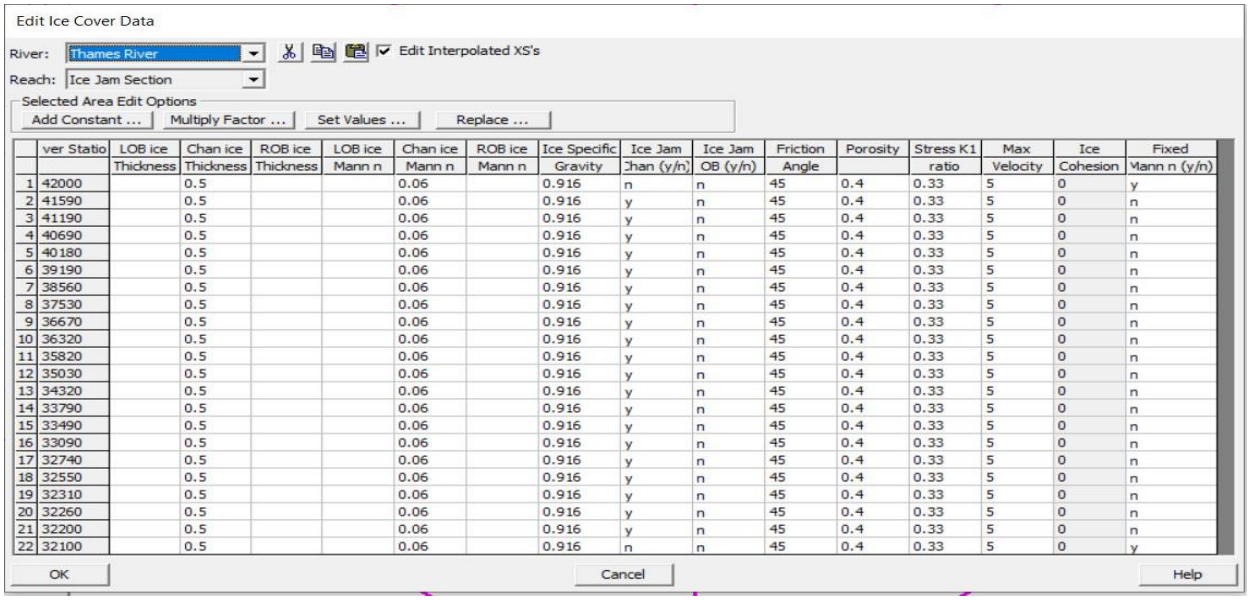

	ver Statio	LOB ice Thickness	Chan ice Thickness	ROB ice Thickness	LOB ice Mann n	Chan ice Mann n	ROB ice Mann n	Ice Specific Gravity	Ice Jam Chan (y/n)	Ice Jam OB (y/n)	Friction Angle	Porosity	Stress K1 ratio	Max Velocity	Ice Cohesion	Fixed Mann n (y/n)
1	42000		0.5			0.06		0.916	n	n	45	0.4	0.33	5	0	y
2	41590		0.5			0.06		0.916	y	n	45	0.4	0.33	5	0	n
3	41190		0.5			0.06		0.916	y	n	45	0.4	0.33	5	0	n
4	40690		0.5			0.06		0.916	y	n	45	0.4	0.33	5	0	n
5	40180		0.5			0.06		0.916	y	n	45	0.4	0.33	5	0	n
6	39190		0.5			0.06		0.916	y	n	45	0.4	0.33	5	0	n
7	38560		0.5			0.06		0.916	y	n	45	0.4	0.33	5	0	n
8	37530		0.5			0.06		0.916	y	n	45	0.4	0.33	5	0	n
9	36670		0.5			0.06		0.916	y	n	45	0.4	0.33	5	0	n
10	36320		0.5			0.06		0.916	y	n	45	0.4	0.33	5	0	n
11	35820		0.5			0.06		0.916	y	n	45	0.4	0.33	5	0	n
12	35030		0.5			0.06		0.916	y	n	45	0.4	0.33	5	0	n
13	34320		0.5			0.06		0.916	y	n	45	0.4	0.33	5	0	n
14	33790		0.5			0.06		0.916	y	n	45	0.4	0.33	5	0	n
15	33490		0.5			0.06		0.916	y	n	45	0.4	0.33	5	0	n
16	33090		0.5			0.06		0.916	y	n	45	0.4	0.33	5	0	n
17	32740		0.5			0.06		0.916	y	n	45	0.4	0.33	5	0	n
18	32550		0.5			0.06		0.916	y	n	45	0.4	0.33	5	0	n
19	32310		0.5			0.06		0.916	y	n	45	0.4	0.33	5	0	n
20	32260		0.5			0.06		0.916	y	n	45	0.4	0.33	5	0	n
21	32200		0.5			0.06		0.916	y	n	45	0.4	0.33	5	0	n
22	32100		0.5			0.06		0.916	n	n	45	0.4	0.33	5	0	y

Figure 6.2 Ice cover editor table window in HEC-RAS

6.2 MODELING ICE-COVERED RIVERS

Modeling of ice-covered rivers can basically be understood on two levels. The first level is an ice cover with known geometry, where the user specifies the ice cover thickness and roughness at each cross section. The second level is a wide-river ice jam where the ice jam thickness is determined at each section by balancing the forces on it. The material properties of the wide-river jam can be selected by the user and can vary from one cross-section to another.

6.2.1 MODELING ICE COVERS WITH KNOWN GEOMETRY

The exact processes by which an ice cover forms rely on the parameters of channel flow as well as the volume and type of ice produced. River ice coverings typically float in hydrostatic equilibrium because they respond to variations in water level both elastically and plastically. Along and across the channel, ice cover thickness and roughness can differ dramatically. A floating, stationary ice cover adds a new fixed boundary and a corresponding hydraulic roughness. A portion of the channel's cross-sectional area is likewise blocked from flow by an ice cover. The end outcome is typically a reduction in the channel conveyance, mostly through an increase in the wetted perimeter and a decrease in hydraulic radius, but also through changes to the effective channel roughness and channel flow area.

Conveyance of a channel or any subdivision of an ice-covered channel, K_i, can be estimated using Manning's equation:

$$K_i = \frac{1.486}{nc} A_i R_i^{2/3} \quad (6.1)$$

Where, n_c = composite channel roughness

A_i = Flow area beneath ice cover

R_i = hydraulic roughness modified to account for the presence of ice

Composite roughness is calculated using Belokon-Sabaneev formula as:

$$n_c = \left(\frac{n_b^{3/2} + n_i^{3/2}}{2} \right)^{2/3} \quad (6.2)$$

where, n_b = bed Manning's roughness value including channel bottom and sides on the left/right

n_i = ice-cover Manning's roughness value

The hydraulic radius of an ice-covered channel is found as:

$$\text{Ri} = \frac{A_i}{P_b + B_i} \quad (6.3)$$

Where, P_b = wetted perimeter associated with the channel bottom and side slopes

B_i = width of the underside of the ice cover

Separate values of ice thickness and roughness can be entered for the main channel and each overbank (Figure 6.1 and Figure 6.2) giving the user with the ability to have three separate ice thickness and ice roughness at each cross section. The amount of a floating ice cover that is beneath the water surface is determined by the relative densities of ice and water. The suggested range of Manning's *n* values for river ice covers is listed in Table 6.1 and Table 6.2.

Table 6.1 Manning's *n* value for river ice covers under different conditions

Type of Ice	Condition	Manning's *n* Value
Sheet ice	Smooth	0.008 to 0.012
	Rippled ice	0.01 to 0.03
	Fragmented single layer	0.015 to 0.025
Frazil ice	New 1 to 3 ft thick	0.01 to 0.03

	3 to 5 ft thick Aged	0.03 to 0.06 0.01 to 0.02

Table 6.2 Manning's *n* values for different types of ice with varying ice thickness

Thickness (ft)	Manning's n values		
	Loose frazil	Frozen frazil	Sheet ice
0.3	-	-	0.015
1.0	0.01	0.013	0.04
1.7	0.01	0.02	0.05
2.3	0.02	0.03	0.06
3.3	0.03	0.04	0.08
5.0	0.03	0.06	0.09
6.5	0.04	0.07	0.09
10.0	0.05	0.08	0.10
16.5	0.06	0.09	-

6.2.2 MODELING WIDE RIVER ICE JAMS

This is probably the most common type of river ice jam. Here, all the stresses acting on the jam are ultimately transmitted to the channel banks. The stresses are estimated using the ice jam force balance equation (6.2):

$$\frac{d(\sigma_x\, t)}{dx} + \frac{2\,\tau_b t}{B} = \rho' g S_w t + \tau_i \qquad (6.4)$$

where, σ_x = the longitudinal stress (along stream direction)

t = the accumulation thickness

τ_b = the shear resistance of the banks

B = the accumulation width

ρ' = the ice density

g = the acceleration of gravity

Sw = the water surface slope

τ_i = the shear stress applied to the underside of the ice by the flowing water.

Equation (6.2) balances changes in the longitudinal stress in the ice cover and the stress acting on the banks with the two external forces acting on the jam: the gravitational force attributable to the slope of the water surface and the shear stress of the flowing water on the jam underside.

For wide river ice jam, force balance equation and the energy equation (6.3) are solved alternatively until the ice jam thickness and water surface equations converge to fixed values at each cross section. This is "global convergence."

Energy equation is given as:

$$Z_2 + Y_2 + \frac{a_2 V_2^2}{2g} = Z_1 + Y_1 + \frac{a_1 V_1^2}{2g} + h_e \qquad (6.5)$$

where, Z_1, Z_2 = elevation of the main channel inverts at sections 1 (upstream) and 2 (downstream)

Y_1, Y_2 = depth of water at cross sections

V_1, V_2 = average velocities (total discharge/total flow area)

a_1, a_2 = velocity weighting coefficients

g = gravitational acceleration

h_e = energy head loss

6.3 TESTING OF RIVER ICE DATA

Analysis of ice-covered river is carried out on Thames River, for testing purpose. The geometry and flow data for Thames River are available from the HEC-RAS example data files for testing purpose.

The water surface elevations resulting from the presence of an ice cover, or an ice jam can be compared to the equivalent open water case. An ice cover changes the effective geometry, thus a separate testing for open water case, ice cover case, and the ice jam case is carried out and the water surface profile is examined.

6.3.1 OPEN WATER CASE

First, a geometry file was created that modeled the existing conditions for a reach of Thames River, which is a natural channel where an ice jam occurred. The modeled reach is 9720 m long with 22 cross sections, and main channel lengths to downstream section range from 50 m to 1030 m. Manning's *n* values in the main channel and overbank areas is taken as 0.025. Next, the steady flow data file was created in HEC-RAS. The profile selected to be analyzed corresponds to the estimated flow during the ice jam event. The flow value of 261 cubic meters per second (cms) was entered at the upstream river station, and a known downstream water surface elevation of 177.64 meters was entered in the Boundary Conditions. Next, the observed water surface elevations during the ice jam event were given and entered for all river stations. A steady flow simulation was run, and a straightforward open water output is received. The water surface elevations (Figure 6.3) calculated from HEC-RAS assuming open water, do not match the observed ice jam elevations at all. The profile plot showing the water surface and ground level with observed water surface in open water case is shown on Figure 6.3.

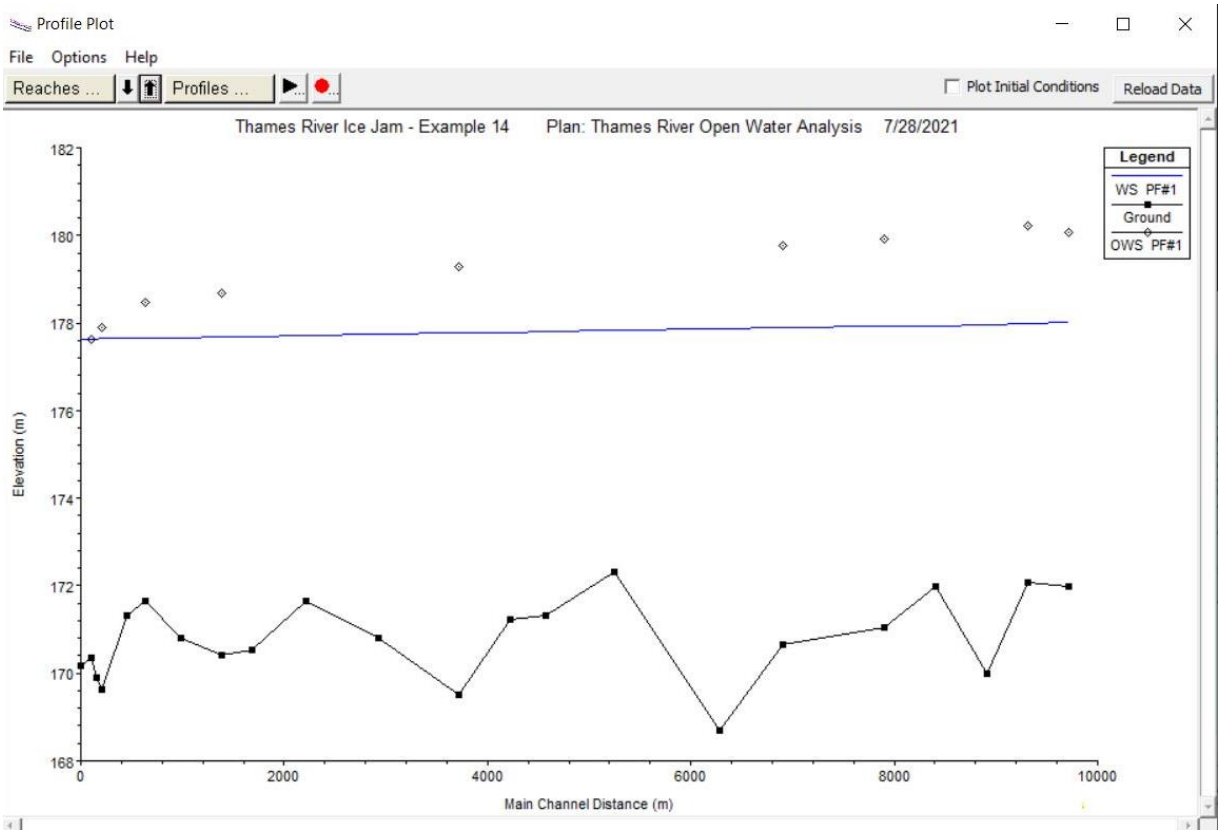

Figure 6.3 Profile plot of Thames River for open water case.

6.3.2 ICE COVER ANALYSIS

For analysis of ice cover case, the HEC-RAS geometry file was edited from that of an open water case. An ice cover with a constant thickness (assumed 0.5 m) and roughness (0.06) is placed on the channel. The geometry file is modified to reflect the presence of the ice cover, and a new plan for steady flow simulation is created with the original steady flow file. The profile plot showing the water surface and ground level with observed water surface and ice cover for ice covered case is shown on Figure 6.4.

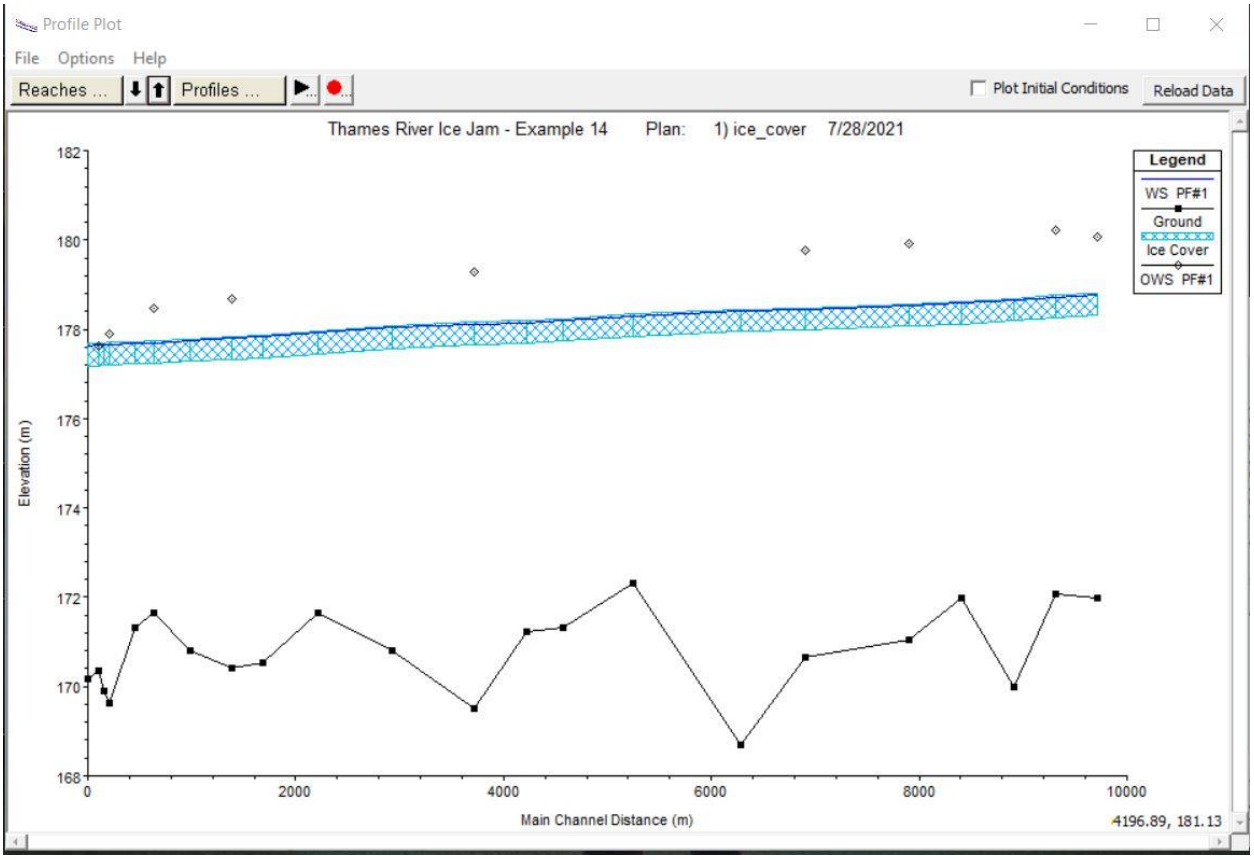

Figure 6.4 Profile plot of Thames River for ice cover case.

6.3.3 ICE JAM ANALYSIS

For ice jam analysis, the previous geometry file was modified to reflect the presence of the ice jam (Figure 6.5) with the original steady flow.

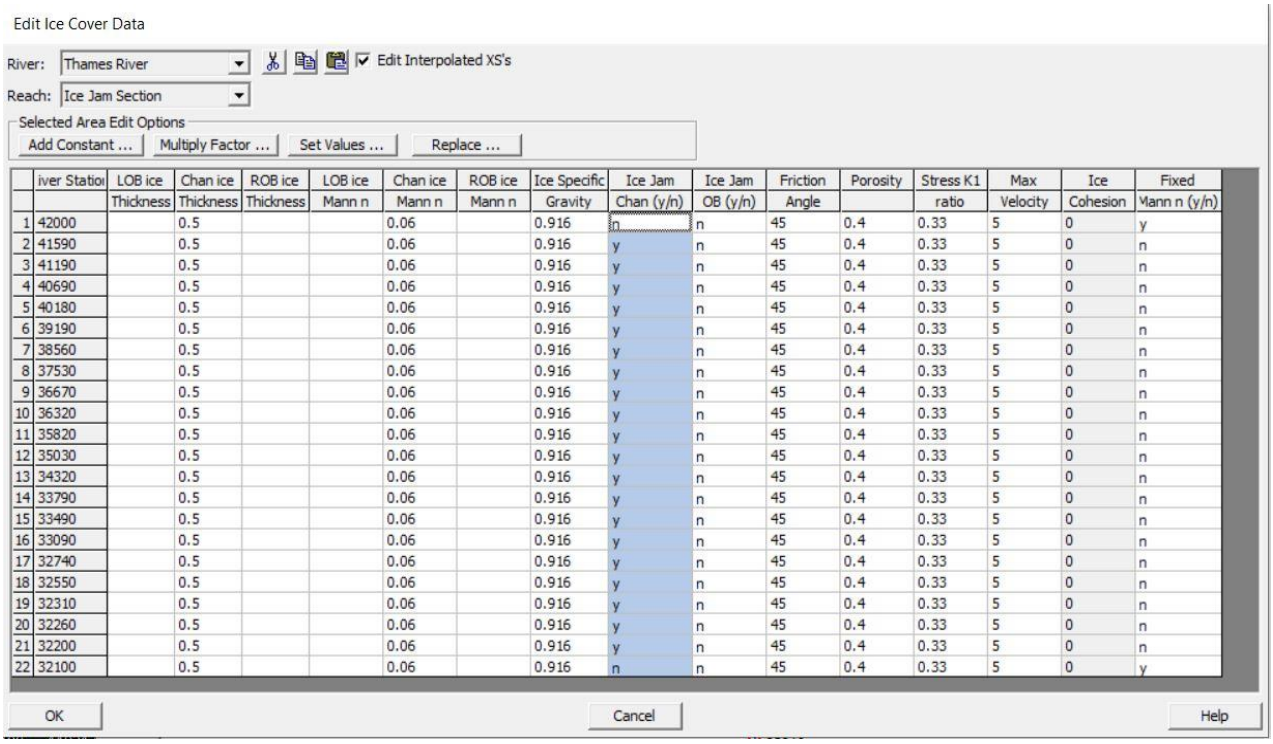

	iver Statio	LOB ice Thickness	Chan ice Thickness	ROB ice Thickness	LOB ice Mann n	Chan ice Mann n	ROB ice Mann n	Ice Specific Gravity	Ice Jam Chan (y/n)	Ice Jam OB (y/n)	Friction Angle	Porosity	Stress K1 ratio	Max Velocity	Ice Cohesion	Fixed Mann n (y/n)
1	42000		0.5			0.06		0.916	n	n	45	0.4	0.33	5	0	y
2	41590		0.5			0.06		0.916	y	n	45	0.4	0.33	5	0	n
3	41190		0.5			0.06		0.916	y	n	45	0.4	0.33	5	0	n
4	40690		0.5			0.06		0.916	y	n	45	0.4	0.33	5	0	n
5	40180		0.5			0.06		0.916	y	n	45	0.4	0.33	5	0	n
6	39190		0.5			0.06		0.916	y	n	45	0.4	0.33	5	0	n
7	38560		0.5			0.06		0.916	y	n	45	0.4	0.33	5	0	n
8	37530		0.5			0.06		0.916	y	n	45	0.4	0.33	5	0	n
9	36670		0.5			0.06		0.916	y	n	45	0.4	0.33	5	0	n
10	36320		0.5			0.06		0.916	y	n	45	0.4	0.33	5	0	n
11	35820		0.5			0.06		0.916	y	n	45	0.4	0.33	5	0	n
12	35030		0.5			0.06		0.916	y	n	45	0.4	0.33	5	0	n
13	34320		0.5			0.06		0.916	y	n	45	0.4	0.33	5	0	n
14	33790		0.5			0.06		0.916	y	n	45	0.4	0.33	5	0	n
15	33490		0.5			0.06		0.916	y	n	45	0.4	0.33	5	0	n
16	33090		0.5			0.06		0.916	y	n	45	0.4	0.33	5	0	n
17	32740		0.5			0.06		0.916	y	n	45	0.4	0.33	5	0	n
18	32550		0.5			0.06		0.916	y	n	45	0.4	0.33	5	0	n
19	32310		0.5			0.06		0.916	y	n	45	0.4	0.33	5	0	n
20	32260		0.5			0.06		0.916	y	n	45	0.4	0.33	5	0	n
21	32200		0.5			0.06		0.916	y	n	45	0.4	0.33	5	0	n
22	32100		0.5			0.06		0.916	n	n	45	0.4	0.33	5	0	y

Figure 6.5 Ice cover data editor table for ice jam analysis.

The Manning's *n* value and the channel ice thickness was specified for every cross section. Initially, the ice thickness of 0.5 meter is specified, and it represents the assumed minimum allowable ice thickness in jam. The ice cover editor table (Figure 6.2) was changed to indicate ice jamming in the river section. Figure 6.5 is the edited ice cover editor table, indicating ice jamming in the river.

For ice jam analysis, number of iterations are required to solve the steady flow equation and the ice jam force balance equation for the entire reach. These calculations iterate until the calculated jam thickness and water surface elevations converge to a constant value within the minimum tolerance. Figure 6.6 shows the calculated ice jam thickness along the channel, the water surface elevations, and the observed water surface elevations.

Also, it can be noticed that in this case, the ice jam water surface elevation matches to the observed water surface elevation reasonably well. Figure 6.7 compares the water surface profile for a same steady flow on all three cases, showing the water surface elevation, ice thickness, and observed water surface elevation.

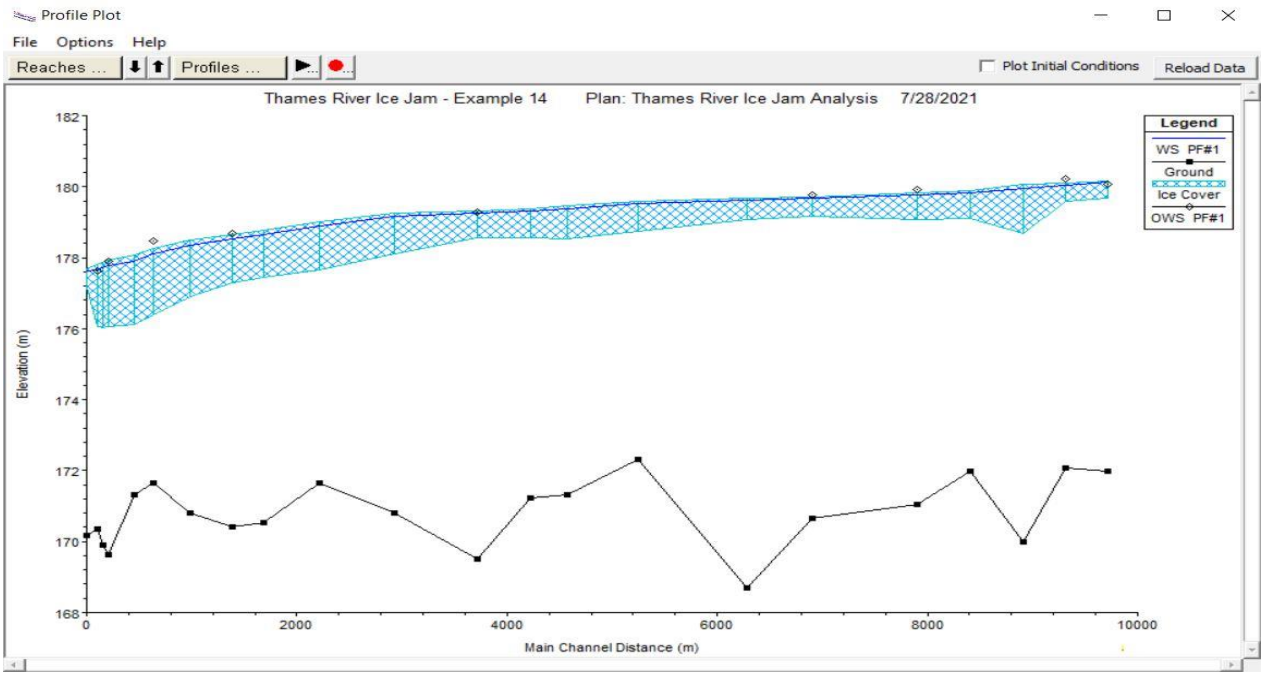

Figure 6.6 Profile plot of Thames River for ice jam case

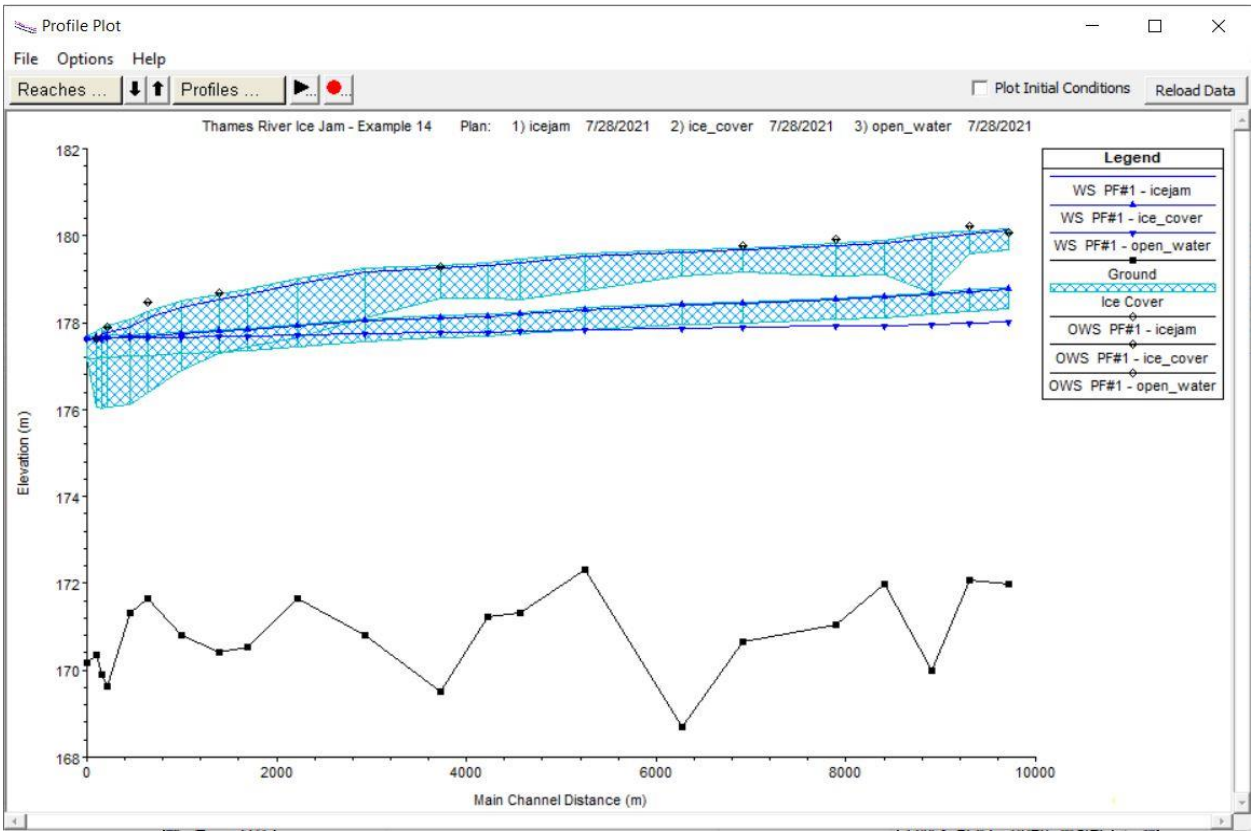

Figure 6.7 Comparison of the profile plot of Thames River for open water case, ice cover case, and ice jam case.

6.4 ICE JAM SENSITIVITY ANALYSIS

Sensitivity analysis of ice jam modeling is run for the Thames river under different flow rates and initial ice thicknesses. The steady flow as input data is varied and the resulting ice jam or water surface profile is compared. This sensitivity analysis demonstrates a potential approach to estimate the inflow when the inflow reduction at the upstream is unknown but the resulting water surface elevations at several locations are known or measured.

Three cases of steady flow are taken here, once the same steady flow which was used for ice jam analysis, i.e., 131.5 cms is used and categorized as Profile 1 (PF#1). Second, the profile flow is halved from the original value, and a discharge of 261 cms is taken and categorized as Profile 2 (PF#2). Finally, the profile flow is doubled from the original value, and a discharge of 522 cms is taken and categorized as Profile 3 (PF#3). The resulting profile plot after ice jam analysis is seen in Figure 6.8. The amount of ice jamming is seen increasing with higher flow rate. And if the inflow was unknown, then analyzing the resulting water surface elevation and observed water surface elevation, the steady flow in the real scenario can be concluded as 261 cms when the range of cross sections with ice cover is known.

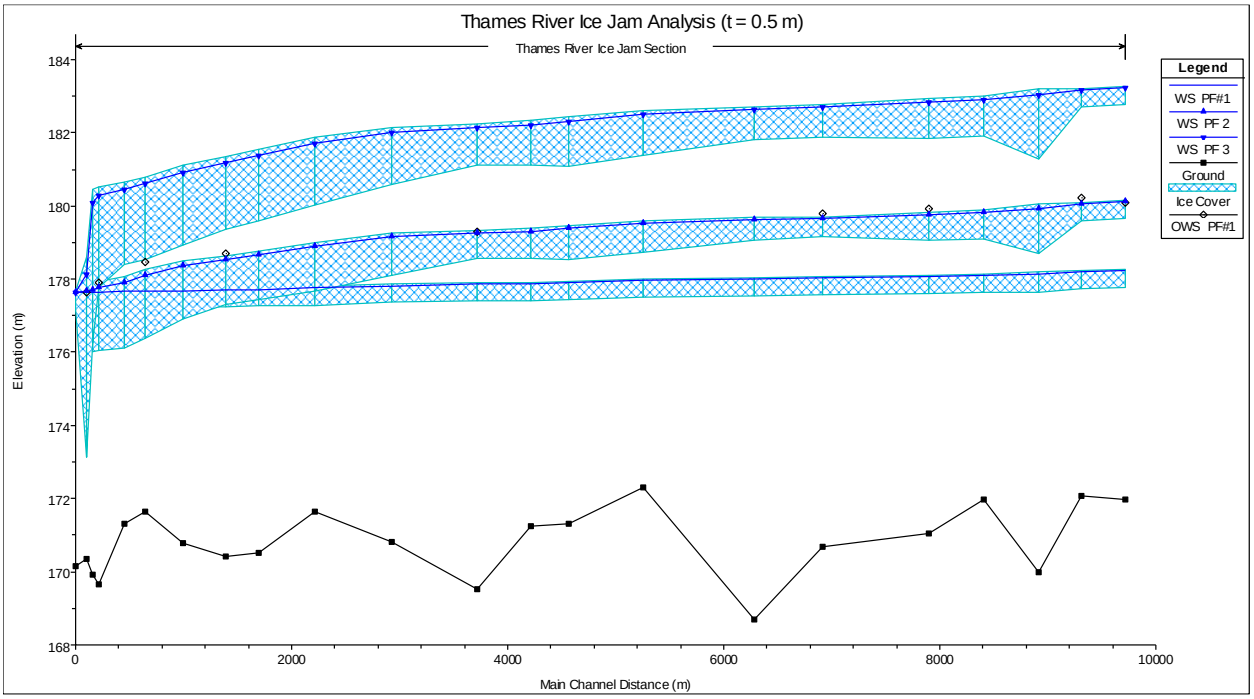

Figure 6.8 Comparison of profile plot of Thames River for ice jamming case when the steady flow is changed.

Figure 6.8 shows the ice cover of Thames River at three discharges: 131.5 cms, 261 cms, and 522 cms, i.e., PF#1, PF#2, and PF#3, respectively, with the constant initial ice thickness of 0.5 m. The initial ice thickness provided during the ice jam simulation works as the minimum ice cover thickness achieved during the simulation period. Further testing with varying initial ice cover thickness is carried out. Figure 6.9 shows the variation of simulated ice cover thickness for three profiles (PF#1, PF#2, and PF#3) under the same three flow rates when the initial ice cover thickness of 1.0 m is provided. Again, Figure 6.10 shows the variation of simulated ice cover thickness for the same three profiles with initial ice cover thickness of 1.5 ft.

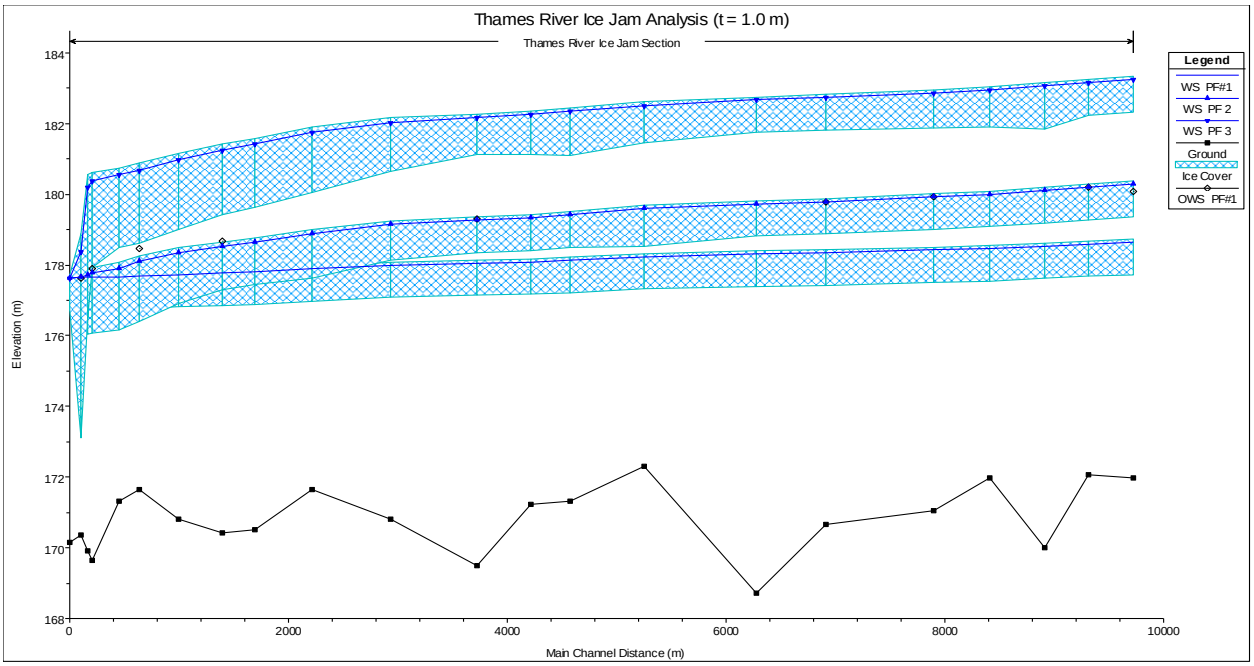

Figure 6.9 Comparison of ice cover thickness at varying steady flow with initial ice cover thickness of 1.0 m.

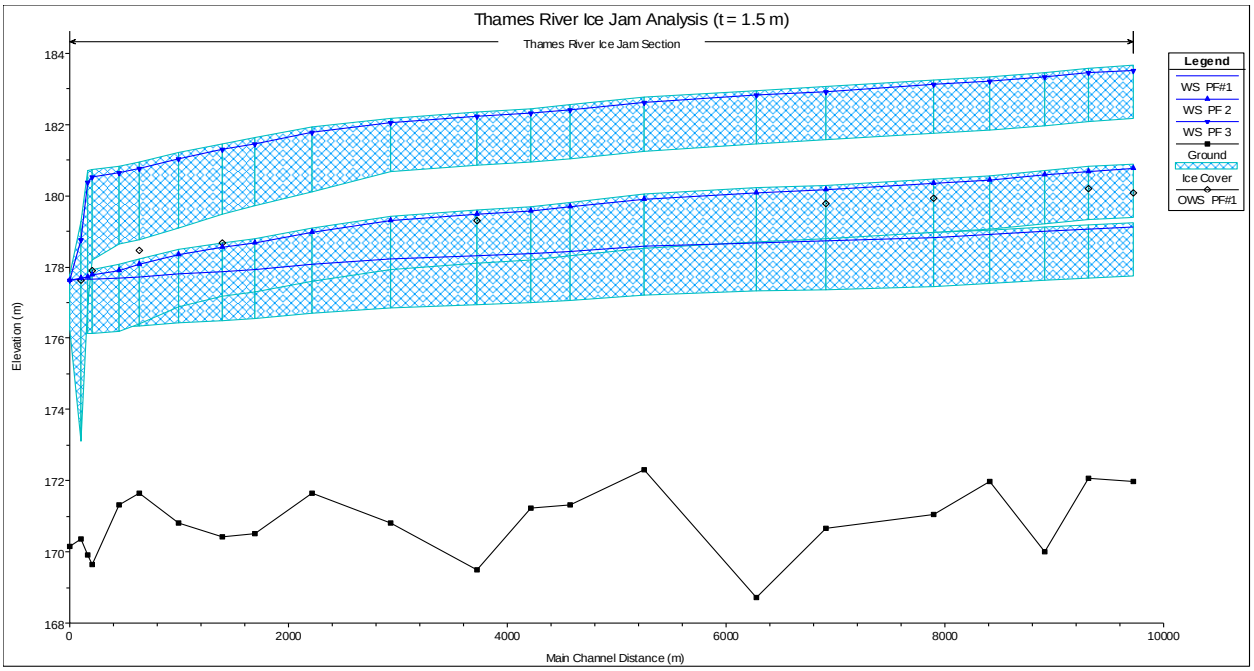

Figure 6.10 Comparison of ice cover thickness at varying steady flow with initial ice cover thickness of 1.5 m.

The ice thickness values during an ice jam on Thames River, for a constant discharge and varying initial ice cover thickness is shown in Figure 6.11. Figure 6.11 (a) shows that simulated ice thickness throughout the river reach remains constantly at the same value which was provided when the discharge was the lowest, i.e., 131.5 cms. Initially, with higher discharge, the ice jam phenomenon is noticed in the river reach. The value of ice thickness is seen increasing with increasing discharge.

Here, the ice jam thickness in the river reach is seen fairly same although the initial thickness assumed was different, until the ice thickness goes below the assumed ice thickness value. Figure 6.11 (d) shows that the ice thickness in the jam during 783 cms flow rate remains the same indifferent of the assumed initial thickness. But, as the ice jam thickness gets below the assumed value of ice cover, the ice thickness remains constant. This phenomenon is evident on all the cases of discharge above 261 cms on Figure 6.11(b), Figure 6.11(c), and Figure 6.11(d).

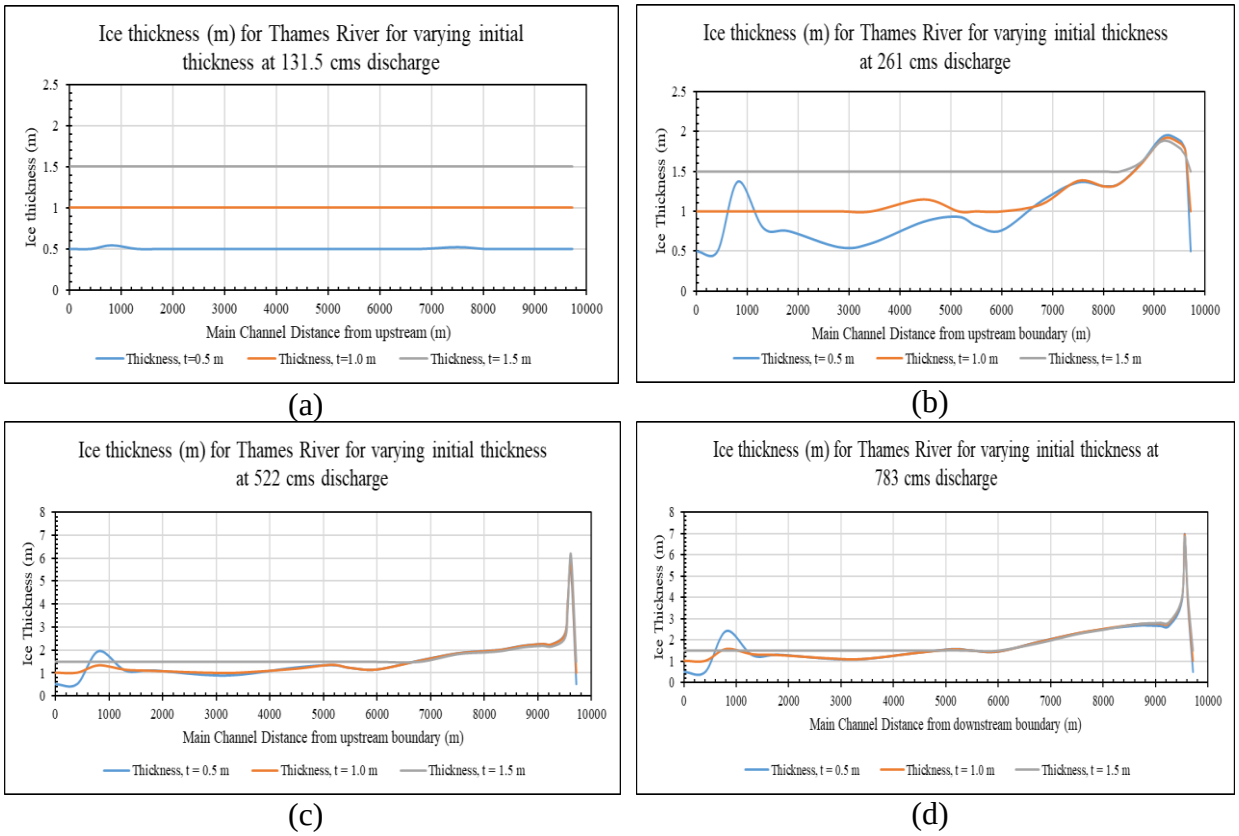

Figure 6.11 Comparison of ice thickness simulated on Thames River using HEC-RAS when the initial thickness is varied (a) when the flow rate is 131.5 cms (b) when the flow rate is 261 cms (c) when the flow rate is 522 cms and (d) when the flow rate is 783 cms.

6.5 MODELING ICE-COVER IN MISSOURI RIVER

The preliminary ice jam analysis is also carried out on Missouri River using the bathymetry data developed using geometry data developed using manual method, where the study area ranges from upstream of the junction of Dearborn River and Missouri River to the downstream of Cascade. In the ice jam analysis process, the ice cover was not added for the entire river reach but was assumed to happen after 7.5 miles (39,600 ft) downstream from the upstream boundary of the study area. The initial minimum thickness of ice cover provided for the simulation was assumed to be 1.65 ft on main channel and 1.3 ft on left and right over bank. The steady flow analysis was carried out with discharge of 5000 cfs, which is an approximate discharge noticed on USGS gage station below Holter lake.

Figure 6.8 shows the steady flow simulation of Missouri River, with ice jam analysis. The ice cover thickness is seen changing throughout the reach. The verification of the water profile elevation with observed water level could not be done because of the lack of observed water level data. Also, for the ice jam analysis using HEC-RAS, no meteorological data is used, and only flow data and geometry data is used for calculation, keeping normal depth as boundary condition of steady flow simulation. Therefore, simulated ice cover cannot be connected with either historical weather in observed ice jam events (e.g., ones analyzed in CHAPTER 3) or future weather forecast in order to forecast ice jam event. With observed ice cover information discussed in section 6.3, it is possible to quantify or predict ice cover in Missouri River during operation conditions.

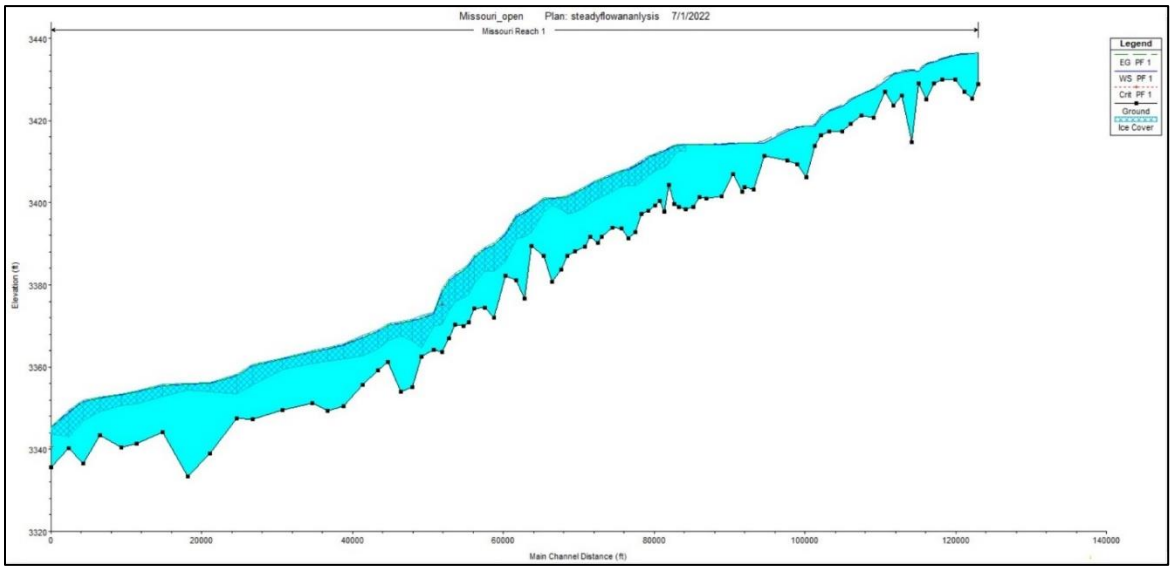

Figure 6.12 Ice jam analysis on Missouri River using steady flow simulation.

Figure 6.13 shows the ice cover thickness when the ice jam steady state simulation with ice cover is performed on the Missouri River. Two different cross-section from 0 – 20000 ft from Cascade and the cross-section from 70,000–90,000 ft from Cascade is considered to be ice covered with the initial ice thickness of 1.65 ft on the main channel and 1.3 ft on the overbank areas.

The two tests of ice jam modeling was carried out at the initial phase of the study to verify the working of HEC-RAS ice jam simulation, when the ice cover is continuous (Figure 6.12), and when the ice cover was discontinuous (Figure 6.13).

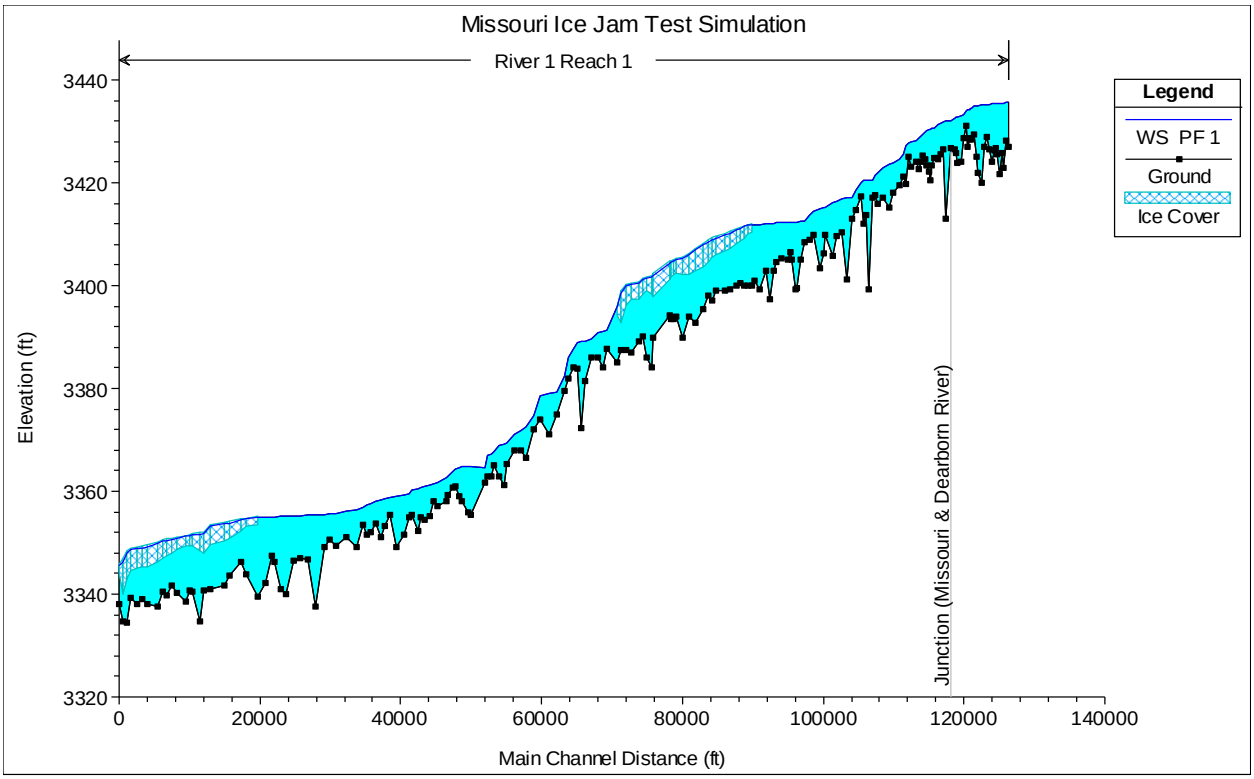

Figure 6.13 Missouri River ice jam analysis on selected river reach on HEC-RAS using bathymetry data obtained from GIS Method (Lidar DEM).

6.6 ICE JAM SENSITIVITY ANALYSIS FOR MISSOURI RIVER

Ice jam simulation of the Missouri River is carried out in HEC-RAS for different conditions, to analyze the ice cover thickness, and volume of ice observed during an ice jamming event. Before calibration of the ice cover simulation of the Missouri River, ice cover locations in the Missouri River were determined. One of the identified ice cover reaches is shown in Figure 6.14. This is a Google Earth image of the December of 2006. Here, ice cover on the Missouri River is seen over a long distance. The ice cover here started from around 20,000 ft downstream from the junction of the Missouri and Dearborn Rivers (red arrow) and ended around 20,000 ft upstream of the Cascade (read arrow in Figure 6.14(a)), and short red line segments cross Missouri River show the start and end of ice cover. On Figure 6.14(a), some parts of Missouri River seems not to be ice covered due to the angle of view, but Figure 6.14(c) more clearly shows those parts are ice covered. For the upstream part on Figure 6.14(b), ice cover shows different colors: white and lighter dark; the lighter dark parts could be open water or ice covered in a different color or transparency. The ice might not cover every part of Missouri River over 16.7 miles from Google Earth image.

Figure 6.15 shows a satellite image and two zoomed images in the summertime for the downstream part of the ice cover reach in Figure 6.14. Figure 6.15(b) and (c) clearly show the potential ice bridging locations where the river width decreases, constriction to the flow is present, or river bifurcation or trifurcation splits flow into two or three channels through island(s). There are various

(a)

(b)

(c)

Figure 6.14 Google Earth image of the Missouri River in December 2006, (a) showing ice cover from downstream of Dearborn River and upstream of Cascade, (b) zoomed view near upstream, and (c) zoomed view near downstream ice cover.

meandering or complex flow paths in small channels. These locations serve as the starting points of the potential ice jam formation, and then ice cover or jam would propagate upstream to have ice cover over a river reach, e.g., about 16.7 miles in Figure 6.14, when the below-freezing weather condition lasted weeks. Ice jam formation points could be dynamic and move from an upstream location, e.g., Figure 6.15(c), to a downstream location, e.g., Figure 6.15(b), when the hydrostatic force due to the build-up of the water level breaks the ice jam.

Figure 6.15 Google Earth image of Missouri River showing the ice bridging locations. (a) Portion of Missouri River with narrow width, and bifurcation of river with small higher elevation land mass in the river. (b) Enlarged portion of (a) showing the bifurcation portion of the river and immediately a constriction downstream. (c) Portion of the Missouri River with trifurcation of the river with small land masses in the river serving as constriction to the flow.

6.6.1 VARIATION OF ICE COVER THICKNESS AND TOTAL ICE ACCUMULATION WITH DISCHARGE

The HEC-RAS geometry data of the Missouri River set up using the GIS method (Lidar DEM) is edited to have the initial ice cover thickness for this reach of 87,939 ft (16.7 miles). The uppermost boundary of the ice cover region is 19,182 ft downstream of the most upstream boundary (near Dearborn River) and the lowermost boundary of the ice cover region is 19,296 ft upstream of the most downstream boundary (Cascade) of the study area. An initial ice cover with 1.65 ft of ice

thickness and 1.65 ft of ice cover on the over banks was provided. One of the limitations of the steady or equilibrium ice cover simulation on HEC-RAS is that it cannot simulate the cross-sections where ice cover forms and ends, thus that should be manually input in the HEC-RAS. The beginning and ending cross sections for ice cover can also be a part of sensitivity analysis.

The ice cover thickness with steady flow data of 4000 cfs, 5000 cfs, and 6500 cfs was simulated for three cases to determine the amount of ice thickness and the volume of ice cover noticed in the Missouri River and its variation with discharge.

The ice cover thickness for three different steady flows is shown in Figure 6.16. The minimum ice cover thickness along the channel is 1.65 ft, as the HEC-RAS ice jam simulation restricts the ice thickness to below the provided initial ice thickness. The average and maximum ice cover thicknesses in the region with ice cover for different discharges are summarized in Table 6.3. HEC-RAS ice simulation results report cumulative total ice volume (ft^3) over the cross section, in the main channel, and the left and right overbank areas. The total ice accumulation over 16.7 miles of the ice cover reach during the three different discharges is shown in Figure 6.17.

The total volume of ice accumulation at 4000 cfs results to 378,856,000 cubic feet. If the density of water is considered to be 1 gm/ft^3, and the density of ice is considered as 0.916 gm/ft^3, the resulting loss in volume of water due to ice jam formation is 340,620,096 cubic feet, i.e., 340.6×10^6 ft^3 when the discharge is 4000 cfs. Similarly, the volumetric loss in water due to ice jam formation during 5000 cfs discharge is 447.9×10^6 ft^3. And that during 6500 cfs is 597.1×10^6 ft^3.

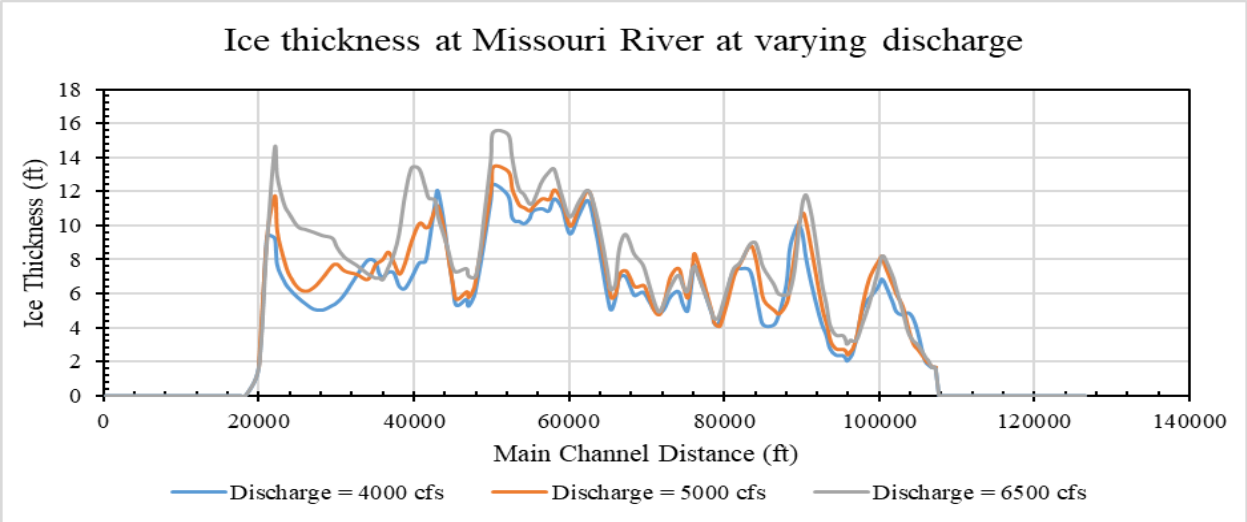

Figure 6.16 Ice thickness at Missouri River simulated from HEC-RAS ice jam simulation with varying discharges of 4000 cfs, 5000 cfs, and 6500 cfs.

Table 6.3 Average ice cover thickness for varying discharge simulated from HEC-RAS for the Missouri River

Discharge (cfs)	Average ice cover thickness (ft)	Maximum ice cover thickness (ft)
4000	5.85	12.43
5000	6.91	13.47
6500	6.89	15.45

With increasing discharge, a rise in the ice cover throughout the reach as well as the rise in total ice volume is seen in Figure 6.16 and Figure 6.17.

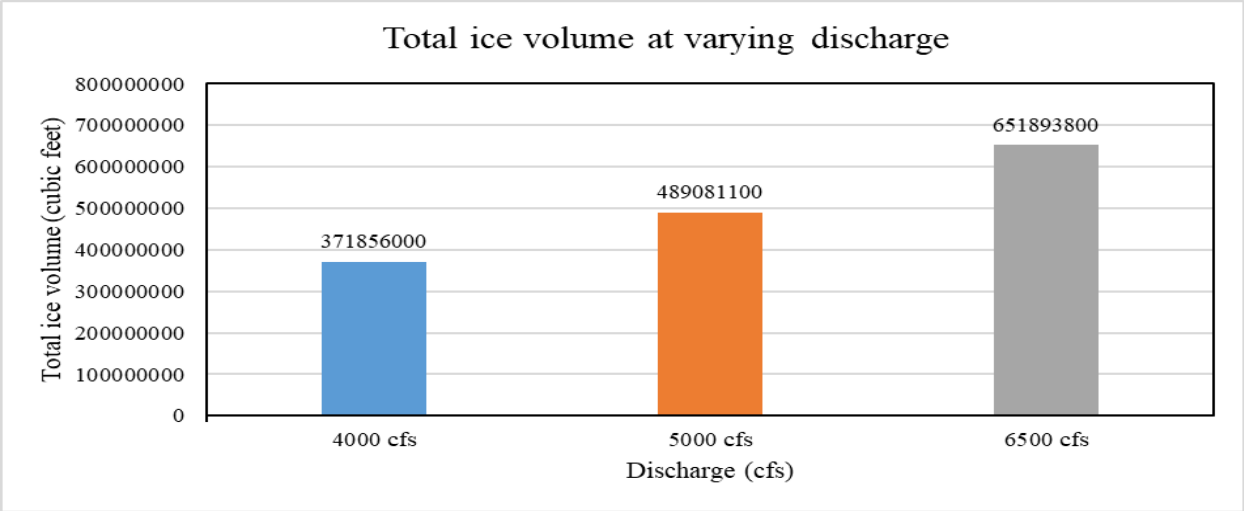

Figure 6.17 Total ice volume on the main channel at the Missouri River during ice jam simulation with varying discharges of 40000 cfs, 5000 cfs, and 6500 cfs.

As this event of ice jam formation shown in Figure 6.14 is an event of December of 2006, the flow analysis of December of 2006 is carried out for Holter and Morony Dam, using the flow analysis spreadsheet. The average discharge for the month of December 2006 is 3669.4 cfs. Thus, the ice jam simulation with the discharge of 4000 cfs is used for the comparison of volume of water loss observed in HEC-RAS to the actual volume of water loss observed during an ice jam event on the Missouri River. Figure 6.18 shows the discharge below Morony and has a loss of 2350 cfs of discharge from 14:30 December-16, 2006 to 22:40 December 18 2006 within a span of 55 hours at the flow loss rate of 42.73 cfs/hour. The discharge loss is a result of ice jam formation seen in Figure 6.14.

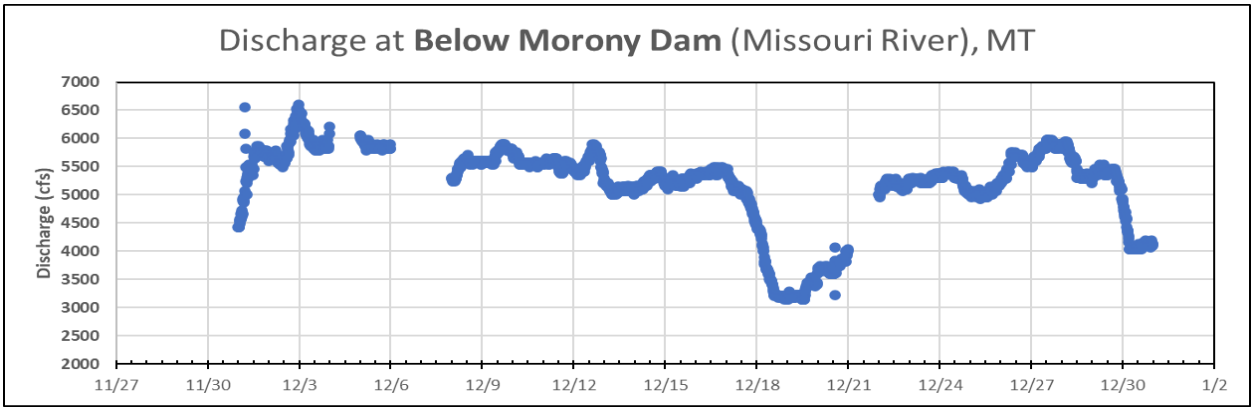

Figure 6.18 Discharge below Morony from December 1, 2006, to December 31, 2006.

The volume of water lost during this event is calculated as the product of loss in discharge to the duration of event (*Volume of water loss (cubic feet) = Sum of Discharge loss (cfs) × Hours (s)*). The total amount of water loss observed during the event is seen to be 465.3×10^6 cubic feet. Comparing with the amount of water loss simulated during the ice jam simulation in HEC-RAS, which is 340.62×10^6 cubic feet, observed volume of loss of water is not totally wrong. Various factors that are observed during the real ice jam simulation, like meteorological parameters, unsteady flow on natural river, are ignored during the ice jam simulation using HEC-RAS, which has resulted in the difference of 124.68×10^6 cubic feet of loss of water.

6.6.2 VARIATION OF ICE COVER THICKNESS WITH VARYING ICE COVER DISTANCE AT CONSTANT DISCHARGE

To observe the ice jam behavior when the reach length of the ice cover at the Missouri River is changed with constant discharge, is analyzed here. The same geometry data derived from the GIS method (Lidar DEM) is used in this sensitivity analysis as well. The length of the reach with ice cover is adjusted in the ice cover editor, to show the change in ice cover thickness.

The discharge of 5000 cfs is taken for all the cases. Thus, the steady flow data of HEC-RAS for all the cases is constant. Initially, similarly as Section 6.6.1 , the ice cover reach length of 87939 ft is taken for simulation. This distance was assumed based on Figure 6.14, thus this distance of 87,939 ft is picked as a base run. Other trials with ice cover reach lengths of around 65,000 ft (12.3 miles) and 40,000 ft (7.6 miles) are taken into consideration. The ice cover reach length is evenly deducted from both the ends as taken in the case of 87939 ft of ice covered reach length.

The three reach lengths of ice cover based on the cross-section distance in HEC-RAS are 87,939 ft, 65,090.4 ft, and 40,175.4 ft. The geometry data is edited for three different cases with, initial ice thickness on the main channel and overbank as 1.65 ft. The simulated ice cover thickness for three different cases with varying reach lengths of ice cover is shown in Figure 6.19. The average ice cover thickness for the case with a longer ice cover reach length is greater than the one with a shorter ice cover reach length, likewise, the total ice volume is greater with a longer ice cover reach length.

The ice cover thickness at the common location, at the ice cover length of 470,175.4 ft, is simulated almost exactly the same, as seen in Figure 6.19, except for the initial 8,000 ft at the upstream portion of the ice cover and the final 12000 ft at the downstream portion of the ice cover. The ice cover thickness at the common part of the ice cover region of 47,075.4 ft shows an average thickness of 8.72 ft. And the ice cover thickness at the common part of 65090.4 ft for the ice jam simulation at two reach lengths of 87,939 ft and 65,090.4 ft shows an average of 8.43 ft.

It is observed that the ice cover thickness during an ice jam simulation for different reach lengths of ice cover, coincides except for some change in ice cover thickness at the upstream part of the ice cover region and downstream part of the ice cover region.

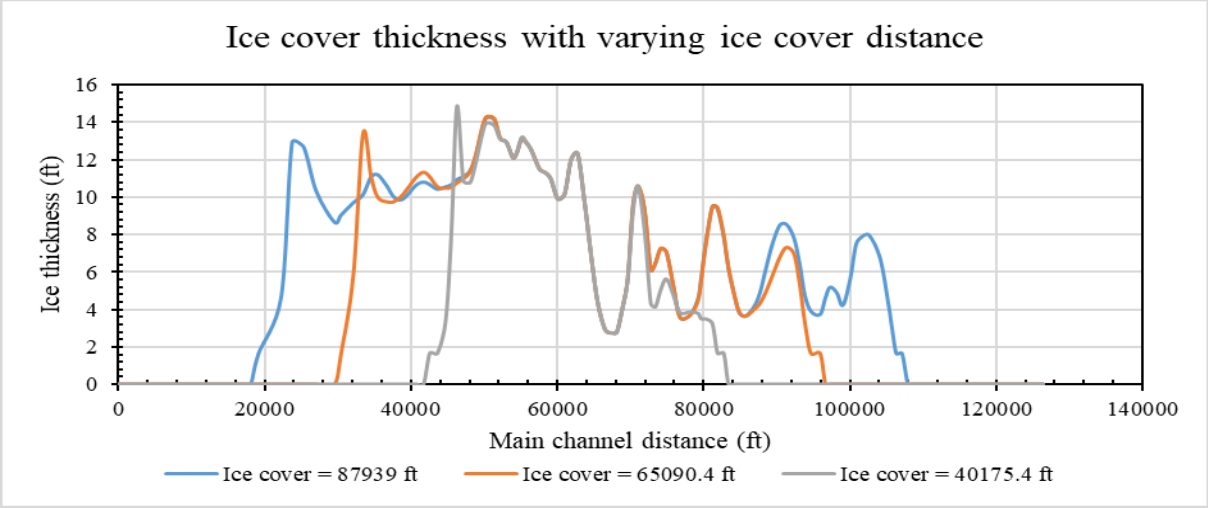

Figure 6.19 Ice cover thickness simulated from HEC-RAS for a discharge of 5000 cfs with varying ice cover distance.

CHAPTER 7. WATER TEMPERATURE SIMULATION

7.1 INTRODUCTION

Water temperature simulation can be done in HEC-RAS under water quality analysis. During the winter cold weather condition, when the simulated water temperature at a cross section reaches 0 ºC, this indicates the potential ice cover formation would start from that cross section. HEC-RAS does not simulate the super cooling event so that the simulated water temperature does not get slightly below 0 ºC. Ice cover initially formed moves and flows to downstream so that stable ice cover could form at further downstream from the cross section where water temperature reaches 0 ºC. Water temperature simulation in HEC-RAS is directly resulted from weather conditions so that one can simulate 0 ºC water temperature and ice cover potential using historical climate for checking or validating historical ice jam events (CHAPTER 3) and weather forecast to predict future ice jam event, which is the key objective of the study.

The first component to be modeled with a new water quality module being created for HEC-RAS is water temperature. The advection-dispersion equation is used by the water quality model to calculate the concentrations at each computing node. Cross-sections are positioned halfway between computational nodes. The advection-dispersion equation is solved by HEC-RAS using the QUICKEST (Quadratic Upstream Interpolation for Convective Kinematics with Estimated Streaming Terms) scheme created by Leonard (1979) and the ULTIMATE (Universal Limiter) algorithm (Leonard 1991). The water quality model CE-QUAL-W2 has successfully applied the QUICKEST ULTIMATE methodology (Cole and Wells 2003). A complete energy budget is used to construct the water temperature model. The heat exchange between the waterbody and the atmosphere occurs through the water surface only. For modeling the heat budget at the water surface, a heat balance can be developed. The heat balance states that for a finite volume of water over a unit time period;

$$Accumulation = Inflow - Outflow \pm Surface\ Heat\ Exchange \quad (7.1)$$

Some factors involved on the surface heat exchange includes the input from shortwave solar radiation and longwave atmospheric radiation, while discharge heat to atmosphere by back radiation, evaporation, and conduction. Other parameters involved in the energy budget for water temperature simulation involves the meteorological parameters like: air temperature, cloudiness, wind speed, atmospheric pressure, and humidity.

7.2 INPUT DATA

In order to perform a water quality simulation, a completed, calibrated hydraulic model (steady or unsteady) is required. In addition, some of the other requirements for water temperature modeling includes:

- Water temperature time series at all hydraulic boundaries (e.g., tributary inflows)
- At least one initial condition value in each reach
- Meteorological time series data

The input data for water temperature includes: (1) Geometry data and (2) Meteorological data assembled.

7.2.1 GEOMETRY DATA

The geometry data required for water temperature simulation includes the same components as required for steady or unsteady flow simulation. Here, the geometry data with bathymetry obtained from manual method, is used for water temperature simulation.

7.2.2 WATER TEMPERATURE DATA

The water temperature data includes the time series at all hydraulic boundaries. The water temperature data at the upstream river station is used for Missouri River reach. The water temperature data below Holter was therefore used for the water temperature simulation. The water temperature at USGS gage station below Holter is available from October 1, 2011 (15-minute interval). This time series data acts as boundary condition. Even there are a few small tributaries (Little Prickly Pear Creek, Rock Creek, Dog Creek, Dearborn River, and Sheep Creek, MT) that add inflow to Missouri River from Holter Dam to Cascade, these small inflows were not considered for winter temperature simulation since small streams could be frozen earlier than Missouri River.

7.2.3 METEOROLOGICAL DATA

At least one complete set of meteorological data must be supplied in order to model water temperature. The following weather data must be included in every meteorological data set: atmospheric pressure, air temperature, humidity (in vapor pressure, relative humidity, wet bulb, or dew point), solar radiation, wind speed, and cloudiness. For the modeling of diurnal water temperature change, a time series of air temperature, humidity, and wind speed radiation with a sample frequency of at least once every three hours is required (USACE 2016). It is not

recommended to utilize a constant value for air temperature, humidity, wind speed, or solar radiation other than for testing. It is best to measure solar radiation over time, however, only very limited weather stations have the equipment to measure solar radiation. The site's longitude and latitude, the day of the year, and the time of day can all be used to estimate and construct a time series of solar radiation in the absence of solar radiation data when cloudiness data are available. The water temperature model requires atmospheric pressure as an input. Site elevation can be used to estimate a time series if one cannot be acquired. Each data collection also contains a limited amount of physical data, such as latitude, longitude, and site elevation, in addition to meteorological time series. Along with meteorological data sets, water temperature model calibration parameters are also recorded. The dust coefficient (used only if a synthetic solar radiation time series is employed) and wind function parameters are calibration parameters (used to control the magnitude of sensible and latent heat) (USACE 2016).

1. Atmospheric Pressure: The pressure that all gases in humid air exert is known as atmospheric pressure. It is a strong function of elevation, fluctuates with the local climate, and often drops off as altitude rises. The water quality model accepts input of atmospheric pressure in millibars (mb), millimeters of mercury (mmHg), inches of mercury (inHg), or atmospheres (atm). At the time of the simulation, the data will be converted to millibars (mb) (USACE 2016). Time series data of atmospheric pressure (Figure 7.1) is entered from an excel spreadsheet.

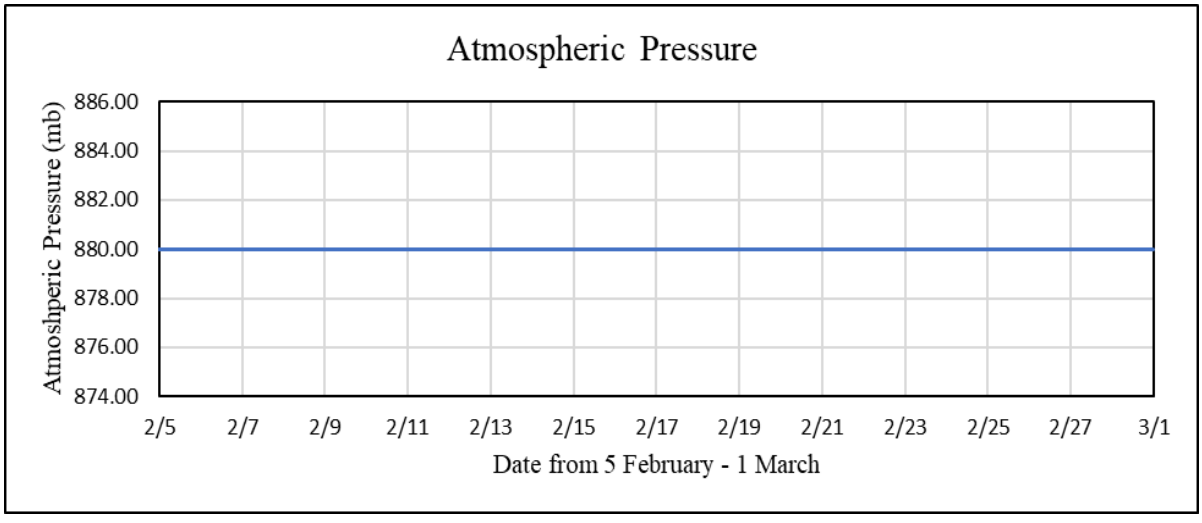

Figure 7.1 Atmospheric pressure time series input data for water temperature modeling from February 5,2022 – March 1, 2022

2. Air Temperature: The water temperature model needs a time series of air temperature as input, either on °C or °F. The plot showing the time series data for air temperature is shown in Figure 7.2

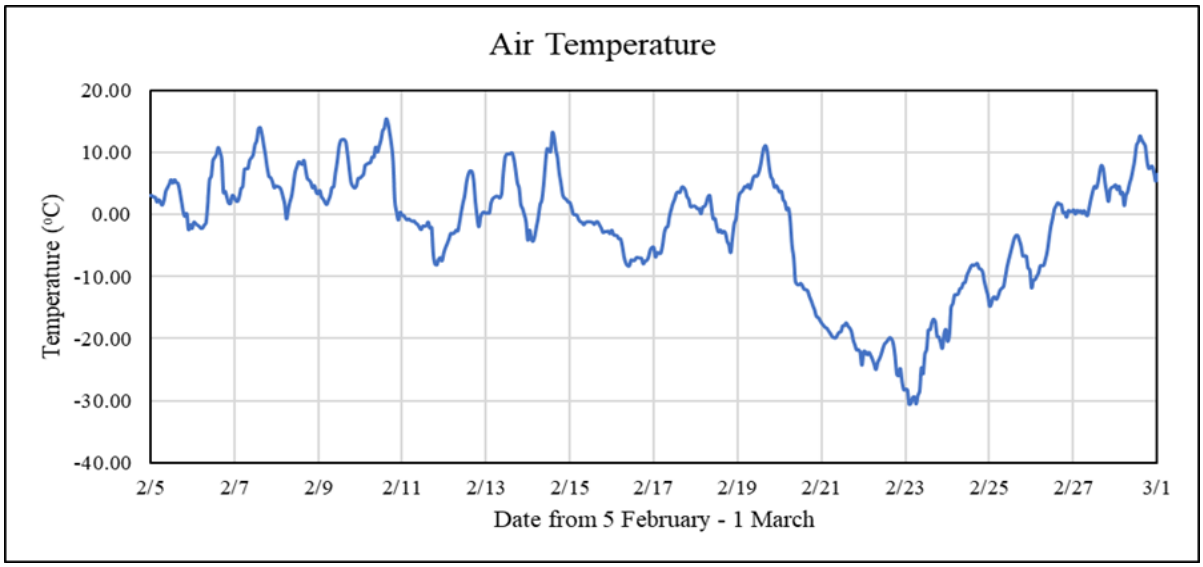

Figure 7.2 Air temperature (ºC) time series input data for water temperature modeling from February 5,2022 – March 1, 2022.

3. Humidity: The water temperature model needs an input of a time series of humidity. Relative humidity (%), wet-bulb temperature (°C or °F), dew-point temperature (°C or °F), or vapor pressure are all ways to represent humidity (mmHg, inHg, or mb). The plot showing the time series data from relative humidity is shown in Figure 7.3.

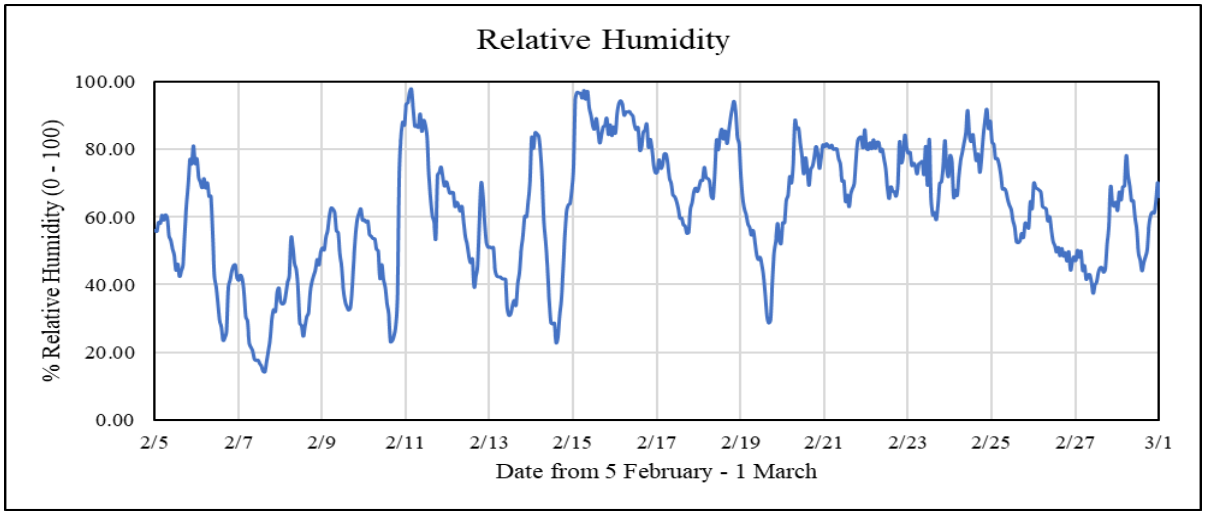

Figure 7.3 Relative Humidity (%) time series input data for water temperature modeling from February 5,2022 – March 1, 2022.

4. Solar Radiation: A nearby weather station may have data on measured solar radiation. Data from satellites is also accessible. W/m^2, $cal/cm^2/day$, and $MJ/m^2/day$ are the most popular measures for measuring solar radiation. Any of these units can be used to submit data, and internal calculations are done in W/m^2. In the absence of a direct measurement, solar radiation can be calculated using the location's longitude and latitude, the time of day, the presence of clouds, and a user-supplied dust coefficient, which simulates local atmospheric attenuation and is frequently employed as a calibration parameter. The main force behind the water temperature model is solar radiation. The plot showing the time series data from solar wave radiation is shown in Figure 7.4.

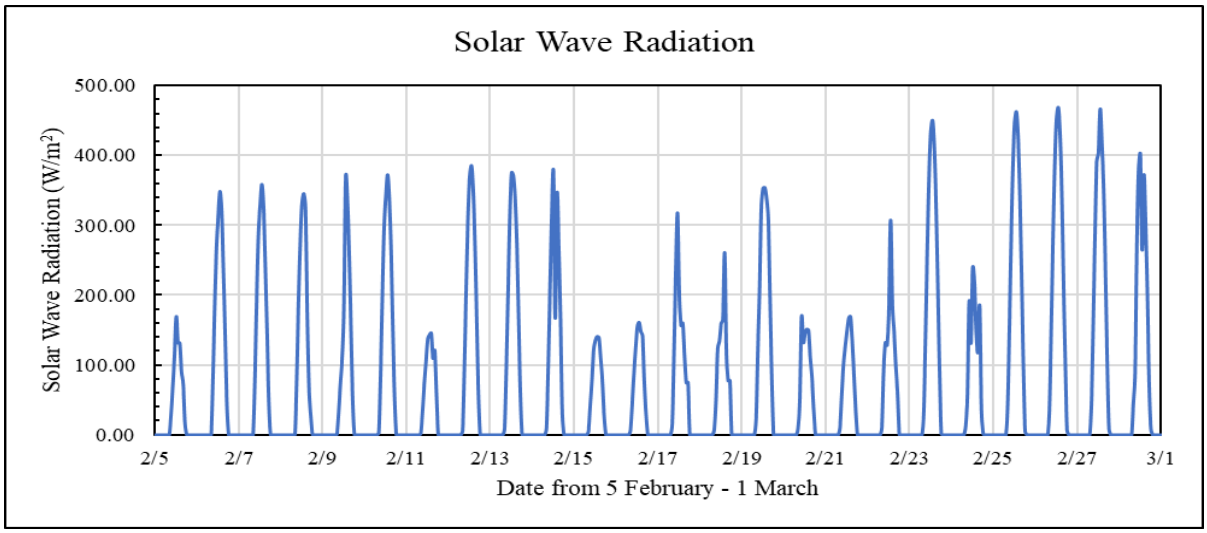

Figure 7.4 Solar wave radiation (W/m^2) time series input data for water temperature modeling from February 5,2022 – March 1, 2022.

5. Cloudiness: Cloudiness ranges from 0 to 0.9 and measures the percentage of the sky that is cloud-covered. Both calculated solar radiation and downwelling longwave radiation must take cloudiness into account. Increasing cloud cover causes computed solar radiation to drop while computed downwelling longwave radiation rises. A rough guideline for cloudiness is:

Overcast skies:	0.9
Broken skies	0.5 – 0.9
Scattered clouds	0.1 – 0.9
Clear skies	0.1

The plot showing time series data for cloudiness in fraction (0 – 1) is shown in Figure 7.5.

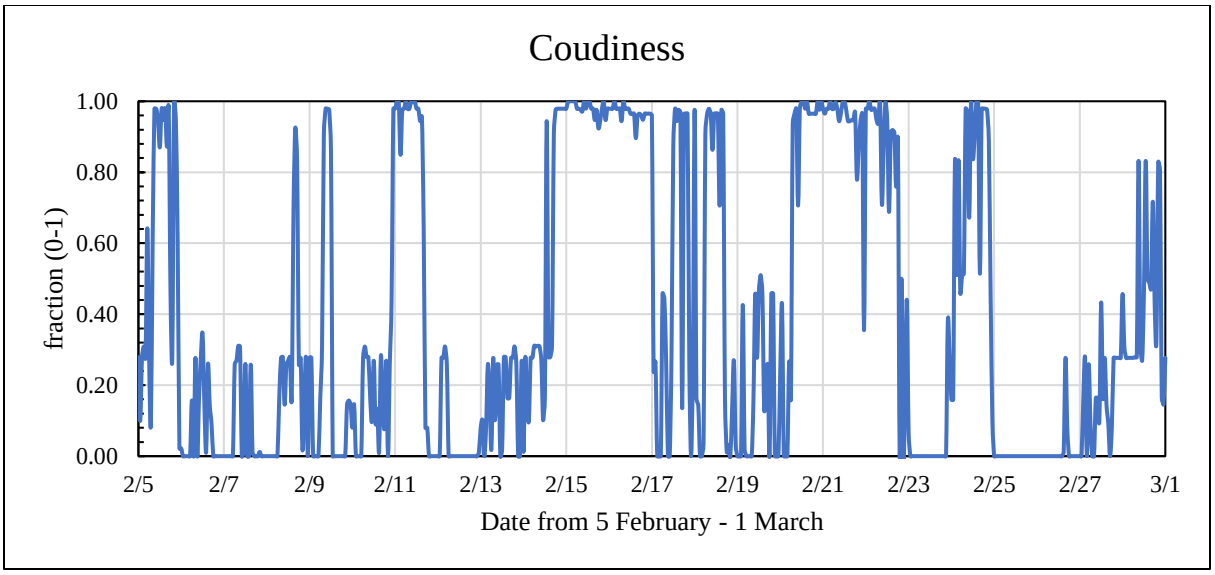

Figure 7.5 Cloudiness (fraction of 0-1) time series input data for water temperature modeling from February 5,2022 – March 1, 2022.

6. Wind: For the assessment of surface flux (latent and sensible heat), wind is a crucial element. Meters per second, miles per hour, and feet per second are common units for measuring wind speed. Any of these units may be used to submit data; internal computations are done in meters per second. The plot showing time series data for wind speed (m/s) is shown in

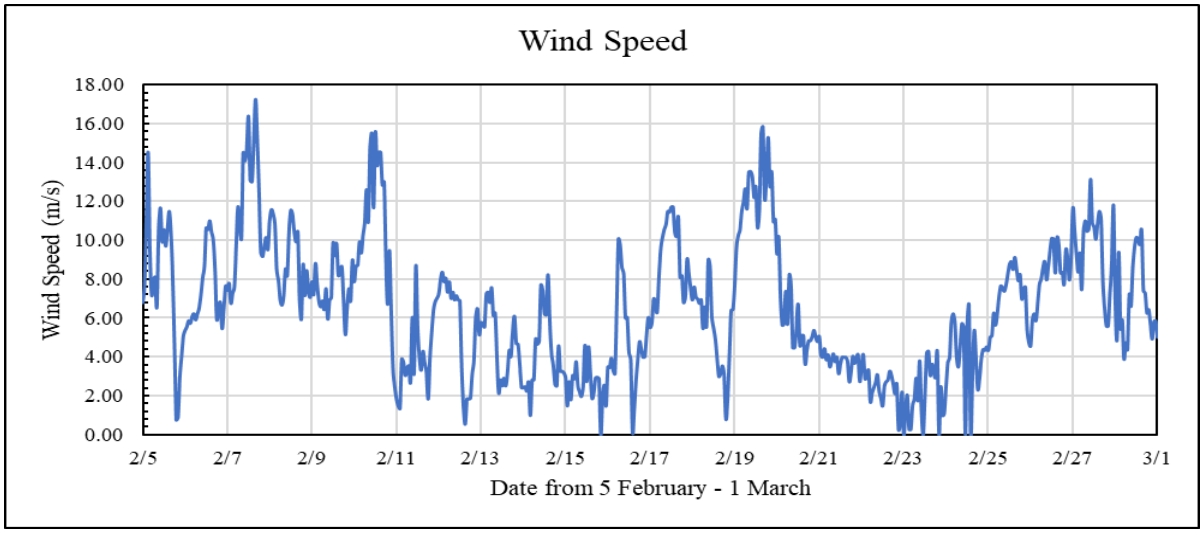

Figure 7.6 Wind speed (m/s) time series input data for water temperature modeling from February 5,2022 – March 1, 2022.

Meteorological data are derived from the weather data for our water temperature simulation. The weather data is accessed from https://www.visualcrossing.com/ website. This visual crossing website provides historical as well as 15-day forecast weather data. The weather data derived from this website is compared against the NOAA (National Oceanic and Atmospheric Administration – Government Agency) for historic as well as forecast data to verify its credibility as shown in Figure 7.7.

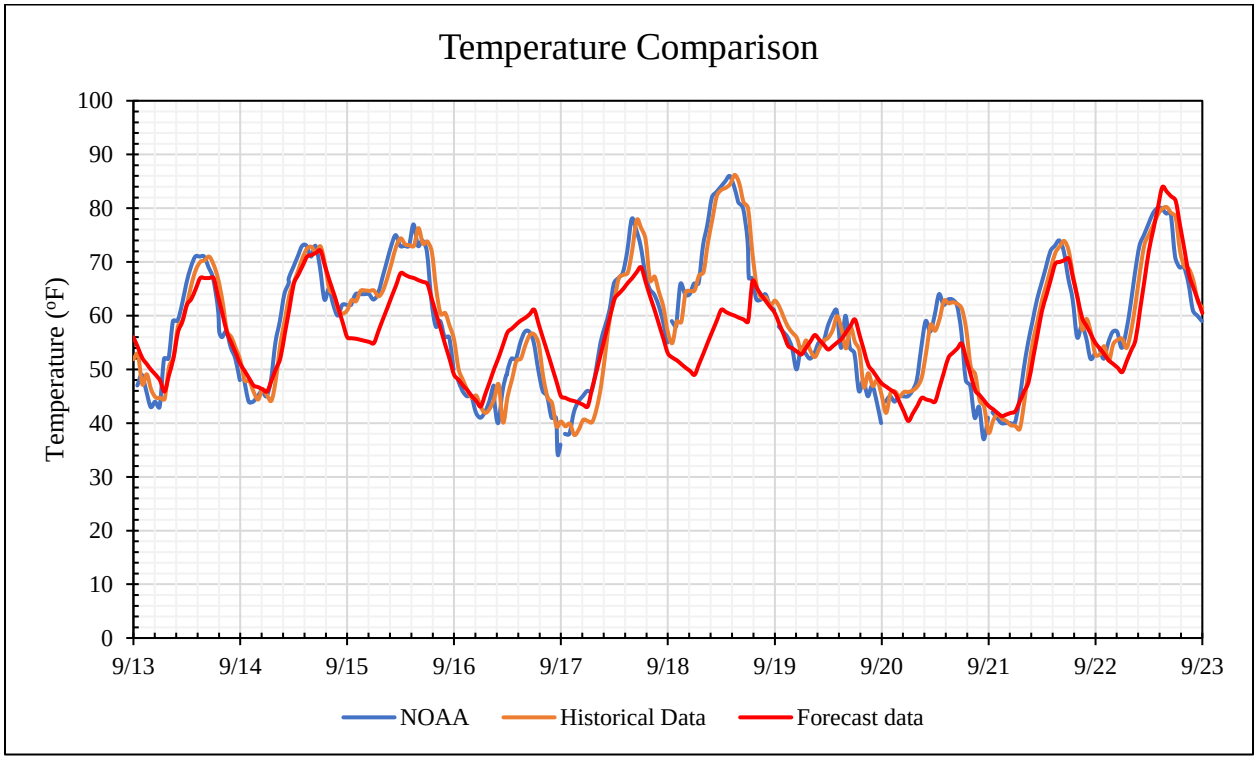

Figure 7.7 Comparison of historical and forecast data obtained from www.visualcrossing.com with NOAA data from 9/13/2021 to 9/23/2021

From Figure 7.7 comparison, it is seen that the historical data provided from this website is accurate with that of NOAA, while the forecast data is acceptable for around 7 days. Thus, for future prediction, forecast data up to 7 days can be taken from this website.

An excel spreadsheet was revised from visual crossing spreadsheet by Dr. Xing Fang, which can easily download the weather data from visual crossing website after specifying weather station information and time period. The user can input the date, either historical or future, and the spreadsheet will be able to extract the weather data and import it to the spreadsheet, Figure 7.2 is the user interface of the spreadsheet, where the date, hour aggregation level (to indicate whether hourly (1), or sub-daily (12), or daily (24) data), and API key for each registered user in visual

crossing website. The spreadsheet with developed VBA code can also convert the extracted weather data to meteorological data inputs, as acceptable by HEC-RAS for atmospheric pressure, air temperature, humidity, solar radiation, cloudiness, and wind speed.

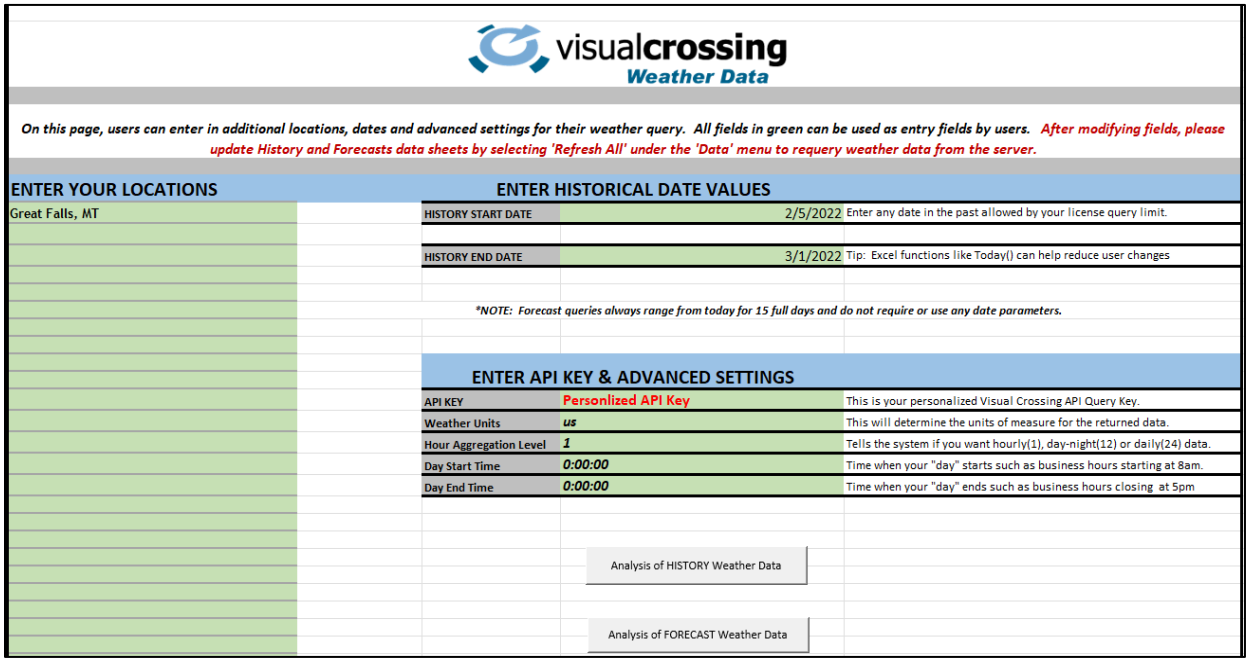

Figure 7.8 User interface of an Excel spreadsheet to import weather parameters from www.visualcrossing.com website to excel worksheet.

7.3 RESULTS

Water temperature simulation was run for several events that were identified in CHAPTER 3, where the ice jamming events was predicted. The input data for HEC-RAS simulation is prepared and the meteorological and water temperature data for the event was identified using the flow analysis spreadsheet (CHAPTER 3.11).

Figure 7.9 shows the water temperature plot along the channel distance (m) from Cascade to Holter for Feb-22, 2022. The water temperature simulation was run from Feb-5, 2022 to Mar-1, 2022, which is identified as a period of ice jam event. Figure 7.10 shows the discharge below Morony from Feb-15 to Mar-2, 2022, which highlights the loss in discharge in between Feb-21 to Feb-24.

Figure 7.11 shows the water temperature at the downstream boundary of the study area, along the date. The water temperature at different dates is seen at 0^{o}C in addition to the Feb-22, 2022 event.

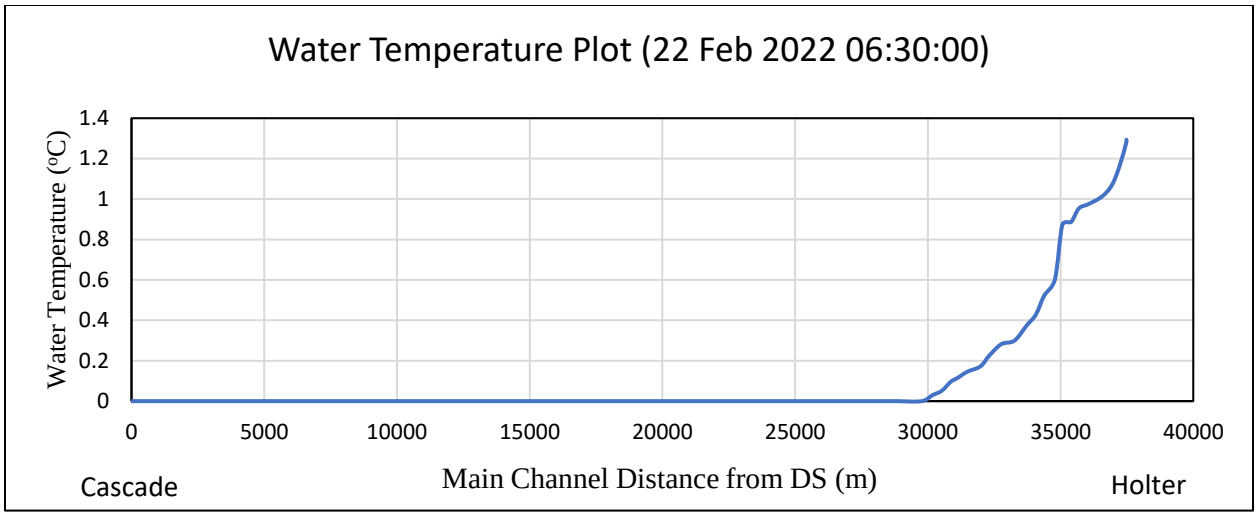

Figure 7.9 Water temperature (°C) versus channel distance (m) from downstream, Cascade to Holter.

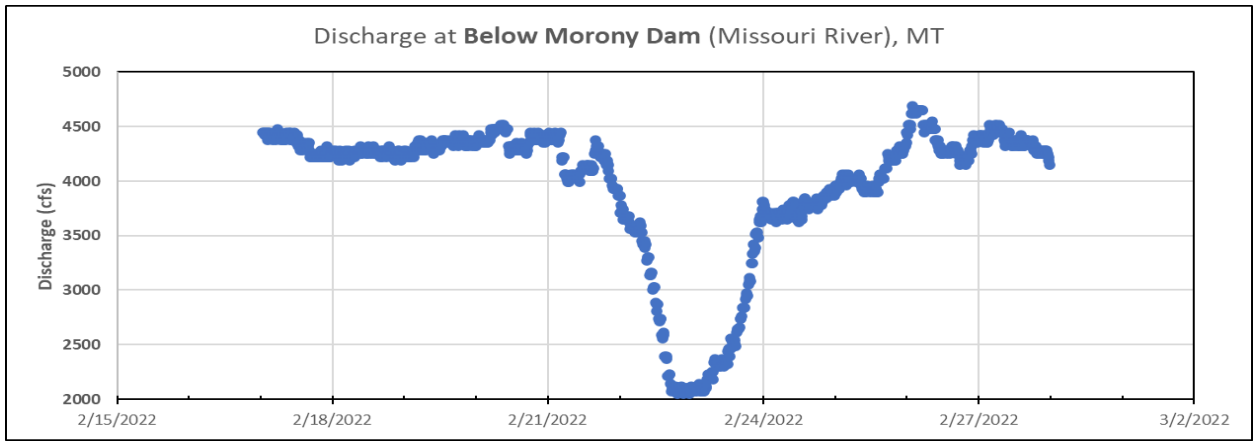

Figure 7.10 Discharge time series at Below Morony Dam from Feb-15, 2022 to Mar-02, 2022.

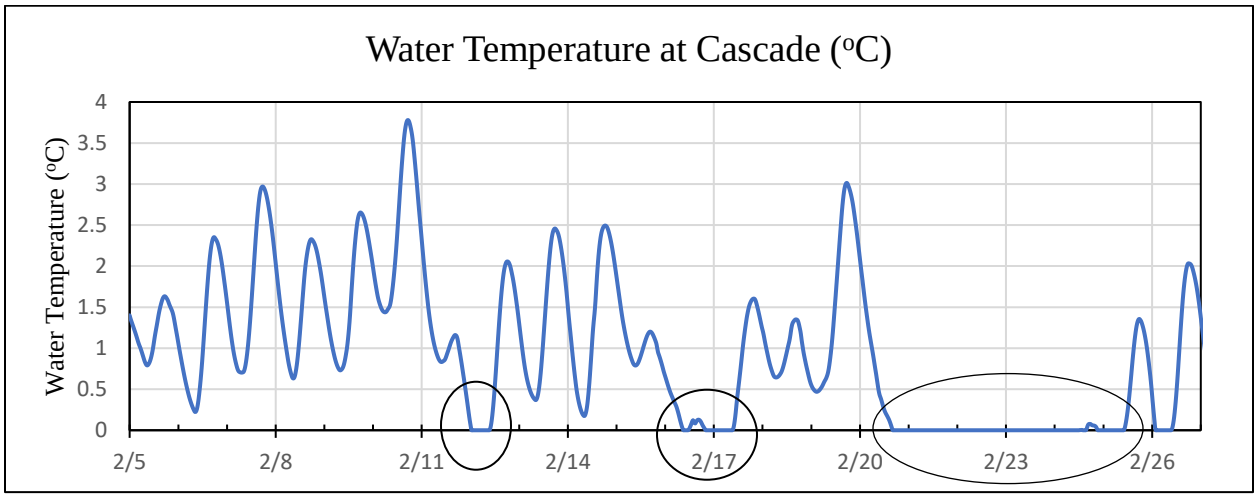

Figure 7.11 Simulated water temperature time series at Cascade showing periods (events) when the water temperature reaches 0°C

7.4 DISCUSSION

The HEC-RAS simulation results obtained after water temperature simulation shows that the water temperature reading downstream from the Holter to Cascade goes to 0 ^{o}C for the event when ice jamming is predicted. Also, a point to note is that water temperature does not go below 0 ^{o}C indicating supercooling phenomena is not seen in HEC-RAS, unlike RIVER1D.

This result of water temperature simulation indicates a probable ice jam in between Cascade and Holter on 22nd February. To support this claim, the simulation shows temperature at 0 ^{o}C for a more than 3 days, Figure 7.11, which is also backed by the reduction in discharge.

To validate the simulation result, the USGS flow data at below Morony dam is examined, Figure 7.10. It shows that there is a reduced discharge of 2000 cfs at below Morony dam from 21st February to 23rd February. This reduction in discharge could be because of the ice jam that occurred downstream of Holter and upstream of Cascade.

This method of water temperature simulation is helpful in prediction purpose as well, because the input data for water temperature simulation consists of mainly meteorological data, which can be forecast data from visual crossing, and the water temperature at boundary conditions can be the present water temperature at below Holter. This helps in the prediction of future ice jam events, which is one of the major aim of the project.

CHAPTER 8. RIVER1D

8.1 INTRODUCTION

River1D is a software in the public domain and developed by researchers in the University of Alberta: Drs. Julia Blackburn and Yongtong She. The Sain Venant equations are resolved using the Characteristic Dissipative Galerkin method, while the ice transport equations are resolved using the Streamline Upwind Petrov-Galerkin finite element method (Blackburn and She 2019). Water temperatures and supercooling, frazil ice production, accretion, and re-entrainment, dynamic and static border ice growth, border ice decay, ice pan production, and ice cover formation, multiple user-defined bridging locations, ice front propagation using leading edge stability criteria, ice front retreat, anchor ice growth and release, and the thermal growth and decay of ice are all things that River1D is capable of simulating. In addition, River1D contains a standalone ice-jam program.

Several studies have utilized River1D, including those looking into the effects of ice on flow distributions in the Mackenzie Delta (Blackburn et al. 2015), modeling ice cover consolidation on the Peace River, and researching the effects of climate change on the thermal regime of the Peace River (Andrishak and Hicks 2005). Additionally, Ye and She (2019) used River1D and data from the Athabasca and Peace Rivers to test mechanical break-up criteria (Ye and She 2019). Data from the Susitna River in Alaska was used to calibrate and validate the most recent version of River1D (Blackburn et al. 2015).

River1D is developed with the ultimate goal to develop a comprehensive river ice process model that is capable of simulating dynamic ice process in natural river systems with complex ice and flow regimes. River1D is proven to be consistently more stable and accurate than other models when modeling extreme dynamic and thermal ice processes. It considers water cooling and supercooling, frazil ice concentration, frazil rise and re-entrainment, border ice growth and decay, anchor ice evolution, under-cover transport of frazil, and ice cover progression based on leading edge stability criteria.

Figure 8.1 illustrates the vertical ice process considered in the model. The processes involved and modeled in the ice jam process are better depicted using the River1D model. Figure 8.1(a) shows the formation of border ice on the left and right banks (widths B_{bl} and B_{br}) with moving surface ice layers (velocity $U_i = U_w$ flow velocity) of solid ice (thickness t_{si}) and frazil slush layers

(thickness t_{fs}) in the middle of the cross section (opening wdith B_o). B_{WS} is the toal width of the cross section as a function of water level based on discharge and channel geometry. *CiBo* is the width of the surface ice formed, where *Ci* is the surface ice concentration. The frazil rise from the underneath water and suspended ice mixture is denoted by $Bo\eta C_f$, where η is the rate of frazil rise. The re-entrainment is denoted by $B_o\beta_{re}C_i$ where β_{re} is denoted by rate of surface ice re-entrainment. New pans formed on the surface of the water and the thickness of new frazil pan is denoted by t_f'. The net rate of heat exchange between water and air is denoted by Φ_{wa}, the net rate of heat exchange between water and ice by Φ_{wi}, and the net rate of heat exchange between water and air through the floating ice layer is denoted by Φ_{ia}.

Figure 8.1 (b) shows the vertical ice process with anchor ice on the bed of the river. The anchor ice thickness on the bed of the river is denoted by t_{an}. The width of the bed anchor ice is denoted by $C_{an}P_b$, where C_{an} is the fraction of bed covered by anchor ice and P_b is the bed-affected wetted perimeters of the channel. The amount of water and suspended ice mixture accretion to the bed is given by $C_{an}P_b\gamma C_f$, where γ is denoted by frazil accretion rate and C_f is the volumetric concentration of suspended frazil.

Figure 8.1 (c) shows the formation of border ice on the banks similar to that of Figure 8.1 (a), but the surface layer of solid ice is stationary here, with moving under-cover frazil layer. The velocity of the under-cover moving frazil layer (U_{ui}) is equal to the average water velocity in the cross-section (U_w). As the surface ice here is stationary, the ice velocity (U_i) is equal to zero. Here, S_{ui} represents the exchange of heat between moving and stationary frazil layer.

Figure 8.2 shows the longitudinal profile definition of modelled ice layers (Blackburn and She 2019). The modelled ice layers using River1D incorporates the moving ice floes from upstream having solid ice layer top and frazil slush layer below, the leading-edge stationary ice cover with solid ice layer, frazil slush layer, and under-cover frazil transport layer from top to bottom, where top two layers have zero velocity and the lowest layer has the water velocity (U_w). Figure 8.2 also shows that the anchor ice at channel bottom is modelled using River1D.

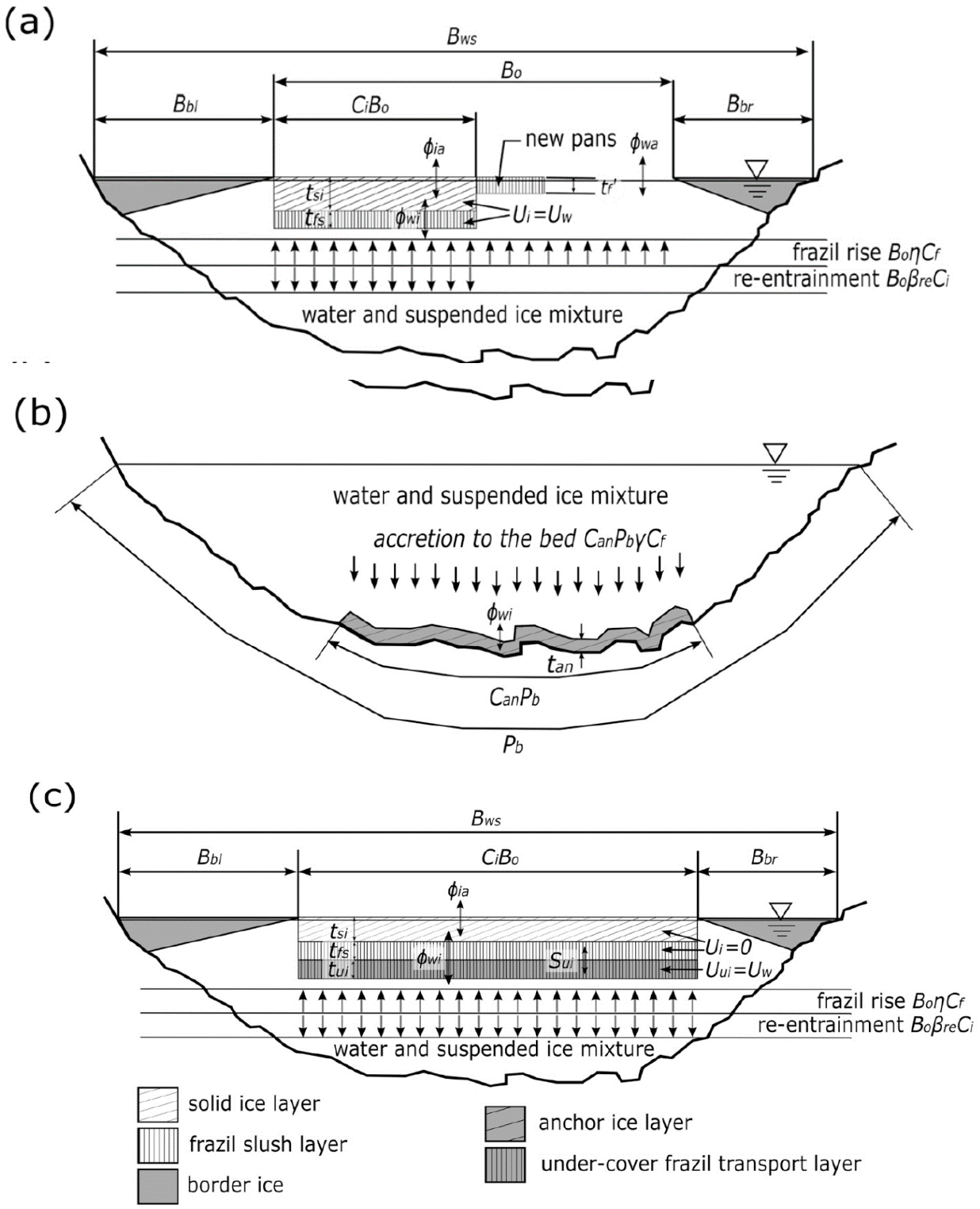

Figure 8.1 Cross-section definition sketch of the vertical processes considered in the model for (a) moving surface ice layers, (b) anchor ice, and (c) stationary surface ice layers with moving under-cover frazil layer (Blackburn and She 2019)

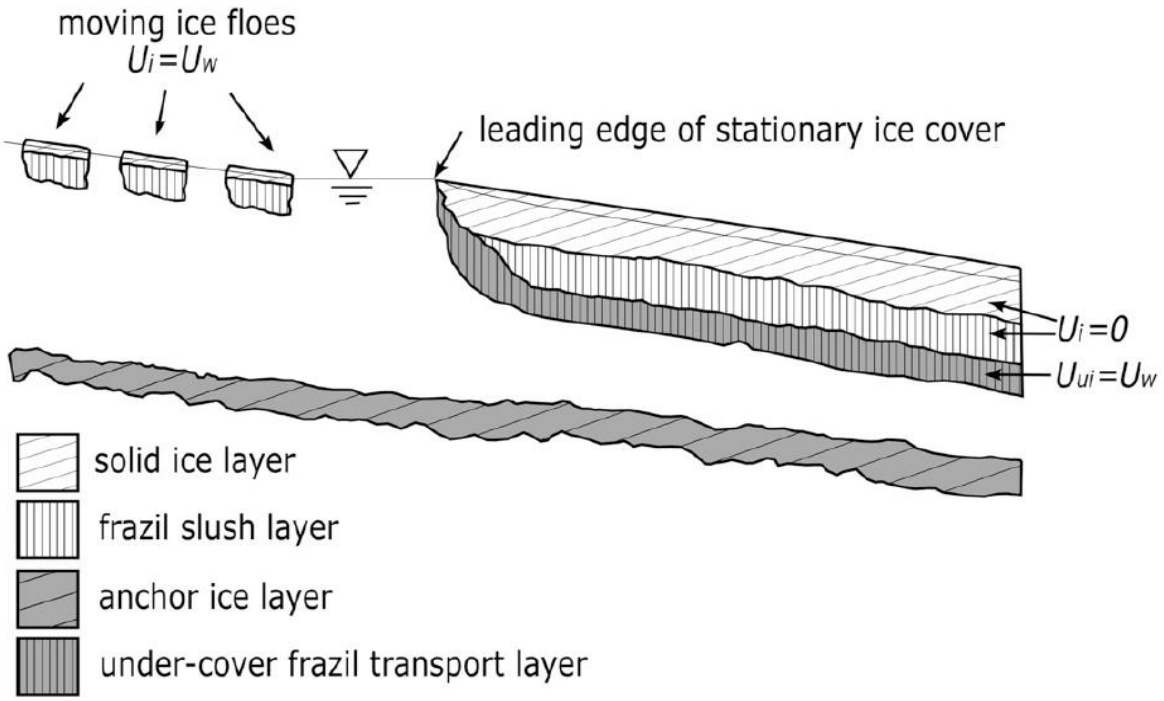

Figure 8.2 Longitudinal profile definition sketch showing the modelled ice layers.

8.2 RIVER1D MODEL DESCRIPTION

River1D is a model that is available in the public domain and was first designed as a hydrodynamic model. It solves the Saint Venant equations by employing the characteristic dissipative Galerkin approach (Hicks and Steffler 1992). Since then, the model has been modified on a number of occasions to include a variety of river ice processes. As a result of these modifications, the model is currently regarded as a physically based, one-dimensional, comprehensive river ice process model. The ice jam modules are housed in a separate standalone component, which was not utilized in this investigation. The River1D suite is able to simulate river ice processes from the beginning of the freezing phase all the way through the melting process.

When Andrishak and Hicks (2005) improved the rectangular channel approximation model to include thermal ice processes by employing control volume principles inside a Eulerian frame of reference, River1D began its transition from a hydrodynamic model to an ice process model. This innovation made it possible to simulate the temperature of the water, the generation of suspended frazil, the formation of surface ice and solid ice, the location of the ice front, and the growth and melting of thermal ice (Andrishak, 2005; Andrishak, 2008; Hicks, 2009). The heat transfer between the water and the air was made simpler by switching from a full energy budget, which requires a substantial amount of data, to a linear heat transfer technique, which just requires data

on the air temperature and the solar radiation (Andrishak and Hicks 2008). Separately, She and Hicks modified the model in order to incorporate the steady ice jam profile equation as well as the impacts of ice resistance on ice jam release waves (She and Hicks 2005). She et al model's includes a component that accounts for the emergence of dynamic ice jams (She et al. 2009). The model capability was enhanced to include simulation of dynamic wave propagation in multi-channel networks (She et al. 2012). These are examples of recent developments in the field (Blackburn et al. 2015).

Both Andrishak and Hicks (2005) and She and Hicks (2005) acknowledged the potential limitations of using rectangular channel approximations and acknowledged that improvements in simulated results could be achieved using natural channel geometry (Andrishak and Hicks 2005; She and Hicks 2005). Additionally, both authors acknowledged that the potential limitations of using natural channel approximations were acknowledged. Blackburn and She (2019) modified the River1D model such that it considers the natural channel geometry (Blackburn and She 2019). During the process of developing this version of the model, it was improved to incorporate supercooling, frazil accretion, re-entrainment, anchor ice formation and release, border ice formation, under-cover transport of frazil, and ice cover formation. These features were added to the model during its development (Blackburn and She 2019). The equations for ice transport are solved by employing a finite element approach known as the Streamline Upwind Petrov-Galerkin method (Blackburn and She 2019).

By utilizing atmospheric zones, River1D makes it possible to utilize meteorological data collected from a number of different weather stations. It is up to the user to decide which parts of a model domain should be represented by each of the many atmospheric zones. Multiple upstream (and/or downstream) boundary conditions, each with their own distinct inflow hydrographs and ice inputs, can be incorporated in the model so that it can account for confluences and difluences.

A thorough dataset taken from the Susitna River in Alaska was utilized in the process of calibrating and validating the model (Blackburn and She 2019). Ye and She (2019) additionally used the defined ice conditions component of the model to test six mechanical break-up criteria using data from the Athabasca and Peace Rivers in Alberta (Ye and She 2019). Even though the impacts of urban influences on the ice formation processes of rivers have not yet been modeled, the most recent version of River1D provides a chance to examine how these influences play a role.

Additionally, one of the reasons why River1D was selected as the model to use in the research project entitled "Studying effects of sub-zero temperatures on the volume of water and discharge in the Missouri River" is because it provides the opportunity to conduct additional validation on the natural channel geometry version of the program.

8.3 RIVER1D APPLICATION

For analysis of the ice jam process, River1D software developed by Dr. Yuntong She and team at the Department of Civil and Environmental Engineering, University of Alberta will be used. The software provides the ability to perform one-dimensional analysis of steady and unsteady open water flows, flow underneath a static ice cover, and steady flow underneath a stable ice jam and the associated ice jam profile.

8.3.1 OPEN CHANNEL FLOW SIMULATION

Open water simulation function is for modeling open-channel flow events during the summer periods for rivers in cold regions, e.g., Alaska, Montana, Alberta. Open channel flow simulation can also be performed using HEC-RAS. The four main types of input data required to model the open channel events using River1D includes:

1. Cross sectional geometry for the reach to be modelled.
2. Channel and floodplain roughness (either Manning's n or roughness height; k).
3. Boundary conditions including tributary inflows.
4. Initial conditions describing water level and discharge at each channel cross-section.

The cross-sectional geometry and channel floodplain roughness (left overbank, channel bed, and right overbank) can be imported from HEC-RAS to River1D. The inflow and outflow boundary conditions are set up as: inflow hydrograph at upstream, and water surface elevation as shown in Figure 8.3.

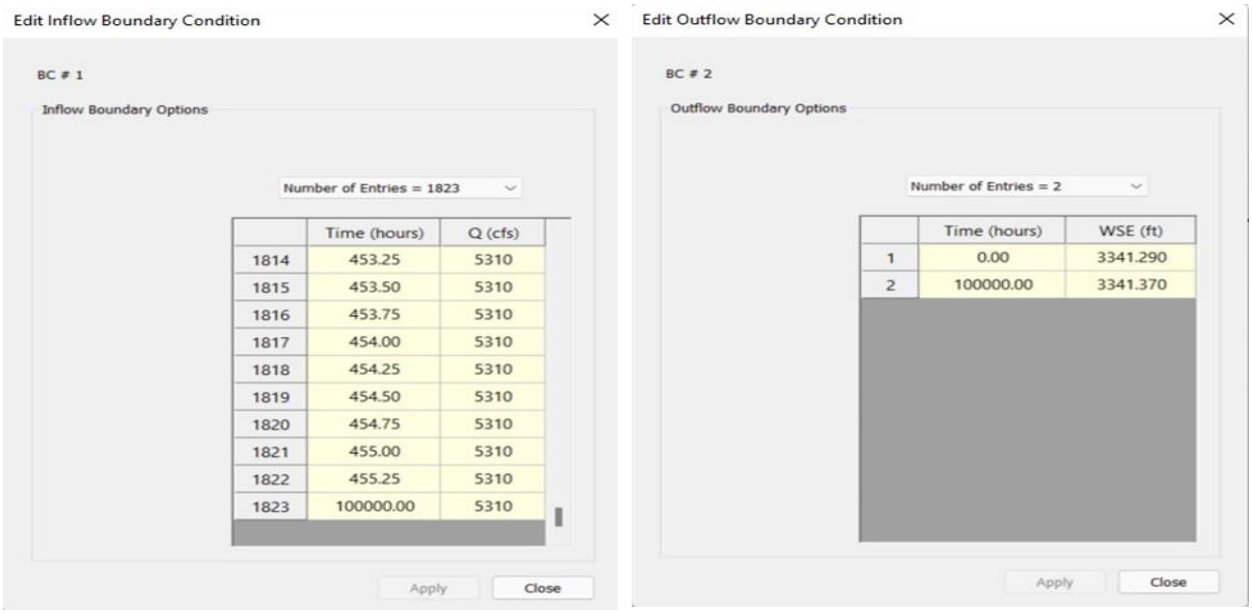

Figure 8.3 Inflow and outflow boundary conditions for open channel simulation on River1D for Missour River simulations.

The simulation is run on Missouri River with discharge data from the USGS gaging station below Holter from 2/29/2020 – 3/19/2020. Thus a steady state simulation for 455.25 hours with a time step of 0.25 hours (15-minute inflow data) is run. Figure 8.4 displays the profile view after the steady simulation of 455.25 hours, for open channel case of Missouri River.

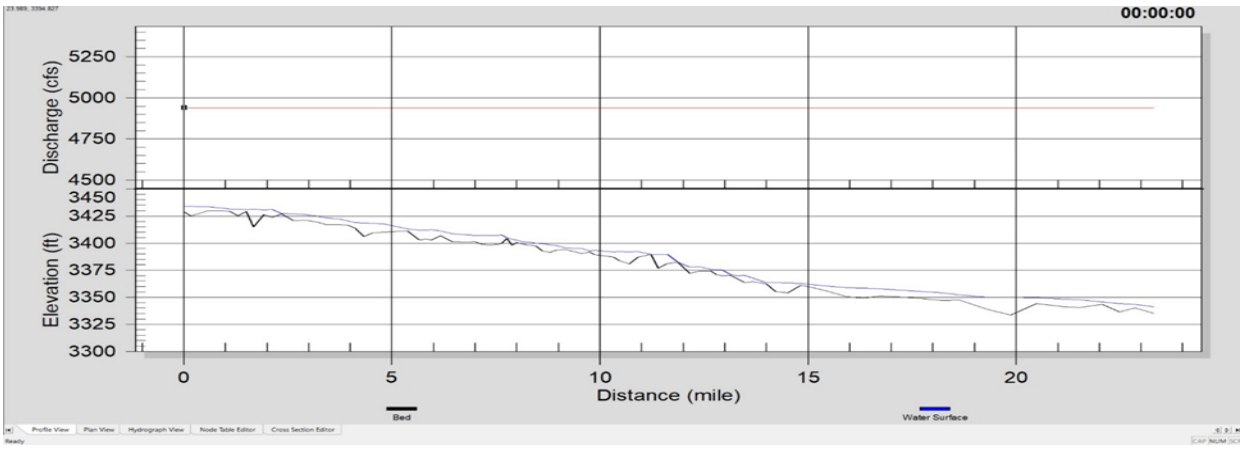

Figure 8.4 Profile view at 455.25 hours of steady state simulation and discharge (cfs) along distance (mile) for open water of Missouri River in River1D.

Figure 8.4 satisfies the assumption of steady simulation as the discharge (cfs) has not changed for the entire river reach, as no lateral flow is introduced. Figure 8.5 shows the transient flow

simulation result for the same case and the Figure 8.6 shows the hydrograph view for transient flow simulation of open water case.

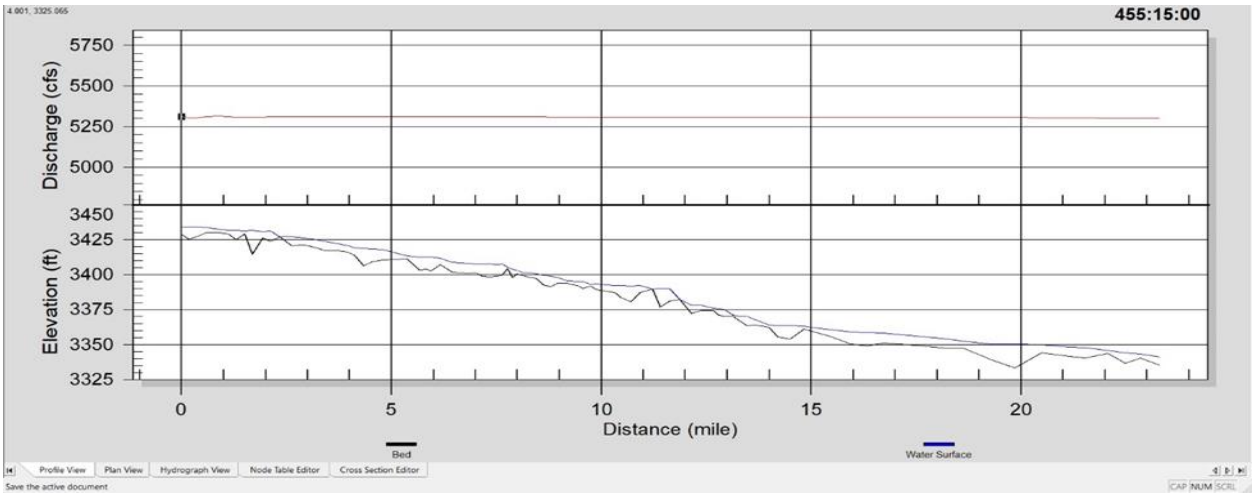

Figure 8.5 Profile view at 455.25 hours of transient (unsteady) simulation and discharge (cfs) along distance (mile) for open water of Missouri River in River1D.

Figure 8.6 Hydrograph view for transient (unsteady) solution for open water case of Missouri River on River1D.

Figure 8.7 shows the profile view of the discharge along the distance at 160 hours of simulation, and the discharge decreases from upstream to downstream. This is because inflow increase rapidly (~4600 to >5000 cfs) from 150 to 160 hours, Figure 8.6.

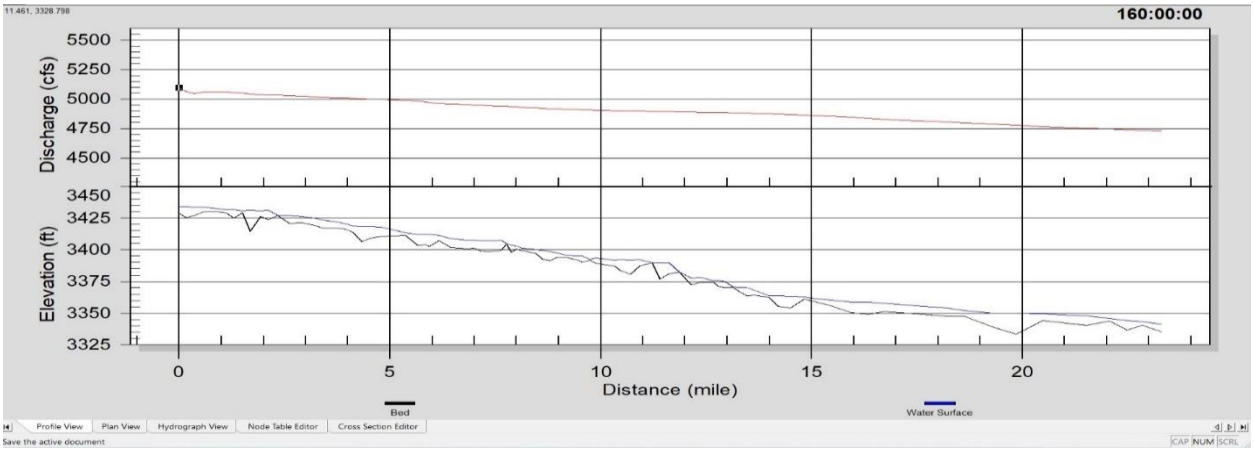

Figure 8.7 Profile view at 160 hours of simulation for open water case showing discharge (cfs) along the distance (mile) on River1D

Unsteady flow simulation on HEC-RAS is carried for the December-2006 on HEC-RAS and on River1D. Figure 8.8 shows the result obtained from transient simulation done in River1D and unsteady flow simulation from December-1, 2006 to December-31, 2006. The simulation result is shown for the Cascade. The result obtained is very identical from both the model. The only difference is seen on the initial phase of the simulation where River1D shows a better result compared to that of HEC-RAS.

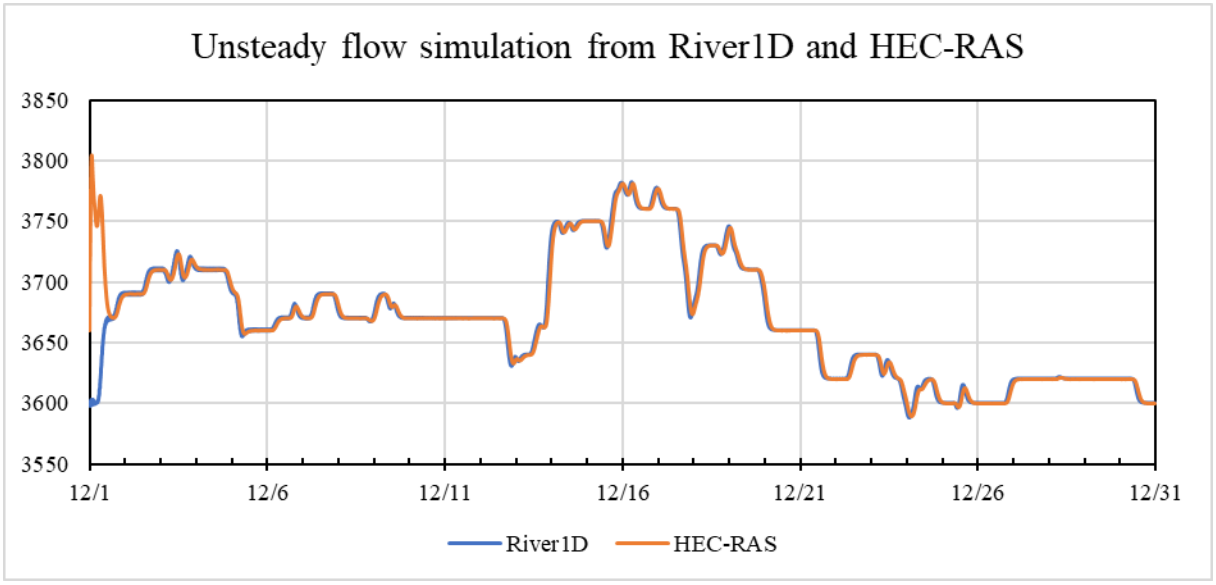

Figure 8.8 Comparison of unsteady flow simulation from River1D and HEC-RAS

8.3.2 STATIC ICE COVER/ICE JAM PROFILE SIMULATION

Static ice cover simulation is for when a static ice cover or an ice jam is present in the channel. The model will compute the ice jam profile based on the ice jam stability equation (Pariset et al. 1966; Uzuner and Kennedy 1976) using the algorithm adapted from the ICEJAM model (Flato and Gerard 1988). This type of simulation contains certain parameters additional than the open water case simulation. Some of the additional parameters includes surface ice concentration, thickness of the specified stationary ice cover in feet or meters, ice roughness, ice roughness mode, and jam flag.

Surface ice concentration (C_i in Figure 8.1a) should be between 0 and 1 with 1 being 100% surface ice coverage. The thickness of specified stationary ice cover will remain constant throughout the simulation; in the case of ice jam profile simulation, these values will be used as an initial condition to calculate the thickness of the ice jam. Ice roughness value is the Manning's n value, and ice roughness mode is a function of ice thickness based on coefficients of Manning's roughness of the under surface of ice. Ice jam flag is used to determine whether to perform the ice jam profile calculation or not.

For the static ice cover simulation of Missouri River, same boundary conditions are used as for the open water case. The initial solid thickness of 1.65 ft was assumed at desired cross-section, the ice roughness *n* of 0.06 was used, with ice roughness mode of 0, as it was user defined. Jam flag was set as 1 for the sections where the jam simulation was desired (indicating jam flag on).

Figure 8.9 shows the profile view for steady state simulation for static ice conditions showing solid ice thickness after the simulation of 455.25 hours along the distance. The constant discharge throughout the river reach satisfies the steady state simulation. Figure 8.10 shows the profile view after the transient simulation was carried out with solid ice thickness along the channel distance.

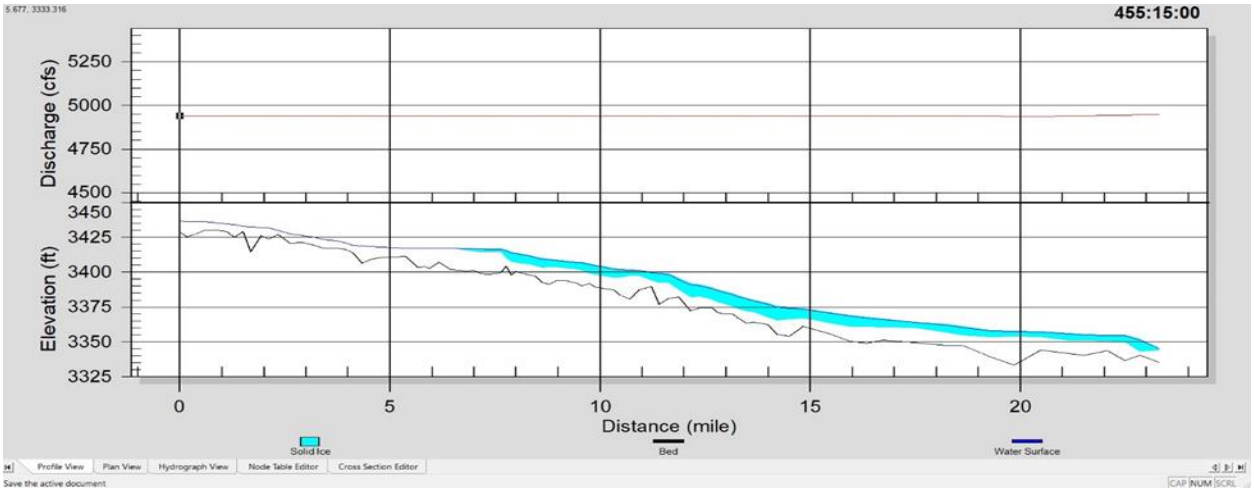

Figure 8.9 Profile view at 455.25 hours of steady state simulation and discharge (cfs) along distance (mile) for static ice conditions of Missouri River in River1D.

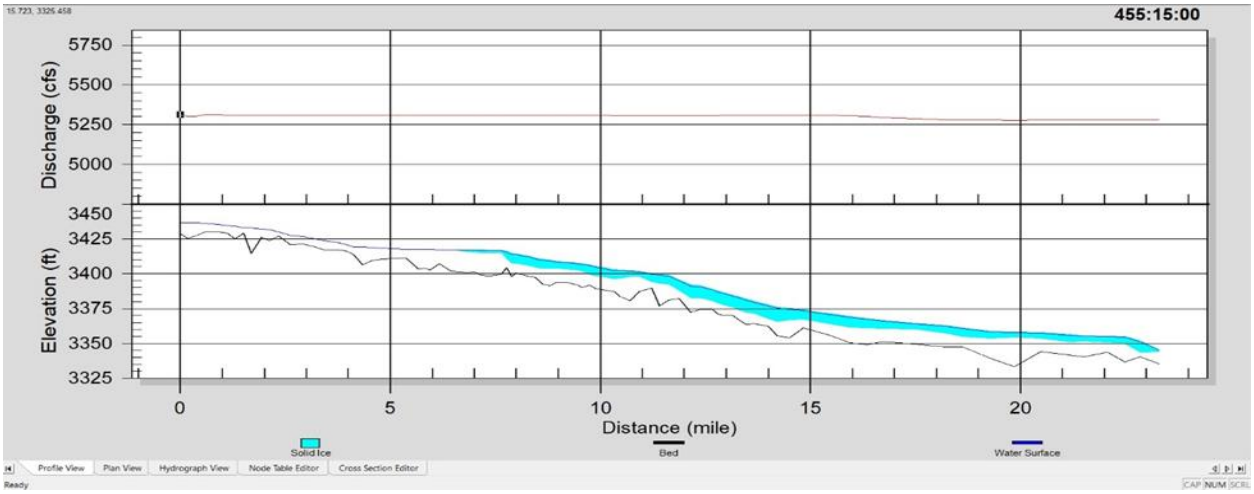

Figure 8.10 Profile view at 455.25 hours of transient simulation and discharge (cfs) along distance (mile) for static ice conditions of Missouri River in River1D.

8.3.3 THERMAL ICE PROCESS SIMULATION

Thermal ice process simulation is the main aim of using the River1D because of the dynamic functionality. Simulation of the surface ice jam processes is a key component in river ice modeling during freeze-up and breakup periods. Static ice process simulation can be done using HEC-RAS but River1D is able to simulate the thermal process simulation. Static ice jam models cannot determine whether, when, and where a jam will form. The thermal ice process simulation includes several thermal ice processes like supercooling, frazil formation, frazil accretion, frazil re-

entrainment, anchor ice formation and release, border ice formation, and under-cover transport of frazil. It is also incorporating the dynamic ice process like ice jam formation and release.

Once the water becomes supercooled (water temperature going slightly below 0^{o}C), frazil ice will form in the water column. The concentration of suspended frazil ice changes with the thermal growth and decay of frazil ice in the water column and mass transfer between and the surface ice, under-cover moving frazil, and anchor ice layers. This method of simulation produces results which is very close to the observed results and provides better understanding of river ice process. Thus, the main output for prediction of river ice process depends on the success of thermal process simulation. The input data for thermal ice process simulation includes:

1. River elevation data for the entire river reach.
2. Inflow at Holter and lateral inflow data along the river reach.
3. Water surface elevation data at the outflow.
4. Water temperature and air temperature data along the study reach.
5. Net solar radiation.

The application of thermal ice process simulation on Missouri River is a part of future study of this project.

Figure 8.10 shows a sample outcome of the profile view of Sustina river, south-central Alaska (Blackburn and She 2019). The outcome shows the water temperature and elevation along the distance for the river.

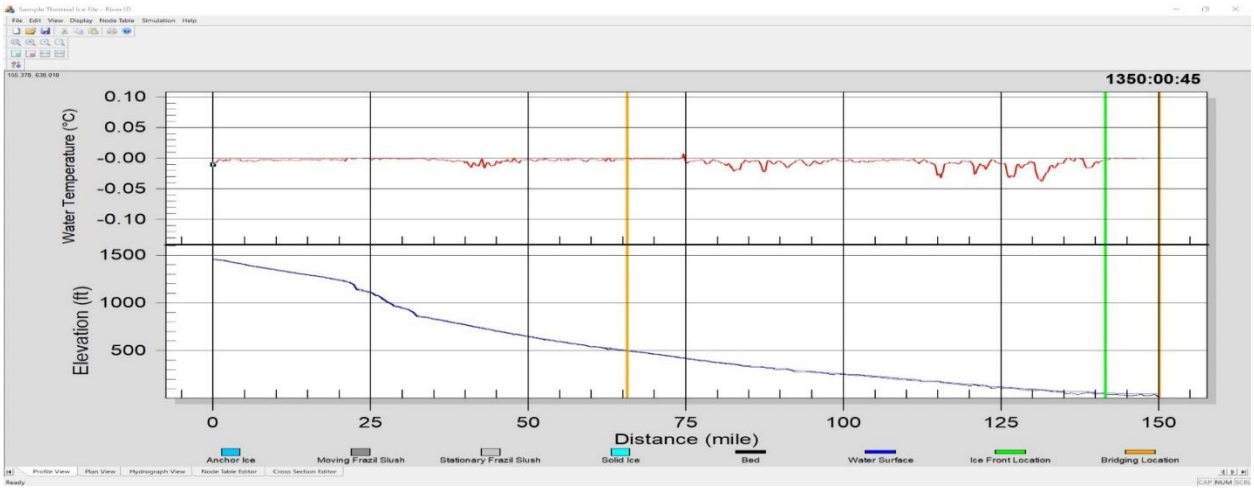

Figure 8.11 Profile view showing elevation and water temperature with distance for the Sustina River, Alaska.

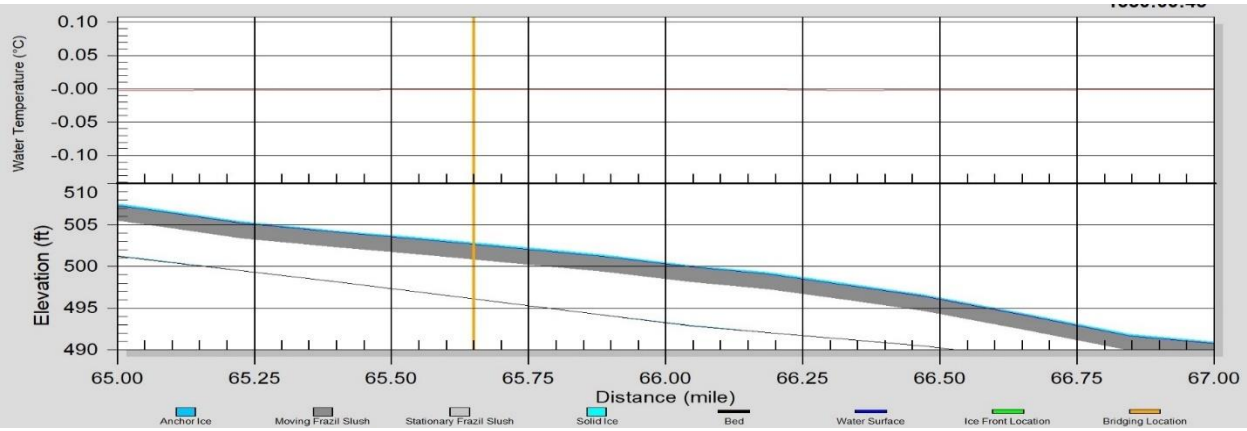

Figure 8.12 Profile view showing the formation of moving frazil slush and solid ice on River1D with bridging location.

Figure 8.12 is a detailed version of Figure 8.11, where we can see the solid ice and beneath it, the moving frazil slush ice. The bridging location of the river is also seen here, and the water temperature shows the water temperature below 0 ^{o}C for some location, showing the supercooling phenomenon. This is the desired result for Missouri River after thermal process simulation.

8.4 COMPARISON TO HEC-RAS

River1D is a dynamic model which can analyze the river process for open channel cases, static ice cover cases, and thermal cases. River ice process is a phenomenon where meteorological parameters play a vital role, and these parameters are accounted very well in River1D, thermal ice process simulation. In contrast, HEC-RAS is applicable and produces results for open water case and static ice cover case, but do not account for the meteorological parameters.

For river from upstream of the junction of Dearborn River and Missouri river to the Cascade, derived from the manual method, HEC-RAS simulation and River1D simulation is carried out. The ice jam steady simulation is carried out on the Missouri River, with assumed ice cover thickness of 1.65 ft starting 6.83 miles downstream from the most upstream cross-section. The profile plot of the ice jam simulation in this case is shown in Figure 6.12. For the same geometry data, River1D steady state simulation is also carried out. The profile view of the steady state simulation with ice cover is shown in Figure 8.9.

The resulting ice thickness achieved from River1D and HEC-RAS is compared in Figure 8.13.

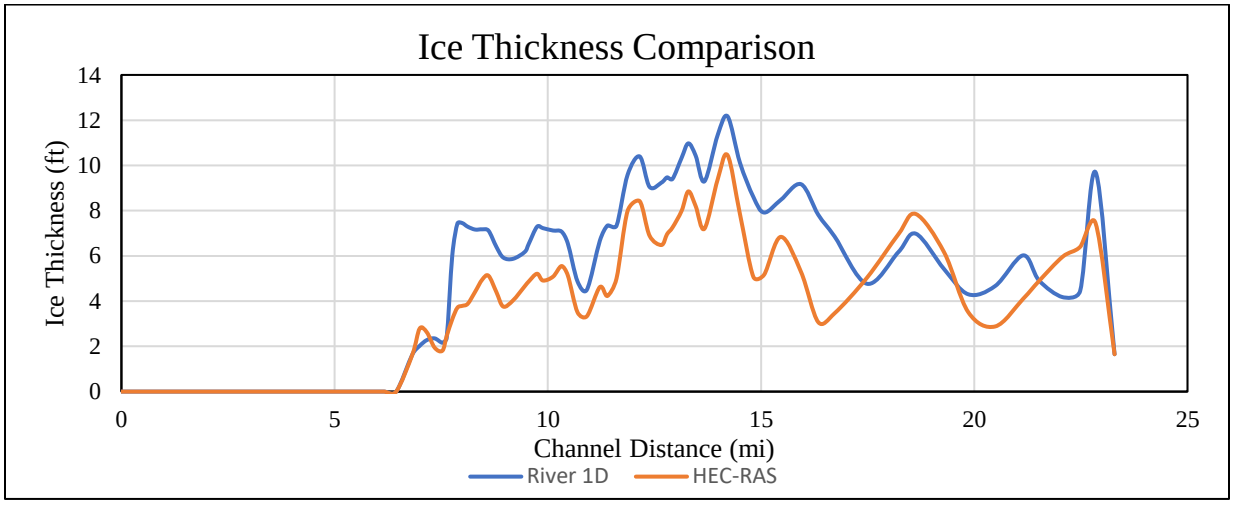

Figure 8.13 Comparison of ice thickness simulated by HEC-RAS and River1D.

The vertical ice process model as in Figure 8.1, are taken into consideration for River1D model. The longitudinal profile, Figure 8.2, shows the longitudinal stretch of river ice modelled on River1D. River1D shows the amount of anchor ice, stationary frazil slush, moving frazil slush, solid ice, ice front location and bridging location. These parameters are missing on HEC-RAS. The ice jam profile calculation on HEC-RAS depends on the amount of ice cover thickness introduced to the river stretch, and do not include the dynamic ice process phenomenon like supercooling, frazil formation, frazil accretion and re-entrainment, anchor ice formation and release, border ice formation, and under-cover transport of frazil. This is the reason, River1D model comparatively provides better understanding of river ice process than HEC-RAS model.

CHAPTER 9. SUMMARY AND CONCLUSIONS

9.1 SUMMARY

In addition to the river ice process, this thesis presents a summary of the river hydrometric data, and meteorological data available for the study reach. The hydrometric data includes the discharge, water temperature, and gage height data, which were obtained from the USGS website. The data analyses conducted in CHAPTER 3 presents the study of discharge, water temperature, and gage height at different USGS gage stations from Holter to Great Falls. The basic concept used on this analysis is, when there is ice jamming in the river, the downstream of the river has loss in discharge, while the upstream of the jamming location has increase in gage height. The water temperature data at the time supports the claim, whether ice formation is feasible or not in the scenario. Also, as river ice formation process is a very dynamic process, and depends on various parameters, making judgements based on discharge, water temperatures, and gage height about the location of ice jam formation is not always accurate.

This thesis also discusses the use of HEC-RAS for simulation of river ice process. HEC-RAS primarily is an one and two-dimensional steady flow, one and two-dimensional unsteady flow calculations, sediment transport/mobile bed computations and water temperature/water quality modeling tool. In addition to the open channel simulation in HEC-RAS, the static ice cover simulation and ice jam simulation can also be carried out in HEC-RAS. This process has been tested in the thesis. The basic input data required for the HEC-RAS is the geometry data, which is imported from RAS Mapper in HEC-RAS. Lidar data and USGS DEM data are used for preparation of input data, which is digitized on RAS Mapper to get the geometry data. The Lidar and DEM data consists of elevation data, which is used in HEC-RAS.

The thesis also discusses about two methods used to generate bathymetry data for the geometry data. One method is the manual method, where contour map available from C-Map genesis website is used to develop bathymetry data for available cross-sections. While other method is the GIS method, where the survey data provided by NWE Hydro was used to create a different DEM raster file, which was used to extract the bathymetry data.

The thesis also discusses about the use of water temperature simulation in HEC-RAS. Water temperature simulation uses geometry data, flow data, and initial water temperature data along with meteorological time series data. The meteorological time series data is prepared using the

spreadsheet developed by Dr. Xing Fang, which imports weather data from visualcrossing.com, and converts that weather data into HEC-RAS required meteorological parameters. This spreadsheet uses power query function of excel along with VBA coding. The water temperature simulation is carried out on HEC-RAS for steady simulation of the river reach. The results obtained by the water temperature simulation aligned with the result obtained from the data analysis of discharge, gage height and water temperature.

The land cover map prepared on this thesis uses the GIS and ERDAS Imagine for unsupervised classification of study area, to identify those date when ice jamming probably occurs and view them. This gives the picture of location of ice jamming, and more susceptible places where ice jamming occurs.

Finally, the thesis presents the idea of using River1D, which is a model that is developed with the main objective to develop a comprehensive river ice process model capable of simulating dynamic ice process in natural river systems with complex ice and flow regimes. River1D has the ability to perform open channel flow simulation and static ice cover simulation, which is similar to what HEC-RAS offers. In addition to that, thermal ice process simulation is possible in River1D, which differentiates River1D from HEC-RAS.

9.2 CONCLUSIONS

The flow analysis method for identifying the ice jam events using discharge, water temperature, and gage height is capable to identify the events and the probable location of ice jamming. This analysis to identify events aids the further process in modeling of river ice, as it helps to identify the time while analyzing river ice process. Number of events are identified using this process in CHAPTER 3. The number of such events identified every year are enlisted in Table 9.1.

Table 9.1 Events identified after analyzing the discharge, water temperature, and gage height on CHAPTER 3.

Year	Number of events identified	Events
2014	3	28 Dec – 31 Dec, 2014 27 Jan – 29 Jan, 2015 31 Jan – 02 Feb, 2015
2015	3	02 Mar – 03 Mar, 2015 16 Dec – 17 Dec, 2015 20 Dec – 27 Dec, 2015
2016	5	30 Jan – 31 Jan, 2016

		07 Dec – 08 Dec, 2016 16 Dec – 19 Dec, 2016 21 Dec – 25 Dec, 2016 25 Dec – 28 Dec, 2016
2018	7	10 Jan – 13 Jan, 2018 04 Feb – 05 Feb, 2018 09 Feb – 11 Feb, 2018 18 Feb – 20 Feb, 2018 14 Mar – 15 Mar, 2018 17 Mar – 21 Mar, 2018 26 Mar – 27 Mar, 2018
2019	7	30 Dec, 2018 – 02 Jan, 2019 04 Jan – 09 Jan, 2019 21 Jan – 25 Jan, 2019 27 Jan – 28 Jan, 2019 31 Jan, 2019 03 Feb – 05 Feb, 2019 28 Mar – 30 Mar, 2019
2020	4	07 Jan – 12 Jan, 2020 02 Feb – 05 Feb, 2020 14 Mar – 19 Mar, 2020 19 Mar, 2020

The land cover classification is done on the LANDSAT image available for such event on the study area of Missouri River from Holter, MT to Great Falls, MT. The land cover classification is carried out for two winter events: 15 December, 2015 and 24 February, 2007, and one summer event: 05 September, 2019. Use of LANDSAT 5 is done for the event of 2007 and LANDSAT 8 for the event of 2015 and 2019. Figure 4.2 and Figure 4.3 shows the land cover classification for winter events and Figure 4.4 shows the land cover classification for summer events.

Geometry data of the river system, including the river reach, and cross section is a vital component for river analysis. HEC-RAS and River1D both requires the cross-section data with elevation for modeling. Lidar data and USGS DEM provides the elevation data on the surface of the earth. They are used for digitizing the river on RAS Mapper. The elevation data provided by them do not contain the bathymetry data, as shown in Figure 5.3. For river analysis process either on HEC-RAS or River1D, bathymetry data is the most important part. Bathymetry data is acquitted by contour map method manually, and survey data of depth on river using GIS method. Figure 5.9 shows the cross-section of river after importing the bathymetry data using manual method, and Figure 5.12 shows the cross-section of river after importing bathymetry data using GIS method.

After the acquisition of bathymetry data, HEC-RAS is able to simulate open channel flow simulation, and static ice cover or ice jam simulation. The steady flow simulation and unsteady flow simulation of the HEC-RAS model from June 1 – July 15, 2020 is carried out for open water case. Figure 5.17 and Figure 5.23 shows the profile plot with water surface elevation for steady and unsteady flow simulation. Ice cover of 1.65 ft was assumed after 6.83 miles downstream from the most upstream cross-section from Figure 5.4, ice jam analysis. Figure 6.12 shows the profile plot after ice jam analysis was carried out, showing the simulated ice cover thickness and water surface elevation through the river reach.

HEC-RAS is used to simulate water temperature for any ice jamming events with water temperature and meteorological data as input. For meteorological data, an excel spreadsheet was developed which can download the weather data from visual crossing website, and convert that to HEC-RAS input table format. The event of ice jamming between 05 February – 01 March, 2022 is analyzed for testing the water temperature simulation in HEC-RAS. The water temperature plot Figure 7.9 showed time series plot of an event on 22 February, 2022 at 06:30:00, when the water temperature remains at 0 ^{o}C. This event is validated with Figure 7.10 where loss of discharge of around 2000 cfs is identified. Thus, water temperature simulation method can be used to predict future conditions of water temperature, like events when water temperature remains at 0 ^{o}C for prolonged period of time, whenever forecast weather data is available.

River1D is the most effective model right now for modeling the river ice process because of its dynamic abilities compared to that of HEC-RAS. River1D incorporates the open channel, static ice cover, and thermal ice simulation processes, which is an advancement to what HEC-RAS performs in ice jam simulation. The comparison of ice thickness shown by HEC-RAS and River1D is made on Figure 8.13 for steady state solution. River1D incorporates the meteorological data while simulation and has various other parameters that are taken into consideration, like vertical ice processes, water cooling and supercooling, under-cover transport of frazil, ice cover progression, bridging location, etc. which results to anchor ice, border ice, moving frazil slush, stationary frazil slush, and solid ice. Thus, thermal ice simulation process is the main objective to accomplish in order to achieve the aim of predicting discharge during ice jam events. River1D model can be developed from the HEC-RAS geometry file, as River1D has the ability to convert the geometry file of HEC-RAS to River1D form. After this, boundary conditions need to be set

up, which includes hydrograph on inflow boundary and water surface elevation on outflow boundary. The nodal flux and initial depth are specified at the beginning of the conversion from HEC-RAS to River1D. These are for the open water simulation. For static ice simulation, other parameter such as ice concentration, solid ice thickness, ice roughness and ice flag are specified. And for the thermal state simulation, in addition to the earlier data, meteorological parameters and bridging events can be added. Some of which include: number of atmospheric zone, number of user defined bridging events, air temperature, and heat transfer constants between water and air. Some of these could only be edited manually on the River1D text editor. The profile view of Missouri river for static ice case using steady and transient simulation is done. The profile view showing the profile elevation and discharge along the distance for steady state simulation is shown in Figure 8.9 and transient simulation is shown in Figure 8.10.

9.3 FUTURE WORK

The main aim of starting the project is to develop a predictive model, to predict an ice jamming event and the amount of discharge lost during such event. NEW Hydro loses a significant amount of energy loss every year during winter season because of these ice jamming events, and the aim is to develop a predictive model, which can be handed over to NWE Hydro after getting it ready.

The future work remaining for completing this project can be incorporated into following bullet points:

- Acquisition of bathymetry data for the study river starting from the Holter lake to Great Falls, with higher accuracy, such that no workaround measures is required to create bathymetry data.
- Create a HEC-RAS project for the entire river reach, with update bathymetry file and do steady and unsteady flow analysis, with ice cover. Ice cover thickness should be used after proper surveying on the river during some of the events.
- Since river flow is a dynamic process, so unsteady flow water temperature simulation should be carried out for the entire reach.
- River1D should be used for the analysis, and thermal process simulation should be carried out. Thermal process simulation is the ultimate outcome as this model incorporates the parameters that are not addressed by HEC-RAS and are very important in river ice process.

- After successful trial of River1D thermal process simulation, this should be automized and programmed to a user-friendly GUI (Graphical User Interface), where the user can specify the forecast meteorological data, initial temperature, solar radiation, water surface level, and other boundary condition parameter, and resulting outcome show the events on the forecast period.
- Handling over the successful project to NWE Hydro, after successfully running the trial.

Many theoretical parts of the project with testing of HEC-RAS and River1D, has been accomplished till date with very limited source of data. This is the foundation for the future work to be carried out in the project.

.

REFERENCES

Altena, B., and Kaab, A. (2021). "Quantifying river ice movement through a combination of European satellite monitoring services." *International Journal of Applied Earth Observation and Geoinformation*.

Andrishak, R., and Hicks, F. (2005). "Impact of climate change on the winter regime of the peace river in Alberta." *Climate Change Research Users Group Alberta Environment*.

Andrishak, R., and Hicks, F. (2008). "Simulating the effects of climate change on the regime of the Peace River." *Canadian Journal of Civil Engineering*, 35, 461-472.

Ashton, G. D. (1979). "River Ice: The presence of ice on rivers changes their behavior, interferes with their use, and causes severe economic disruption." *American Scientist*, 67(1), 38-45.

Beltaos, S., and Wong, J. (1986). "Downstream Transition of River Ice Jams." *Journal of Hydraulic Engineering*.

Beltaos, S. (1987). "River Ice Jams- Theory, Case-Studies and Applications - Closure." *Journal of Hydraulic Engineering Association*, 2-19.

Beltaos, S., and Burrell, B. C. (2003). "Hydraulic Interaction Between Ice And Bridges." *12th Workshop on the Hydraulics of Ice Covered Rivers*.

Beltaos, S. (2008). "Progress in the study and management of river ice jams." *Cold regions science and technology*.

Beltaos, S. (2013). "Freezeup Jamming and Formation o Ice Cover, in River Ice Formation." Committee on River Ice Process and the Environment.

Bijeljanin, M., and Clark, S. P. (2011). "Application of Numerical Modelling Towards Prediction of River Ice Formation on the Upper Nelson River." *CGU HS Committee on River Ice Processes and the Environment*.

Blackburn, J., She, Y., Hicks, F., and Nafziger, J. (2015). "Ice Effects on Flow Distribution in the Mackenzie Delta." 18th Workshop on the Hydraulics of Ice Covered Rivers, Committee on River Ice Processes and the Environment, Quebec City, Quebec, Canada.

Blackburn, J., and She, Y. (2019). "A comprehensive public-domain river ice process model and its application to a complex natural river." *Cold regions science and technology*, 163, 44-58.

Brown, S. R., Beltaos, S., Power, G., and Beddow, T. (2000). "Effects of hanging dams on winter movements and swimming activity of fish." *Journal of Fish Biology*.

Canada, N. R. (2013). *Fundamentals of Remote Sensing*.

Carson, R. W., and Groeneveld, J. L. (1997). *Evolution of the ICESIM model*, Canada.

Chaouch, N., Temimi, M., Romanov, P., Cabrera, R., McKillop, G., and Khanbilvardi, R. (2012). "An automated algorithm for the river ice monitoring over the Susquehanna River using the MODIS data." *Hydrological Processess*.

Clark, S. (2013). "Border and Skim Ice, in RIver Ice Formation." Committee on River Ice Processes and the Environment, Edmonton, Alberta, 77-106.

Cole, T. M., and Wells, S. A. (2003). "CE-QUAL-W2: A Two-Dimensional, Laterally Averaged, Hydrodynamic and Water Quality Model, Version 3.1, User Manual." U.S. Army Corps of Engineers.

Daly, S. F., and Ettema, R. (2006). "Frazil Ice Blockage of Water Intakes in the Great Lakes." *Journal of Hydraulic Engineering*.

Dey, S., and Merwade, V. (2020). "1D HEC-RAS Model Developement using RAS-Mapper."

Duguay, C. R., Bernier, M., Gauthier, Y., and Kouraev, A. (2015). "Remote sensing of lake and river ice." *Remote Sensing of the Cryosphere*.

ESRI. (1998). "ESRI Shapefile Technical Description." Environmental Systems Research Institute, Inc.

Federal Emergency Management Agency, F. (2018). "Guidance for Flood Risk Analysis and Mapping." *Ice-Jam Analyses and Mapping*.

Flato, G. M., and R., G. (1986). "Calculation of ice jam thickness profiles."

Flato, G. M., and Gerard, R. (1988). "Calculation of ice jam profiles," Master's Thesis, University of Alberta, Edmonton, Alberta.

Gebre, S., TImalsina, N., and Alfredsen, K. (2014). "Some Aspects of Ice-Hydropower Interaction in a Changing Climate. Energies." *Energies, MDPI*, 7(3), 1-15.

Hains, M. D. B., and Zabilansky, L. J. (2005). "The Effects of River Ice on Scour and Sediment Transport." *CGU HS Committee on River Ice Processes and the Environment*.

Hicks, F., and Steffler, P. (1992). "A characteristic dissipative galerkin scheme for open channel flow." *Journal of Hydraulic Engineering*.

Hicks, F. (2016). "An Introduction to River Ice Engineering for Civil Engineers and Geoscientists." CreateSpace Independent Publishing Platform.

Howley, R., Ghobrial, T. R., and She, Y. (2019). "Thermal regime in the North Saskatchewan River in Edmonton." *Committee on River Ice Processes and the Environment 20h Workshop on the Hydraulics of Ice Covered Rivers*, Ottawa, Ontario, Canada.

Jasek, M., and Lavalley, J. (2003). "Safety during River Ice Data Collection " *CGU HS Committee on River Ice Processes and the Environment*.

Jasek, M., and Pryse-Phillips, A. (2015). "Influence of the proposed Site C hydroelectric project on the ice regime of the Peace River." *Canadian Journal of Civil Engineering*.

Jasek, M. (2019). "An Emerging Picture of Peace River Break-up Types that Influence Ice Jam Flooding of the Peace-Athabasca Delta " *20th Workshop on the Hydraulics of Ice Covered Rivers*.

Kalke, H., McFarlane, V., Ghobrial, R. T., and Loewen, M. (2019). "Field Measurements of Supercooling in the North Saskatchewan River." *Committee on River Ice Processes and the Environment 20th Workshop on the Hydraulics of Ice Covered Rivers*, Ottawa, Ontario, Canada.

Kempema, E., Kengo Osada, Brian Remlinger, and Ettema, R. (2019). "Anchor-Ice-Related Flooding along Flat Creek, Jackson, Wyoming: Insights from a Stream in Mountainous Terrain." 20th Workshop on the Hydraulics of Ice Covered Rivers.

Khan, A. O. (2006). *Open Channel Hydraulics*, Elsevier.

Leonard, B. P. (1991). "The ULTIMATE conservative difference scheme applied to unsteady one-dimensional advection." *Computer Methods in Applied Mechanics and Engineering*, 88, 17-74.

Lindenschmidt, K.-E., Baulch, H. M., and Cavaliere, E. (2018). "River and Lake Ice Processes—Impacts of Freshwater Ice on Aquatic Ecosystems in a Changing Globe." *Water*.

Lindenschmidt, K., A. Das, P. Rokaya, and Chu, T. (2016). "Ice-jam flood risk assessment and mapping." *Hydrological Processess*.

Lindenschmidt, K. (2017). "RIVICE - A Non-Proprietary, Open-Source, One-Dimensional River-Ice Model." *Water*, 9(5), 314.

Liu, N., Kells, J., and Lindenschmidt, K. E. (2015). "Mapping River Ice Cover Breakup Induced by Hydropeaking Operations." 18th Workshop on the Hydraulics of Ice Covered Rivers, Committee on River Ice Processes and the Environment., Quebec City, Quebec, Canada,.

Malenchak, J. J. (2012). "Numerical Modelling of Ricer Ice Processes on the Lower Nelson River," University of Manitoba, Winnipeg, Canada.

Montana Department of Natural Resources & Conservation. (2022). "Ice jam potential rising across E. Montana." Helena, MT.

Olaode, A., Naghdy, G., and Todd, C. (2014). "Unsupervised Classification of Images: A Review." *International Journal of Image Processing (IJIP)*, 8(5).

Pariset, E., Hausser, R., and Gagnon, A. (1966). "Formation of ice covers and ice jams in rivers." *ASCE Journal of Hydraulics Divison 92(HY6)*, 1-24.

Prowse, T. D. (2001). "River-Ice Ecology. I: Hydrologic, Geomorphic, and Water-Quality Aspects." *Journal of Cold Regions Engineering*.

Prowse, T. D., Bonsal, B. R., Duguay, C. R., and Lacroix, M. P. (2007). "River-ice break-up/freeze-up: a review of climatic drivers, historical trends and future predictions." *Analysis of Glaciology*.

Rokaya, P., Howard, W., and Lindenschmidt, K.-E. (2019). "Promoting Sustainable Ice-Jam Flood Management along the Peace River and Peace-Athabasca Delta." *Journal of Water Resources Planning and Management*.

Rokaya, P. M.-M., Luis; Lindenschmidt, Karl-Erich. (2020). "A physically-based modelling framework for operational forecasting of river ice breakup." *Advances in Water Resources*.

She, Y., and Hicks, F. (2005). "Incorporating Ice Effects in Ice Jam Release Surge Models." 13th Workshop on the Hydraulics of Ice Covered Rivers, Committee on River Ice Processes and the Environment, Hanover, New Hampshire, USA.

She, Y., Hicks, F., Steffler, P., and Healy, D. (2009). "Constitutive model for internal resistance of moving ice accumulations and Eulerian implementation for river ice jam formation." *Cold Regions Science and Technology*, 55.

She, Y., Hicks, F., and Andrishak, R. (2012). "The role of hydro-peaking in freeze-up consolidation events on regulated rivers." *Cold Regions Science and Technology*.

Shen, H. T. (2003). "Research on river ice processes: progress and missing links." *Journal of Cold Regions Engineering*, 135-142.

Shen, H. T. (2010). "Mathematical modeling of river ice processes." *Cold Regions Science and Technology*, 62, 2-13.

Turcotte, B., Burrell, B. C., and Beltaos, S. (2019). "The Impact of Climate Change on Breakup Ice Jams in Canada: State of knowledge and research approaches." 20th Workshop on the Hydraulics of Ice Covered Rivers.

Tuthill, A. M., Wuebben, J. L., and Gagnon, J. J. (1998). "ICETHK User's Manual Version 1 98-11."

Urroz, G. E., and Ettema, R. (1994). "Small-scale experiments on ice-jam initiaion in a curved channel." *Canadian Journal of Civil Engineering*, 719-727.

USACE. (2016). "HEC-RAS River Analysis System, Hydraulic Reference Manual (version 5.0)." U.S. Army corps of Engineers (USACE), Hydrologic Engineering Center (HEC), Davis, CA.

Uzuner, M. S., and Kennedy, J. F. (1976). "Theoretical Model of River Ice Jams." *ASCE Journal of Hydraulics Divison 102(HY9)*, 1365-1383.

Wang, J., Chen, P.-p., and Sui, J.-y. (2011). "Progress in studies on ice accumulation in river bends." *Journal of Hydrodynamics, Ser. B*, 737-744.

Whitfield, P. H., and McNaughton, B. (1986). "Dissolved-oxygen depressions under ice cover in two Yukon rivers." *Water Resources Research*, 1675-1679.

Ye, Y., and She, Y. (2019). "Evaluating Criteria for Mechanical Breakup Initiation Using Field Data." 20th Workshop on the Hydraulics of Ice Covered Rivers, Committee on River Ice Processes and the Environment, Ottawa, Ontario, Canada.